Role of Reelin in synaptogenesis and synaptic stabilization in the adult brain

Carles Bosch

UNIVERSITAT DE BARCELONA
FACULTAT DE BIOLOGIA
DEPARTAMENT DE BIOLOGIA CEL·LULAR

INSTITUTE FOR RESEARCH IN BIOMEDICINE, BARCELONA
PARC CIENTÍFIC DE BARCELONA

Role of Reelin in synaptogenesis and synaptic stabilization in the adult brain

Carles Bosch

Barcelona, juny 2014

Programa de Doctorat en Biomedicina

UNIVERSITAT DE BARCELONA
FACULTAT DE BIOLOGIA
DEPARTAMENT DE BIOLOGIA CEL·LULAR

INSTITUTE FOR RESEARCH IN BIOMEDICINE, BARCELONA
PARC CIENTÍFIC DE BARCELONA

Role of Reelin in synaptogenesis and synaptic stabilization in the adult brain

Paper de la Reelina en la formació i estabilització de sinapsis en el cervell adult

Programa de Doctorat en Biomedicina

Memòria presentada per Carles Bosch, llicenciat en Biotecnologia, per optar al grau de Doctor per la Universitat de Barcelona

Els estudis de tercer cicle s'han emmarcat en el programa de doctorat en Biomedicina de la Universitat de Barcelona. El projecte de Tesi Doctoral està inscrit al Departament de Biologia Cel·lular de la Facultat de Biologia de la Universitat de Barcelona. El treball experimental i la redacció de la memòria que es presenten han estat dirigits pel **Dr. Albert Martínez Garcia**, Professor Agregat a la Universitat de Barcelona, i pel **Dr. Eduardo Soriano García**, Catedràtic de Biologia Cel·lular de la Universitat de Barcelona.

Barcelona, juny de 2014.

Vist-i-plau dels directors de la tesi:

Dr. Albert Martínez Garcia

Dr. Eduardo Soriano García

El Candidat a Doctor,

Carles Bosch Piñol

Als pares, al Sergi, i a la Bea.

Quan surts per fer el viatge cap a Ítaca,
has de pregar que el camí sigui llarg,
ple d'aventures, ple de coneixences.
(...)
Has d'arribar-hi, és el teu destí,
però no forcis gens la travessia.
És preferible que duri molts anys,
que siguis vell quan fondegis l'illa,
ric de tot el que hauràs guanyat fent el camí,
sense esperar que et doni més riqueses.
(...)
Més lluny, heu d'anar més lluny
dels arbres caiguts que ara us empresonen,
(...)
I quan sereu deslliurats
torneu a començar els nous passos.
Més lluny, sempre molt més lluny,
més lluny del demà que ara ja s'acosta.
I quan creieu que arribeu, sapigueu trobar noves sendes.

Kavafis - Carles Riba - Lluís Llach

Caminante, son tus huellas
el camino, y nada más;
caminante, no hay camino:
se hace camino al andar.

Al andar se hace camino,
y al volver la vista atrás
se ve la senda que nunca
se ha de volver a pisar.

Caminante, no hay camino,
sino estelas en la mar.

A. Machado

Agraïments

Aquests han estat uns anys intensos i emocionants, durant els quals han vingut, han marxat i s'han quedat nombrosos actors parcials d'aquesta tesi. A ells van dirigides aquestes breus paraules.

En primer lloc, voldria agraïr als directors de tesi la oportunitat rebuda. A l'Eduardo, per haver-me obert les portes d'aquest laboratori, i a l'Albert per la paciència mostrada i demostrada. I a tots dos, per haver dirigit els meus primers passos dins de la carrera científica.

Als companys de laboratori. A TOTS. GRÀCIES. En una feina que no és individual, i que està plagada d'errors i contratemps, poder comptar amb un equip humà d'aquest nivell és més que un luxe. Em deixaré gent, però doneu-vos per aludits.

Però si hem de dir noms... comencem pel principi. El primer equip de ex-predoctors, Anna, Ale, Vane... i els "grans" que ja van arribar crescudets, Cátia, Ana, Franc, i els que ja estaven crescuts quan vaig arribar, Lluís, Ash. Vàreu ser els primers contactes amb algú que ja havia passat pel clot, i fent gala de l'experiència vau advertir de perills i amenaces (prohibit començar experiments més enllà de les 20h!), vau guiar passos insegurs (quants protocols de WB calen per fer-ne un?) i vau permetre luxes primerencs (creo que con el siguiente sueldo ya me tocará devolver mojitos a alguien... ;D). I també els que han arribat més tard, però s'han guanyat un lloc enorme. Ramon, ets un crack.

Tot i que en el pot petit hi va la bona confitura... i aquí em falten paraules per descriure el que ha set aquesta colla de novatos que hem pujat junts. Óscar, amfitrió de les jornades L'Hos Pintxos (cal fer-ne una International Edition!), Román, superhéroe sin complejos, fonts inacabables de motivació com la Sara o el Martí, liantes capaços de tot i més (menys quan fa pal), la delegació de la bella Italia, els "Tonis", el Toni (et quedes de guardià!), la Mar, vida paral·lela gairebé (necessitaràs algú que piqui la cadira de tant en tant?), la Núria (sí, has d'anar al costat de la Mar, i tant), els tècnics que han ajudat dins i fora el lab, Natalia. Repetim? jejej...

En segundo lugar, también agradecer a Javier abrirme las puertas de su laboratorio en tantas ocasiones, por los libros y por los consejos. A Ángel, por el trabajo impecable y dejar que jugara con ese microscopio. Y por las conversaciones sobre viejas cámaras... Y a Isabel, por el día a día. Y a Asta, por

hacerme de taxista y profesora de microinyección a tiempo parcial. Y a toda la plantilla del laboratorio, Paula, Lidia (habrá que hacer una inmersión algún día no?), Gonzalo... Gracias por la acogida.

También a gente como Alfonso o Ignacio, que sin tener nada que ver con este trabajo me habéis dedicado un poco de vuestro tiempo y experiencia. Y por las cervezas también.

Seria injust no parlar de les plataformes tècniques on s'han desenvolupat gran part dels experiments. Pel nivell tècnic, per l'habilitat comunicativa, i per l'ambient humà. A la plataforma de microscòpia electrònica, des de la Carmen fins la Lídia, passant per tots. I a la de microscòpia digital avançada ("els confos" pels entesos). Lídia, Seb, Anna, Julien. No sabria dir què ompliria realment les pàgines que seguiexen a aquesta sense la vostra col·laboració, suport i discussió.

Però no ens quedarem al laboratori. Els pisos per on he passat m'han permès conèixer gent excepcional. La terrasseta de Maurici, Can Caballero amb el foc a terra i la play... Amb vosaltres he compartit alegries i penes durant tot aquest temps, i en guardaré un record increïble. Voldria mencionar als amics de sempre, els que et fan saber qui ets. Als de Puigverd, que ens coneixem des del bressol i seguim reunint-nos a desenes. I als tres de Lleida, Godo, Jose i Isaac. Fer fer fàcil l'impossible, i atractives les bajanades. Per ser capaços d'imaginar el món de l'inrevés.

I sobretot, als meus. Als tiets i tietes, cosins i cosines. Per ser-hi, per preocupar-vos, per formar part de mi. Als padrins i padrines, a tots quatre. Per fer de la vida un lloc bonic per viure-hi.

Al Sergi. Perquè és una passada tenir-te de germà. Ets genial, sàpigues-ho. Ah, i per la maquetació de la tesi, que no és poca cosa! ;)

Als pares. Per haver-me ensenyat a viure, a ser feliç, a treballar i a estimar.

I a la Bea. Per ser-hi. Per no ser com jo. Per complementar-me. Per aguantar-me quan em faig pesat. I perquè sense tu no seria jo, i per tant aquesta tesi tampoc seria la que és.

A tots, GRÀCIES.

Indexes

Index of Contents

Indexes 1
Index of Contents 3
Index of Figures and Tables 9
Index of abbreviations 13

Introduction 17
1. Synapse formation during development 19
The compartmentalized brain: Patterning process of the nervous system 19
Generation and survival of nerve cells. 19
Axon guidance: how to find the target 20
Synapse formation 20
Synaptic compartmentalization: helping cells do the right choice 20
Synapse development 22
Excitatory synapses 23
Inhibitory synapses 25
Signal integration: To fire or not to fire, this is the question 25
Location of synapses depends on synapse type 26
Dendritic spines: function 26
Spinogenesis during development 27
Purkinje cells and the Sotelo model 28
Pyramidal neurons: the Miller/Peters Model and the Filopodial Model. 28

2. Spine and synapse plasticity in the adult brain 31
Spine plasticity in the adult: learning rules and plasticity 31
Molecular effectors in synaptic plasticity 33
Ca^{2+} dynamics 33
Actin and ABPs: the compartmentalized spinoskeleton 34
Glutamate receptors during synaptic plasticity 35

3. Reelin: Functions in the developing and adult brain 39
The Reelin pathway and its role in brain development 39
Molecular biology of Reelin: the gene, the mRNA, the protein 39
The Reelin pathway: receptors, Dab1 and signaling cascades 40
The Reelin expression and function in brain development 41

Reelin in the adult brain 43
The Reelin expression and function in the adult brain 43
Reelin and synaptic plasticity 44
Reelin and dendritic spines 45
Reelin and brain pathologies 47
Animal tools to study the role of the Reelin pathway in the adult brain 48
Adult-specific conditional overexpression of Reelin: The Reelin-OE mouse model 48
Conditional deletion of Dab1: floxed Dab1 mouse model-based approaches 48

Aims of the study 53

Results 57
1. Role of Reelin in the presynaptic connectivity of the adult hippocampus 59
Reelin over-expression modulates the structural complexity of presynaptic elements 59
Presynaptic proteins in Reelin-OE mice: Synapsin and SNAP25. 61

2. Role of Reelin in the postsynaptic connectivity of the adult hippocampus 65
Reelin over-expression triggers dendritic spine hypertrophy 65
Reelin modulates the complexity of spine apparatus in a lamina-specific manner 67
Reelin regulates the distribution of synaptic NMDA receptors 69
Reconstructions of apical dendrites from CA1 pyramidal cells evidence spine hypertrophy in Reelin-OE mice 71

3. Reelin signaling regulation of dendritic spines in pyramidal cells 77
Introduction to chapter 3: Pyramidal neurons in the neocortex 77
Hippocampal CA1 pyramidal cells of Reelin-OE mice display similar spine features as controls 79
Cortical S1BF Layer 5 pyramidal cells of Reelin-OE mice display reduced spine density and spine hypertrophy 79
Hippocampal CA1 pyramidal cells of Cre/flDab1 + TAM mice display unaltered spine density but reduced complexity of spine morphologies 83
Cortical S1BF Layer 5 pyramidal cells of Cre/flDab1 + TAM mice display increased spine density and increased complexity of spine morphologies 83

4. High-throughput 3D reconstruction of dendritic spines and synapses in GFP-traced adult-generated neurons by using FIB/SEM technology 87
Introduction to Chapter 4: High-throughput correlative electron microscopy approach to study hippocampal adult neurogenesis 87
FIB/SEM technology allows the analysis and 3D reconstruction of synaptic interactions from identified neurons with high resolution 89

FIB/SEM analysis of input synapses onto mature adult-generated granule cells. 93
Developmental analysis of input synapses onto adult-generated GCs. 98
Spines from adult-generated GCs are preferentially innervated by multi-synaptic axon terminals. 101

5. Role of Reelin signaling in the synaptic integration of developing new-born granule cells in the adult hippocampus. 105
Introduction to Chapter 5: Reelin and adult neurogenesis. 105
Reelin role on new-born GCs can be assessed by a correlative light microscopy-FIB/SEM imaging protocol. 106
Mature new-born granule cells exhibit structural alterations upon both up- and down-regulation of the Reelin signaling pathway. 108
Developmental analysis of input synapses onto adult-generated GCs under gain and loss-of-function paradigms of Reelin signaling 111
Reelin signaling regulates presynaptic multiinnervation of spines of developing new-born GCs 113

Discussion 117
1. Presynaptic plasticity in the hippocampus of Reelin-OE mice 119
Reelin confers unique structural properties to adult hippocampal dendritic spines. 121

2. Postsynaptic plasticity in the hippocampus of Reelin-OE mice 121
Reelin levels do not regulate postsynaptic protein expression levels but do determine their synaptic/extrasynaptic distribution. 122
Is there a layer-specific synaptic responsiveness to Reelin? 124

3. Reelin-triggered spine plasticity in pyramidal cells 127
Reelin overexpression effect on dendritic spines of pyramidal cells 127
Downregulation of Reelin signaling effect on dendritic spines of pyramidal neurons 129
Reelin regulates spine plasticity in a cell-specific and dendritic domain-specific way 130

4. Imaging adult neurogenesis with a FIB/SEM microscope 133
Postsynaptic structures in developing new-born GCs 134
Quantitative analysis of spine morphologies in developing new-born GCs 135
Correlation of paired morphological measurements inside a spine-synapse couple 136
Presynaptic innervation of newborn GCs 137

5. Reelin signaling and hippocampal adult neurogenesis 141
Reelin signaling in dendritic spines of developing new-born GCs 142
Reelin signaling in the presynaptic innervation to developing new-born GCs 143

Conclusions 147

Materials and Methods 151
Materials 153
Animals 153
Chemicals 154
Antibodies 154
Software 154

Methods 155
Tamoxifen Injection 155
Retroviral (RV) tracing 155
Synaptosome extracts 155
Western Blots 156
Immunohistochemistry and mean intensity measurements 156
Intracellular injections of fluorophore 157
Deconvolution 157
Spine density 158
Spine morphological analysis from confocal stacks 158
Electron microscopy 159
Post-embedding immunogold immunohistochemistry 159
Pre-embedding electron microscopy 159
Three-dimensional electron microscopy using FIB/SEM technology 160
Connectomics analysis 161
Image segmentation and quantitative morphometric analysis 161

Resum 165
Introducció 167
Espines dendrítiques 169
Plasticitat sinàptica i d'espina en el cervell adult 170
Efectors moleculars en la plasticitat sinàptica 170
Funcions de la Reelina en el sistema nerviós 172
Reelina al desenvolupament del sistema nerviós 173
Reelina en el cervell adult 173
Reelina i patologies del sistema nerviós 174
Models animals per l'estudi del paper de la via de Reelina en el cervell adult 175

Resultats i discussió 177
Plasticitat presinàptica en l'hipocamp de ratolins Reelin-OE 177
Plasticitat postsinàptica en l'hipocamp d'animals Reelin-OE 179
La Reelina regula la plasticitat estructural de les espines dendrítiques en l'hipocamp adult 179
Els nivells de Reelina no regulen l'expressió de proteïnes postsinàptiques però sí la seva distribució sinàptica-extrasinàptica 179
Els efectes derivats de la sobreexpressió de Reelina són dependents de capa 180
La Reelina promou la plasticitat d'espina en neurones piramidals 140
Efectes de la sobreexpressió de Reelina sobre espines dendrítiques de neurones piramidals 181
Efectes de la disrupció de la via de senyalització de Reelina sobre

espines dendrítiques de neurones piramidals 181
Anàlisi de la neurogènesi adulta per microscòpia FIB/SEM 183
Estructures postsinàptiques en noves GCs en desenvolupament 183
Anàlisi quantitatiu de morfologies d'espina en el desenvolupament de GCs de nova generació 184
Correlació de mesures morfològiques aparellades de conjunts espina-sinapsi 184
Innervació presinàptica de GCs de nova generació 185
La Reelina en la neurogènesi adulta a l'hipocamp 186
Reelina i les espines de noves GCs en desenvolupament 186
Reelina i la innervació presinàptica a noves GCs en desenvolupament 187

Conclusions 189

References 191

Appendix 215
Coauthored publications 217

Index of Figures and Tables

Introduction

1. Synapse formation during development

Figure i.1.1 Histological compartmentalization of synapses. 21
Figure i.1.2 Histological compartmentalization of presynaptic afferences in a single cell. 22
Figure i.1.3 Synapses can be classified in Types 1 and 2 according to ultrastructural features. 24
Figure i.1.4 Distinct types of glutamate receptors elicit particular contributions to the synaptic activity. 25
Figure i.1.5 Drawings of Cajal illustrating different types of dendritic spines. 27
Figure i.1.6 Models for developmental spinogenesis and dendritic spine classification into morphological types. 29

2. Spine and synapse plasticity in the adult brain

Figure i.2.1 Learning rules for spines are regulated by the actin cytoskeleton. 32
Figure i.2.2 Calcium compartmentalization in spines. 33
Figure i.2.3 Distribution of actin-binding proteins in the spinoskeleton defines spine microdomains. 35
Figure i.2.4 NMDA receptor subunit composition is modulated during synaptic plasticity. 36

3. Reelin: Functions in the developing and adult brain

Figure i.3.1 Structure of the Reelin protein. 40
Figure i.3.2 Reelin-initiated events in developing neurons. 41
Figure i.3.3 Reelin role in the development of layered structures in the neocortex, hippocampus and cerebellum. 43
Figure i.3.4 Reelin signaling in synaptic plasticity. 45
Figure i.3.5 Reelin-OE mice as a model for adult-specific Reelin gain of function studies. 49
Figure i.3.6 Mouse models derived from the flDab1 line permitting the conditional deletion of Dab1. 50

Results

1. Role of Reelin in the presynaptic connectivity of the adult hippocampus

Figure r.1.1 Reelin overexpression in vivo triggers presynaptic hypertrophy and increased connectivity in the hippocampus. 61
Figure r.1.2 Expression of presynaptic proteins synapsin and SNAP-25 is not altered in the hippocampus of Reelin-OE mice. 62

2. Role of Reelin in the postsynaptic connectivity of the adult hippocampus

Figure r.2.1 Reelin overexpression in vivo triggers postsynaptic hypertrophy in the hippocampus. 67
Figure r.2.2 Spine apparatus and synaptopodin in dendritic spines of Reelin-OE mice. 69
Figure r.2.3 Western Blot analysis and quantification of distinct post-synaptic proteins. 71
Figure r.2.4 Expression of NMDA receptor subunits NR2a and NR2b in Reelin-OE mice. 73
Figure r.2.5 Expression of p-cofilin in Reelin-OE mice. 74
Figure r.2.6 3D reconstructions of dendrites in the stratum radiatum of the CA1 illustrate spine hypertrophy in Reelin-OE mice. 75

3. Reelin signaling regulation of dendritic spines in pyramidal cells

Figure r.3.1 Reelin-OE mice CA1 pyramidal neurons exhibit similar spine densities and morphologies as controls. 80
Figure r.3.2 Reelin-OE mice S1BF Layer 5 pyramidal neurons exhibit fewer but larger spines than controls. 82
Figure r.3.3 Conditional deletion of the Dab1 gene alters spine morphology in hippocampal CA1 pyramidal cells. 84
Figure r.3.4 Conditional deletion of the Dab1 gene alters spine density and morphology in S1BF Layer 5 pyramidal neurons. 85

4. High-throughput 3D reconstruction of dendritic spines and synapses in GFP-traced adult-generated neurons by using FIB/SEM technology

Figure r.4.1 Dendritic spines and postsynaptic densities visualized in developing GCs. 89
Figure r.4.2 Correlative light and FIB/SEM microscopy of DAB-stained GC dendrites allows high-resolution 3D reconstruction. 90
Figure r.4.3 FIB/SEM microscopy allows high resolution fine ultrastructural analysis of identified synapses. 92
Figure r.4.4 Infrequent types of dendritic spines in 8 week-old GFP/DAB labeled GCs as reconstructed with FIB/SEM microscopy. 93
Figure r.4.5 Types of dendritic spines arising from 8 week-old GFP/DAB labeled GCs as reconstructed with FIB/SEM microscopy. 94
Figure r.4.6 FIB/SEM images and the corresponding 3D reconstructions illustrating branched spines in 8 week-old GCs. 95
Figure r.4.7 Quantitative correlations of spine volumes with other

morphological parameters of spines and synapses from 8 week-old GCs. 96
Table r.4.1 Correlation analysis of spine volume against other variables. 97
Table r.4.2 Regression analysis of binned spine volume against other variables (below threshold) for 8-9 week-old GCs. 97
Table r.4.3 Data imaged for the analysis of WT, new-born GCs 98
Figure r.4.8 Comparative analysis of dendritic spines in 3-4 and 8-9 weeks old GCs. 98
Table r.4.4 Number of analyzed features in WT new-born GCs 100
Table r.4.5 Correlation analysis of young neuron's spine volume against other variables for 8-9 week-old GCs 101
Figure r.4.9 Characteristics of presynaptic innervation of GC dendritic spines at 3-4 and 8-9 weeks. 103
Figure r.4.10 Multisynaptic boutons innervate equally all spine types and morphologies. 103

5. Role of Reelin signaling in the synaptic integration of developing new-born granule cells in the adult hippocampus.

Table r.5.1 Data imaged for the analysis of Reelin-OE and Dab1-KO new-born GCs 106
Table r.5.2 Number of analyzed features in Reelin-OE and Dab1-KO new-born GCs 107
Figure r.5.1 Comparative analysis of dendritic spines in 3-4 and 8-9 weeks-old GCs of Reelin-OE mice and Dab1-KO GCs. 108
Table r.5.3 Spine and synapse maximal records found for morphological parameters. 110
Figure r.5.2 Correlations of spine volumes with other morphological parameters of spines and synapses in Reelin-OE and Dab1-KO 8-9 week-old GCs. 111
Table r.5.4 Correlation analysis of spine volume against other variables in Reelin-OE and Dab1-KO new-born GCs. 111
Figure r.5.3 Characteristics of presynaptic innervation of Reelin-OE and Dab1-KO GC dendritic spines at 3-4 and 8-9 weeks. 114
Figure r.5.4 Multisynaptic boutons innervate equally all spine types and morphologies in Reelin-OE and Dab1-KO assays. 115

Index of abbreviations

ABP	actin-binding protein
ACPD	trans-(1S,3R)-1-amino-1,3-cyclopentanedicarboxylic acid
AD	Alzheimer's Disease
AMPA	alpha-amino-3-hydroxy-5-methylisoxazole-4-propionic acid
AP	action potential
APP	Amyloid Precursor Protein
APV	2-amino-5-phosphonovaleric acid
ATP	adenosine triphosphate
Aβ	beta-amyloid
CNQX	6-cyano-7-nitroquinoxaline-2,3-dione
CNS	central nervous system
CR	Cajal-Retzius cells
Cre/flDab1	UbiCre / floxed Dab1 mouse line
DAB	diaminobenzidine
DG	dentate gyrus
DOX	Doxycycline
EGL	external granular layer
EPSC	excitatory postsynaptic current
EPSP	excitatory postsynaptic potential
FIB/SEM	focused ion beam scanning electron microscopy
flDab1	floxed Dab1 (mouse line name)
GABA	gamma-amino-butyric-acid
GluN2A, NR2a	NMDA receptor subunit 2A
GluN2B, NR2b	NMDA receptor subunit 2B
IGL	inner granular layer
IML	inner molecular layer
IPL	inner plexiform layer
IPSP	inhibitory postsynaptic potential
LTD	long-term depression
LTP	long-term potentiation
MML	medial molecular layer
NMDA	N-methyl-D-aspartate

OB	olfactory bulb
OM	optical microscopy
OML	outer molecular layer
ORC	olfactory receptor cell
P5	postnatal day 5
PC	purkinje cell
PCP	phencyclidine
PNS	peripheral nervous system
PPF	paired-pulse facilitation
PSD	postsynaptic density
PTP	post-tetanic potentiation
Reelin-OE	Reelin-overexpressing mouse line
RER	rough endoplasmic reticulum
RGC	retinal ganglion cell
SGSS	spontaneous generation, selection and strengthening of spines
SLM	stratum lacunosum-moleculare
SLR	spine learning rule
SO	stratum oriens
SP	stratum pyramidale
SR	stratum radiatum
TAM	tamoxifen
TARP	AMPA receptor regulatory protein
VGCC	Voltage-gated cation channel
WT	wild-type

Introduction

1. Synapse formation during development

The compartmentalized brain: Patterning process of the nervous system

Cada [célula nerviosa] es un cantón fisiológico absolutamente autónomo.(Cajal, 1888)

The brain is a highly compartmentalized organ in both an anatomical, physiological and functional way. The developmental process that gives rise to this subdivided architecture is complex and can be depicted as a series of functional events. It starts with the generation of progenitor cells in the neural plate and neural tube from ectodermal undifferentiated cells. The next striking process is the formation of regional differences within the neural tube, which will later develop the different regions of the central nervous system. A third important process is the specification of distinct neuronal subtypes, and a fourth key step is the influence of neuronal inputs on the morphogenesis. These first stages are characterized by a series of inductive interactions, where signals secreted by a localized cell population drive the differentiation of the neighboring cells. These signaling molecules are highly conserved in evolution and the same signals are used in different developmental stages for different actors.
The nervous system early differentiates in two different zones: the central nervous system (CNS), composed at later stages by the brain, the cerebellum and the spinal cord, and the peripheral nervous system (PNS), composed by the sensory neurons that conduct sensory experience information to the CNS and the motor neurons that transmit inputs received in the spinal cord to the muscular fibers. The main focus of the research exposed in this work is based on the CNS, and therefore the argumentations made will be directed to this zone, although some similarities might exist in the PNS.

Generation and survival of nerve cells.

During embryonic development an initial overabundance of neurons is generated, to be subsequently pruned by a programmed cell death of the superfluous ones. This process can be explained by a neurotrophic hypothesis: Many axons reach initially the target cell, which secretes low levels of neurotrophic factors. The axons internalize these factors, which promote neuronal survival. Finally, only axons that have incorporated sufficient amounts of neurotrophic factors survive, while the others die through apoptosis. At these stages, intracellular signaling events also drive the differentiation of progenitors into either neuronal cells or glia. Overall, these mechanisms are highly conserved evolutively.

Axon guidance: how to find the target

To ensure specificity of connections, axon terminals must travel long distances away from their somata, and different mechanisms have been developed to perform this process. Guidance cues of different nature are received along the path (attractive and repulsive, contact and gradient). Some axons grow during early embryonic stages, when the distances are short, and serve as guidance scaffolds for future migrating axons. Similarly, other physical paths can be useful to guide axon migration, such as epithelial surfaces or extracellular matrices. The axon terminal part, called growth cone, is the structure that responds to all these stimuli by integrating the guidance cues found along the migrating path.

Synapse formation

[…] la propagación de la acción nerviosa se verifica por contactos al nivel de ciertos aparatos o disposiciones de engranaje, cuyo objeto es fijar la conexión, multiplicando considerablemente las superficies de influencia. (Cajal, 1889)

Synapse formation is the step that closes the wiring process, which ends with a structure stable enough to last a lifetime but with plastic properties enabling modification upon sensory experience.
Some requirements govern this process: First, axon terminal must reach the right target cell at the right membrane region. This region will constitute the postsynaptic membrane, and must be responsive to the neurotransmitter released by the terminal. Second, both pre- and postsynaptic membranes apposed must match perfectly, so as to allow signal responsiveness to happen in the millisecond range. And third, the overall structure must present both robustness and plastic properties, so it can be activity-modulated. These requirements are accomplished through a signaling crosstalk between the pre- and postsynaptic compartments.

Early synapse formation in development occurs with a certain similarity as with the neuronal generation and survival, this is, usually early multiple synapse generation processes are followed by sensory experience selection of synaptic inputs that promotes elimination of the inefficient or inactive synapses while ensures maturation of the more effective or active ones. This effect is also evident from the presynaptic view: axons perform small synapses on many targets at early stages, and end up making large synapses on relatively few targets after a sensory refinement process.

Synaptic compartmentalization: helping cells do the right choice

Confined brain structures (such as cortical layers) simplify the task of a given cell to find the right postsynaptic partner, and vice versa. This strategy is present in many different examples, some of which I will review:

One scenario can be that in a given zone, a specific pre- or postsynaptic actor is the predominant synaptic partner. This is seen in the dendrites and axons of retinal ganglion cells (RGCs) (**Fig. i.1.1a**). Every kind of RGC receives inputs of one interneuron type (among a dozen) in the inner plexiform layer (IPL) of the retina. To facilitate the correct pre/post match, IPL is subdivided in ten sublayers, and every afferent interneuron type extends its axons in a single sublayer. Additionally to the spatial cue, there is a molecular specificity cue: different RGC types express different adhesion molecules, also expressed by the right presynaptic partner. Therefore, the matching problem is subdivided: the postsynaptic cell must extend the dendritic branches along the right IPL sublayer, and this branching and synaptic specificity is further activity-refined by molecular cues, ending in a layered distribution of the

different synaptic couples.

Other examples can be found in cortical neurons innervating specific layers, and in olfactory receptor cells (ORC) (**Fig. i.1.1b**). In the latter, one ORC expresses only one receptor (among a thousand possible). Although somata are interspersed in the olfactory epithelium, the axons of ORCs expressing the same receptor converge in the same glomerulus of the olfactory bulb, thus providing a homogenous presynaptic input in this area.
Target specificity requirement may also refer to a subregion of the postsynaptic dendritic tree. This is useful for cells that distribute different presynaptic partners in different compartmentalized dendritic regions.

Examples of these innervations can be found in the cerebellar Purkinje Cell (PC) whose dendrites extend to the cerebellar molecular layer (**Fig. i.1.2a**). Granule cell axons innervate distal dendritic spines.

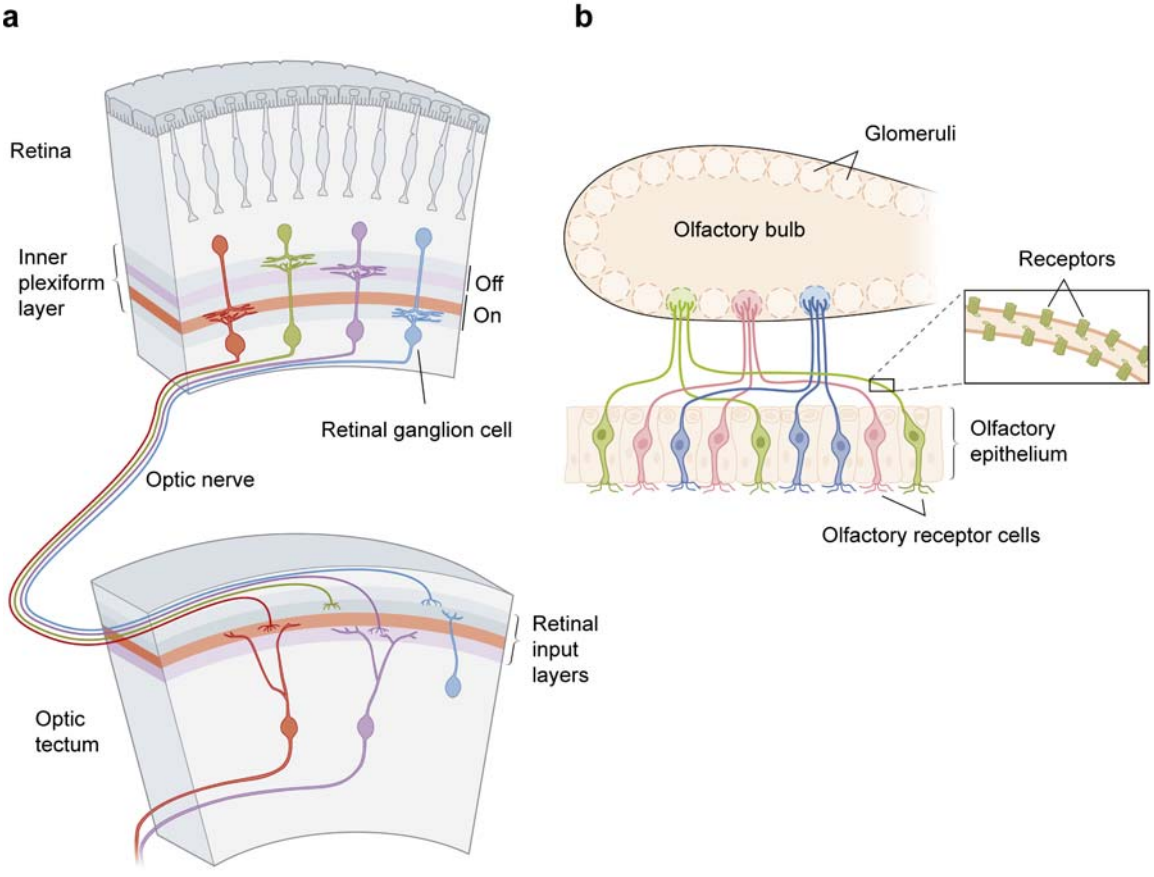

Figure i.1.1 Histological compartmentalization of synapses.
(**a**) Retinal ganglion neurons form layer-specific synapses. The inner plexiform layer of the retina is innervated by different amacrine and bipolar cells, whose axons distribute along different sublayers. The dendrites of Off and On retinal ganglion cells distribute at the inner and the outer portion of the plexiform layer, respectively, and therefore they receive synapses from different interneuron types. Similarly, ganglion cell axons belonging to these different synaptic couples innervate different zones in the optic tectum. (**b**) Targeting of sensory axons to discrete glomeruli in the olfactory bulb is directed by olfactory receptors. The axons of olfactory sensory neurons expressing the same receptor form synapses with target neurons in the same glomerulus. Notably, these sensory neurons are sparsely distributed along the olfactory epithelium of the nose. This specificity is driven by molecular recognition processes involving their odorant receptors. Adapted from (Kandel et al., 2012).

Climbing fiber axons establish synapses on proximal dendritic shafts and basket cell axons contact the axon hillock and initial segment. Molecular cues might drive this distribution, namely the expression of neurofascin coupled to basket cell axons' synapses. This spatial synaptic distribution is further replicated by divergent dendritic spines' properties: while distal dendritic spines are intrinsic to the neuron, proximal dendritic spines present activity-dependent maintenance (Yuste and Bonhoeffer, 2004).

The hippocampal CA1 pyramidal neuron presents a similar compartmentalized presynaptic afferences (**Fig. i.1.2b**): CA3 pyramidal cells' axons innervate CA1 pyramidal cells at basal dendrites in stratum oriens and proximal apical dendrites in an spatially correlated pattern, this is, CA3 neurons that are distant from the CA1 project primarily to apical dendrites in the stratum radiatum, whereas CA3 neurons that are closer project more consistently to basal dendrites. On the other hand, axons of entorhinal cortex pyramidal neurons and from thalamic regions innervate CA1's apical tuft dendrites at stratum lacunosum-moleculare. (Andersen et al., 2007).

This spatial confinement of presynaptic afferences may provide also an ability to integrate the locally homogenous received impulses in the dendritic tree, therefore contributing to the signal integration process of the cell (Chadderton et al., 2014).

Synapse development

The synaptic development involves a crosstalk between the pre- and postsynaptic compartments. Both anterograde and retrograde signals ensure a correct organization of synaptic machineries so as the end product becomes a proper, functional synapse. The molecular synaptic machinery presents some specificity to the major neurotransmitter involved, which defines the presynaptic neuron type.

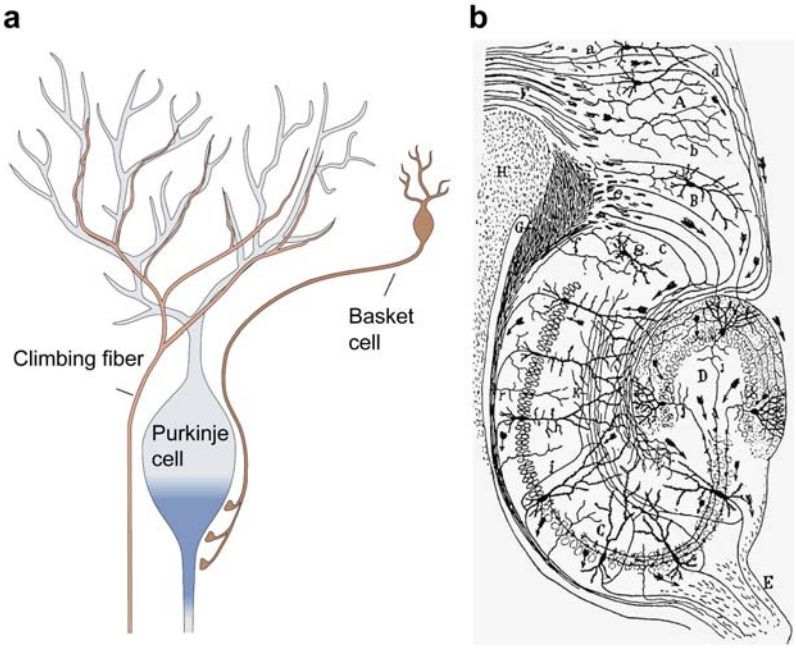

Figure i.1.2 Histological compartmentalization of presynaptic afferences in a single cell.
(**a**) Many neurons form synapses on cerebellar Purkinje neurons, and these are located at different dendritic domains. While parallel fibers from granule cells contact distal dendritic spines, climbing fiber axons establish synapses at the proximal dendritic tree. Besides, inhibitory basket cells establish synapses on the axon hillock and initial segment. (**b**) In hippocampal CA1 pyramidal cells different dendritic domains receive distinct synaptic inputs. Axons from the entorhinal cortex and from the thalamus innervate distal tuft apical dendrites, whereas proximal apical and basal dendrites are innervated by commissural axons from the CA3. (**a**) is adapted from (Kandel et al., 2012); (**b**) is adapted from (Cajal, 1911).

Most neurotransmitters are generally low molecular weight molecules, although some peptides can act as messengers at synapses. The precise effect that a neurotransmitter triggers depends much on the receptor involved. These receptors can be ionotropic, where the receptor itself is an ion channel that

opens in response to the neurotransmitter binding, or metabotropic, where the receptors can trigger the opening of ion channels via second messengers. Therefore, few neurotransmitters and a rich variety of receptors permit a number of different possible effects.

In the CNS, synaptic inputs can be either excitatory or inhibitory depending essentially on the type of ion channels involved. Although the same transmitter can trigger different effects depending on the receptors activated, a transmitter is usually excitatory or inhibitory. Typically, excitatory synapses involve glutamate neurotransmitter and its receptors are associated with Na^+ and Ca^{2+} permeable-ion channels. On the other hand, inhibitory synapses in the CNS are usually mediated by γ-amino-butyric-acid (GABA) or glycine neurotransmitters, which involve the permeation of Cl^- channels. Whereas excitatory signals promote the appearance of excitatory postsynaptic potentials (EPSP), inhibitory synapses promote the appearance of inhibitory postsynaptic potentials (IPSP) and their role remains in both counteracting synaptic excitation as well as sculpting the pattern of firing of some spontaneously active neurons.

Excitatory and inhibitory synapses present morphologically different ultrastructure, and correspond to the synapse classes Gray Type 1 or asymmetric, and Gray Type 2 or symmetric, respectively (Gray, 1959) (**Fig. i.1.3**). Type 1 synapses present round vesicles, an electron-dense region close to the active zone in the presynaptic membrane and a thick electron-dense region adjacent to the postsynaptic membrane, known as the postsynaptic density (PSD). Type 2 synapses exhibit oval vesicles and less obvious pre- and postsynaptic membrane specializations and PSD.

Excitatory synapses

Excitatory synapses account for the vast majority of synapses in the brain, and the aminoacid L-glutamate is the major excitatory transmitter. Ionotropic glutamate receptors are ligand-gated ion channels that can be classified in three groups in basis of the synthetic agonist that specifically triggers their activation (**Fig. i.1.4a**): AMPA receptors (α-amino-3-hydroxy-5-methylisoxazole-4-propionic acid), kainate receptors (kainate) and NMDA receptors (N-methyl-D-aspartate). Pharmacological inhibition of these receptors can be assessed through concrete drugs: NMDA receptors are blocked by APV (2-amino-5-phosphonovaleric acid), PCP (phencyclidine) and MK801, whereas AMPA and kainate receptors are both blocked by CNQX (6-cyano-7-nitroquinoxaline-2,3-dione). The metabotropic glutamate receptors are G protein-coupled receptors that can be selectively activated by ACPD (trans-(1S,3R)-1-amino-1,3-cyclopentanedicarboxylic acid).

All glutamate-gated channels are permeable to Na^+ and K^+, but the NMDA receptor, besides those ions, is permeable also to Ca^{2+}. The NMDA receptor needs extracellular glycine as a cofactor to be active, and its opening depends on membrane voltage via a Mg2+ plug removal mechanism, behaving thus as a coincidence detector of pre and postsynaptic activity.

Postsynaptic glutamate-responding membranes exhibit both AMPA and NMDA receptors, and each receptor type contributes differently to the total EPSP (**Fig. i.1.4b**). In rest, following presynaptic Glutamate secretion NMDA receptor pore is blocked by the Mg^{2+} plug, and thus AMPA receptors are responsible for the whole current (EPSC), resulting in a rapid current rise. As membrane becomes depolarized, Mg2+ is expelled from the NMDA receptor pore and the latter becomes permeable to Na^+, K^+ and Ca^{2+} ions, contributing to a late, slow phase of the postsynaptic current as well as triggering Ca^{2+}-depending postsynaptic signaling cascades, such as activation of the calcium-calmodulin-dependent

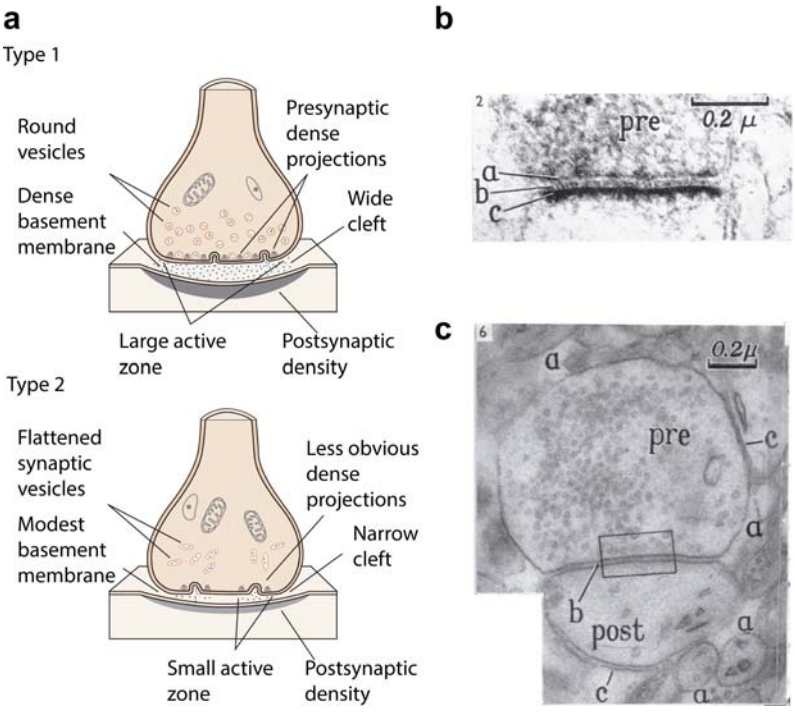

Figure i.1.3 Synapses can be classified in Types 1 and 2 according to ultrastructural features. (**a**) Schema depicting main ultrastructural characteristics defining both types. Most striking differences are the shape of synaptic vesicles, the total area of the active zone and the relative prominence of the presynaptic and postsynaptic densities, which confers either an asymmetric (type 1) or symmetric (type 2) appearance. (**b**, **c**) Electron micrographs depicting axospinous synapses classified as Type 1 (**b**) and Type 2 (**c**). Scale bars are 0.2 μm. Abbreviations: *pre*, presynaptic terminal; *post*, postsynaptic terminal. (**a**) is adapted from (Kandel et al., 2012); (**b**, **c**) are adapted from (Gray, 1959).

protein kinase II (CaMKII) (Lisman et al., 2007). Thus, NMDA receptors establish a link between the electrical signals and the biochemical signals that govern synaptic function, what points them in a key role in the plasticity mechanisms.

Ionotropic receptors are formed by subunits that ensemble around a central pore, and can be classified in three families according to evolutionary linkages among their structures, which differ in the number of subunits per receptor. One is the pentameric nicotinic ACh receptor family, which encloses ACh, $GABA_A$ and Glycine receptors. A second family is formed by the tetrameric ionotropic Glutamate receptors (AMPA, kainate and NMDA receptors). Different genes code for variants of each receptor type: four AMPA (GluA1-GluA4) and five kainate (GluK1-GluK5) receptor subunits combine to form homomers or heteromers with two subunits of each type. NMDA receptor subunits comprise two groups, the GluN1 and the four GluN2A-GluN2D genes. Two GluN1 and two of the different types of GluN2 subunits compose the final NMDA receptor, giving rise to a considerable amount of different combinations. The third family of ionotropic receptors is the purinergic P2X receptors, or ATP receptor-channels, composed by three subunits.

The postsynaptic density is a stable, electron-dense structure located beneath the postsynaptic membrane of excitatory synapses. Ionotropic glutamate receptors are located along this structure, while metabotropic ones tend to locate on the periphery (Baude et al., 1993; He et al., 2000; Racz and Weinberg, 2013). A relevant protein in this area is PSD-95, which contains three PDZ domains that can bind to several cytosolic and transmembrane proteins, including NMDA receptors, the transmembrane adhesion protein neuroligin, AMPA receptor regulatory proteins (TARPs) such as stargazin or actin cytoskeleton organizers. Therefore, the postsynaptic density serves as a scaffold for the clustering of postsynaptic proteins.

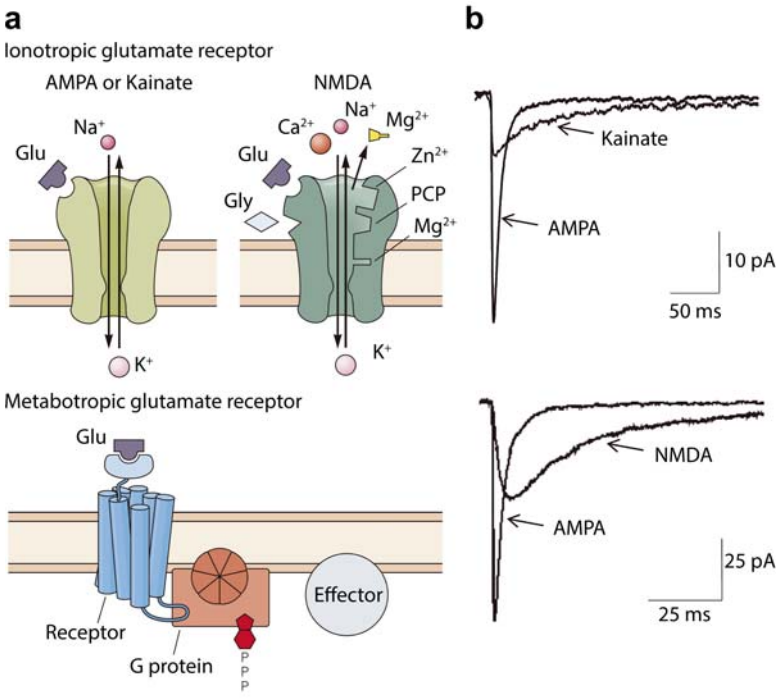

Figure i.1.4 Distinct types of glutamate receptors elicit particular contributions to the synaptic activity. (**a**) AMPA and kainate ionotropic receptors contain a channel permeable to Na^+ and K^+. The NMDA receptor contains a channel that is permeable to Ca^{2+}, Na^+ and K^+. These receptors bind multiple modulators of their activity, some of which are depicted in the figure. The metabotropic glutamate receptors regulate the opening of ion channels through the activation of an intermediate GTP-binding protein. (**b**) AMPA receptors mediate fast spontaneous mEPSCs, whereas kainate receptors mediate slower responses. NMDA receptors, in turn, mediate late, slow contributions to the mEPSCs. Abbreviations: *Glu*, Glutamate; *Gly*, Glycine; *PCP*, phencyclidine; *mEPSC*, miniature excitatory postsynaptic current. (**a**) is adapted from (Kandel et al., 2012); (**b**) is adapted from (Traynelis et al., 2010).

Inhibitory synapses

Although less abundant, inhibitory synapses play an important role in the brain connectivity regulation, both by preventing excess of excitatory activity and in terms of helping coordinate activity between networks of neurons.

GABA and Glycine are the neurotransmitters involved in the generation of inhibitory postsynaptic potentials. GABA can act through the ionotropic $GABA_A$ receptor, which channel is permeable to Cl^-, or through the metabotropic $GABA_B$, which regulates the opening of a K^+ channel. Glycine is less abundant in the brain and has a more prominent role in the spinal cord, and its action is mediated by an ionotropic receptor permeable to Cl^-.

Since the chemical transmembrane gradient of Cl^- generates a force greater than the electron-repulsive force, Cl^- channels opening in response to GABA results in a net entry of Cl^-. This triggers an increase in the negative charge on the inside of the membrane: the membrane becomes hyperpolarized. Similarly, $GABA_B$ receptors promote the opening of K^+ channels. Here, the outflow of K^+ through these channels drives the membrane to the above-mentioned hyperpolarization. Hyperpolarized membranes offer a greater resilience to trigger an action potential in response to excitatory stimuli-derived depolarization, and are thus inhibited.

Signal integration: To fire or not to fire, this is the question

Although a single neuron can receive up to thousands of presynaptic inputs, a single synapse is almost never strong enough to trigger an action potential (AP) at the axon initial segment, a zone with an in-

creased density of voltage-dependent Na^+ channels that confers a lower threshold for action potential generation. The integration of the input signals is therefore the crucial process that leads to the cell's decision of whether to fire or not an action potential. The parameters involved in this process are the location, size and shape of the synapse, the proximity and strength of synergistic or antagonistic synapses, and the resting potential of the cell. Moreover, the passive membrane properties of the cell may regulate the feasibility of two signals proximal in time or space to become summed. Voltage-gated Na^+, K^+ and Ca^{2+} channels in dendrites permit some EPSPs to generate a dendritic AP, which will further be integrated with the other signals in the cell body and axon initial segment. Also, they allow APs generated in the axon's initial segment to back-propagate towards the dendritic tree, which could temporally facilitate the removal of the Mg^{2+} plug of NMDA receptors and therefore their opening.

Location of synapses depends on synapse type

According to the neuronal domains comprising the presynaptic and postsynaptic elements, most synapses are axodendritic, axosomatic or axoaxonic. In the latter, the postsynaptic neuron is indirectly affected, since the signal controls the amount of neurotransmitter released from the target axon terminals. Axosomatic contacts are common among inhibitory neurons, since inhibitory activity is more effective when located near the axon hillock than when produced in a remote dendritic shaft. Axodendritic contacts can be either at the dendritic shaft or on dendritic spines. However, the majority of excitatory inputs are located on dendritic spines (Colonnier, 1968).

Dendritic spines: function

[…] la superficie [de las dendritas de las células de Purkinje] aparece erizada de puntas o espinas cortas que […] están representadas por ligeras asperezas. (Al principio creíamos que estas eminencias eran resultado de una precipitación tumultuosa de la plata; pero la constancia de su existencia y su presencia, hasta en las preparaciones en que la reacción aparece con gran delicadeza en los demás elementos, nos inclina á estimarlas como dispoción normal). (Cajal, 1888)

Dendritic spines are small protrusions that arise from the dendrites of many neurons, and are the postsynaptic site of the majority of excitatory contacts in the brain (Gray, 1959). Although some rare inhibitory contacts have been documented to be located on spines too, these spine heads receiving such inputs did also receive excitatory innervation (Gulyas et al., 1993; Sik et al., 1995). Almost all spines bear synapses, and those who don't exhibit a filopodial structure (Arellano et al., 2007b). Spines vary in size and shape, and even though their existence and relationship with synaptic connections and learning has been documented since a century ago by Santiago Ramón y Cajal (**Fig. i.1.5**), their specific function is still a matter of controversy (Cajal, 1888; Yuste and Majewska, 2001b).

A first explanation for their existence was appointed by Cajal as an attempt to increase the dendritic surface available for receiving synapses, as it happened with intestinal microvilli (Cajal, 1891). However, since most of the dendritic shaft is devoid of synapses this idea was early discarded. In turn, this connection hypothesis evolved and other researchers exposed that dendritic spines could enlarge the synaptic field of the dendrite, making it able to connect synaptic boutons within a wider range (Peters and Kaiserman-Abramof, 1970) and therefore minimizing the wiring length in the CNS neuropil (Swindale, 1981). Spines were also proposed as dendritic correlates of the axonal growth cone, and such dendritic growth cone would help incoming axons contact nearby dendrites (Cajal, 1904; Shepherd, 1996).

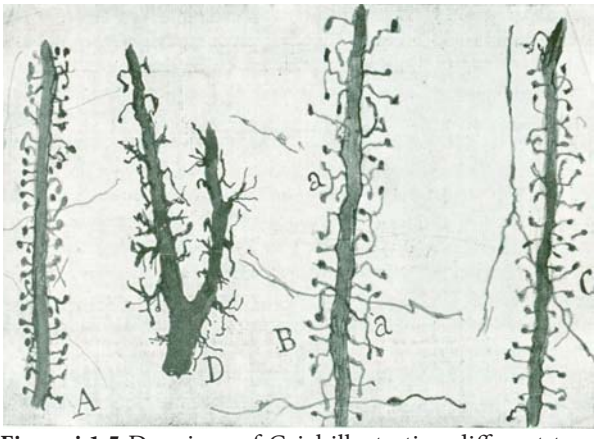

Figure i.1.5 Drawings of Cajal illustrating different types of dendritic spines.
Hand-made drawings depict dendritic segments from pyramidal cells belonging to different cortical layers and animal species (*A*, rabbit; *B*, 2 month-old human; *C*, *D*, cat). Reproduced from (Cajal, 1933).

A second explanation points the spines as information input-ouptut devices, behaving as processing units analogous to logical gates (Shepherd, 1996). This hypothesis is based on the fact that back-propagating action potentials that occur during long-term potentiation (LTP) would make spines capable of some output function. In the same direction, some evidences point to spine ability of signal filtering or amplification (Shepherd et al., 1985; Svoboda et al., 1996; Araya et al., 2006).

A third hypothesis describes the spines as a biochemical compartment, isolated from the dendrite by the spine neck. It has been shown that the neck exerts a diffusional barrier for 10000 kDa dextrans (Majewska et al., 2000a; Yuste and Majewska, 2001b), and therefore to any molecule or macromolecular complex above this threshold. This compartmentalization has well defined implications in Ca^{2+} dynamics (Majewska et al., 2000a; Noguchi et al., 2005), which govern and link spine structural and functional plasticity (Yuste and Majewska, 2001b). Dendritic spines exhibit different Ca^{2+} concentrations than the adjacent dendritic shafts, spines present different Ca^{2+} dynamics than shafts, Ca^{2+} diffusion is restricted by the spine neck and CaMKII is highly present in dendritic spines. Interestingly, Ca^{2+} concentration in the dendritic spine can be modulated by multiple molecular effectors, as well as by changes in spine morphology and shape. Altogether, dendritic spines function might be the implementation of input-specific calcium-based local learning rules that mediate synaptic plastic properties (Yuste and Majewska, 2001b; Yuste, 2011).

The existence of these learning rules in the postsynaptic terminal becomes only necessary when the connectivity is sparse, either if one presynaptic cell innervates different targets or if one postsynaptic cell receives inputs of different afferents. In these cases the optimal wiring process might involve a huge postsynaptic arborization and a low rate of presynaptic contacts per cell, as it happens with spine-bearing pyramidal cells. In contrast, in synaptic circuits exhibiting a homogenous connectivity of one presynaptic cell innervating one postsynaptic target the synaptic plasticity should occur preferentially at the presynaptic compartment, which might contact dendritic shafts establishing many synapses next to each other, preferentially close to the soma to avoid dendritic attenuation. The latter situation is in accordance with the connectivity pattern of neocortical interneurons, which tend to perform multiple synapses to the same postsynaptic target.

Spinogenesis during development

The establishment of excitatory synapses is a process that includes in many cases the formation of dendritic spines, as previously stated. Developmental synaptogenesis and spinogenesis, therefore, are closely associated processes (although different) that configure the last steps of brain development. The observation of spinogenesis in different systems led to different models, some of which in some cases might overlap (**Fig. i.1.6a-c**).

Purkinje cells and the Sotelo model

Purkinje cells in the cerebellum receive different afferences at different somatodendritic domains, and exhibit two differently regulated populations of dendritic spines.

Spines on distal dendrites of Purkinje cells receive contacts from parallel fibers of Granular cells. The generation of these spines is intrinsic to the neuron, irrespectively of the presynaptic activity, which configured the Sotelo model for spinogenesis (**Fig. i.1.6a**) (Sotelo, 1978). Evidences pointed that 'naked' spines without terminals could be identified at early postnatal stages (Sotelo, 1975), and that these spines displayed a helical distribution from the shaft in both fish and mice (O'Brien and Unwin, 2006). Finally, mutant mice lacking the presynaptic cells develop spines with normal ultrastructure (Sotelo et al., 1975).

In contrast, spines on proximal dendrites of Purkinje cells receive contacts from climbing fibers of inferior olive neurons. After an initial intrinsic pruning of spines and synapses spine maintenance in this case is activity-dependent. This helps the maturation of the climbing fiber – Purkinje cell connectivity, ending with each Purkinje cell being innervated by a single climbing fiber.

Pyramidal neurons: the Miller/Peters Model and the Filopodial Model.

Dendritic spines exhibit diverse morphologies. Recent studies point to a unimodal distribution of morphological parameters (Trommald and Hulleberg, 1997; Arellano et al., 2007a; Tonnesen et al., 2014). However, since individual spine's morphology is closely related to its function (Yuste and Majewska, 2001b), dendritic spines have been traditionally classified in morphological types, commonly filopodia, stubby, thin and mushroom (**Fig. i.1.6d**) (Peters and Kaiserman-Abramof, 1970; Tashiro and Yuste, 2003; Rochefort and Konnerth, 2012). Some developmental studies point that certain spine types are most common at early ages, while mushroom spines become predominant at mature stages (Trachtenberg et al., 2002). Miller and Peters proposed a mechanism by which in a first stage, the axon terminal establishes a synapse on the dendritic shaft, resulting in a stubby spine. Next, the spine develops to more mature phenotypes and the axon terminal enlarges its vesicular content, giving rise to thin and mushroom spines (**Fig. i.1.6b**) (Miller and Peters, 1981). However, ultrastructural volume reconstructions of two neighboring spines from the same parent dendrite establishing synapses with the same bouton revealed up to seven neurites passing inside the closed loop (Knott et al., 2006). These complex structures are hardly explained by this model, as well as the fact that axonal trajectories through the neuropil are largely straight.

The Filopodial Model, in turn, establishes that dendritic filopodia might become stabilized by transforming into spines in an activity-dependent manner (**Fig. i.1.6c**) (Dailey and Smith, 1996; Ziv and Smith, 1996). Therefore, initial spine and synapse pruning might be an intrinsic process, but spine maintenance is activity-dependent. Dendritic filopodial motility appears to be developmentally regulated and spatially confined: activity regulation is only evident on filopodia arising from the dendritic shaft, but not in dendritic growth cone filopodia. The latter constitute a different population that respond to a synaptotropic behavior and which would guide the growth and branching of dendrites (Portera-Cailliau et al., 2003).

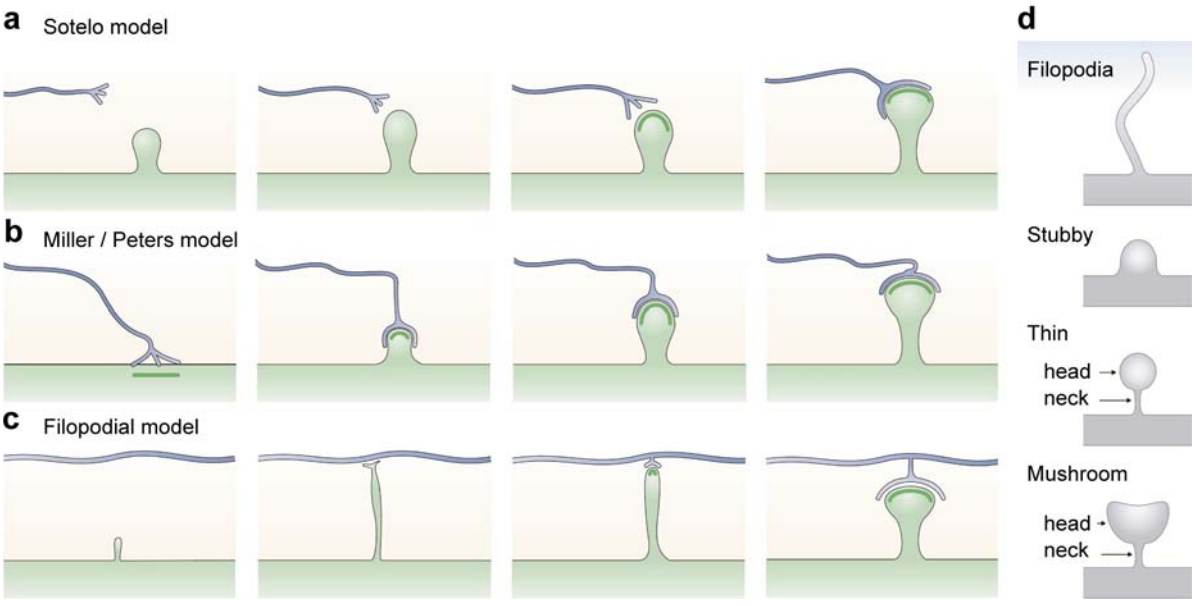

Figure i.1.6 Models for developmental spinogenesis and dendritic spine classification into morphological types. (**a**-**c**) The diagram illustrates the essential figures of the three models of spinogenesis. In the Sotelo model (**a**), spines emerge independently of the axon terminal. In the Miller/Peters model (**b**), the terminal induces the generation of the spine by contacting first the dendritic shaft. In the Filopodial model (**c**), a spontaneously generated dendritic filopodium establishes a synaptic contact with a nearby axon, and spine stabilization depends on synaptic activity. (**d**) Schematic drawings of spine morphologies based on the most common four-category classification. Additionally, a fifth category referred to branched spines is usually added, which consists of spines with more than one head. (**a**-**c**) is adapted from (Yuste and Bonhoeffer, 2004); (**d**) is adapted from (Rochefort and Konnerth, 2012).

2. Spine and synapse plasticity in the adult brain

Spine plasticity in the adult: learning rules and plasticity

Dendritic spines exhibit a great morphological plasticity in an individual's lifetime, both involving spine appearance and removal and changes in its shape and volume, as well as molecular changes in relevant proteins, resulting in modifications of the spine physiological properties. This plasticity has been pointed as a physical correlate for learning and memory processes. The global process linking spine and synaptic plasticity has been thoroughly discussed, and the compilation of all experimental evidences can be included in a mechanism describing the spontaneous generation, selection and strengthening of spines (SGSS) (**Fig. i.2.1**) (Kasai et al., 2010b). This mechanism is composed by fifteen spine learning rules (*SLRs*):

SLR1: Spine synapses form spontaneously during early development.

SLR2: Spine elimination and generation occur frequently.

SLR3: Spine synapses are the major sites for structural plasticity of cortical excitatory circuits.

SLR4: Spines arise from filopodia. Filopodia do not have PSD or head.

SLR5: Spine-head volumes vary over a wide range, but the distribution is conserved: small spines are abundant and large ones are rare.

SLR6: Newly generated spines are small, and older spines tend to be large.

SLR7: Spine head volume reflects the strength of the synapse.

SLR8: Spine necks vary in thickness and length, thereby regulating rapid signaling events in spines: membrane potential, calcium concentration and the flow of the polymerized actin gel.

SLR9: Spine head enlargement or shrinkage can be induced by repetitive stimulation.

SLR10: Spine enlargement and LTP can be induced at the level of single spines, and spines can act as memory elements.

SLR11: The likelihood of spine enlargement depends on the spine's initial size. Persistent enlargement is more frequent on small spines.

SLR12: Spine volumes fluctuate spontaneously, and this fluctuation is greater in large spines.

SLR13: Larger spines are more persistent than smaller ones.

SLR14: An individual spine can persist throughout the entire life of an animal.

SLR15: Actin-based cell motility is a fundamental mechanism for plasticity and fluctuation of dendritic spines.

Therefore, spine generation would occur in some degree in a spontaneous, slow way (new spine appearance occurs 0.5-1h after stimulation (Nagerl et al., 2004)). Activity-dependent enlargement, otherwise, is a much faster process that could reflect the rapid acquisition of memory.

Altogether, SGSS model for spine creation and function predicts the following mechanism: Filopodia emerge spontaneously and those who find a presynaptic terminal form silent synapses. The resulting spines that become triggered during the network operation will undergo activity-dependent enlargement and will become integrated in the functional circuit, persisting for a longer time. Otherwise they will be eliminated. Persistent spines may become stabilized and strengthened by both activity-dependent and intrinsic size fluctuations, finally being able to last for a lifetime (**Fig. i.2.1a**).

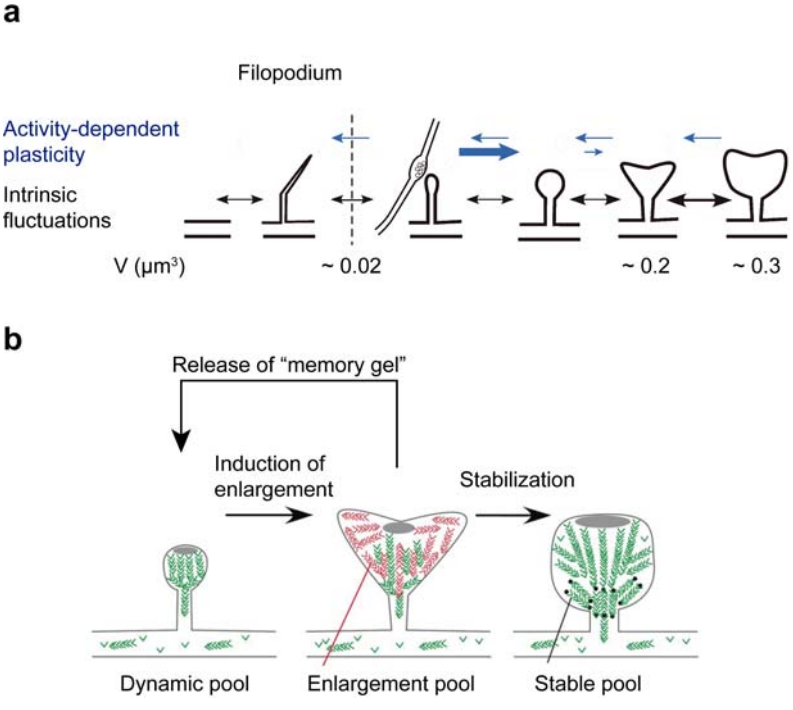

Figure i.2.1 Learning rules for spines are regulated by the actin cytoskeleton.
(**a**) Variations in spine size occur both in an activity-dependent manner and spontaneously, as illustrated by blue and black arrows, respectively. However, both scenarios reflect different motility patterns (larger arrows indicate larger fluctuations). Whereas the amplitude of intrinsic fluctuations is proportional to the spine size, activity-dependent fluctuations are directed preferentially to enlarge small spines only, ensuring their persistence. Indeed, big spines rarely undergo activity-dependent enlargement. Typical spine sizes are indicated below some spine types. Note that, whereas initial stages involve large volume variations of several orders of magnitude, across last stages of spine maturation volume variations are relatively small, despite of notable changes in the shape of the spine. (**b**) Three different actin pools underlie spine structure and plasticity. The dynamic pool exhibits a fast turnover rate and it is supposed to maintain the spine shape by counteracting external compressive forces. Enlargement pool is exclusively present under activity-dependent induction. Its highly cross-linked structure provides a gel-like consistence, and its diffusion through the spine neck precedes spine shrinkage and prevents subsequent enlargements. Conversely, confinement of this gel in the spine head ensures persistence of the enlarged spine. Finally, the size of the stable pool is proportional to the spine volume. Thus, stabilization of a recently enlarged spine might involve the creation of more stable pool to substitute the transient enlargement one. Abbreviations: *V*, volume.

(**a**) was adapted from (Yasumatsu et al., 2008; Kasai et al., 2010b); (**b**) was adapted from (Honkura et al., 2008).

Spine maintenance is strongly regulated by compartmentalized actin pools inside the spine (Honkura et al., 2008) (**Fig. i.2.1b**), allowing individual spines to last thousands of times longer than the lifetime of their constituent molecules. Resting spines exhibit two actin pools: The dynamic pool is located at the apex of the spine and polymerizes faster in larger spines, generating continuously the expansive force to maintain the spine volume. The stable pool is located close to the spine neck, its volume is higher in larger spines, and its size determines the amplitude of spontaneous volume fluctuations. A third pool of actin appears distributed along the spine head after induction of activity-triggered spine enlargement. The enlargement pool requires higher concentrations of monomeric G-actin and is composed by cross-linked actin fibers that behave as a gel. The consistence of this gel can be made more rigid by some molecular effectors such as CaMKII. More interestingly, this gel can be released to the dendritic shaft through the spine neck (which would occur easier in spines with wider spine necks). If this occurs, the enlarged spine reverts to the initial smaller size and cannot be enlarged again. Therefore, this 'memory gel' exerts the force needed to increase the spine volume. Afterwards, the bigger spine may develop a larger stable pool and the dynamic pool will maintain the new spine size.

Molecular effectors in synaptic plasticity

Ca^{2+} dynamics

Synaptic plasticity of dendritic spines remains tightly associated to transient variations in Ca^{2+} concentration inside the spine. Local Ca^{2+} dynamics can be regulated by two main mechanisms: control of calcium influx and efflux (**Fig. i.2.2**) (Yuste and Majewska, 2001b).

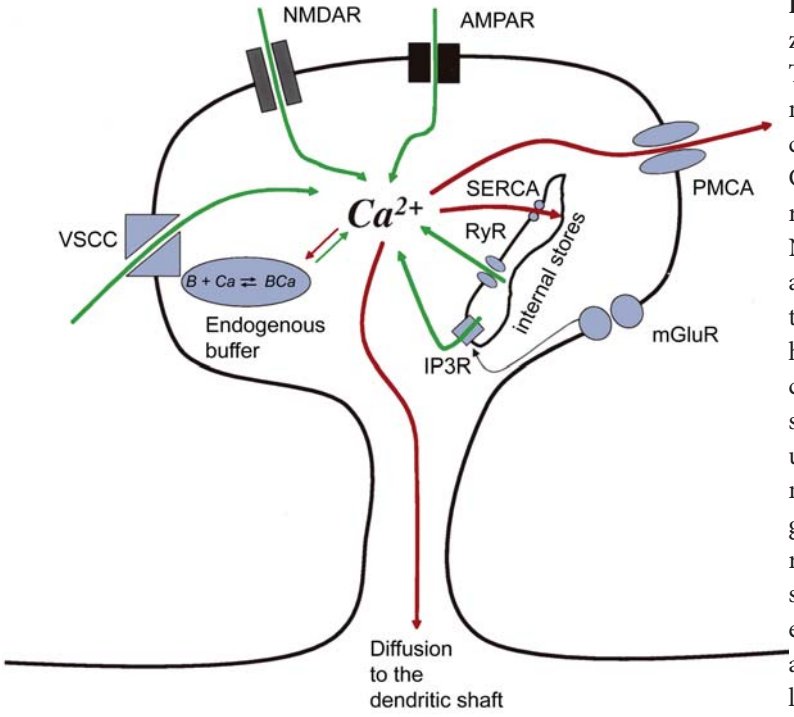

Figure i.2.2 Calcium compartmentalization in spines.
The schema illustrates different mechanisms that control calcium concentration dynamics in the spine. Green arrows depict calcium influx, red arrows show calcium efflux. Both NMDA and some AMPA receptors allow influx of calcium from the extracellular space, which can also happen through voltage-sensitive calcium channels (VSCC). Internal stores can serve as a source of calcium, which can be triggered by several mechanisms, including metabotropic glutamate receptors. Also, calcium retrieval by cytoplasmic proteins may serve as a buffering system. Calcium extrusion mechanisms include both active deployment to the extracellular space or to internal reservoirs and passive diffusion through the dendritic shaft. The kinetics of this diffusion are influenced by the geometry of the spine neck. Abbreviations: *VSCC*, voltage-sensitive calcium channel; *NMDAR*, NMDA receptor; *AMPAR*, AMPA receptor; *PMCA*, plasma membrane calcium ATPase; *mGluR*, metabotropic glutamate receptors; *B*, buffer; *SER-*

CA, sarco/endoplasmatic Ca^{2+} ATPase; *RyR*, ryanodine receptors; *IP3R*, inositol triphosphate receptor; IP3, inositol triphosphate. Adapted from (Yuste and Majewska, 2001b).

First, local influx of Ca^{2+} can be attained by the regulation of calcium-permeable receptors, such as NMDA receptors and some AMPA receptors. Also, back-propagated action potentials might induce calcium influx by opening voltage-dependent calcium channels at the spine surface. Moreover, calcium deployment from internal stores can raise local concentration. A well characterized calcium store present in mature mushroom-type spines is the spine apparatus, a specialized form of endoplasmic reticulum composed of several stacks (Gray, 1959; Spacek and Harris, 1997) which has also been related to post-translational modification and transport of proteins (Jedlicka et al., 2008). Synaptopodin is an actin-binding protein that localizes at the spine apparatus and whose function is determinant for activity-triggered spine plasticity (Vlachos et al., 2009; Segal et al., 2010; Vlachos et al., 2013). Synaptopodin mRNA is expressed by both pyramidal neurons and granule cells of the hippocampus (Mundel et al., 1997) and the protein shows a lamina-specific distribution in the mouse hippocampus (Deller et al., 2000; Roth et al., 2001; Bas Orth et al., 2005).

Second, calcium dynamics can be regulated by mechanisms governing Ca^{2+} extrusion from the synapse. This can be attained by active or passive mechanisms. Calcium pumps located at either the plasma membrane (Plasma Membrane Ca^{2+} ATPases or PMCAs) or in the surface of internal stores (sarco/endoplasmatic Ca^{2+} ATPases or SERCA pumps) can deliver the spine Ca^{2+} to extracellular space or spine apparatus, respectively. Spine Ca^{2+} can also diffuse to the dendritic shaft and its kinetics depend on spine neck morphology (Majewska et al., 2000b; Noguchi et al., 2005).

Actin and ABPs: the compartmentalized spinoskeleton

Spine morphology is closely regulated by the actin cytoskeleton, which is the main component of the spine cytoskeleton (Matus et al., 1982; Kaech et al., 1997). Actin fibers form bundles in the spine neck, while in the spine head interact with the plasma membrane and the PSD at their barbed ends. Functionally distinct actin binding proteins (ABPs) distribute along functionally different microdomains within the spine cytoskeleton, also known as spinoskeleton (**Fig. i.2.3**) (Racz and Weinberg, 2008; Colgan and Yasuda, 2014). Since actin dynamics comprise the typical "trendmilling" model (in which monomers add at the 'barbed' end and dissociate from the 'pointed' end), their regulation involves mechanisms controlling either their polymerization or depolymerization kinetics.

In the apex of the dendritic spine, the probably more relevant function for actin in the PSD is the stabilization of glutamate receptors. NMDA receptors can be linked through α-actinin, whereas AMPA receptors interact with F-actin via different scaffolding proteins such as PSD-95, Abp1, PICK1 and neurabin (Racz and Weinberg, 2013). Moreover, α-actinin can bind CaMKII and work cooperatively with this enzyme to either modify synaptic efficacy or actin cytoskeleton dynamics. Finally, α-actinin is also associated to the spine apparatus, since it can bind its associated protein synaptopodin.

Below the spine surface, cofilin enzyme is an actin severing protein that becomes inactive when phosphorylated. It enhances actin turnover by both increasing depolymerization rate and by cutting long filaments to expose uncapped barbed ends. Its phosphorylation (and therefore activity) is regulated by LIMK and the phosphatase slingshot. Cofilin is located in the immediate vicinity of the plasma membrane, in the most dynamic part of the spinoskeleton, and is also present in the PSD.

Below this shell, branching of F-actin is modulated by Arp2/3 complex, which is further regulated by a number of upstream modulators (WASP, N-WASP, WAVE/Scar, cortactin and PICK1, among others). Arp2/3 locates 20-100 nm from the plasma membrane, on the side of the spine, away from the PSD,

and its distribution might depict a branching and nucleation-specialized actin microdomain in the spine.

Inside the spine core it is described to be located the stable pool of F-actin (Honkura et al., 2008). There are three ABPs described to be localized in this region: cortactin, profilin and drebrin. Cortactin is an ABP related to actin branching and nucleation, and can activate the Arp2/3 complex. It can bind NMDA receptors, but it is preferentially located inside the spine core (Racz and Weinberg, 2004). Profilins mediate filament enlongation by attaching G-actin to the barbed end, and can be recruited from the dendritic shaft to the spine core during LTP (Ackermann and Matus, 2003). Finally, drebrin can bind to F-actin and inhibit its interaction with tropomyosin and α-actinin, and has been found to modify the mechanical properties of actin filaments, thereby regulating spine expansion and stabilization. Although during development is also present proximal to the membrane, the neuron-specific isoform drebrin A concentrates in the core region of mature spines (Racz and Weinberg, 2013).

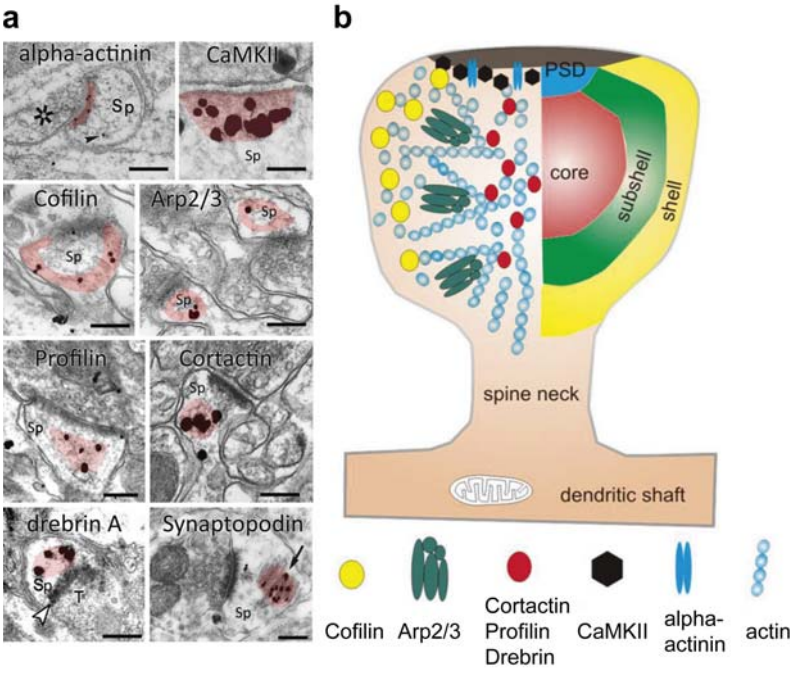

Figure i.2.3 Distribution of actin-binding proteins in the spinoskeleton defines spine microdomains. (**a**) Electron micrographs depicting ultrastructural localization of eight actin-binding proteins in the dendritic spine obtained by immunogold approaches. Shaded area represents the zone of concentration for each protein. (**b**) Different concentric microdomains can be defined attending to the distribution of a number of actin-binding proteins. These asymmetries are somewhat reminiscent of the functionally different actin pools. Notably, actin-severing protein cofilin distributes at the apex of the spine, which would be occupied by the previously defined dynamic actin pool. In the other side, branching-promoting complex Arp2/3 locates at the subshell, which could be occupied by the enlargement pool, while proteins located at the spine core could be related to the above mentioned stable pool. Scale bars are 0,2 μm. Adapted from (Racz and Weinberg, 2013).

Glutamate receptors during synaptic plasticity

Ultrastructural spine and PSD morphology has been correlated to the receptor content and distribution (Nusser et al., 1998), as well as to the current injected at the synapse and the glutamate sensitivity of the spine (Matsuzaki et al., 2001). Moreover, rapid changes in the distribution of glutamate receptor subunits in the spine and their trafficking are also activity-regulated (Greger and Esteban, 2007), providing a link between molecular rearrangements and synaptic plasticity.

AMPA type glutamate receptors are responsible for the first rapid excitatory depolarizing events in the synaptic process. The phosphorylation of the AMPA receptor subunits regulates their activity by modifying their conductance (Derkach et al., 1999; Kristensen et al., 2011). Different kinases in the

spine are involved in the phosphorylation of these subunits, such as CaMKII, PKA, PKC, PKG, FYN and JNK (Huganir and Nicoll, 2013). These events can be activity-regulated bidirectionally, this is, LTP increasing phosphorylation and long-term depression (LTD) decreasing phosphorylation (Barria et al., 1997; Lee et al., 1998). Besides, AMPA receptors exhibit a dynamic membrane trafficking. Indeed, some synapses are devoid of AMPA receptors and are therefore synaptically 'silent' (Gomperts et al., 1998). Those might become active after AMPA receptor recruitment triggered in response to NMDA activity (Liao et al., 2001). AMPA receptor trafficking and recruitment to the synapse might occur in two scenarios: by exo- and endocytosis (Park et al., 2004; Greger and Esteban, 2007) or by lateral diffusion in the plasma membrane (Opazo et al., 2012). In both mechanisms AMPA receptors become more stable when located in the synaptic cleft by means of scaffolding proteins located at the PSD (Huganir and Nicoll, 2013).

The protein levels of NMDA receptor are independent of the amount of F-actin in the spine or the size of the PSD (Kasai et al., 2003) or of the synaptic activity (Gardoni et al., 2009). However, subunit-specific trafficking and phosphorylation events are closely regulated in an activity-dependent manner, thereby modifying the final subunit composition of the synaptic and extrasynaptic NMDA receptors (**Fig. i.2.4a**) (Tovar and Westbrook, 2002; Yashiro and Philpot, 2008; Paoletti et al., 2013). Also, NMDA receptor activity is necessary for LTP and LTD (Liu et al., 2004; Foster et al., 2010), and for the late-LTP-triggered spine pruning (Maletic-Savatic, 1999; Gambrill and Barria, 2011).

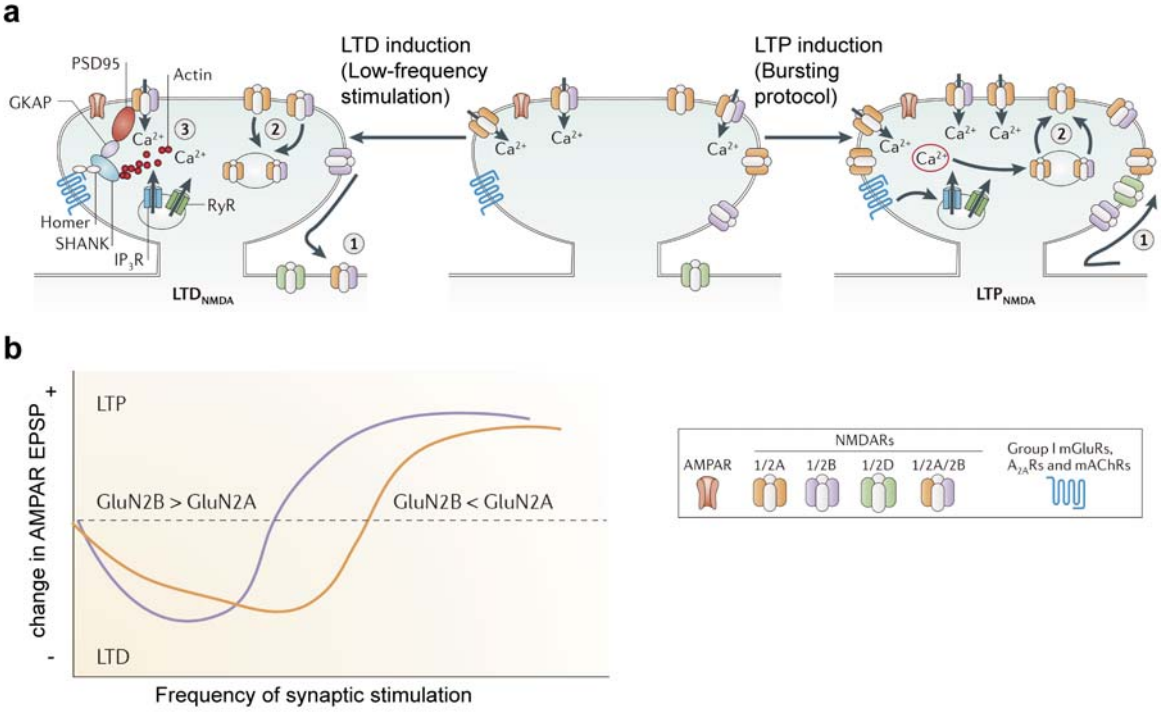

Figure i.2.4 NMDA receptor subunit composition is modulated during synaptic plasticity.
(**a**) At adult synapses, NMDARs can undergo plasticity independently of AMPARs. Both LTP and LTD induction protocols trigger increases in Ca^{2+} concentrations at the spine, which can be attained through a variety of mechanisms. NMDAR subunit composition is also modified in response to these plasticity events, and mechanisms involved include lateral diffusion (1), exocytosis and endocytosis (2) and actin depolymerization (3). (**b**) The ratio of GluN2A-to-GluN2B in the synaptic NMDAR population influences the AMPAR-mediated synaptic plasticity. Briefly, when the synaptic GluN2A-to-GluN2B ratio is low following synaptic stimulation, LTP is more likely to occur rather than LTP. In the opposite situation, LTD is favoured. Abbreviations: *NMDAR*, NMDA receptor;

AMPAR, AMPA receptor; mGluR, metabotropic glutamate receptor; *IP3R*, inositol triphosphate receptor; *GKAP*, guanylate kinase-associated protein; *RyR*, ryanodine receptor; *LTP*, long-term potentiation; *LTD*, long-term depression; *EPSP*, excitatory postsynaptic potential. Adapted from (Paoletti et al., 2013).

Moreover, the two GluN2 subunits (2A and 2B) confer different properties to the receptor with relevant effects in synaptic plasticity. In contrast to neonatal synapses, NMDA receptors in adult synapses contain predominantly GluN2A subunits. This switch occurs during the synaptic maturation process and implies several changes in NMDAR-mediated synaptic currents such as decay time kinetics or temporal integration properties (Paoletti et al., 2013). Similarly, neuronal activity drives the switch of GluN2A-to-GluN2B in mature synapses, by specifically regulating the drift of GluN2A subunits (Barria and Malinow, 2002; Groc et al., 2006) among other mechanisms. Lateral diffusion of NMDA receptors also differs depending on the GluN2 subunit (Groc et al., 2006). GluN2B retention at synapse requires binding to scaffolding MAGUK proteins located in the PSD, whereas GluN2A receptors are more stable and localize to postsynaptic sites even in the absence of PDZ binding (Prybylowski et al., 2005; Groc et al., 2006). Finally, 2A and 2B subunits of NMDA receptors contribute differently to the likeliness of a spine to undergo LTP or LTD: although both subtypes contribute to the process, LTP is favoured against LTD when GluN2A-to-GluN2B ratio is low following synaptic stimulation, whereas in the opposite situation LTD is more likely to occur (**Fig. i.2.4b**) (Yashiro and Philpot, 2008; Paoletti et al., 2013). Conversely, a number of studies have associated GluN2A with LTP induction and GluN2B with LTD (Sprengel et al., 1998; Brigman et al., 2010). The fine mechanism behind GluN2A and 2B-mediated plasticity is still to be uncovered, although the role of their respective intracellular C-terminal domains has revealed interesting cues with specific physiological and behavioral correlates (Ryan et al., 2013).

3. Reelin: Functions in the developing and adult brain

The Reelin pathway and its role in brain development

Reelin is a high-molecular weight glycoprotein targeted to the extracellular matrix with a key role in both brain development and synaptic plasticity. It was first discovered after mapping the spontaneous autosomal recessive mutation *reeler* in mice (Goffinet and Dernoncourt, 1991; Miao et al., 1994; Bar et al., 1995). The first *reeler* strain characterized originated in Edinburgh (strain B6C3Fe *ala-Reln*^{rl}/J), although other similar mutations resulting in the absence of functional Reelin protein were further identified (Hirotsune et al., 1995). Gene subcloning and protein characterization analyses identified the absence of Reelin as the cause for the *reeler* phenotype (D'Arcangelo et al., 1995). The human *RELN* gene was also cloned (DeSilva et al., 1997), and subjects with an inherited form of truncated *RELN* gene were identified. The lack of Reelin in humans triggers lissencephaly with cerebellar hypoplasia (LCH), a phenotype that parallels much the one observed in the *reeler* mice (Hong et al., 2000).

Molecular biology of Reelin: the gene, the mRNA, the protein

The *reln* gene in mouse is located in chromosome 5 and extends over 450 Kb (Royaux et al., 1997). It contains 65 exons and two different polyadenylation sites, and different transcripts can be generated by alternative splicing events. The promoter region lacks canonical TATA and CAAT boxes, but it contains 3 potential transcription starts with recognition sites for transcription factors Sp1 and AP2. The human *RELN* gene characterization (located in 7q22) revealed also binding sites for other transcription factors such as CREB, NF-κβ, Tbr1 and Pax6 (Chen et al., 2002; Levenson et al., 2008). Besides this classical, transcription-factor based gene expression process Reelin expression may undergo an epigenetic-mediated regulation. Potentially methylation sites include several CpG islands in the promoter region, as well as other sites within the gene itself. The existence of this abundance of regulator sites suggests that Reelin expression is finely tuned. The full-length mRNA isoform is the most frequent one and contains 11673 base pairs.

The full-length Reelin protein is composed by 3461 amino acids (**Fig. i.3.1a**) (D'Arcangelo et al., 1997). The relative molecular mass of the glycosylated secreted protein is 427 kDa, although mass prediction after signal peptide cleavage was ~385 kDa (D'Arcangelo et al., 1997; Tissir and Goffinet, 2003; Knue-

sel, 2010). It is highly conserved between mouse and human. It exhibits a modular structure. The N-terminal region contains a signaling peptide that targets for secretion, an F-spondin homology domain and an epitope recognized by the CR-50 monoclonal antibody that is essential for Reelin dimerization and function. The protein is mainly composed by eight repeats, each containing two subrepeats separated by an EGF-like motif. The C-terminal region is highly conserved and necessary for signaling (Derer et al., 2001; Nakano et al., 2007). Following secretion, Reelin is cleaved by proteases at two sites (Jossin et al., 2004), generating five different proteolytic fragments (**Fig. i.3.1b**) (Knuesel, 2010). Although the specific role of each fragment has not entirely been elucidated, some findings indicate that blocking the N-terminus with CR-50 epitope has neutralizing activity on Reelin function (Del Rio et al., 1997), and that the central fragment (composed of repeats 3 to 6) is necessary and sufficient to rescue the *reeler* phenotype and can trigger signal transduction by binding to receptors (Jossin et al., 2004; Jossin and Goffinet, 2007).

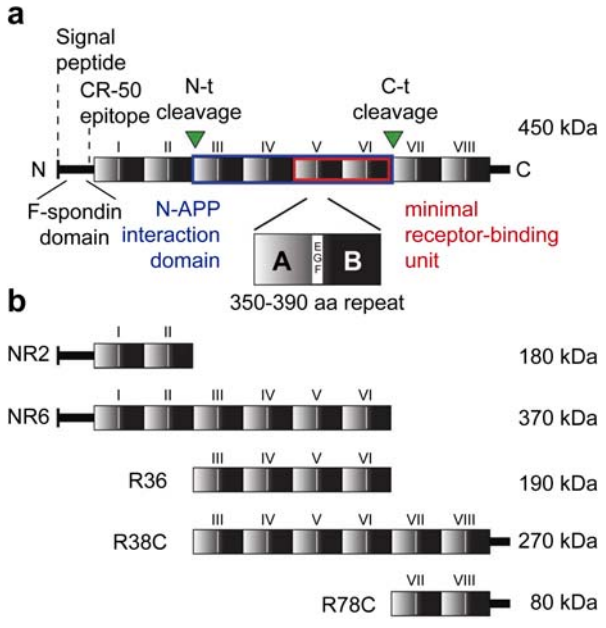

Figure i.3.1 Structure of the Reelin protein.
(**a**) The schema depicts the modular structure of the full Reelin protein. Each element (I-VIII) is composed by two subrepeats A, B separated by an EGF-like motif. Dashed lines point to approximate localization of the signal peptide and the CR-50 epitope needed for dimerization. Green triangles indicate cleavage sites by extracellular proteases. Blue box outlines the region identified to interact with APP, whether red box indicates the region interacting with its receptors. (**b**) Different transcriptional starts and proteolytic cleavage of the protein generates five different Reelin peptides ranging from 80 to 370 kDa in size. Abbreviations: *N-t*, N-terminal; *C-t*, C-terminal; *aa*, amino acid. Adapted from (Knuesel, 2010).

The Reelin pathway: receptors, Dab1 and signaling cascades

Full-length Reelin forms dimers and processed fragments containing the CR-50 epitope can form larger homomeric complexes (Utsunomiya-Tate et al., 2000; Kubo et al., 2002). Reelin dimerization has been suggested to be able to bind and activate its receptors including the very low density lipoprotein receptor (VLDLR) and the apolipoprotein E receptor 2 (ApoER2) (D'Arcangelo et al., 1999; Hiesberger et al., 1999). Although other receptors have been described for Reelin, such as the cadherin-related neuronal receptor family members (Senzaki et al., 1999; Jossin and Cooper, 2011), integrins (Dulabon et al., 2000; Dong et al., 2003; Sekine et al., 2012) or ephrins (Sentürk et al., 2011; Bouche et al., 2013) only VLDLR and ApoER2 double-mutant mice reproduce the *reeler*-like phenotype (Trommsdorff et al., 1999), pointing these receptors as the most prevalent ones during physiological Reelin signaling events.

Reelin homomers bind to VLDLR and ApoER2, which triggers receptor clustering and phosphorylation of the cytoplasmic disabled1 (Dab1) by Fyn and Src, two kinases of the Src family tyrosine kinases (SFK) (Howell et al., 1999; Arnaud et al., 2003b; Kuo et al., 2005). The pattern of expression of Dab1 is largely complementary to that of Reelin, being expressed at high levels by principal neurons of the

embryonic cerebral cortex and hippocampus and by Purkinje cells in the cerebellum (Rice et al., 1998; Borrell et al., 2007), and absence of Dab1 triggers the appearance of *reeler*-like phenotypes (Sweet et al., 1996; Goldowitz et al., 1997; Sheldon et al., 1997; Yoneshima et al., 1997), suggesting an exclusive relationship of Dab1 with Reelin-induced signaling events. Dab1 activation leads to the emergence of different intracellular signaling cascades by means of recruitment and activation of other non-receptor tyrosine kinases (**Fig. i.3.2**). The signaling cascades triggered by Reelin include the mitogen-activated protein kinase/extracellular signal-regulated kinase (MAPK/ERK) pathway (Simo et al., 2007), the phosphatidylinositol-3-kinase (PI3K)/Akt pathway (Beffert et al., 2002; Gonzalez-Billault et al., 2005) and the Crk/CrkL-C3G pathway (Ballif et al., 2004; Matsuki et al., 2008; Feng and Cooper, 2009), reaching both the actin and the microtubule cytoskeleton. The signaling duration is terminated by the ubiquitination of phosphorylated Dab1, whose degradation is triggered by the Cul5 cascade (Arnaud et al., 2003a; Suetsugu et al., 2004; Feng et al., 2007; Simo et al., 2010; Simo and Cooper, 2013), and by the endocytosis of the Reelin/receptor complex (Morimura et al., 2005; Duit et al., 2010).

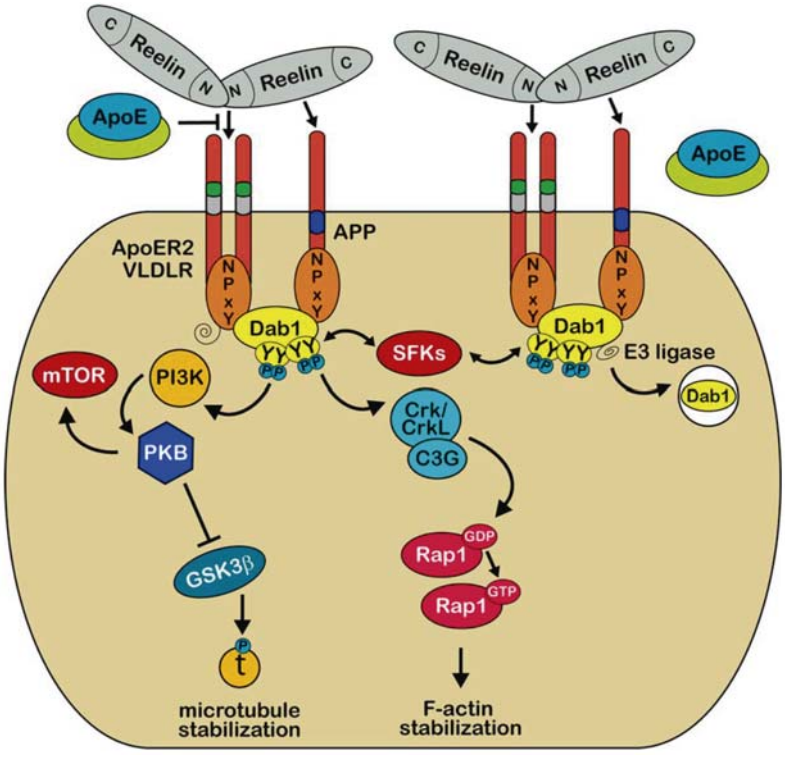

Figure i.3.2 Reelin-initiated events in developing neurons.
The illustration shows some of the signaling pathways downstream of Reelin signaling at developmental stages. Multimeric Reelin binding to its receptors triggers the intracellular clustering and phosphorylation of Dab1 by Src family tyrosine kinases (SFKs). Phosphorylated Dab1 further promotes the activation of other intracellular cascades through the recruitment and activation of additional non-receptor tyrosine kinases. Notably, PI3K cascade regulates the activity of GSK3β, one of the main kinases phosphorylating the microtubule-stabilizing protein Tau (τ), also involved in the pathogenesis of Alzheimer's disease. Phosphorylated Dab1 is also a target for ubiquitin ligases, which by promoting the degradation of Dab1 limit the duration of the Reelin-triggered signaling. Reproduced from (Knuesel, 2010).

The Reelin expression and function in brain development

Reelin expression during development and adulthood is not constrained to the nervous system. Beyond it, it has been reported to be expressed in a number of tissues including embryonic somite, foregut, yolk sac, optic cup, blood vessels, precartilage, stomach, pituitary, vibrissae and tooth germ, and also in adult liver, kidney, adrenal and pituitary glands, testis and ovary. Moreover, Reelin protein levels have been observed in serum and platelet-poor plasma, and the liver has been pointed as the putative origin for circulating Reelin pool generation and maintenance (Ikeda and Terashima, 1997; Smalheiser et al., 2000). However, since the most prominent phenotypes on Reelin-deficient mice were nervous system-related injuries, most of the research interest has been driven to this structure (Alcantara et al., 1998).

Developmental expression of Reelin in the brain is driven by specific cellular populations, the most important being Cajal-Retzius (CR) cells in the forebrain and granule cell precursors in the cerebellum. Besides, Reelin is also expressed in other zones including hypothalamus, caudate-putamen, medial septum and olfactory bulb (OB) (Alcantara et al., 1998). CR cells are a transient, Reelin and p73-positive cell population that migrate from diverse yet specific production sites to the marginal zone of the cortex and hippocampus and disappear 1-2 weeks after birth (Cajal, 1891; Retzius, 1893; Meyer et al., 2002; Soriano and Del Rio, 2005). CR cells are eliminated through programmed cell death after completion of cell migration and layer formation processes (del Rio et al., 1995). Reelin is secreted by CR cells from E10 onwards by specialized form of rough endoplasmic reticulum (RER) in the cortical marginal zone (Derer et al., 2001). This process constitutes a key regulator event of neuronal migration in the formation of the cortical plate, during which the preplate splits into the marginal zone and a subplate layer (**Fig. i.3.3a**) (Del Rio et al., 1997; Super et al., 1998). More specifically, Reelin secretion by CR cells directs the radial migration and the formation of cellular layers by principal, excitatory cortical neurons born in the ventricular zone and proper Reelin secretion is needed to configure the inside-out gradient of the layered cortical structures (Caviness and Sidman, 1973; Caviness, 1982; Tissir and Goffinet, 2003; Boyle et al., 2011). Migration of pyramidal neurons of the hippocampus and generation of its typical layered pattern is similarly regulated by Reelin. Besides, CR cells located in the outer molecular layer (OML) of the dentate gyrus (DG) secrete Reelin throughout life, thereby regulating the migration of new-born neurons in the dentate gyrus (**Fig. i.3.3b**) (Forster et al., 2006). Furthermore, loss of Reelin is related with granule cell dispersion in the DG in both human patients and *reeler* mice (Haas et al., 2002; Duveau et al., 2011).

In the cerebellum, Reelin is expressed by granule cell precursors in the external granule layer (EGL) (D'Arcangelo et al., 1995). The cerebellum contains two principal cell types, granule and Purkinje cells, and its development starts at E11. Reelin-expressing granule cell precursors migrate tangentially from the rhombic lip over the surface forming the EGL, whereas Purkinje cells migrate radially from the ventricular zone to right below the EGL, giving rise to the Purkinje cell layer. At this point, granule cells migrate radially from the EGL inwards across the molecular and Purkinje cell layer and form the internal granule layer (IGL). This last event of migration and the proper refinement of the Purkinje cell layer are finely regulated by Reelin, which is only present extracellularly in the molecular layer and at the premigratory zone of the EGL (Miyata et al., 1996). Accordingly, Reelin deficiency triggers ectopic positioning of Purkinje cells and a reduction in the number of granule and Purkinje cells (**Fig. i.3.3c**) (Goffinet, 1983).

Finally, Reelin function has also been related to axonal and dendritic growth phenomena during the early formation of the hippocampus and cortex. Reelin secreted by hippocampal CR cells diffuses to the adjacent layers OML and stratum lacunosum-moleculare (SLM). These layers are the target of the perforant pathway, composed by axons migrating from the entorhinal cortex, and Reelin plays a crucial role in their early growth and branching (**Fig. i.3.3b**). More interestingly, Reelin promotes synaptogenesis to these entorhinal afferents. (Del Rio et al., 1997; Borrell et al., 1999; Borrell et al., 2007). Similarly, dendritic arbor maturation comprising dendritic elongation and branching in both DG granule cells and cortical pyramidal neurons has also been shown to depend on Reelin signaling (Niu et al., 2004; Olson et al., 2006; Nichols and Olson, 2010).

Altogether, Reelin exerts different functions in the developing brain. It is a key regulator of radially migrating principal neurons in cortical structures, and is also involved in axonal growth processes leading to hippocampal innervation, as well as in the establishment of synapses of these axons in their target zones. Finally, it also regulates the development of the dendritic arbors of DG granule cells and cortical neurons.

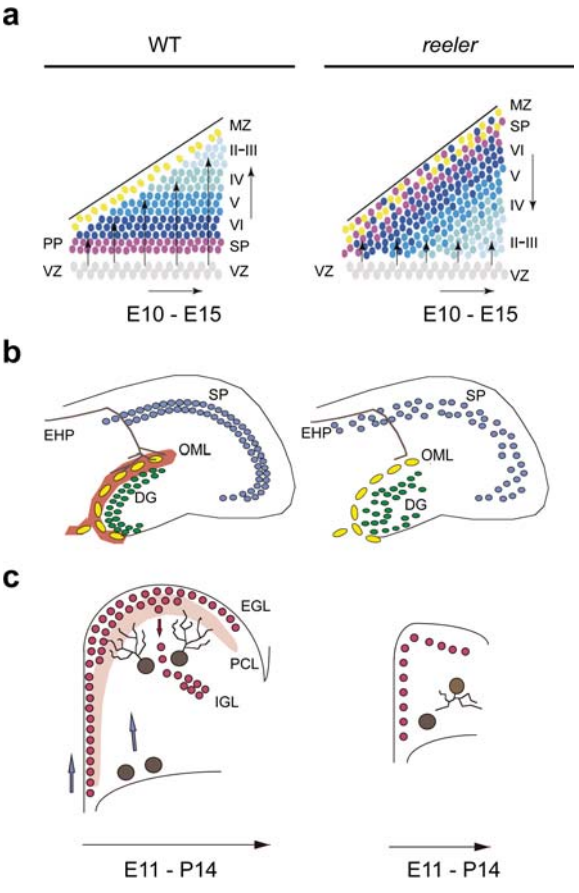

Figure i.3.3 Reelin role in the development of layered structures in the neocortex, hippocampus and cerebellum.
(**a**) Normal cortical development involves the splitting of the preplate (PP) into the marginal zone (MZ) and the subplate (SP). Further, new neurons migrate radially upon the older ones (arrows) and settle under the MZ, where Cajal-Retzius cells (CR) (yellow) secrete Reelin. This process generates the typical inside-out pattern of cortical structures (neuron age is color-coded in shades of blue). In reeler mice, conversely, splitting of the PP does not take place and radial migration becomes impaired, further disrupting the layering pattern and sometimes inversing it to an outside-in (arrows in the right). (**b**) In normal mice Cajal-Retzius cells (yellow) express Reelin (shaded red) in the outer molecular layer (OML), and exhibit a compact layer of pyramidal neurons at the stratum pyramidale (SP). *Reeler* mice, in turn, present a more dispersed SP as well as dispersion of the Granule cells in the dentate gyrus (green). Further, entorhinohippocampal fibers (EHP) (brown) display reduced branching in these mice. (**c**) In the developing cerebellum Reelin is secreted (shaded red) by Granule cells (red), which migrate tangentially to form the external granule layer (EGL). Purkinje cells (brown) migrate radially towards these Reelin-producing cells. Finally, Granule cells migrate inwardly across the Purkinje cell layer (PCL) to form the inner granule layer (IGL). In *reeler* mice, Purkinje cells Purkinje cells remain in a deep subcortical location, and granule cells are reduced in number, resulting in a smaller cerebellum. Abbreviations: *WT*, wild-type; *E10*, embrionary day 10; *II-VI*, cortical layers 2-6; *VZ*, ventricular zone. (**a**) was adapted from (Cooper, 2008); (**b**, **c**) were adapted from (D'Arcangelo and Curran, 1998).

Reelin in the adult brain

The Reelin expression and function in the adult brain

The expression of Reelin undergoes an important change after completion of the neuronal migration processes. The developing marginal zones become layer I in the neocortex and SLM and OML in the hippocampus (Frotscher, 1998). CR cell population progressively disappears during the first postnatal weeks, although some cells have been reported to remain during adulthood in these layers (Abraham and Meyer, 2003). In the same direction, Reelin starts being expressed in GABAergic interneurons located along the neocortex and hippocampus, in glutamatergic mitral cells in the olfactory bulb, in glutamatergic granule cells in the cerebellum and in layer II pyramidal cells in the piriform and entorhinal cortex (Alcantara et al., 1998; Pesold et al., 1998; Abraham and Meyer, 2003; Pappas et al., 2003; Herz and Chen, 2006; Ramos-Moreno et al., 2006). This change in expression early suggested the existence of a new function for Reelin in the postnatal and adult brain, since the previously described for neuronal migration or dendritic development was no longer applicable in these stages.

Reelin and synaptic plasticity

The first evidence of Reelin being involved in synaptogenesis came from late developmental studies of entorhino-hippocampal connections reporting this effect in addition to a previously known role in axon growth regulation (Borrell et al., 1999). Later on, more evidences came from the observation of the structure and function of retinal synaptic circuitry in *reeler* and *scrambler* mice (Rice et al., 2001) which showed defects in connectivity and physiological responses. Reelin role in the adult retina has been further characterized and both ApoER2 and VLDLR are required for the establishment and maintenance of a normal synaptic connectivity, although specific functions have been described for each receptor in this tissue (Trotter et al., 2011).

Mice lacking Reelin or its signaling effectors were used as tools to evaluate the role of Reelin in the adult brain. *Reeler* mice brains display large cell mispositioning events, but heterozygous *reeler* mice (*HRM*) present an overall conserved histological disposition concomitant with a decrease in the amounts of Reelin signaling (Liu et al., 2001; Badea et al., 2007; Katsuyama and Terashima, 2009). Mutants for ApoER2 or VLDLR show impairments in adult hippocampal LTP, and blockade of LDL receptors with RAP peptide blocks LTP. Besides, hippocampal LTP is enhanced when perfusing Reelin to wild-type (WT) slice cultures (Weeber et al., 2002). Moreover, hippocampal spontaneous IPSCs were also reduced in these mice, suggesting that Reelin might exert a role in the development of inhibitory synapses (Qiu et al., 2006b).

A detailed study of the Reelin ApoER2 receptor revealed that Reelin-mediated enhancement of LTP was dependent on an alternatively spliced exon of ApoER2 (Beffert et al., 2005). Although non-essential for Reelin downstream signaling, exon 19 of ApoER2 is necessary for the Reelin-induced enhancement of LTP, with a mechanism specifically involving NMDA receptors rather than AMPARs. ApoER2 interacts directly with NMDA receptors and exon 19 is necessary for Reelin-induced phosphorylation of 2A and 2B subunits of NMDA receptors. More interestingly, alternative splicing giving rise to the expression of exon19-containing mRNA is activity-dependent, and mice lacking this variant exhibit learning and memory deficits.

Reelin-triggered tyrosine phosphorylation of NMDA receptor subunits 2A and 2B occurs via SFKs and Dab1 and is accompanied by an increased calcium influx through these receptors (**Fig. i.3.4a**) (Chen et al., 2005; Qiu et al., 2006a). Moreover, Src is associated with ApoER2 through PSD-95, and is recruited to PSD-95 after Reelin application, whereas in the other side NMDAR activity modulates the interaction between ApoER2 and PSD-95 (Hoe et al., 2006; Qiu et al., 2006a). NMDAR activity can also be modulated by the relative ratio of 2A-to-2B-containing NMDA receptors at the synapse, and this can be attained by lateral mobility of receptors (Groc et al., 2006). Reelin also participates in this regulation, by means of increasing the surface mobility of NR2B-containing NMDARs, which results in NR2A-enriched synapses (**Fig. i.3.4b**) (Sinagra et al., 2005; Groc et al., 2007; Qiu and Weeber, 2007).

In brief, Reelin-mediated ApoER2 activation leads to Src recruitment to PSD-95, which triggers interaction with and phosphorylation of NMDAR subunits 2A and 2B, therefore, increasing their calcium influx. Besides, long-term Reelin signaling promotes an enrichment of the 2A-to-2B ratio of NMDA receptor subunits at the synapse. Altogether, these effects promote an enhancement of the NMDAR synaptic response.

Reelin infusion on cultured slices triggers an enhancement of CA1 synaptic plasticity mediated by both NMDARs and AMPARs. However, the mechanism by which Reelin potentiates synaptic activity differs depending on the receptor type involved (Qiu et al., 2006a). As previously described, postsynaptic modifications might account for the enhancement of NMDAR synaptic responses after Reelin treat-

ment. On the other side, although AMPAR channel activity can also be regulated through phosphorylation (Barria et al., 1997) Reelin-triggered AMPAR plasticity does not rely on changes in AMPAR phosphorylation. Conversely, it appears to be related to an increased presence of AMPA receptors in the surface (Qiu et al., 2006a; Qiu and Weeber, 2007), and this insertion is dependent on PI3K – but in this case is independent of Src. Reelin-induced AMPAR insertion also underlies a decrease in the number of silent synapses, this is, synapses that initially contained only NMDARs (Qiu and Weeber, 2007). Therefore, Reelin signaling through PI3K (but not Src) promotes the exposure and insertion of new AMPARs in the synaptic membrane, what in turn enhances the synaptic function, leading to increased AMPAR-mediated whole-cell currents.

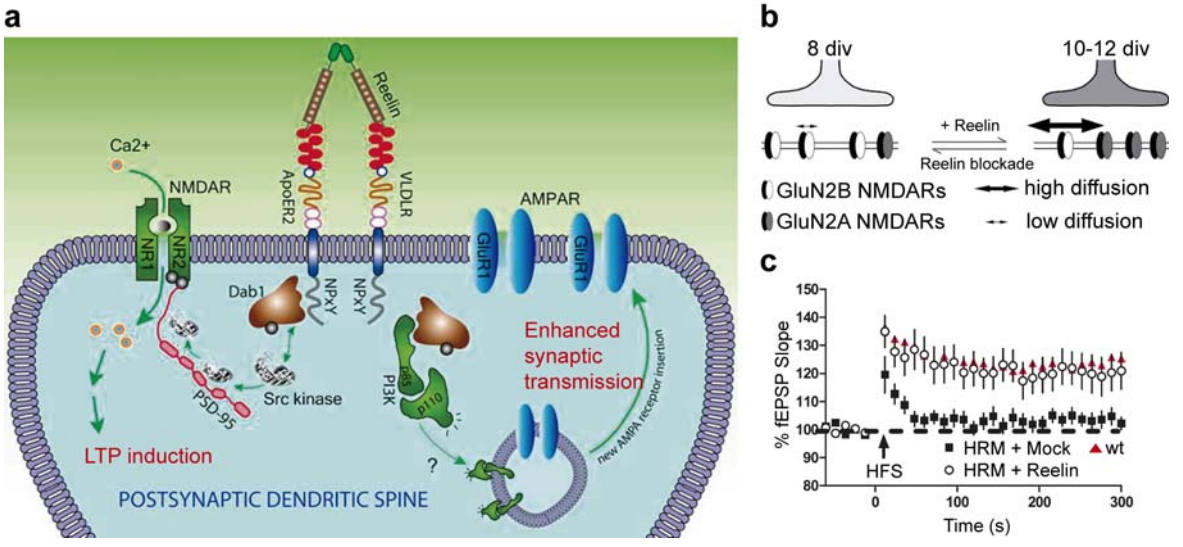

Figure i.3.4 Reelin signaling in synaptic plasticity.
(**a**) Reelin can modulate the postsynaptic response to excitatory stimuli through a number of mechanisms. Activated Dab1 promotes the association of Src with PSD-95, which in turn serves as scaffold for NMDA receptors (NMDARs). The phosphorylation of their GluN2 subunit follows Reelin signaling, leading to increased NMDA response. In the other side, Reelin promotes the surface expression of AMPA receptors (AMPARs) through a PI3K-mediated exocytic process, thereby promoting AMPA excitability. (**b**) Reelin also modulates the GluN2A-to-GluN2B ratio of synaptic NMDARs through the lateral diffusion of the GluN2B-containing receptors, which in turn would facilitate the induction of LTP in these spines. (**c**) AMPAR-mediated LTP is recovered in heterozygous *reeler* mice (*HRM*) upon 5 days from Reelin supplementation. Abbreviations: *div*, days *in vitro*. (**a**) was adapted from (Qiu et al., 2006a); (**b**) was adapted from (Groc et al., 2007) and (**c**) was adapted from (Rogers et al., 2013).

Reelin and dendritic spines

Dendritic spines receive most excitatory synapses in the brain, and their morphology is tightly related to their synaptic efficacy (Bourne and Harris, 2008; Rochefort and Konnerth, 2012). *Reeler* mice exhibit lower spine densities in different cortical zones and spines present a smaller, less complex appearance (Liu et al., 2001). Cultured hippocampal neurons from *reeler* mice exhibited less glutamate receptor-immunoreactive puncta, which could be partially restored by Reelin supplementation in the media (Qiu and Weeber, 2007). Similarly, *HRM* and *reeler* mice exhibited a decreased density of dendritic spines on apical dendrites of CA1 pyramidal neurons (Niu et al., 2008), while hippocampal synaptosomal fractions (but not total extracts) showed decreased levels of PSD-95 and NMDA receptor subunit 2A (Niu et al., 2008; Ventruti et al., 2011). More interestingly, Reelin supplementation to *reeler* organo-

typic hippocampal slice cultures recovered normal spine density in a lipoprotein-receptor dependent manner. Dab1-KO mice exhibited very similar phenotypes: CA1 pyramidal neurons displayed a lower density of dendritic spines which was dependent on SFK activity, and hippocampal synaptosomal fractions (but not total extracts) presented lower levels of PSD-95 and NR2A, thereby confirming a role for Dab1 in dendritic spine formation. Therefore, Reelin signaling in the adult regulates dendritic spine development, which is independent of the former regulation of neuronal processes. On the other side, a close view to the presynaptic compartment revealed that hippocampal synaptic boutons of *reeler* mutants bore more vesicles, and membrane extracts revealed reduced levels of SNAP-25, a SNARE protein. Moreover, these phenotypes could be rescued by Reelin supplementation (Hellwig et al., 2011).

Structural and synaptic plasticity are two co-regulated, although different, processes (Matsuzaki et al., 2004; Kopec et al., 2006; Sdrulla and Linden, 2007; Cingolani and Goda, 2008). Combined analysis of the Reelin role on structural and physiological properties of synapses was approached by injecting recombinant Reelin intraventricularly on wild-type mice (Rogers et al., 2011). Acute Reelin infusion to wt mice provoked an increase of spine density at both apical and basal dendrites of CA1 pyramidal cells. However, this effect appeared to be a late phenomenon, since it was only evident five days post-infusion and not at earlier time points. On the other side, Reelin-injected mice displayed an enhanced LTP, whereas presynaptic function did not evidence any changes when evaluated by paired-pulse facilitation (PPF). Finally, Reelin-injected mice performed better in spatial learning and memory tasks. A similar approach was performed on *HRM* (Rogers et al., 2013) in order to evaluate whether it could revert some of the physiological, structural or behavioral impairments of this mouse model. Acute Reelin supplementation triggered an early increase in GAD67 protein levels. However, spine density remained unaltered in *HRM* Reelin-supplemented mice. In contrast, some morphological alterations of dendritic spines (e.g. spine length or width) could be partially or totally reverted to wt values by Reelin infusion. This treatment could also rescue some synaptic plasticity deficits present in the *HRM* (**Fig. i.3.4c**). Both presynaptic-related (post-tetanic potentiation, PTP) and postsynaptic-related (LTP) plasticity evaluations revealed that Reelin-supplemented *HRM* scored undistinguishable results than the ones attained by wt mice. Finally, Reelin-injected *HRM* recovered the associative learning deficit observed in *HRM*. Therefore, biochemical, morphological and physiological deficits present in the *HRM* could be rescued by a single *in vivo* injection of Reelin.

Due to the relevant roles of Reelin signaling during the development of the nervous system, transgenic models based on constitutive modification of Reelin expression raise the question of whether defects observed might be secondary to the mispositioning of neurons. To overcome this caveat, conditional and directed transgene constructs have been developed.

Using an adult-forebrain specific and excitatory neuron-specific conditional Dab1 knock-out (Dab1 cKO) mouse line, Trotter et al. (Trotter et al., 2013) analyzed the role of this protein in adult synaptic plasticity. Dab1 cKO mice displayed unaltered spine density in apical dendrites of CA1 pyramidal cells, but displayed smaller spines in these dendrites. Conversely, presynaptic and postsynaptic-associated proteins such as glutamate receptors or PSD-95 showed similar levels in Dab1 cKO hippocampal extracts and synaptosomal fractions. Dab1 cKO mice exhibited impaired LTP induction and maintenance, and were insensitive to Reelin-triggered LTP enhancement. Finally, Dab1 cKO exhibited long-term associative memory deficits. Therefore, adult-specific impairement of Reelin signaling provokes synaptic plasticity-related deficits.

Reelin and brain pathologies

Reelin exerts a key function in both the development of the brain and its function in the adulthood. Therefore, irregularities in the Reelin function are likely to be associated with a diverse range of neurological disorders, both psychiatric and neurodegenerative.

Reelin expression abnormalities have been reported in patients for various psychiatric disorders, including schizophrenia, bipolar disorder, autism and major depression (Impagnatiello et al., 1998; Fatemi et al., 2000; Guidotti et al., 2000; Costa et al., 2001; Persico et al., 2001; Knable et al., 2004; Abdolmaleky et al., 2005; Knuesel, 2010; Folsom and Fatemi, 2013). Reelin relationship with these disorders has been pointed to be both active and passive, agreeing with the two-hit hypothesis for the expression of such diseases: Underlying neurodevelopmental abnormalities increase the vulnerability of individuals to the manifestation of the disease, and several of the putative disturbances are dependent on Reelin-mediated signaling. In the other side, abnormal Reelin signaling promotes the development of cognitive dysfunction. Reduced Reelin expression in different brain regions has been reported in patients for all the previously mentioned psychiatric diseases (Folsom and Fatemi, 2013), Reelin expression correlates positively with the age of illness onset and negatively with the illness duration (Knable et al., 2004) and Reelin downregulation in these diseases has been associated with a decrease in glutamic acid decarboxylase (GAD67) (Impagnatiello et al., 1998; Fatemi et al., 2000; Guidotti et al., 2000; Costa et al., 2001; Knuesel, 2010). Moreover, one of the genes responsible for the familial form of schizophrenia, disc1 (Blackwood et al., 2001; Li et al., 2007), displays molecular crosstalks by the Reelin signaling pathway (Assadi et al., 2003; Young-Pearse et al., 2010). Reelin has also been related with mesial temporal lobe epilepsy (Haas et al., 2002; Haas and Frotscher, 2010). One characteristic feature of epilepsy is granule cell dispersion, which is also evident in reelin signaling-deficient mice.

Multiple mechanisms have been proposed to account for the altered Reelin expression in neuropsyhiatric disorders. Epigenetic methylation of the Reelin promoter has been shown as a feasible method for a sustained long-term downregulation of its expression in mice (Dong et al., 2007), and postmortem analysis of brains from subjects with schizophrenia and studies in mice revealed strong correlation between S-adenosyl-methionine (SAM), DNMT1, hypermethylation of the reelin promoter and decreased Reelin expression (Veldic et al., 2004; Abdolmaleky et al., 2005; Guidotti et al., 2007). However, other mechanisms might induce a decrease in Reelin signaling: Inherited spontaneous mutations could provoke the absence of circulating protein levels, early perinatal insults such as viral or bacterial infections have been reported to be able to modify the expression of Reelin in an otherwise critical developmental period, and abnormal microRNA expression present in some psychiatric disorders could regulate the expression of Reelin, among other putative processes (Folsom and Fatemi, 2013).

Reelin signaling has increasingly been linked with the pathophysiology of Alzheimer's disease (AD) (Knuesel, 2010). Different evidences point to this relationship: First, the ApoE isoform ε4 is the major risk factor for AD. ApoE regulates the lipid metabolism and therefore the clearance of the β-amyloid (Aβ) deposits. This specific isoform correlates with worse clearance kinetics and a major accumulation of soluble and fibrillary Aβ (Schmechel et al., 1993; Tsai et al., 1994; Urosevic and Martins, 2008). ApoE-mediated clearance occurs through different lipoprotein receptors, two of them shared with the Reelin signaling pathway: ApoER2 and VLDLR (Herz and Chen, 2006). Moreover, Aβ deposits colocalize with Reelin and amyloid precursor protein (APP) interacts with both Reelin and Dab1 (Trommsdorff et al., 1998; Homayouni et al., 1999; Hoe et al., 2009; Doehner et al., 2010), while it has been reported that Reelin can counteract Aβ-induced synaptic disfunction (Durakoglugil et al., 2009). Therefore, Reelin-mediated signaling can exert an active role in the regulation of the processing and trafficking of APP. Second, mouse models deficient in Reelin signaling exhibit increased phosphorylation of the microtubule-stabilizing protein Tau, which might be regulated through GSK3β and

Cdk5 (Hiesberger et al., 1999; Beffert et al., 2002; Gonzalez-Billault et al., 2005). Hyperphosphorylated Tau protein is the structural component of paired helical filaments and neurofibrillary tangles, hallmarks of AD progression. It has been reported that Reelin levels decline with age (Knuesel et al., 2009), whereas in the other side Reelin expression and glycosylation patterns have been found altered in AD patients (Botella-Lopez et al., 2006; Chin et al., 2007; Botella-Lopez et al., 2010) and some Reelin polymorphisms have been associated to AD pathology (Seripa et al., 2008; Kramer et al., 2011). Altogether, age-related impaired Reelin signaling could both trigger abnormal Tau phosphorylation and impair the clearance of Ab peptides. This would facilitate the appearance of neurofibrillary tangles and promote amyloidogenesis, respectively, which might underlie the progressive decline in cognitive abilities found in AD (Pujadas et al., 2014).

Animal tools to study the role of the Reelin pathway in the adult brain

As mentioned previously, the striking role of Reelin in brain development can be a source of confusion when studying its function on the adult brain. To avoid such caveats, we used some models that focus the up- or down-regulation of the Reelin signaling pathway to the already developed brain.

Adult-specific conditional overexpression of Reelin: The Reelin-OE mouse model

The Reelin-OE mouse line is a Tet-OFF line composed by two transgenes that overexpresses Reelin under the control of *pCaMKIIα* (**Fig. i.3.5a**). The promoter of CaMKIIα drives the expression of the tetracycline-controlled transactivator (*tTA*), therefore ensuring both a temporal (from P5 onwards) and cellular (mimicking the expression of CaMKIIα) restriction of the transgene expression. In the other side, the second transgene codes for a *tTA*-inducible *tetO* promoter driving the expression of the exogenous reelin gene. In double transgenic mice *pCaMKIIα-tTA* / *tetO-rlM* (Reelin-OE mice), exogenous Reelin expression is directed by the CaMKIIα promoter, in a regulated system that can be repressed by doxycycline (DOX) administration (**Fig. i.3.5b**) (Pujadas et al., 2010).

Reelin-OE mice exhibit exogenous Reelin expression in numerous pyramidal cells in the neocortex, hippocampus (most remarkably in CA1 region), and entorhinal cortex (**Fig. i.3.5c**). DG granular cells are also Reelin-positive, as well as a large percentage of striatal neurons. Finally, mitral cells and plexiform layers of the OB also exhibit an increased Reelin immunostaining in these mice, besides the already reported endogenous one (Alcantara et al., 1998). Protein levels analyses by Western Blot revealed that adult Reelin-OE mice had a threefold increase in Reelin expression in the cerebral cortex and hippocampus, and about a sevenfold increase in the striatum, whereas Dab1 levels were slightly decreased. Reelin-OE mice exhibited enhanced *in vivo* hippocampal LTP (**Fig. i.3.5d**) and some alterations in adult neurogenic profiles, including a mispositioning in the OB periglomerular and granular neurons and abnormal cell migration and positioning of adult-generated DG granule cells. In the other side, histological examination of adult Reelin-OE mice did not reveal neuroanatomical alterations compared to control mice. Therefore, the Reelin-OE mouse model, which exhibits normal cortical lamination, allows the specific examination of Reelin functions in the adult forebrain.

Conditional deletion of Dab1: floxed Dab1 mouse model-based approaches

The floxed Dab1 mouse line (flDab1) is a knock-in mouse with *loxP* sequences flanking the exon III (encoding residues 23-69) of the *dab1* locus (Pramatarova et al., 2008). This allele provokes a transient reduction of Dab1 protein levels during early postnatal stages but normal Dab1 expression is attained from P14 onwards (Pramatarova et al., 2008; Teixeira et al., 2014). Adult homozygous flDab1 mice exhibit permanent structural and layering alterations including reduced cerebellar size (Pramatarova

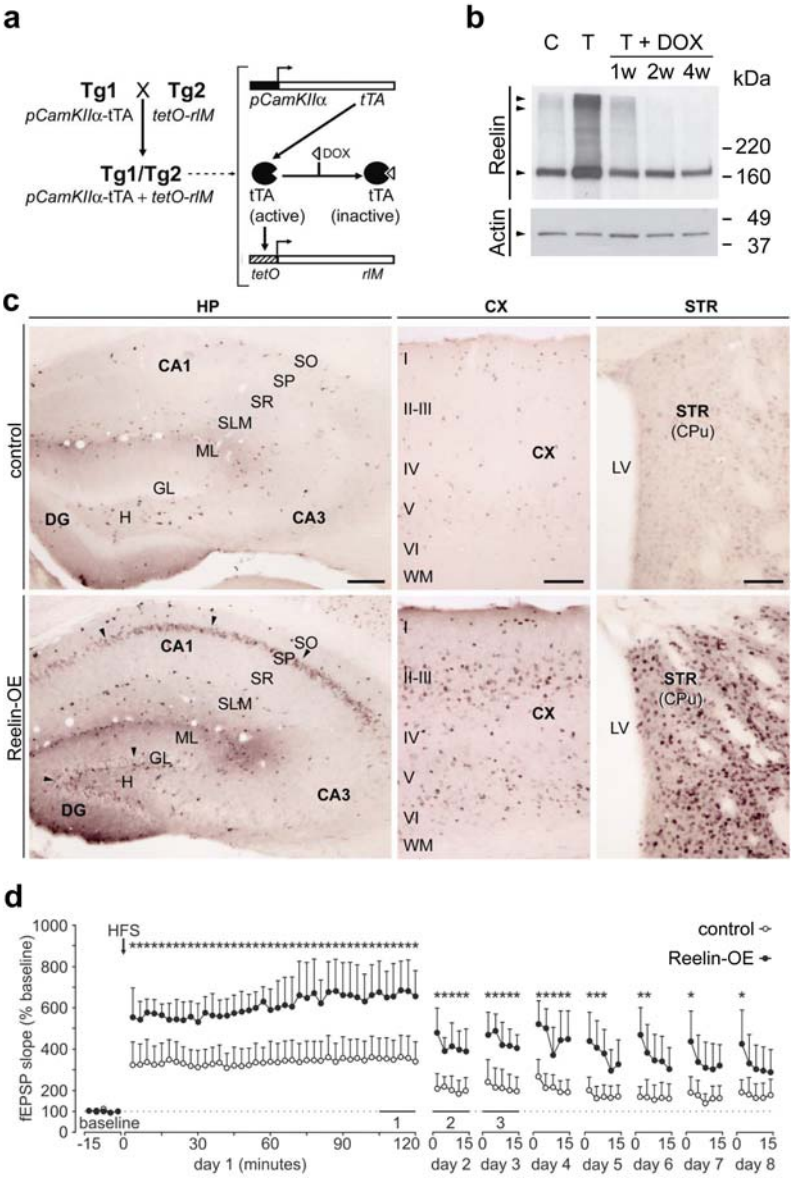

Figure i.3.5 Reelin-OE mice as a model for adult-specific Reelin gain of function studies.
(**a**)Transgenic mice that overexpress Reelin were based on the Tet-off regulated binary system: The first transgene (Tg1) contains the tTA transactivator set under the promoter *pCaMKIIα*, while the second transgene (Tg2) contains rlM controlled by the tetO promoter. Double transgenic mice (Tg1/Tg2) express Reelin in neurons expressing CaMKIIα. (**b**) One week of doxycycline administration to Reelin-OE mice (T + DOX) effectively abolishes the exogenous levels of Reelin protein in homogenates from striatum. (**c**) Exogenous Reelin is expressed in hippocampal pyramidal cells and granule cells of the dentate gyrus (arrowheads, bottom left panel), in neocortical pyramidal cells (bottom middle) and in striatal neurons (bottom right). (**d**) Reelin-OE mice exhibit enhanced *in vivo* hippocampal LTP responses to HFS stimulus (arrow) that last for several days. Scale bars: left, 200 μm; middle and right, 100 μm. Abbreviations: *C*, control; *T*, Reelin-OE mice; *DOX*, doxycycline; *HP*, hippocampus; *CX*, cortex; *STR*, striatum; *H*, hilus; *GL*, granule layer; *ML*, molecular layer; *SLM*, stratum lacunosum-moleculare; *SR*, stratum radiatum; *SP*, stratum pyramidale; *SO*, stratum oriens; *WM*, white matter; *LV*, lateral ventricle; *CPu*, caudate-putamen nucleus; *HFS*, high frequency stimulus. Adapted from (Pujadas et al., 2010).

et al., 2008), ectopic pyramidal cells in hippocampal CA1 and CA3, a mild disorganization of cortical layer II especially evident in the cingulate, retrosplenial, entorhinal and piriform cortices and ectopic neurons in cortical layer I. In the other side, these mice exhibit normal cortical layering and layer width (**Fig. i.3.6c**) (Teixeira et al., 2014). This mouse line exhibits some schizophrenia-like behavioral phenotypes that are exacerbated by factors associated with increased risks, such as a lowered pre-pulse inhibition after chronic stress induced by corticosterone, or enhanced hyperlocomotion upon cocaine administration.

When crossing this mouse line with an Ubiquitous CreER^{T2} mouse line (strain B6.Cg-Tg(UBC-cre/ESR1)1Ejb/J) the resulting model (Cre/flDab1) allows removal of Dab1 expression upon tamoxifen

(TAM) administration (**Fig. i.3.6a-b**). The cell mispositioning defects observed in the flDab1 are not further influenced by adult long-term inactivation of Dab1 (**Fig. i.3.6c**) (Teixeira et al., 2014).

Stereotaxic injection of Cre-GFP expressing retroviruses (Zhao et al., 2006) to the DG of adult flDab1 mice allows for localized adult-born granule cell-specific shutdown of the responsiveness to the Reelin pathway (**Fig. i.3.6d**) (Teixeira et al., 2012). This approach allows for the identification of adult new-born granule cells of a determined age, and therefore permits a developmental time course analysis of the integration of these cells into the preexisting circuitry, and the role of Reelin in this process. Moreover, Dab1-defective adult-born granule cells display abnormal branching pattern and the appearance of basal dendritic processes in the hilus that receive ectopic synapses and therefore generate abnormal reverberant circuitries.

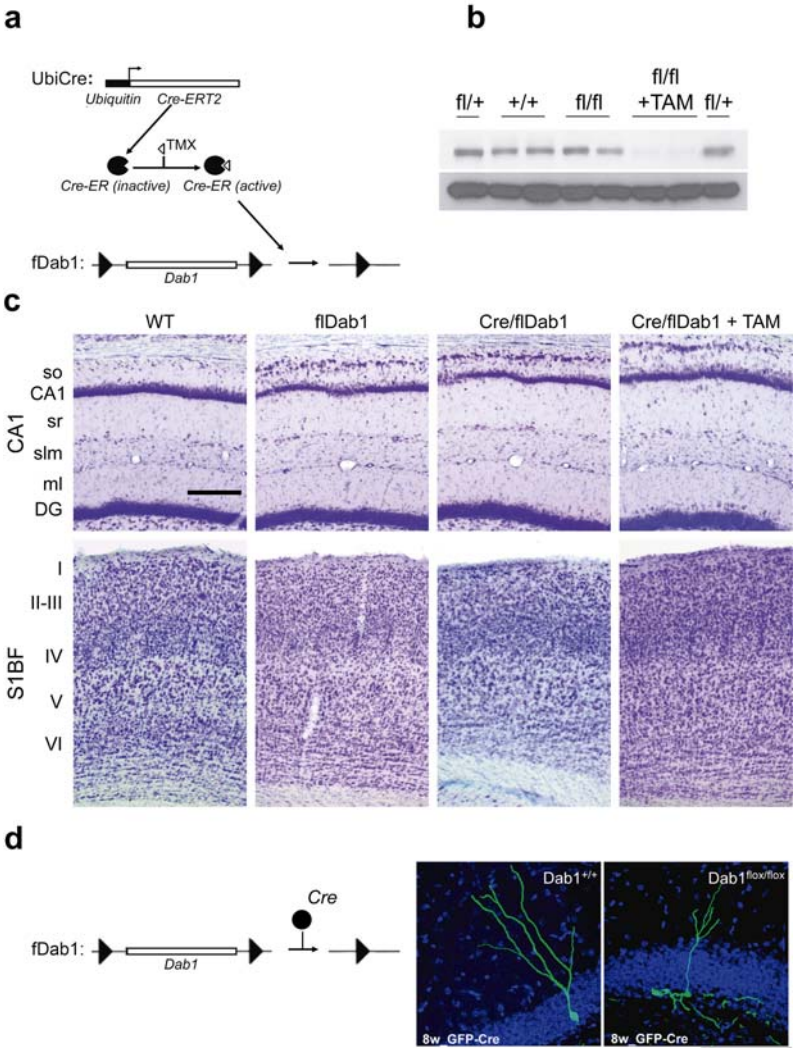

Figure i.3.6 Mouse models derived from the flDab1 line permitting the conditional deletion of Dab1.
(**a**-**c**) Ubiquitous conditional deletion of the *dab1* gene was attained by crossing the floxed Dab1 (flDab1) mouse line with a mouse line expressing a modified Cre recombinase under the ubiquitin promoter (UbiCre) (**a**). This construction expresses a functionally inactive form of Cre. Administration of Tamoxifen (TAM) triggers activation of the recombinase, thereby inducing the deletion of the floxed gene and therefore its expression (**b**). (**c**), flDab1 mice experience a transient downregulation of Dab1 expression at early postnatal stages, leading to localized abnormalities in cell positioning. Besides, overall layering is conserved in these mice, and these phenotypes are not worsened upon inactivation of the *dab1* gene. (**d**), infection of flDab1 mice dentate gyrus new-born granule cells with modified retroviruses expressing Cre recombinase allows for the generation of cell-specific depletion of the *dab1* gene. These cells exhibit alterations in their development, such as the appearance of basal processes in the hilar region which receive functional, aberrant synaptic contacts. Scale bar is 250 µm. Abbreviations: *fl*, *flox*, flDab1; +, wild allele; *DG*, dentate gyrus; *ml*, molecular layer; *slm*, stratum lacunosum-moleculare; *sr*, stratum radiatum; *CA1*, CA1 pyramidal layer; *so*, stratum oriens; *S1BF*, somatosensory cortex 1 – barrel field; *I-VI*, cortical layers 1-6. (**b**, **d**) adapted from (Teixeira et al., 2012); (**c**) adapted from (Teixeira et al., 2014).

In sum, flDab1 mice represent a versatile loss-of-function tool to evaluate adult role of Reelin pathway, as well as to analyze the effects of a transient downregulation of its signaling.

Altogether, these mouse models have provided precise useful resources to study the role of Reelin in the establishment and maintenance of synapses in the adult brain. These questions frame the goals we wished to solve in the present work.

Aims of the study

The goal of this study is to investigate the role of Reelin in synaptic plasticity processes in the adult brain, involving spine and synapse formation and stabilization. To this end, we established the following aims of the study:

1. Role of Reelin in the synaptic ultrastructural and molecular features of the adult hippocampus

1.1 Analysis of the ultrastructural morphology and molecular biology of presynaptic boutons in the adult hippocampus in Reelin-OE mice

1.2 Analysis of the ultrastructural morphology and molecular biology of postsynaptic spines in the adult hippocampus in Reelin-OE mice

2. Role of Reelin in the genesis and growth of dendritic spines in pyramidal cells

2.1 Characterization of the dendritic spines of hippocampal CA1 and S1BF pyramidal cells in Reelin-OE mice

2.2 Characterization of the dendritic spines of hippocampal CA1 and S1BF pyramidal cells in Cre/flDab1 mice

3. Role of Reelin in the synaptic integration process undergone by dentate gyrus (DG) new-born granule cells in the adult hippocampus

3.1 Setup of a reliable, high-throughput method for correlative optical microscopy (OM) – focused ion beam scanning electron microscopy (FIB/SEM) imaging of pre-labeled dendrites.

3.2 Analyisis of the presynaptic connectivity and ultrastructural morphology of dendritic spines in developing DG new-born granule cells.

3.3 Analysis of the presynaptic connectivity and ultrastructural morphology of dendritic spines in Reelin-OE and Dab1-KO developing DG new-born granule cells.

Results

1. Role of Reelin in the presynaptic connectivity of the adult hippocampus

Reelin over-expression modulates the structural complexity of presynaptic elements

Reelin protein has been proposed as a regulator of hippocampal synaptic plasticity. More specifically, Reelin has been reported to exert a physiological function (Pujadas et al., 2010; Rogers et al., 2011; Rogers et al., 2013) as well as structural one (Niu et al., 2008).

To address whether the presynaptic ultrastructure of the hippocampal circuitry was altered, we first performed an electron microscope study of the hippocampus of Reelin-Overexpressing (Reelin-OE) adult mice. Also, to confirm that the phenotypes were caused by the transgene expression, a second control group of Reelin-OE mice treated with doxycycline for 1 week before being killed was present in all tests performed (**Fig. r.1.1a**). This treatment was previously proven to be sufficient to return Reelin protein levels to normal values (Pujadas et al., 2010).

We found an increase in the density of synaptic terminals establishing excitatory synapses in each hippocampal layer (**Fig. r.1.1b**). A morphometric analysis revealed that those terminals were larger in all hippocampal layers (**Fig. r.1.1d**) and a less circular in strata radiatum and oriens (**Fig. r.1.1.e**). Furthermore, the numbers of axon terminals that established two or more synaptic contacts were increased in all hippocampal layers in Reelin-OE mice compared to control littermates (**Fig. r.1.1c**). Finally we found that excitatory synaptic contacts were longer in stratum lacunosum-moleculare of Reelin-OE mice (**Fig. r.1.1f**).

All the phenotypes observed were found to be completely reversed in the doxycycline-treated mice. In some cases, DOX-treated animals showed phenotype reversion even when Reelin-OE mice exhibited only a trend (circularity in mml-oml-slm and contact length in mml-oml). Moreover, the density of synaptic terminals in DOX-treated mice (in layers iml-mml-oml) was even lower than WT values.
Thus, presynaptic terminal ultrastructure appeared to be more complex in the hippocampus of Reelin-OE mice, and an increased density of terminals was also found, while transgene inactivation reversed all the phenotypes observed.

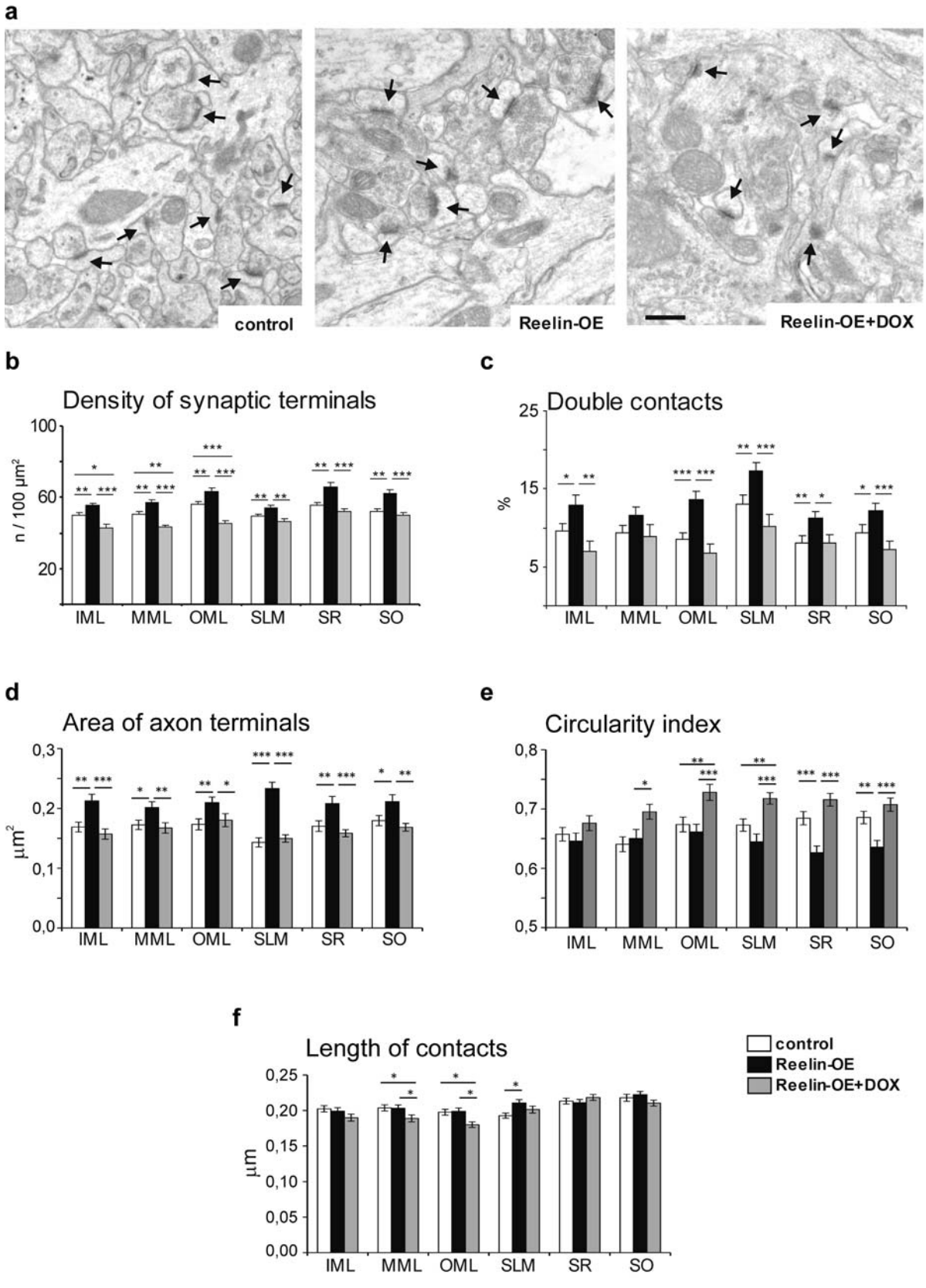
a
control
Reelin-OE
Reelin-OE+DOX
b
Density of synaptic terminals
n / 100 µm²
100
60
20
IML
MML
OML
SLM
SR
SO
c
Double contacts
%
25
15
5
d
Area of axon terminals
µm²
0,3
0,2
0,1
0,0
e
Circularity index
0,8
0,7
0,6
0,5
f
Length of contacts
µm
0,25
0,20
0,15
0,10
0,05
0,00
control
Reelin-OE
Reelin-OE+DOX

Figure r.1.1 Reelin overexpression *in vivo* triggers presynaptic hypertrophy and increased connectivity in the hippocampus.
(**a**) Electron micrographs illustrating axon terminals establishing synaptic contacts (arrows) in the inner molecular layer of control, Reelin-OE, and DOX-treated Reelin-OE mice. (**b**-**c**) Density of synaptic contacts (**b**) and percentage of synaptic terminals establishing at least two contacts (**c**). (**d**-**f**) Histograms depicting bouton's area (**d**) and circularity index (**e**) and the length of synaptic contact (**f**) in different hippocampal layers in control, Reelin-OE and DOX-treated Reelin-OE mice (mean ± SEM; *p < 0.05; **p < 0.01; ***p < 0.001; Student's t test). Scale bar in (**a**) is 0.5 μm. Abbreviations: *IML*, inner molecular layer; *MML*, medial molecular layer, *OML*, outer molecular layer; *SLM*, stratum lacunosum-moleculare; *SR*, stratum radiatum; *SO*, stratum oriens.

Presynaptic proteins in Reelin-OE mice: Synapsin and SNAP25.

We next sought to determine the extent to which the overexpression of Reelin contributes to modify the protein trafficking to the axon terminal. Synaptosomal enrichments from adult mice hippocampi were performed and tested for levels of presynaptic proteins of interest by immunoblot assays. Levels of protein expression remained stable across different groups when we analyzed synapsin 2a and 2b (**Fig. r.1.2a**) and SNAP-25 (**Fig. r.1.2b**).

We performed immunohistochemical assays to assess local changes in hippocampal layer distribution of these proteins. Histological analysis of immunoreactivity revealed identical distribution in Reelin-OE mice compared to control littermates for both synapsin (**Fig. r.1.2c**) and SNAP-25 (**Fig. r.1.2d**).
In sum, presynaptic proteins synapsin and SNAP25 did not suffer evident changes in terms of expression pattern across hippocampal layers and protein levels in the synaptosomsal compartment under Reelin overexpression *in vivo*.

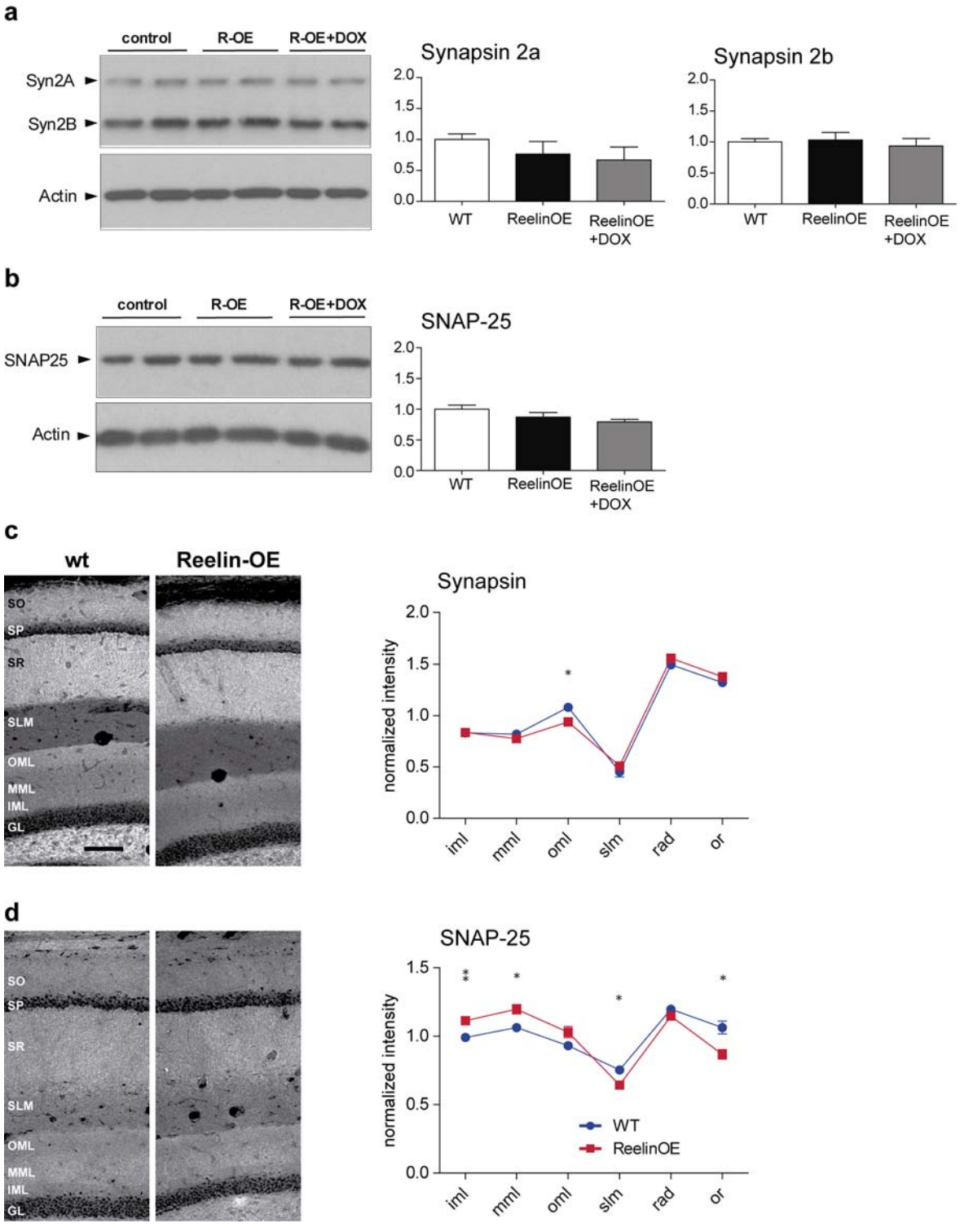

Figure r.1.2 Expression of presynaptic proteins synapsin and SNAP-25 is not altered in the hippocampus of Reelin-OE mice.

(**a**) Western-blot analysis of isoforms a and b of synapsin 2 in synaptosomal fractions of the hippocampus, and the respective quantifications. (**b**) Western-blot analysis and quantification of SNAP-25 protein levels in syn-

aptosomal fractions of the hippocampus. Data corresponds to band intensity normalized to its correspondent actin signal, and are expressed as the average fold change respect to values found in control mice. (**c**-**d**) Immunolabeling for synapsin (**c**) and SNAP-25 (**d**) in hippocampal sections of control, Reelin-OE and DOX-treated Reelin-OE mice. Normalized mean signal recordings from both proteins at the different hippocampal layers are shown at the right. (mean ± SEM; *p < 0.05; **p < 0.01; ***p < 0.001; Student's t test). Scale bar in (**c**) is 100 μm. Abbreviations: *R-OE*, Reelin-OE; *GL*, granule cell layer; *IML*, inner molecular layer; *MML*, medial molecular layer, *OML*, outer molecular layer; *SLM*, stratum lacunosum-moleculare; *SR*, stratum radiatum; *SP*, stratum pyramidale; *SO*, stratum oriens.

2. Role of Reelin in the postsynaptic connectivity of the adult hippocampus

Reelin over-expression triggers dendritic spine hypertrophy

Dendritic spines are the postsynaptic structure of most excitatory synapses in the brain (Colonnier, 1968). We performed a detailed fine electron microscopy analysis of these structures in the hippocampus of both Reelin-OE mice and Doxycycline-treated Reelin-OE mice to validate the specificity of the phenotypes to the transgene expression (**Fig. r.2.1a**).

Spine density was found to be unaltered in Reelin-OE mice in all hippocampal layers (**Fig. r.2.1b**). However, DOX treatment was associated with a spine loss in most layers, similar to what was observed previously in the presynaptic compartment. We next analyzed the morphology of these spines, and we observed that spines appeared to be larger in most of the hippocampal layers in Reelin-OE mice compared to control mice (**Fig. r.2.1a**). Furthermore, those Reelin-OE mice that were treated with DOX showed spines with a similar size than control ones. To substantiate these observations, we performed a morphometric study of dendritic spines in all the hippocampal layers (**Fig. r.2.1c-d**). We observed that dendritic spines were significantly larger in most layers of Reelin-OE mice compared to their control littermates, and differences were higher in those layers that receive entorhinal inputs, i.e. the medial and outer molecular layers and the stratum-lacunosum moleculare (27%-35% of difference) (**Fig. r.2.1c**). Furthermore, the circularity index of dendritic spines, which reflects their complexity, was significantly lower in all the hippocampal layers of Reelin-OE mice (3%-7%) compared to their control littermates (**Fig. r.2.1d**). In both the area and circularity index analysis, dendritic spines in Reelin-OE mice treated with DOX showed no significant differences with those analyzed in control mice.

Dendritic spine shapes are associated to spine function and plasticity. We thus analyzed the morphology of hippocampal dendritic spines in Reelin-OE mice. The most widely used nomenclature to distinguish the morphological diversity of dendritic spines is based on the relative sizes of the spine head and neck (Peters and Kaiserman-Abramof, 1970; Harris et al., 1992; Bourne and Harris, 2008). Following these criteria, dendritic spines are divided in thin, stubby and mushroom types. However, this classification requires fully-imaged dendritic spines. Since our analysis was based on single-section EM micrographs, we implemented new spine classification criteria based on the curvature of the PSD, suitable

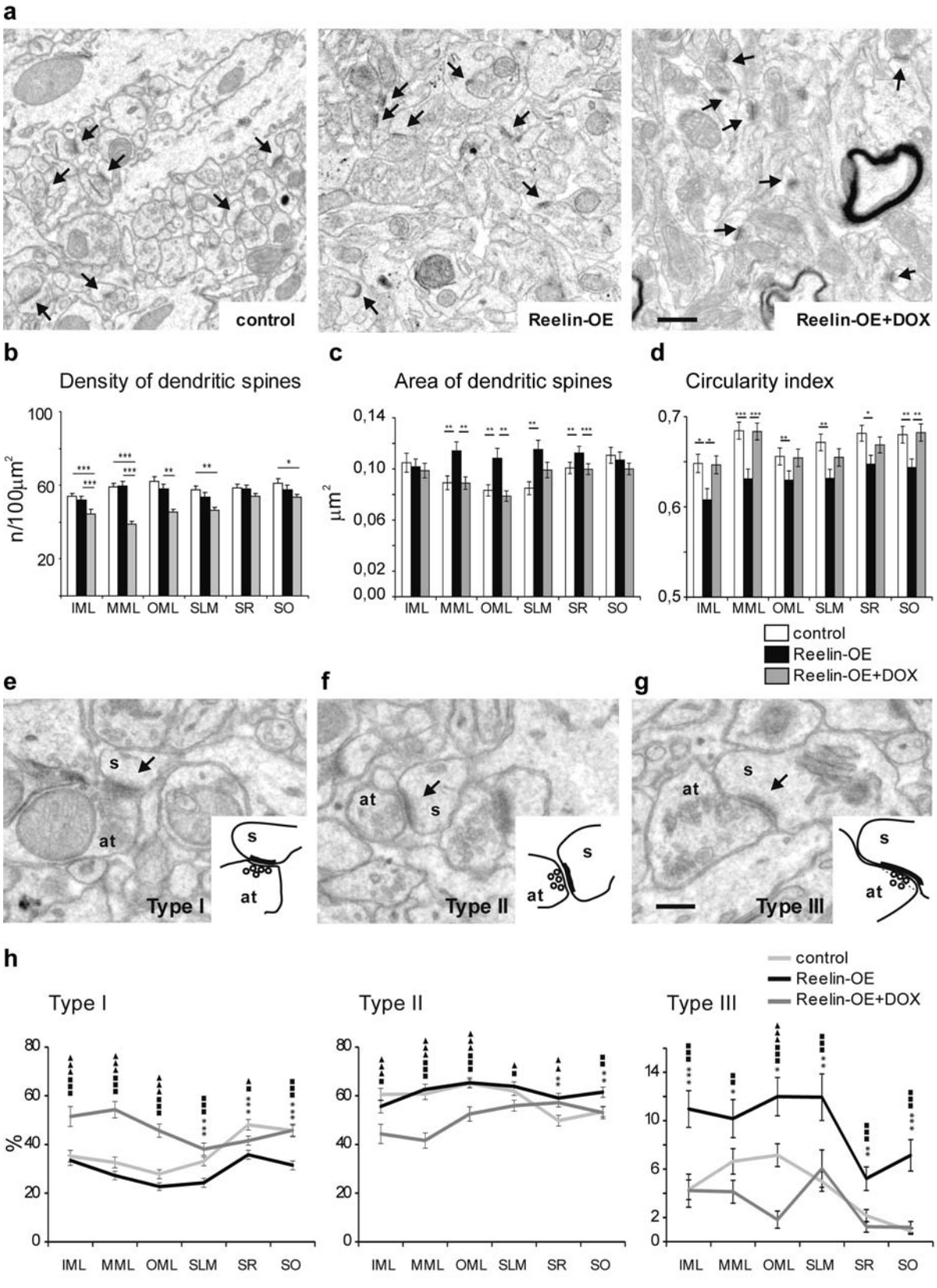
a
control
Reelin-OE
Reelin-OE+DOX
b
Density of dendritic spines
n/100µm²
100
60
20
IML MML OML SLM SR SO
c
Area of dendritic spines
µm²
0,14
0,10
0,06
0,02
0,00
IML MML OML SLM SR SO
d
Circularity index
0,7
0,6
0,5
IML MML OML SLM SR SO
control
Reelin-OE
Reelin-OE+DOX
e
s
at
Type I
f
at
s
Type II
g
at
s
Type III
h
Type I
Type II
Type III
%
80
60
40
20
0
14
10
6
2
IML MML OML SLM SR SO
control
Reelin-OE
Reelin-OE+DOX

for working with incomplete spines. We divided spines into type I, which showed a convex PSD (**Fig. r.2.1e**); type II, which showed a straight or weakly concave PSD (**Fig. r.2.1f**); and type III, which showed a PSD with a sufficiently concave curvature to fit an area of the pre-synaptic bouton large enough to accommodate an entire synaptic vesicle (**Fig. r.2.1g**). Following this nomenclature, we observed that, although only some layers showed significant differences in the percentage of types I and II, the number of type III dendritic spines was higher in all the hippocampal layers of Reelin-OE mice (from 1.5 to 8.2 folds) compared to those found in their control littermates. Moreover, the percentage of this type of spines was mainly reverted to control levels by administration of DOX (**Fig. r.2.1h**).

Altogether, these findings indicate that Reelin increases the structural complexity of postsynaptic elements and therefore their synaptic efficacy, while maintaining spine density constant.

Reelin modulates the complexity of spine apparatus in a lamina-specific manner

The spine apparatus (SA) (**Fig. r.2.2a**) is a specialized form of endoplasmic reticulum composed of stacks of smooth endoplasmic reticulum (Spacek and Harris, 1997). It is present in some dendritic spines in all hippocampal layers. Because it is suggested to play a role in spine plasticity (Jedlicka et al., 2008; Segal et al., 2010), we were interested in analyze possible changes in the density and morphology of this organelle in Reelin-OE mice. We observed an increase in the density of spines containing SA in the outer molecular layer of Reelin overexpressing mice. DOX treatment, in turn, induced a decrease in the remaining layers (**Fig. r.2.2b**). Moreover, when the area occupied by SA was analyzed we found that this organelle was significantly larger in medial and outer molecular layers and in the stratum lacunosum-moleculare of Reelin-OE mice compared to their control littermates (**Fig. r.2.2c**). DOX-treated Reelin-OE mice showed similar values to control ones.

We next analyzed the expression and distribution of the SA-associated protein synaptopodin. To determine whether Reelin-OE affected Synaptopodin expression in the hippocampus, we performed WB and IHC analyses in Reelin-OE mice. No significant differences were found in the levels of protein expression in hippocampal synaptosomal fractions assays (**Fig. r.2.2d-e**). On the other hand, immunohistochemical analysis showed alterations in the laminar distribution of synaptopodin in Reelin-OE mice (**Fig. r.2.2f-g, i**). In accordance with other studies (Bas Orth et al., 2005), control mice showed a highest expression of synaptopodin in dentate molecular layers. However, Reelin-OE mice showed higher expression in stratum lacunosum-moleculare than any other layers. After treatment with DOX, Reelin-OE hippocampus showed no clear layer-specific differences in synaptopodin expression (**Fig. r.2.2h, i**).

Figure r.2.1 Reelin overexpression *in vivo* triggers postsynaptic hypertrophy in the hippocampus.
(**a**) Electron micrographs illustrating dendritic spines receiving synaptic inputs (arrows) in the inner molecular layer of control, Reelin-OE and DOX-treated Reelin-OE mice. (**b**-**d**) Histograms showing density (**b**), area (**c**) and circularity index (**d**) of dendritic spines in different hippocampal layers in control, Reelin-OE and DOX-treated Reelin-OE mice (mean ± SEM; *p < 0.05; **p < 0.01; ***p < 0.001; Student's t test). (**e**-**g**) Electron micrographs showing three types of defined dendritic spines depending on PSD curvature (see text): type I (**e**), type II (**f**) and type III (**g**), as illustrated on the bottom left insets in each photograph. (**h**) Histogram illustrating the percentage of the distinct types of dendritic spines in all the hippocampal layers in control, Reelin-OE, and DOX-treated Reelin-OE mice (mean ± SEM; *p < 0.05; **p < 0.01; ***p < 0.001 for control vs. Reelin-OE mice; squares for Reelin-OE vs. Reelin-OE+DOX; triangles for control vs. Reelin-OE+DOX mice; Student's t test). Scale bars: 500 nm in (**a**); 200 nm in (**e**-**g**). Abbreviations: *IML*, inner molecular layer; *MML*, medial molecular layer, *OML*, outer molecular layer; *SLM*, stratum lacunosum-moleculare; *SR*, stratum radiatum; *SO*, stratum oriens.

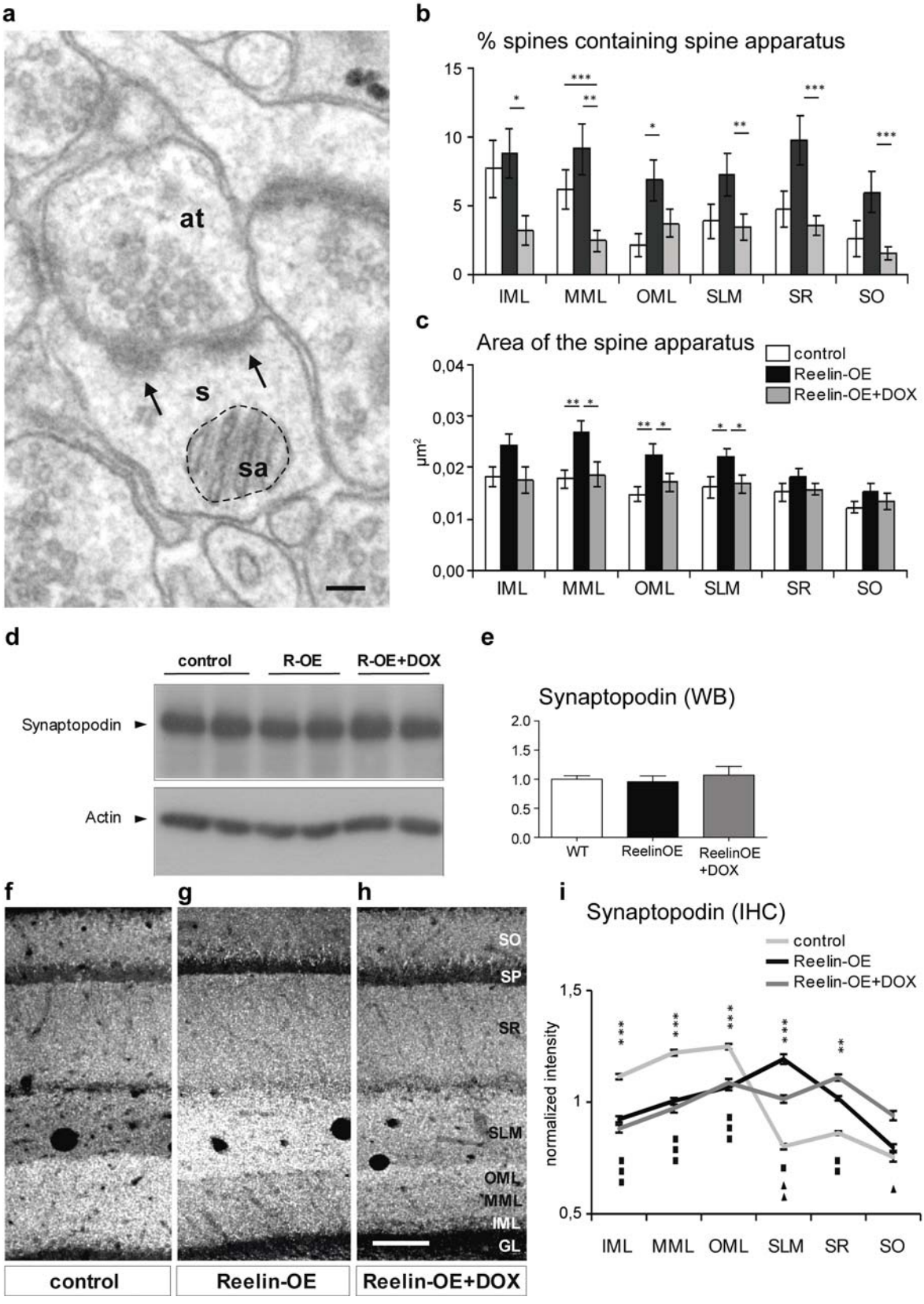
a
at
s
sa
b
% spines containing spine apparatus
15
10
5
0
IML
MML
OML
SLM
SR
SO
c
Area of the spine apparatus
control
Reelin-OE
Reelin-OE+DOX
µm²
0,04
0,03
0,02
0,01
0,00
d
control
R-OE
R-OE+DOX
Synaptopodin
Actin
e
Synaptopodin (WB)
2.0
1.5
1.0
0.5
0.0
WT
ReelinOE
ReelinOE +DOX
f
g
h
SO
SP
SR
SLM
OML
MML
IML
GL
control
Reelin-OE
Reelin-OE+DOX
i
Synaptopodin (IHC)
control
Reelin-OE
Reelin-OE+DOX
normalized intensity
1,5
1
0,5
IML
MML
OML
SLM
SR
SO

Taken together, these results demonstrate that Reelin overexpression is promoting a higher complexity of spine apparatus and a redistribution of the expression of synaptopodin in the hippocampus.

Reelin regulates the distribution of synaptic NMDA receptors

As mentioned above, we observed that protein expression in synaptic terminals was not altered by an increase of Reelin in the hippocampus. In order to evaluate whether molecular composition of post-synaptic elements was altered in Reelin-overexpressing mice, WB analyses were performed from synaptosomal fractions of the hippocampus. Thus, we analyzed the protein levels of glutamate receptors (GluR1, GluR2/3, GluN1, NR2a, NR2b), scaffolding proteins (PSD-95) and downstream proteins (CaMKII, cofilin, p-cofilin, LIMK and P-LIMK) (**Figs. r.2.3**, **r.2.4a-b**, **r.2.5a**). Among all these cases, only the expression of LIMK (**Fig. r.2.3f**) was significantly higher in Reelin-overexpressing mice compared to control littermates.

Because of Reelin expression is linked to surface mobility of NMDA receptors *in vitro* (Groc et al., 2007), we were interested to elucidate whether Reelin influences distribution of these receptors *in vivo*. Thus, immunogold assays were performed using antibodies against NR2A and NR2B and their distribution was analyzed in the stratum radiatum. Distribution of NR2A-gold dots was altered in Reelin-OE mice (**Fig. r.2.4c-e**). Thus, while 90% of dots were found within PSD in control spines, Reelin-overexpressing spines showed a 70% of dots within synaptic contact, a 19% in non-synaptic membrane and 11% inside the spine (**Fig. r.2.4i**). Similarly, immunogold assays against NR2B in control, Reelin-OE and DOX-treated Reelin-OE mice (**Fig. r.2.4f-h**) showed that the percentage of extrasynaptic dots was higher in Reelin-OE than control spines (**Fig. r.2.4j**).

Finally, since it has been reported that phosphorylation of cofilin, an F-actin severing protein, promotes stabilization of mature dendritic spines and is regulated by Reelin (Chai et al., 2009; Shi et al., 2009; Kruger et al., 2010), we tested its distribution in dendritic spines of stratum radiatum in control and Reelin-OE mice. Immunogold staining against p-cofilin (**Fig. r.2.5c-e**) showed that the percentage of the expression of this protein was higher in non-synaptic regions in Reelin-OE mice when compared to their control littermates (**Fig. r.2.5f**). In NR2B and p-cofilin, the effects were mainly reverted in those transgenic mice to which DOX was administrated (**Figs. r.2.4j**, **r.2.5f**).

Figure r.2.2 Spine apparatus and synaptopodin in dendritic spines of Reelin-OE mice.
(**a**) Electron micrograph of dendritic spines (s) containing a spine apparatus (sa) receiving two synaptic contacts (arrows) from an axon terminal (at). Dashed-line circle represents an example of the area of spine apparatus used to perform analysis in (**c**). (**b**-**c**) Histograms illustrating the percentage of dendritic spines containing spine apparatus (**b**) and the area of these organelles (**c**) in distinct hippocampal layers of control, Reelin-OE, and DOX-treated Reelin-OE mice (mean ± SEM; *p < 0.05; **p < 0.01; ***p < 0.001; Student's t test). (**d**) Immunoblot analysis of synaptopodin in Reelin-OE, DOX-treated Reelin-OE mice and control littermates. (**e**) Histogram showing WB quantifications (n=3 blots) represented as average fold change relative to control group after normalization to actin signal. (**f**-**h**) Immunolabeling for synaptopodin in hippocampal sections of control, Reelin-OE, and DOX-treated Reelin-OE mice. (**i**) Quantitative determination of immunoreactivity to synaptopodin in the different hippocampal layers of control, Reelin-OE, and Reelin-OE+DOX mice (mean ± SEM; *p < 0.05; **p < 0.01; ***p < 0.001 for control vs. Reelin-OE mice; squares for Reelin-OE vs. Reelin-OE+DOX; triangles for control vs. Reelin-OE+DOX mice; Student's t test). Scale bars: 100nm in (**a**); 100μm in (**f**-**g**). Abbreviations: *IHC*, immunohistochemistry; *IML*, inner molecular layer; *MML*, medial molecular layer; *OML*, outer molecular layer; *SLM*, stratum lacunosum-moleculare; *SR*, stratum radiatum; *SO*, stratum oriens; *R-OE*, Reelin-OE; *WB*, western blot.

These results show that Reelin is involved in Glu receptor plasticity by regulating the distribution of NMDA receptor subunits inside the spine.

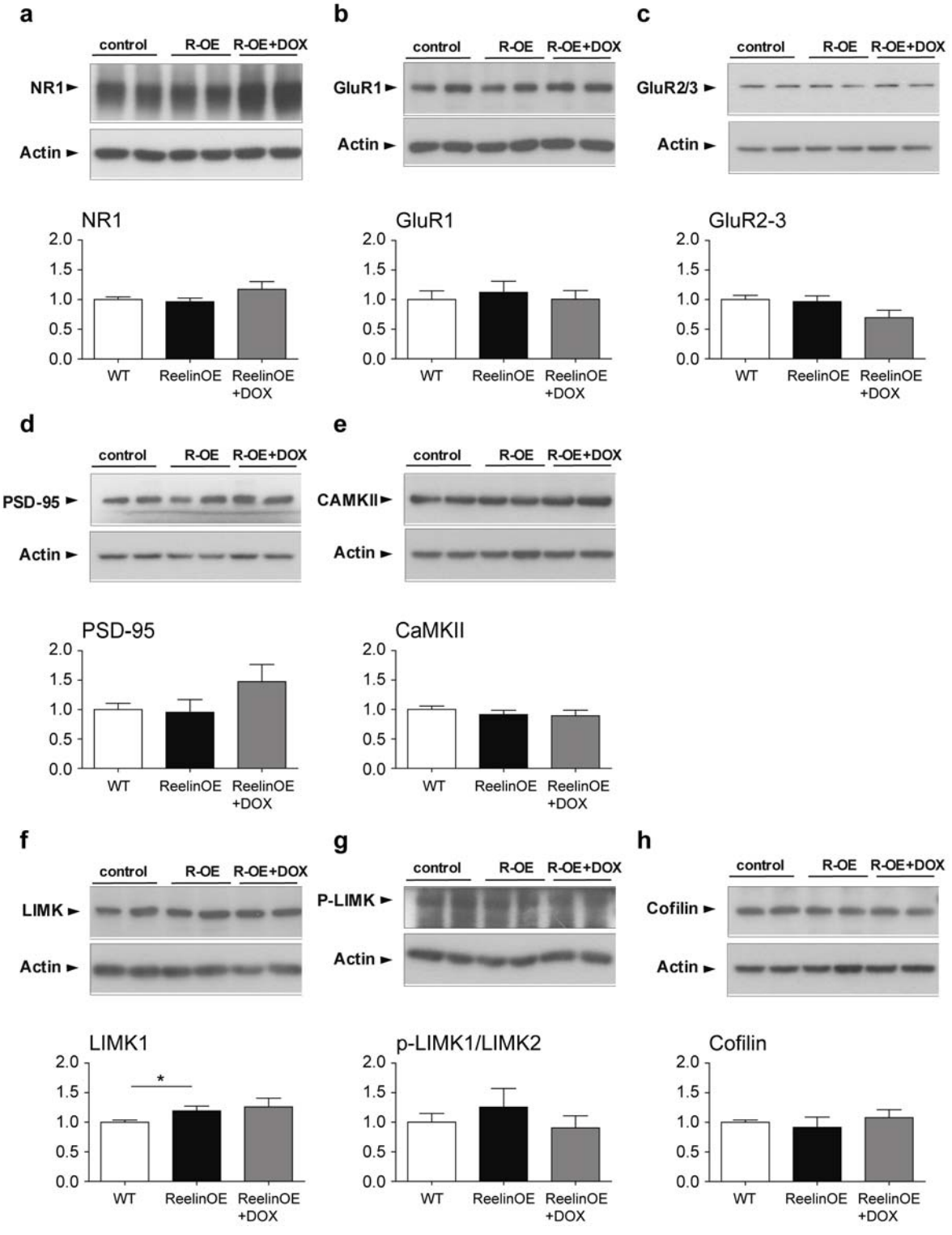

Reconstructions of apical dendrites from CA1 pyramidal cells evidence spine hypertrophy in Reelin-OE mice

In order to visualize the morphological phenotypes described in the previous experiments, a fine reconstruction was performed of a segment of apical dendrites from CA1 pyramidal cells in the stratum radiatum.

Serial-section TEM micrographs were obtained from Reelin-OE mice and control littermates. Manual segmentation and 3D rendering of the dendrite was driven with Reconstruct software. The randomly-chosen segments exhibited several phenotypes consistent with the analyses performed. Reelin-OE's dendrite exhibited larger and more complex mushroom-shaped spines, displaying in some cases extremely large heads of ~1μm in diameter, and often bearing two or more synaptic active zones, while most of the reconstructed dendritic spines in control mice were simple, bearing a thin-type appearance and a single synaptic contact (**Fig. r.2.6**).

These findings illustrate that Reelin overexpression leads to an enlargement and hypertrophy of dendritic spines, which is associated with complex and multiple synaptic junctions.

Altogether, hippocampal dendritic spines in mice overexpressing Reelin in the adulthood exhibited a more complex phenotype. Spines were found to be larger in size, with less compact morphologies, in almost all layers analyzed. Although global spine numbers remained unaltered, spines bearing a concave, invaginated PSD were 2-3 times more frequent, as well as spines bearing a spine apparatus. Moreover, spine apparatuses were larger in entorhinal-innervated layers, and its associated protein Synaptopodin exhibited an altered pattern of expression. Although protein levels of receptors remained unaltered in the spine, NMDA receptor subunits 2A and 2B were redistributed to extrasynaptic locations, similarly to what was observed to the actin severing protein p-cofilin. All these observations were supported with the appearance of ultrastructural reconstructions of apical dendritic segments of CA1 pyramidal cells. More interestingly, most of these phenotypes were fully or partially reverted to control values by the inactivation of transgene expression with Doxycycline administration.

Figure r.2.3 Western Blot analysis and quantification of distinct post-synaptic proteins.
(**a**-**g**) Immunoblot analysis and their corresponding quantifications of NR1 (**a**), GluR1 (**b**), GluR2-3 (**c**), PSD-95 (**d**), CaMKII (**e**), LIMK1 (**f**) and p-LIMK1/LIMK2 (**g**) from synaptosomal fractions of the hippocampus (n=3) in control, Reelin-OE and DOX-treated Reelin-OE mice. Data shown corresponds to average band density normalized with the respective actin, and is expressed as a fold change respect to control values (mean ± SEM; *$p < 0.05$; **$p < 0.01$; ***$p < 0.001$ for control vs. Reelin-OE mice; squares for Reelin-OE vs. Reelin-OE+DOX; triangles for control vs. Reelin-OE+DOX mice; Student's t test). Abbreviations: *R-OE*, Reelin-OE.

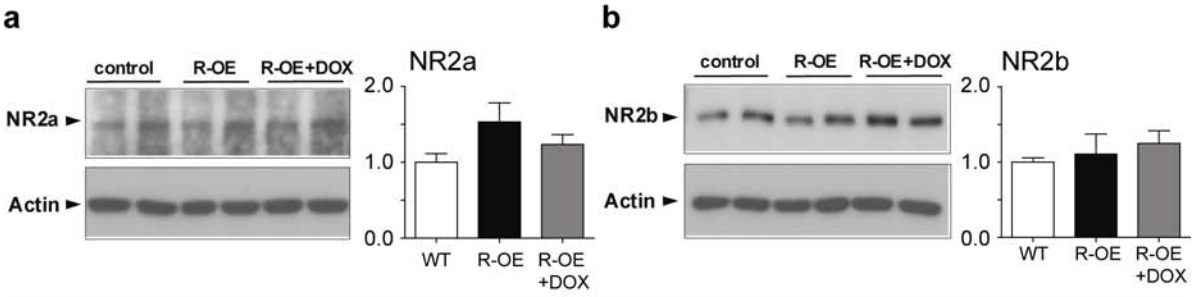
a
control
R-OE
R-OE+DOX
NR2a
Actin
NR2a
2.0
1.0
0.0
WT
R-OE
R-OE +DOX
b
control
R-OE
R-OE+DOX
NR2b
Actin
NR2b
2.0
1.0
0.0
WT
R-OE
R-OE +DOX

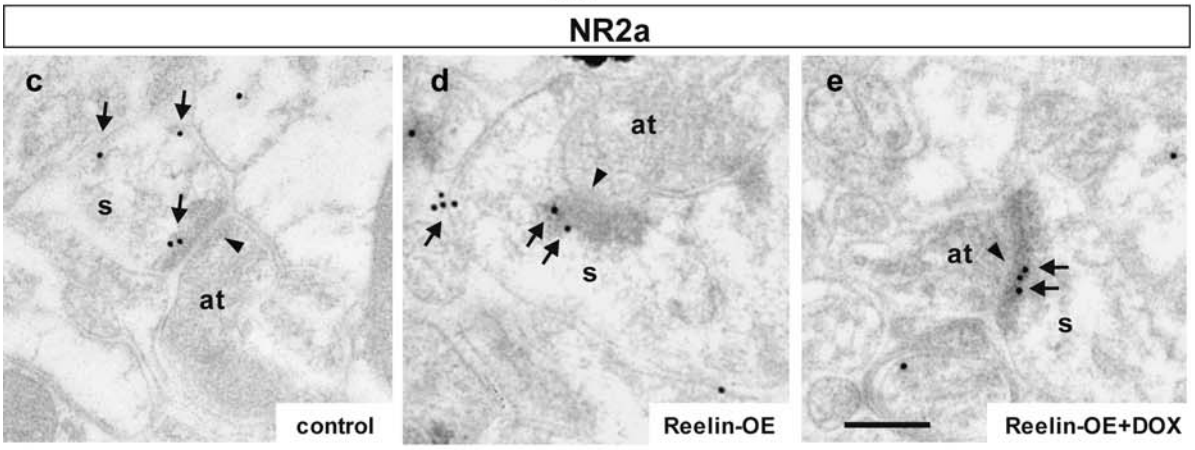
NR2a
c
s
at
control
d
at
s
Reelin-OE
e
at
s
Reelin-OE+DOX

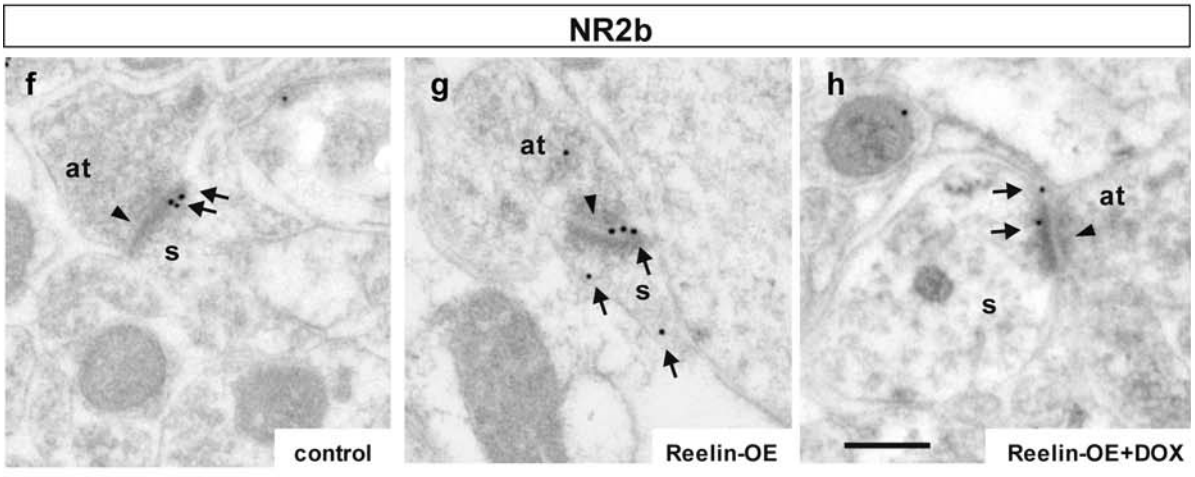
NR2b
f
at
s
control
g
at
s
Reelin-OE
h
at
s
Reelin-OE+DOX

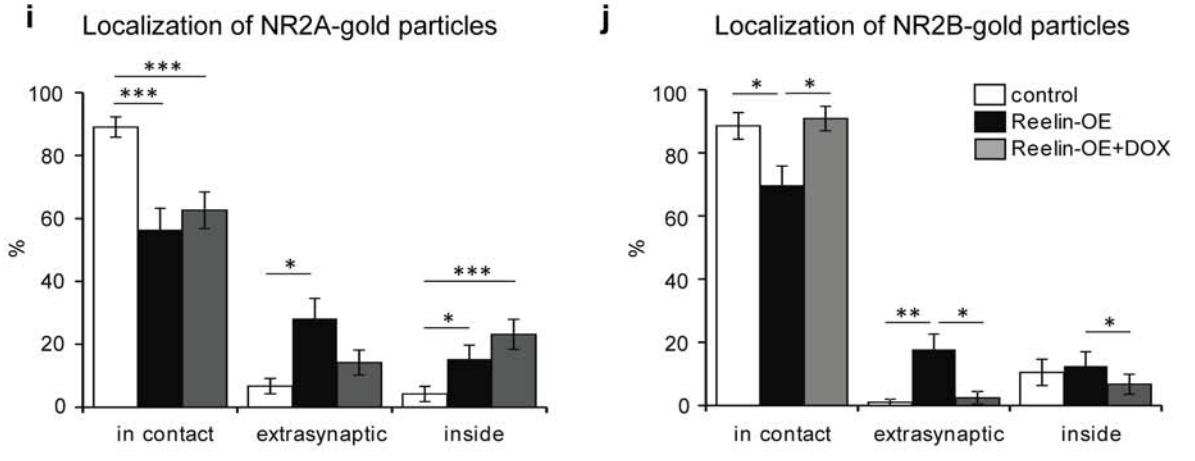
i
Localization of NR2A-gold particles
%
100
80
60
40
20
0
***
***
*
***
*
in contact
extrasynaptic
inside
j
Localization of NR2B-gold particles
control
Reelin-OE
Reelin-OE+DOX
%
100
80
60
40
20
0
*
*
**
*
*
in contact
extrasynaptic
inside

Figure r.2.4 Expression of NMDA receptor subunits NR2a and NR2b in Reelin-OE mice.
(**a**) Left, immunoblot analysis of NR2a in hippocampal synaptosomes from control, Reelin-OE, and DOX-treated Reelin-OE mice. Right, histogram showing densitometric analysis (n=4 animals per group, 3 blots). Results depict fold change respect to control values (mean ± SEM; *p < 0.05; Student's t test). (**b**) Left, immunoblot analysis of NR2b in hippocampal synaptosomes from control, Reelin-OE, and Reelin-OE+DOX mice. Right, histogram showing the respective quantifications. (**c**-**e**) Examples of immunogold labeling against NR2a in dendritic spines (s) receiving a synaptic contact from an axon terminal (at) in the stratum radiatum of control (**c**), Reelin-OE (**d**), and DOX-treated Reelin-OE (**e**) mice. (**f**-**h**) Examples of immunogold labeling against NR2b in dendritic spines (s) receiving a synaptic contact from an axon terminal (at) in the stratum radiatum of control (**f**), Reelin-OE (**g**), and DOX-treated Reelin-OE (**h**) mice. In (**c**-**h**), note synaptic contacts pointed by arrowheads and immunolabeling dots labeled by arrows. (**i**-**j**) Histogram shows the proportion of NR2a (**i**) and NR2b-gold particles (**j**) located at the synaptic contact, at the extrasynaptic membrane and in the intracellular domain of dendritic spines in the stratum radiatum of Reelin-OE and DOX-treated Reelin-OE mice and their control littermates. Scale bar is 250nm. Abbreviations: *R-OE*, Reelin-OE.

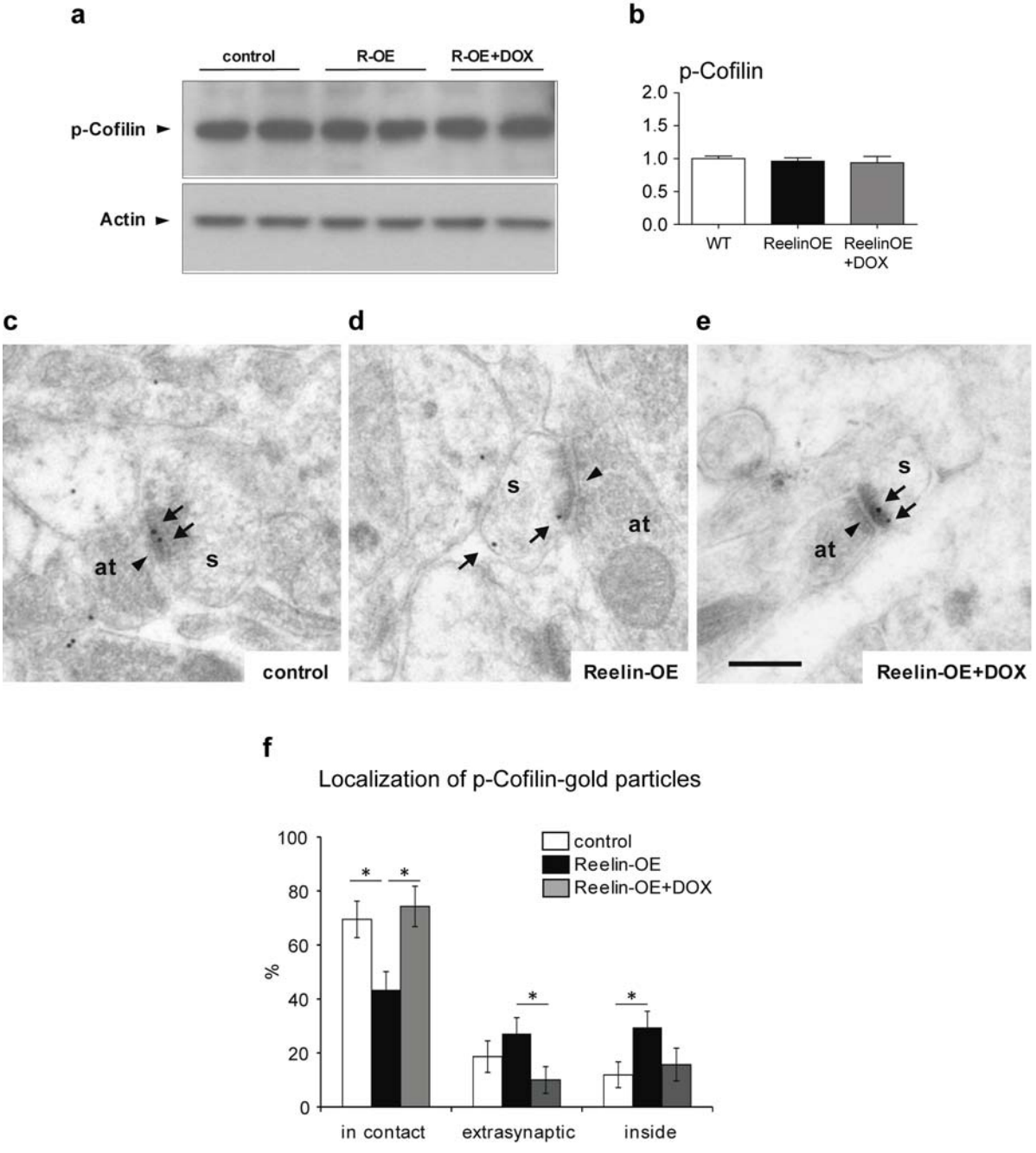

Figure r.2.5 Expression of p-cofilin in Reelin-OE mice.
(**a**-**b**) immunoblot analysis of p-Cofilin in control, Reelin-OE, and DOX-treated Reelin-OE mice (**a**) and histogram showing densitometric analysis (**b**) (n=4 animals per group, 3 blots). Results depict fold change respect to control values (mean ± SEM; *p < 0.05; Student's t test). (**c**-**e**) Examples of immunogold labeling against p-cofilin in dendritic spines (s) receiving a synaptic contact from an axon terminal (at) in the stratum radiatum of control (**c**), Reelin-OE (**d**), and DOX-treated Reelin-OE mice (**e**). Note synaptic contacts indicated by arrowheads and immunolabeling dots by arrows. (**f**) Histogram shows the proportion of p-cofilin-gold dots at the synaptic contact, at extrasynaptic membrane and in the intracellular domain of dendritic spines in the stratum radiatum of Reelin-OE and DOX-treated Reelin-OE mice and their control littermates. Scale bar is 250nm.

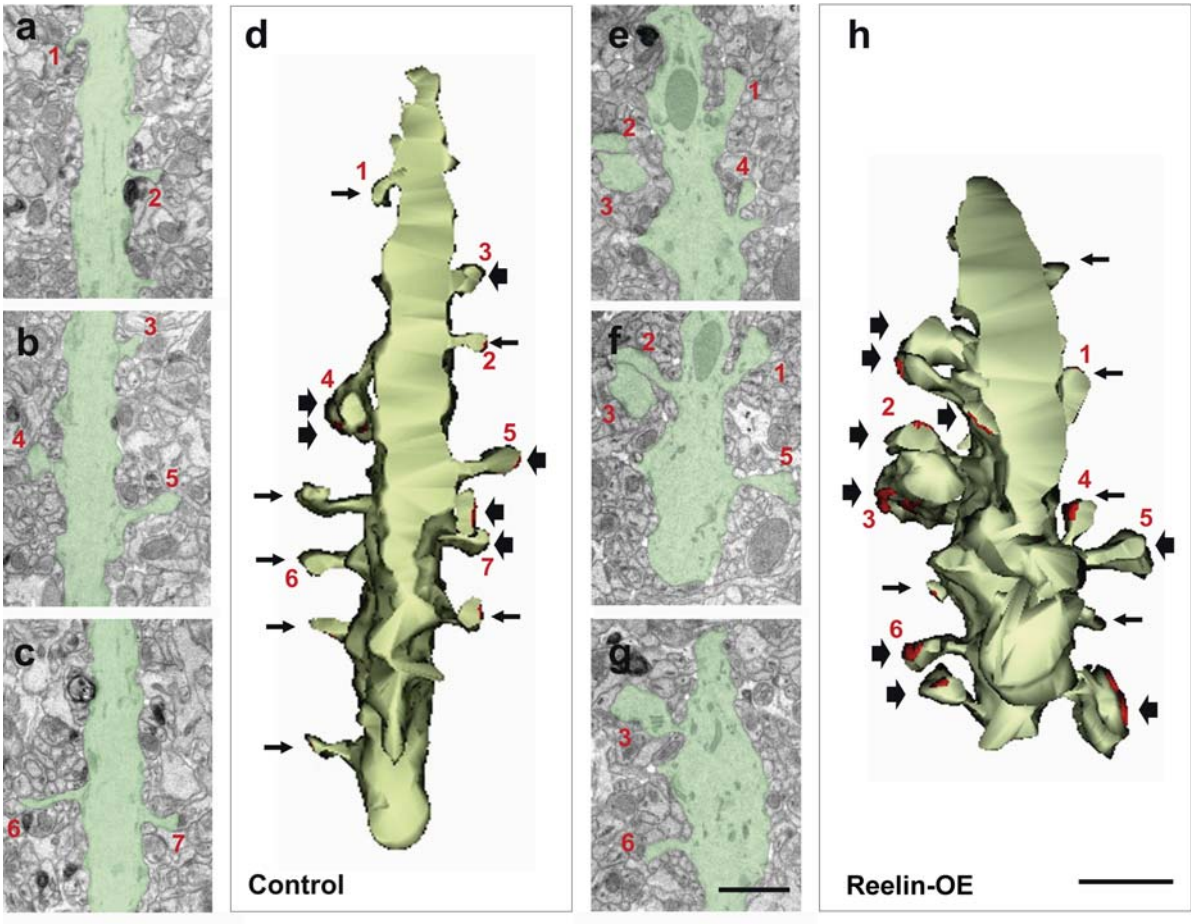

Figure r.2.6 3D reconstructions of dendrites in the stratum radiatum of the CA1 illustrate spine hypertrophy in Reelin-OE mice.

Reconstruction of dendrites of both a control (**a**-**d**) and a Reelin-OE mouse (**e**-**h**) was carried through a serial section electron microscopy approach. (**a**-**c**, **e**-**g**) Examples of serial electron micrographs in which the dendritic shaft and emerging spines have been colored in green; numbers point to examples of reconstructed dendritic spines in d and h. (**d**-**h**) Three-dimensional reconstructions of the identified dendritic segments shown in **a**-**c** and **e**-**g**; note the large hypertrophy of spines in **h**, compared to controls (**d**). Dendritic spine heads with sizes below and above 0,4 µm in diameter are represented by small and large arrows, respectively. Synaptic contacts are drawn in red. Dendritic spines in electron micrographs are labeled by numbers. Scale bar in (**g**) is 1 µm and is applicable to (**a**-**c**, **e**-**g**); scale bar in (**h**) is 1 µm and refers to (**d**, **h**).

3. Reelin signaling regulation of dendritic spines in pyramidal cells

Introduction to chapter 3: Pyramidal neurons in the neocortex

"¿Hay en nuestros parques algún árbol más elegante y frondoso que el corpúsculo de Purkinje del cerebelo ó la célula psíquica, es decir, la famosa pirámide cerebral?" (Cajal, 1917)

Pyramidal neurons represent the predominant neuronal type for excitatory signal transmission in many cortical regions, including the cerebral cortex, the hippocampus and the amygdala, while they are absent in some other areas, such as the olfactory bulb, the striatum, the midbrain, the hindbrain and the spinal cord (Cajal, 1904). These spiny cells are present in mammals, but also in birds, fish and reptiles, although not in amphibians (Benavides-Piccione et al., 2002; Elston, 2003). Therefore, this cell type evidences both an evolutionary conservation and a specific location to areas related to cognitive function, reinforcing the early idea of these cells as key players in high cognitive processes (Cajal, 1890, 1933).

Pyramidal cells exhibit a complex morphology characterized by two main dendritic domains, emerging from the base and apex of the soma respectively, and named in consequence as basal and apical dendritic trees. Both domains display large differences in length, complexity, spine distribution and branching patterns, strongly pointing to different signal integration dynamics and therefore distinct functions (Spruston, 2008). Whereas the basal tree is short and ramified, the apical tree displays two differentiated zones: it is first composed by a thick single trunk dendrite from which some thin oblique branches emerge. This proximal to soma apical dendrite further branches to give rise to a distal ramified dendritic tuft. Overall, this complex morphology conveys particular passive dendritic properties to different dendritic domains (Vetter et al., 2001; Major et al., 2013).

Pyramidal neurons are located in layered structures, and synaptic inputs received on different dendritic domains may come from different cortical regions. Indeed, basal and proximal apical dendrites receive local inputs, whereas the distal dendritic tuft becomes innervated by axons emitted by distant cortical and thalamic neurons (Binzegger et al., 2004; Izhikevich and Edelman, 2008). Due to passive dendritic attenuation properties, signal propagation for inputs on tuft dendrites is strongly reduced and spikes

generated in this region are not able to reach the soma by themselves. Interestingly, coincidence of tuft-received signals with back-propagating action potentials or dendritic depolarizations at more proximal regions allows distal signals to integrate and develop dendritic spikes. Therefore, pyramidal cell function could be to serve as a coincidence detector between distal activity registered at tuft dendrites and local activity received at proximal apical and basal dendrites (Jarsky et al., 2005; Spruston, 2008).

Moreover, different GABAergic interneurons innervate pyramidal cells at specific cellular domains, thereby modulating differently their synaptic integration properties. Basket cells establish multiple perisomatic synapses, and therefore influence the firing of the entire pyramidal cell (Freund and Buzsaki, 1996; Somogyi and Klausberger, 2005). In the other hand, hippocampal OLM cells or cortical Martinotti interneurons establish inhibitory synapses on the apical tuft, thus inhibiting the firing of distal apical synapses only (Silberberg and Markram, 2007). Interneurons might be activated in a feed-forward way, by the same afference that activates the pyramidal neuron, thus limiting the duration of the pyramidal neuron excitation state. Besides, they can be activated in a feedback manner, downstream of their target pyramidal neuron activation, thus limiting the sustained firing of the pyramidal neuron. In this case, two scenarios might be possible: If interneuronal activity is a quick, onset-transient, it might regulate pyramidal local afference activity and innervate it at the soma and proximal dendrites. Otherwise, a sustained late-persistent interneuronal activation occurs in interneurons innervating distal dendrites, and modulates the induction and propagation of Ca^{2+} spikes of the dendritic tuft (Spruston, 2008). Finally, interneuronal activity might also have an excitatory role, as is the case of Chandelier cells. Here, GABAergic innervation is driven to the initial axon segment, where it triggers membrane depolarization due to local Cl^- reversal potential, therefore playing a role in regulating the timing of firing during rhythmic activity (Szabadics et al., 2006). Pyramidal neuron activity modulation is also attained by other mechanisms, such as the presence and distribution of specific voltage-gated ion channels along the dendritic tree, with a clear impact on the diffusion of back-propagated action potentials and dendritic spikes, and different neuromodulators targeting the activity of these channels, like acetylcholine (ACh) and brain-derived neurotrophic factor (BDNF) (Egorov et al., 2002; Gordon et al., 2006).

In this chapter we wanted to analyze the role of Reelin in structural synaptic plasticity of pyramidal neurons. Since Reelin is endogenously expressed by a subset of interneurons in the adult brain, it might exert a function in the regulation of pyramidal cell activity. Conjointly, pyramidal cells are covered by thousands of dendritic spines, these being the postsynaptic partner for most excitatory glutamatergic synapses (Elston and DeFelipe, 2002; Ballesteros-Yanez et al., 2006). Therefore, spines are an estimate of the minimum of excitatory synapses received on a neuron. By using both *in vivo* gain- and loss-of-function approaches combined with different individual cell labeling methods we analyzed the dendritic spine features of hippocampal CA1 and somatosensory cortex 1 – barrel field (S1BF) layer 5 pyramidal neurons.

Hippocampal CA1 pyramidal cells of Reelin-OE mice display similar spine features as controls

We first seeked to analyze the Reelin-triggered hippocampal spine phenotypes previously reported at the ultrastrusctural level. We labeled CA1 individual pyramidal cells from both Reelin-OE mice and control littermates by means of intracellular microinjection and iontophoretic delivery of fluorophore (Dumitriu et al., 2011). Next, Alexa 594-labeled CA1 pyramidal cells were imaged in a Zeiss confocal microscope and images were further blind-deconvolved using AutoDeblur software (Bitplane Inc) (**Fig. r.3.1a-b**).

We first characterized the dendritic spine density distribution in the basal dendritic tree with respect to the distance from the soma by means of a Sholl analysis. We analyzed 69 and 51 dendritic segments from 5 and 4 cells of control and Reelin-OE mice, respectively. Reelin-OE mice exhibited similar spine density distribution as control mice (**Fig. r.3.1c**). We then analyzed the spine density with respect to the beginning of the dendritic branch in apical oblique dendritic segments, from 159 and 207 dendritic segments that corresponded to 19 and 25 cells of 5 mice per group, respectively. We found no differences either between controls and Reelin-OE mice (**Fig. r.3.1d**). Therefore, spine density and their distribution along the dendrites remain unaltered in CA1 pyramidal neurons at both the apical and basal dendritic domains after Reelin overexpression.

Next, we wished to analyze the morphology of these spines. Digital 3D surfaces enclosing each spine were individually generated using the Imaris software package (Bitplane Inc). Volume and sphericity from 1654 and 1553 spines from apical oblique dendrites of 19 and 25 CA1 pyramidal cells and 1071 and 991 spines from basal dendrites of 5 and 4 cells belonging to control and Reelin-OE mice were pooled for analysis. Sphericity parameter returns values comprised between 0 and 1 and relates to the compactness of the shape of a given object, 1 being attributable to a sphere and 0 to a line (**methods** (**1**)). Spines from Reelin-OE mice displayed similar average volume and sphericity with respect to spines of control mice, both at the basal and the apical dendritic tree (**Fig. r.3.1e-f**).
We then addressed the study to the apical dendritic tree of these cells. By analyzing the dendritic spine density in +150 segments of 5 mice per group, we found that Reelin-OE mice presented similar spine distributions and densities as controls (**Fig. r.3.1g-h**). We then applied a similar morphometric approach as mentioned before to +1500 spines in each group, and we found that both the spine volume (**Fig. r.3.1i**) and their sphericities (**Fig. r.3.1j**) were similar across both groups analyzed.
Altogether, we confirmed by optical microscopy that spine density remains unaltered in the hippocampus of Reelin-OE mice. Moreover, spine morphology in the basal domain of CA1 pyramidal cells was similar to that found in controls, as we found in EM analysis on the stratum oriens. Finally, spine size in the apical dendrites of CA1 pyramidal cells did not appear to be different from the one found in control animals.

Cortical S1BF Layer 5 pyramidal cells of Reelin-OE mice display reduced spine density and spine hypertrophy

We next decided to analyze a second type of pyramidal cells. Since different cortical layers receive different synaptic inputs, a distal pyramidal cell type might respond differently to a similar plasticity-inducing Reelin overexpression event. To determine the extent to which Reelin regulation of dendritic spines of pyramidal neurons was restricted to hippocampal CA1 or could be reproduced in other cortical regions we addressed a new study of spine density and morphology in pyramidal neurons. Reelin-

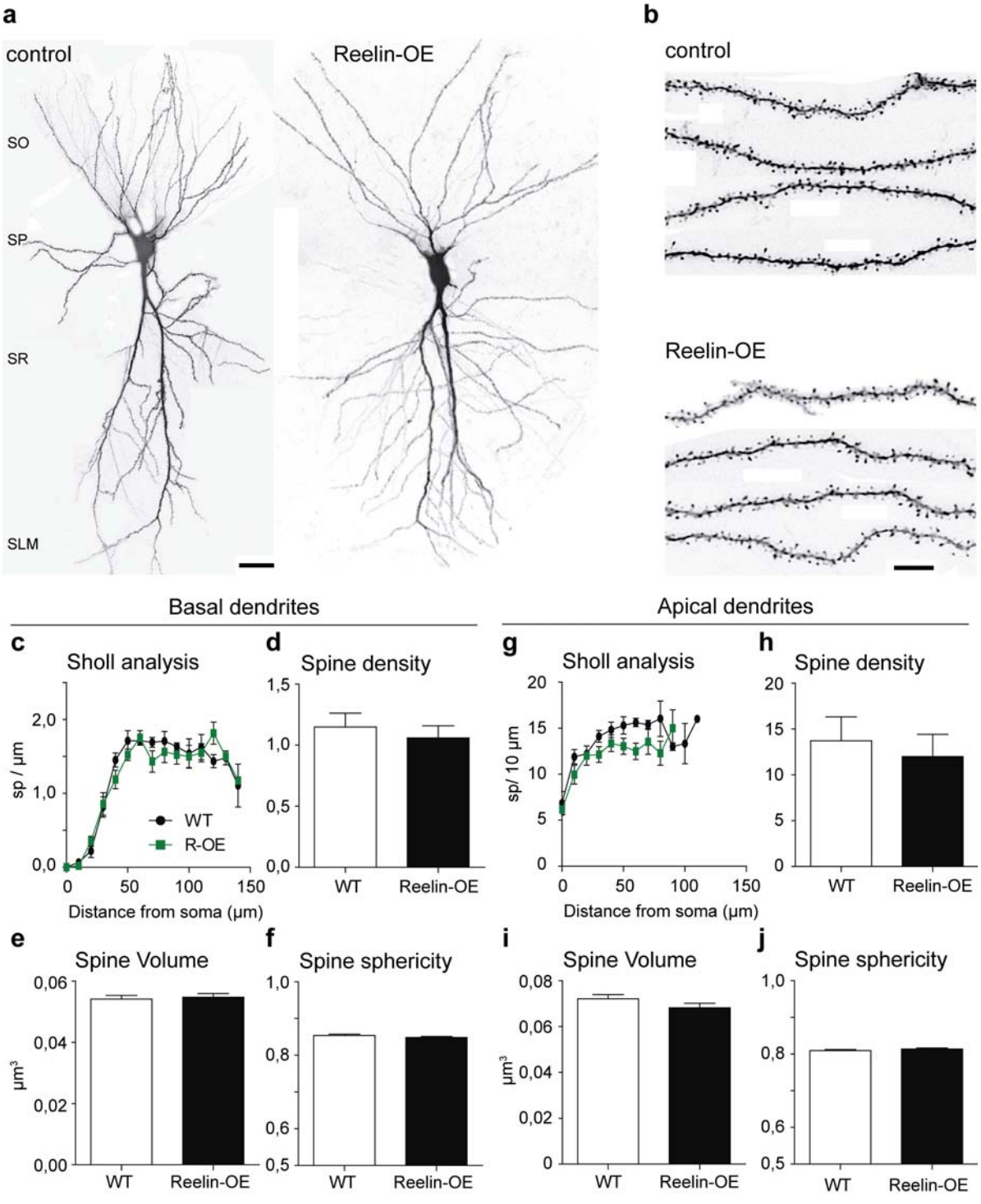

Figure r.3.1 Reelin-OE mice CA1 pyramidal neurons exhibit similar spine densities and morphologies as controls. (**a**-**b**) Low-magnification images of Alexa 594-filled CA1 pyramidal neurons of control and Reelin-OE mice (**a**) and higher magnifications of some basal dendrites from these groups (**b**) are shown. (**c**-**d**) Histograms show spine distribution along the dendrite (**c**) and average spine density measurements (**d**) in basal dendrites of CA1 pyramidal cells of control and Reelin-OE (n = 4 animals per group). (**e**-**f**) Morphometric analysis of these spines included quantifications of their volume (**e**) and sphericity (**f**) (n = 3). (**g**-**h**) Spine density analysis of apical

OE mice express exogenous Reelin in a CaMKII promoter-driven pattern (Pujadas et al., 2010). Thus, in addition to the endogenous pattern of Reelin expression (Alcantara et al., 1998), in Reelin-OE mice numerous pyramidal cells in the neocortex, hippocampus and entorhinal cortex are immunoreactive for Reelin, as well as DG granule cells, among other cell types (Pujadas et al., 2010). In particular, Layer 5 pyramidal cells of S1BF cortex are positive for exogenous Reelin expression. Thus, we chose Layer 5 pyramidal cells in the S1BF cortex for analysis.

Thy1H mouse line display a subpopulation of neurons expressing the GFP reporter protein. In the S1BF cortex the labeled cell population is limited to a number of isolated layer 5 pyramidal neurons and some layer II interneurons (**Fig. r.3.2a**) (Feng et al., 2000). We took advantage of this reporter mouse line by crossing it with our Reelin-OE mouse line to trace the cells of interest in this study.
We focused on the apical dendrite at two different locations: in the trunk, non-ramified dendritic segment that crosses layer 4, and in the tuft, ramified segment present in layers II-III (**Fig. r.3.2b**). To verify that the putative phenotypes would be due to the Reelin overexpression, a third group of Reelin-OE mice were administered DOX to inhibit the transgene expression (Reelin-OE-DOX) and further analyzed. Spine counts were performed a visum under a widefield microscope and the respective dendritic segment lengths measured using the Fiji software package (Schindelin et al., 2012). A total of 120 segments in 40 cells from 4 animals per group were pulled from control, Reelin-OE and Reelin-OE-DOX mice.

Spine density was found to be a 15% and 27% lower in Reelin-OE mice compared to control mice in apical dendrites passing by layers 4 and 2-3, respectively. More interestingly, Reelin-OE-DOX mice displayed dendritic densities similar to control mice in both areas analyzed (**Fig. r.3.2c**, **f**).

We next analyzed the morphology of these spines. High-resolution confocal acquisitions underwent an experimental deconvolution protocol, which allowed for a more accurate spine head surface segmentation using Imaris software. A total of 2501, 1654 and 3476 spines were pooled for the layer 4 analysis and 1832, 1488 and 1750 for the layer 2-3 analyis corresponding to 120 dendritic segments each from control, Reelin-OE and Reelin-OE-DOX mice, respectively. At both layer 4 and layer 2-3, dendrites from layer 5 pyramidal neurons of Reelin-OE mice exhibited hypertrophic spines, which were 33% and 68% larger than control ones (**Fig. r.3.2d**, **g**). Moreover, at both layers these spines were found to be 4% and 5% less spherical (**Fig. r.3.2e**, **h**). More interestingly, Reelin-OE-DOX group presented spine volumes and sphericities similar to those of control animals (**Fig. r.3.2d-e**, **g-h**).

Thus, apical dendrites of S1BF Layer 5 pyramidal cells exhibited a reduction in spine density and an increase in spine complexity under Reelin overexpression. The same effect was observed for these dendrites at two branching levels, both at trunk dendrites passing by layer 4 and at tuft dendrites passing by layers 2-3. Finally, transgene expression inactivation by doxycycline administration rescued the control phenotype.

dendrites of CA1 pyramidal neurons including spine distribution (**g**) and average density (**h**) (n = 5). (**i**-**j**) Spine volume (**i**) and sphericity (**j**) quantification for apical dendrites (n=5) (mean ± SEM; *p < 0.05; Student's t test). Scale bars are 30 μm in (**a**) and 5 μm in (**b**). Abbreviations: *SLM*, stratum lacunosum-moleculare; *SR*, stratum radiatum; *SP*, stratum pyramidale; *SO*, stratum oriens; *sp*, spine.

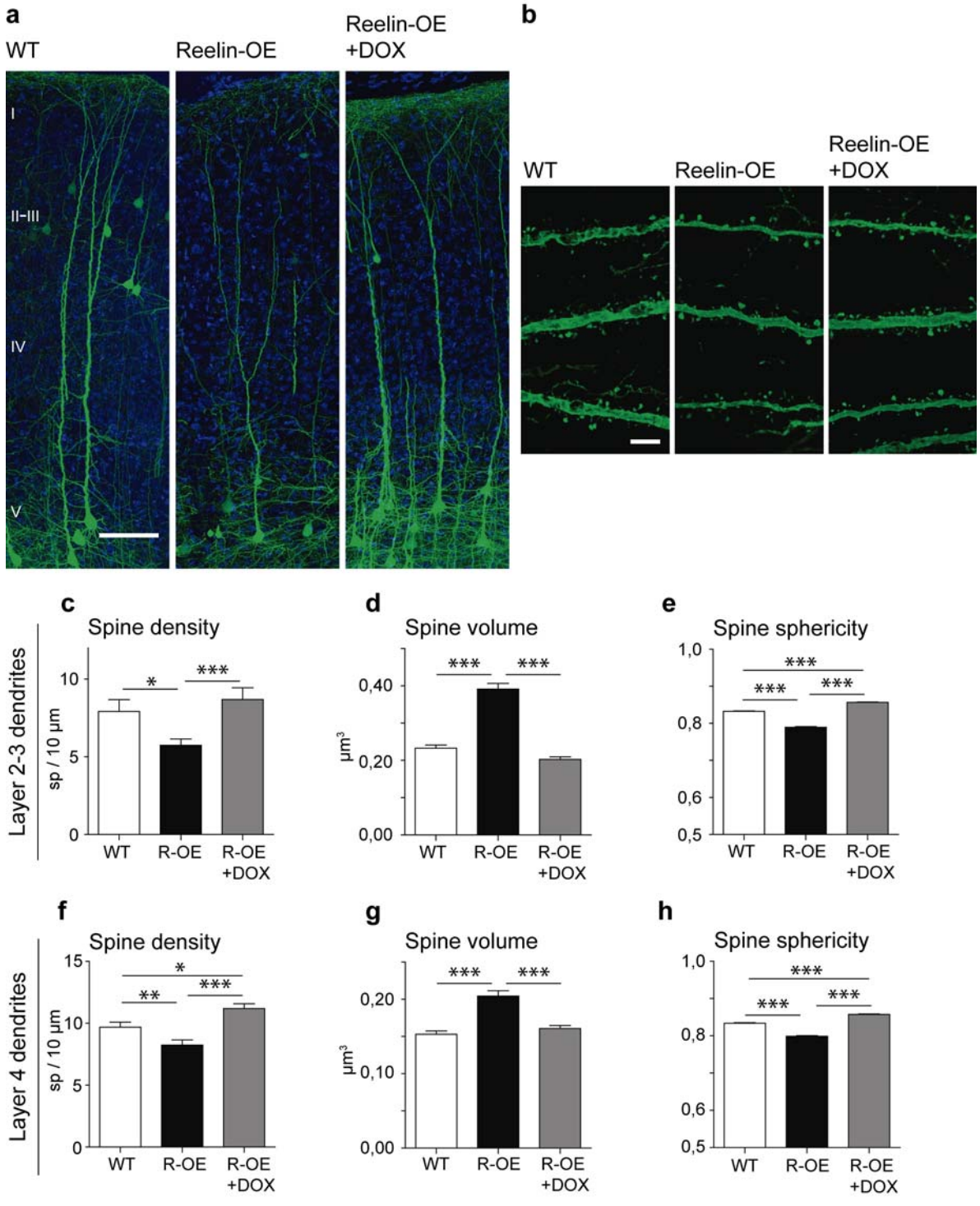

Figure r.3.2 Reelin-OE mice S1BF Layer 5 pyramidal neurons exhibit fewer but larger spines than controls. (**a**-**b**) Low-magnification images of YFP-expressing Layer 5 pyramidal neurons of control, Reelin-OE, and Reelin-OE mice treated with DOX (**a**) and higher magnifications of some dendritic segments corresponding to the layers 2-3 of these mice (**b**). (**c**-**e**) Analyisis of dendritic segments of these cells corresponding to tuft dendrites passing by layers 2-3, including spine density (**c**), volume (**d**) and sphericity (**e**) (n = 4 animals per group). (**f**-**h**) Analysis of dendritic segments of these cells corresponding to trunk dendrites passing by layer 4, including spine

Hippocampal CA1 pyramidal cells of Cre/flDab1 + TAM mice display unaltered spine density but reduced complexity of spine morphologies

Reelin signaling converges in the intracellular adaptor Dab1 after Reelin interaction with its receptors. Also, Dab1 activation by self-phosphorylation precedes the intracellular signaling cascade that reaches its final effectors. Therefore, Dab1 protein is a key target for Reelin signaling regulation. Moreover, Dab1 KO mice reproduce many histological, physiological and behavioral phenotypes found in *reeler* mice (Sheldon et al., 1997).

Pramatarova and colleagues recently generated a floxed Dab1 mouse (flDab1), which allows successful Dab1 depletion after Cre recombinase activity (Pramatarova et al., 2008). We crossed this mouse line with an Ubiquitin promoter-driven Cre recombinase expression mouse line, obtaining a conditional Dab1 KO mouse line (Cre/flDab1) that generates a Dab1-KO mouse upon intraperitoneal injection of tamoxifen (Cre/flDab1+TAM).

In order to complement the previous analyses performed under a gain-of-function paradigm for Reelin expression, we addressed similar experiments under a loss-of-function scenario consisting in the unresponsiveness to the Reelin-triggered signaling.

We first analyzed the hippocampal CA1 pyramidal neuron at basal dendrites. Individual cells were labeled by means of intracellular injection of Lucifer Yellow fluorophore on fixed tissue. Immunohistochemical processing further amplified fluorophore's signal (**Fig. r.3.3.a-b**). High-resolution confocal acquisitions were performed with a Leica SP5 microscope and these underwent previously described experimental deconvolution. Image stacks z-projections were used to quantify spine density relative to distance to the soma, providing 389 and 401 dendritic segments from 36 cells of 3 animals per group from flDab1 and Cre/flDab1+TAM mice, respectively. Density of dendritic spines in the basal dendrites from CA1 pyramidal cells was not affected, nor the distribution of dendritic spines with respect to the soma, in Cre/flDab1+TAM mice (**Fig. r.3.3c-d**).

We next analyzed the morphology of these spines (more than 1500 per group) by means of the same digitizing protocol previously described. Here, spines in basal dendrites of Cre/flDab1+TAM mice were a 21% smaller and 1% more spherical than the control ones (**Fig. r.5.3e-f**).

Therefore, loss of Reelin signaling by means of Dab1 depletion results in shrinkage of the dendritic spines of basal dendrites from CA1 pyramidal cells, whereas spine counts remain unaltered.

Cortical S1BF Layer 5 pyramidal cells of Cre/flDab1 + TAM mice display increased spine density and increased complexity of spine morphologies

We next addressed our interest to the cortical S1BF layer V pyramidal neurons. To test whether the spine phenotype observed in hippocampus could be extrapolated to the whole pyramidal cell population, neurons of interest were labeled following an identical intracellular microinjection approach and processed as previously described (**Fig. r.3.4a-b**).

density (**f**), volume (**g**) and sphericity (**h**) (n = 4) (mean ± SEM; *p < 0.05; **p < 0.01; ***p < 0.001; Kruskal-Wallis test and Dunn's posthoc test). Scale bars are 100 μm in (**a**) and 5 μm in (**b**). Abbreviations: *I-V*, cortical layers 1-5; *sp*, spine.

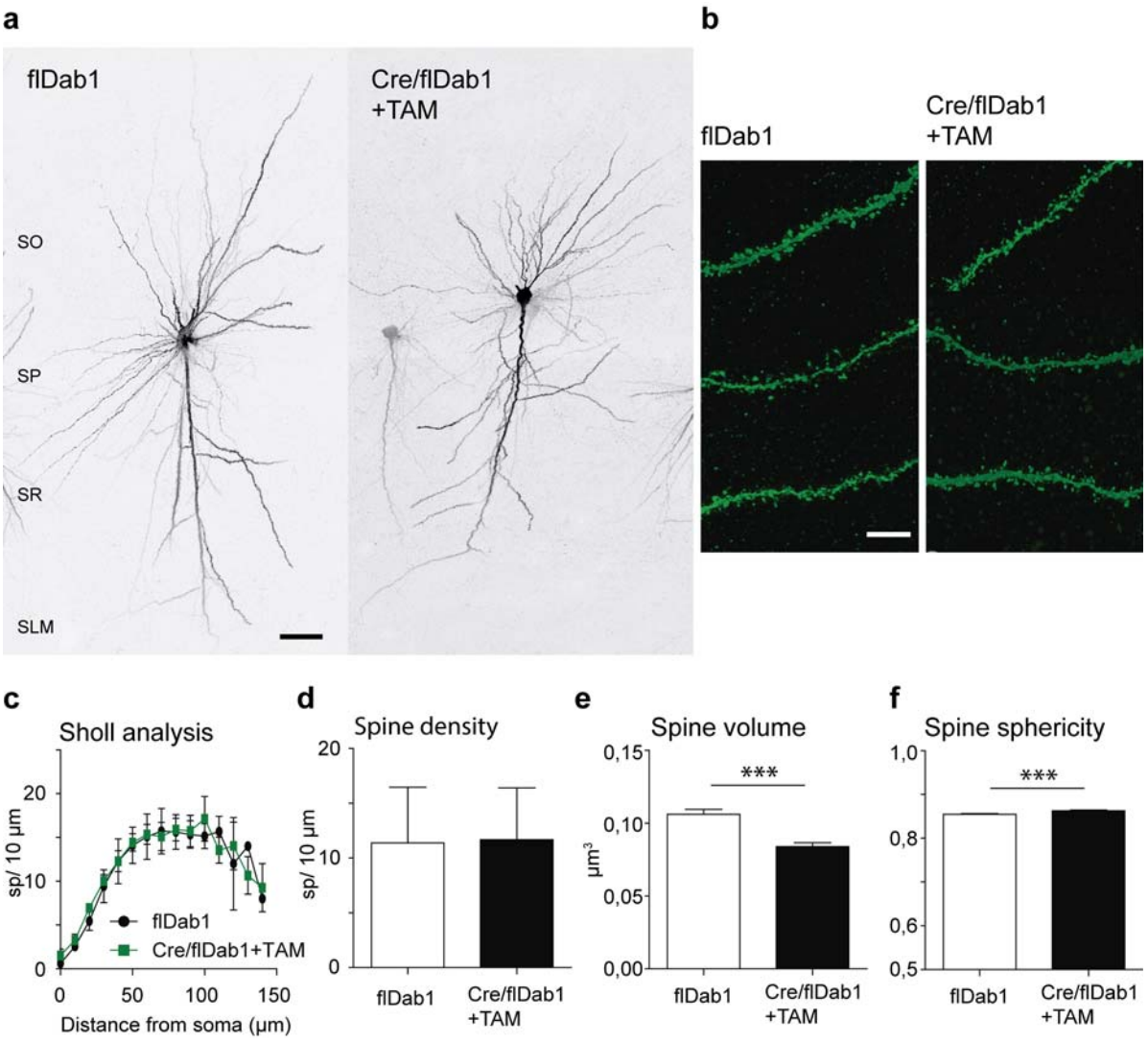

Figure r.3.3 Conditional deletion of the Dab1 gene alters spine morphology in hippocampal CA1 pyramidal cells. (**a**-**b**) Low-magnification images of Lucifer Yellow-filled CA1 pyramidal neurons of flDab1 and Cre/flDab1 mice treated with TAM (**a**) and higher magnifications of dendritic segments belonging to basal dendrites (**b**). (**c**-**d**) Histograms show spine distribution along the dendrite (**c**) and average spine density (**d**) of basal dendrites of CA1 pyramidal cells of these mice (n = 3 mice per group). (**e**-**f**) Morphometric analysis of these spines, including spine volume (**e**) and sphericity (**f**) (n = 3) (mean ± SEM; *p < 0.05; **p < 0.01; ***p < 0.001; Student's t test). Scale bars are 30 µm in (**a**) and 5 µm in (**b**). Abbreviations: *SLM*, stratum lacunosum-moleculare; *SR*, stratum radiatum; *SP*, stratum pyramidale; *SO*, stratum oriens; sp, spine.

Confocal images of trunk dendritic segments passing by layer 4 were Z-projected. 50 and 64 dendritic segments from 7 and 11 cells of 2 and 4 mice of either flDab1 or Cre/flDab1+TAM genotypes were pooled for analysis. Cre/flDab1+TAM mice displayed a 38% increase in spine density by respect to flDab1 controls. (**Fig. r.3.4c**)

To analyze spine morphology, 766 and 933 spine heads were digitized as previously described. In Cre/flDab1-TAM mice, spine heads volumes from apical dendrites of layer 5 pyramidal neurons were 40% larger than in flDab1 mice. More interestingly, these spines were 2% less spherical than their control

counterparts. (**Fig. r.3.4d**).

Therefore, apical trunk dendrites of S1BF layer 5 pyramidal neurons presented an increase of spine density concomitant with an enhanced complexity of these spines when the Reelin signaling pathway was abolished.

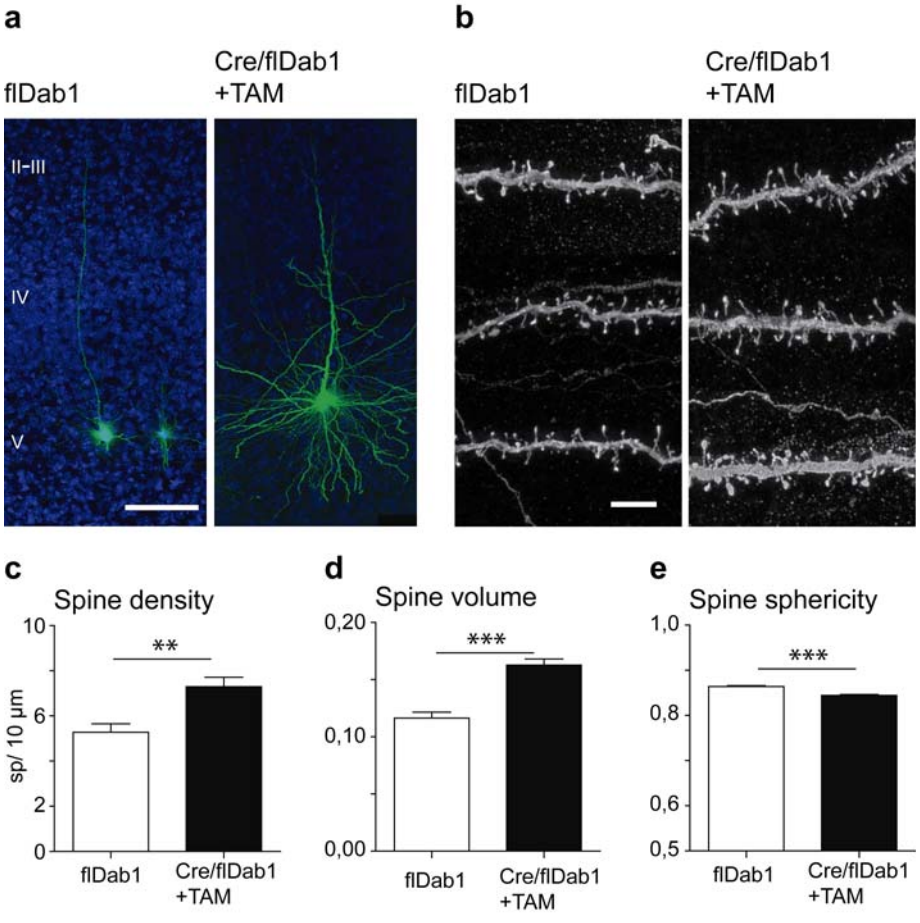

Figure r.3.4 Conditional deletion of the Dab1 gene alters spine density and morphology in S1BF Layer 5 pyramidal neurons.
(**a**-**b**) Low-magnification images of Lucifer Yellow-filled Layer 5 somatosensory 1 barrel field cortex (S1BF) pyramidal neurons of both flDab1 and Cre/flDab1 mice treated with TAM (**a**) and higher magnifications of dendritic segments corresponding to the layer 4 of these mice (**b**). (**c**) Spine density of trunk dendrites passing by layer 4 (n = 2 flDab mice, 4 Cre/flDab1+TAM mice). (**d**-**e**) Spine volume (**d**) and sphericity (**e**) in the same region (n =2) (mean ± SEM; *p < 0.05; **p < 0.01; ***p < 0.001; Student's t test). Scale bars are 100 µm in (**a**) and 5 µm in (**b**). Abbreviations: *II-V*, cortical layers 2-5; *sp*, spine.

Altogether, apical dendrites from S1BF layer 5 pyramidal neurons presented more complex dendritic spines when the Reelin signaling pathway was both enhanced and suppressed. However, in these dendritic segments Reelin overexpression triggered a decrease in spine density whereas Dab1 depletion provoked an increase in spine number. Besides, hippocampal CA1 pyramidal cells in these same mouse models presented particular spine parameters: There, Reelin overexpression did not alter spine density or morphology, whereas Dab1 depletion triggered less complex spine morphologies without modifying spine density.

4. High-throughput 3D reconstruction of dendritic spines and synapses in GFP-traced adult-generated neurons by using FIB/SEM technology

Introduction to Chapter 4: High-throughput correlative electron microscopy approach to study hippocampal adult neurogenesis

The study of the nervous system is to an important degree a study of the connexions of neuronal processes. This is at present an impossible task for the electron microscope (EM), not only because of the impracticability of serially sectioning a useful volume of tissue, but because the cell processes of grey matter twist and turn in all directions […] Nevertheless, electron microscopy should prove invaluable in this connexion in assessing the accuracy of information obtained by the light microscopy […]. (Gray, 1959)

The fine dissection of microcircuits is essential for the understanding of normal brain function and for the identification of structural and physiological modifications associated with neural plasticity and neuropathological conditions. The development of transmission electron microscopy (TEM) represented a revolutionary step allowing the first fine analysis of synapses and revealing the high structural synaptic complexity of the nervous system (Sotelo, 1975, 1978; Peters et al., 1991; Peters and Palay, 1996; Harris and Weinberg, 2012). A further methodological breakthrough was the combination of TEM with single neuron tracing methods (Golgi method, intracellular filling, immunohistochemistry, etc) which allowed the fine analysis of input and output synaptic connectivity in identified neurons (Blackstad, 1965; Fairen et al., 1977; Somogyi and Hodgson, 1985; Fairen, 2005). Although these methods provided fundamental information over the last four decades, the requirement of performing observations in ~60 nm-ultrathin sections limits data analysis to a segmented visualization of synaptic structures, due to the complex 3D architecture of the neural cells. Efforts to successfully overcome this problem include obtaining and analyzing serial ultrathin sections that offer reconstruction of identified dendritic and axonal segments (Stevens et al., 1980; Harris et al., 2006; Hoffpauir et al., 2007; Jain et al., 2010; Mishchenko et al., 2010; Bock et al., 2011). However, obtaining series of serial ultrathin sections is extremely time-consuming and technically-demanding, often making it impossible to reconstruct large volumes of tissue. Hence, the recent development of automated EM techniques represents another crucial step in the study of neuronal circuits (Briggman and Denk, 2006; Knott et al., 2008; Merchan-Perez et al., 2009; Helmstaedter, 2013).

We used a dual-beam electron microscope that combines a focused ion beam column (FIB) and a scanning electron microscope (SEM). The FIB column directs a gallium (Ga^+) ion beam towards the sample, the collision of which resulting in the removal of substrate atoms from the sample. Since the FIB can be focused and controlled on a nanometer scale, this effect is used to mill the specimen, removing a thin layer of material. A backscattered electron image is then obtained from the freshly milled surface using the SEM. The milling/imaging processes are automatically repeated in order to obtain long series of images that represent a three-dimensional view of the tissue (Merchan-Perez et al., 2009; Bushby et al., 2011). Using this methodology we and others have previously shown that synapses can be accurately identified, reconstructed and quantified from large 3D tissue samples obtained in an automated manner (Merchan-Perez et al., 2009; Morales et al., 2011). Further, recent studies have attempted to correlate light microscopy fluorescence and FIB/SEM microscopy (Allegra Mascaro et al., 2013; Maco et al., 2013; Sonomura et al., 2013). With this correlative light microscopy-FIB/SEM method we aimed to analyze developing synaptic inputs on retrovirally-traced adult-generated GCs in the DG.

Adult neurogenesis is a process present in many species, humans included (Lois and Alvarez-Buylla, 1994; Eriksson et al., 1998; Gage, 2000; Deng et al., 2010; Knoth et al., 2010; Sanai et al., 2011; Spalding et al., 2013), that has been observed in two brain regions: the subventricular zone (SVZ) of the lateral ventricle and the subgranular zone (SGZ) of the dentate gyrus (DG). New neurons are continuously generated in these areas, and later on differentiate and become integrated into functional circuits of the olfactory bulb and hippocampus, respectively. Hippocampal adult neurogenesis in mice exhibits a highly accurate temporal development, which has been precisely studied with the help of retrovirally-labeled synchronous neurogenic populations (Zhao et al., 2006; Ge et al., 2007) among other techniques. In brief, new neurons born in the SGZ migrate to the inner granule cell layer during their first week of age, and at two weeks already depict a neuron-like morphology and receive depolarizing GABAergic input from interneurons in the granular layer. 3-week old granule cells (GCs) are described to start becoming integrated with their local network: their dendrites reach the molecular layer, where they receive glutamatergic excitatory input from entorhinal cortex boutons, and GABAergic input at their somata triggers inhibitory hyperpolarizing events. At this time these cells also exhibit mossy fiber boutons that establish efferent synaptic contacts to CA3 pyramidal cells, either on the dendritic shaft or onto preexisting thorny excrecences. From 4 to 6 weeks new-born GCs undergo a critical period during which they exhibit stronger plasticity than mature GCs, both in terms of increased amplitude of LTP and a lower threshold for LTP induction. This process is dependent on NR2b-containing NMDA receptor activity. In contrast, 8-9 week-old new-born granule cells exhibit synaptic plasticity parameters identical to those of mature granule cells, although some features related to structural plasticity last longer to exhibit mature phenotypes (Toni et al., 2007; Toni and Sultan, 2011).

In this chapter we used FIB/SEM technology to completely reconstruct previously identified dendritic segments in a high-throughput approach with a resolution comparable to conventional TEM. Both adult neurogenesis and the recruitment of these neurons into adult circuits are essential for learning and memory and these processes have been implicated in major neurodegenerative and psychiatric diseases (Zhao et al., 2008; Deng et al., 2010). Our experimental design allowed for the full 3D reconstruction of up to 248 dendritic spines and the identification of their synaptic inputs, thereby allowing a detailed analysis of the synaptogenesis in this important neuronal population.

FIB/SEM technology allows the analysis and 3D reconstruction of synaptic interactions from identified neurons with high resolution

To map the onset and development of synaptic inputs on adult-generated GCs in the dentate gyrus, young adult mice were injected with a retroviral vector expressing the postsynaptic protein PSD95 fused to GFP that allows the visualization of postsynaptic densities (MRSVPSD95g virus, as described in (Kelsch et al., 2008)). Whereas dendritic spines were rare in 2 week-old GCs, 3-4 week-old neurons displayed numerous dendritic spines, most of them tipped with PSD95-GFP-positive puncta (**Fig. r.4.1**). Dendritic spines and PSD95-GFP-positive postsynaptic densities were more abundant at 8 weeks, when synaptogenesis is believed to be completed. These findings are consistent with previous studies on adult neurogenesis in the dentate gyrus (Toni et al., 2007; Toni and Sultan, 2011) and prompted us to focus our FIB/SEM analysis on dendrites of adult generated GCs aged 3-4 and 8-9 weeks.

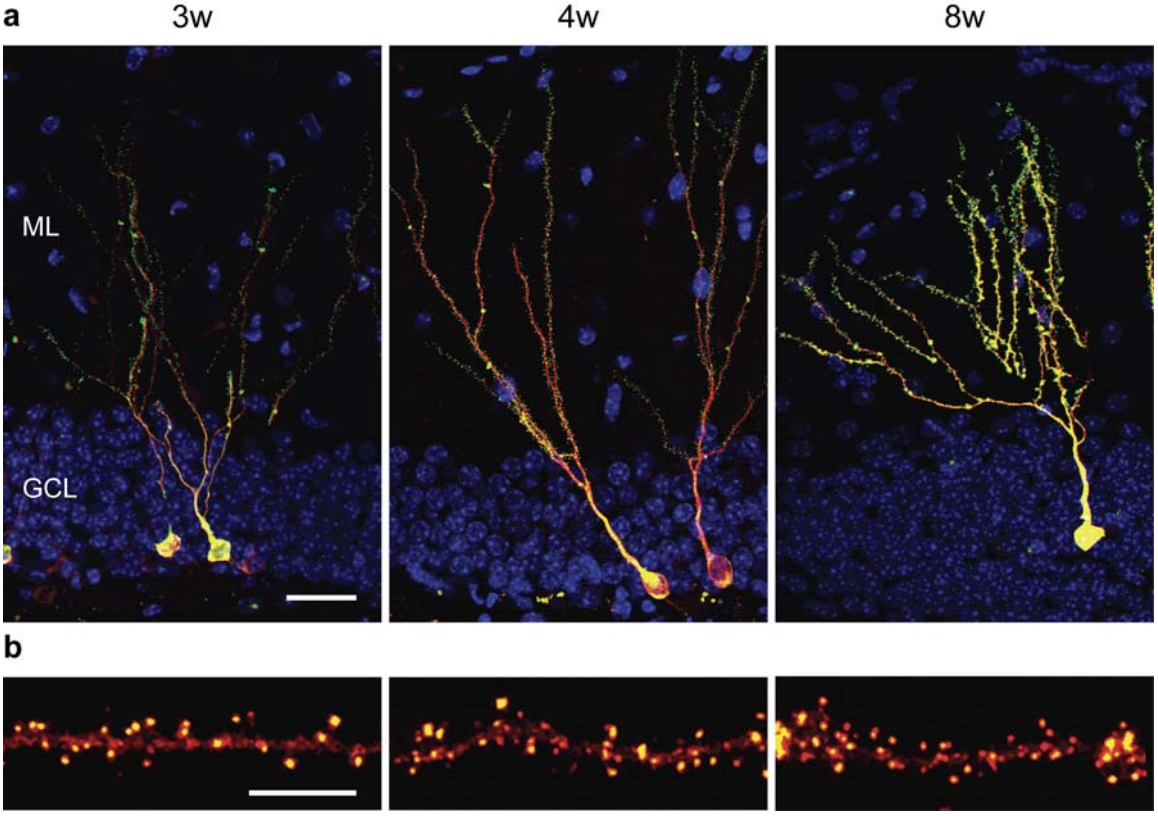

Figure r.4.1 Dendritic spines and postsynaptic densities visualized in developing GCs.
New-born GCs were labelled with a retroviral vector expressing PSD95, and visualized at 3, 4 and 8 weeks post-injection. (**a**) Low magnification views of retrovirally-labelled adult born GCs. (**b**) Confocal reconstructions of GC dendritic segments showing dendritic spines (red color) and postsynaptic densities (yellow color). Notice the increase in dendritic spines concomitant to post-injection times. Scale bars are 20 µm in (**a**) and 5 µm in (**b**). Abbreviations: *GCL*, granule cell layer; *ML*, molecular layer; *3w*, 3 weeks post-infection.

To investigate the development of synaptic inputs with EM resolution, adult-generated neurons were labeled with retroviral vectors expressing GFP. Brain slices were processed for GFP-immunostaining, diaminobenzidine (DAB) development and plastic embedding using conventional TEM procedures. Flat embedding of slices allowed the identification of labeled GCs and the subsequent trimming of tissue blocks. We next designed a correlation procedure that allowed us to apply FIB/SEM technology to identified dendrites that were previously selected under the light microscope (**Fig. r.4.2a**, details in **methods**). In brief, optimally stained and straight, parallel to surface-evolving dendritic segments of interest were identified and their precise position annotated with reference to fiducial landmarks present in both OM and EM images (**Fig. r.4.2b-c**). FIB/SEM serial images were obtained with a Z axis resolution of 25nm and an X-Y resolution of 3.7 nm per pixel (**methods**). We found that 2048x1536 pixel serial micrographs at a resolution of 3.7 nm/pixel (field of view of 7.6 x 5.7 μm, equivalent to 15000x magnification) allowed unambiguous identification of synaptic junctions and fast scanning cycles, and were therefore selected as the routine settings for obtaining image stacks for 3D reconstructions. Examination of these images revealed an overall quality of fine structure and resolution comparable to that of conventional TEM (**Figs. r.4.2g**, **r.4.3**).

As a further step for the automation and analysis of 3D reconstructions we implemented the EspINA program by developing specific softwares for the reconstruction of labeled structures. Alignment of images, segmentation and 3D reconstructions of tissue blocks of up to 10 μm in depth (up to 442 sections) were efficiently obtained in a semi-automatic manner: alignment of FIB/SEM images was assessed by automatic registration with Fiji (Schindelin et al., 2012)and manually checked-up with Reconstruct software (Fiala, 2005). The resulting images were saved as stacks and connectivity parameters were annotated by visualizing them with Fiji (**Fig. r.4.2g**). Examples of 3D reconstructed dendritic segments, using EspINA, are shown in Figure 1i, and were equivalent to segments reconstructed using the standard Reconstruct software (**Fig. r.4.2h**). Moreover, EspINA-based 3D reconstructions allowed quality control by the researcher and the visualization of orthogonal sections in any of the XYZ axis (**Fig. r.4.2i-j**).

Figure r.4.2 Correlative light and FIB/SEM microscopy of DAB-stained GC dendrites allows high-resolution 3D reconstruction.
(**a**) Light microscopy image of the araldite block surface (after trimming) allows the visualization and selection of the DAB-stained dendrite and the annotation of surface conserved traits, such blood vessels (red dashed line). The Course line (blue dashed arrow) defines the trajectory of the dendrite of interest and the selected acquisition direction (black arrow). The Trench line (blue pointed line) indicates the desired acquisition starting plane. (**b**) SEM image of the block surface, revealing conserved traits (red dashed line, green arrowheads), allows the identifications of the pre-selected trench plane and the start of the harvesting. Note that dendritic segments that evolve at the block surface are visible at SEM (green arrowheads), but not dendritic segments evolving entirely below the surface (black arrow in a). (**c**) SEM image after opening a trench before the trench line, allowing the sample to be ready for FIB/SEM serial milling-acquiring cycles. (**d**) Low magnification SEM-ESB image showing the surface of the trench face. The dendrite of interest is labelled by a red arrow. (**e-f**) Image acquisition provides up to several hundreds of serial images (**e**) that require alignment procedures (**f**) to obtain properly oriented stacks ready to tomography sergmentation. (**g-h**) Spine identification in individual micrographs (**g**) and stacks can be further traced to 3D reconstructions performed with either manual segmentation with Reconstruct software (**h**) or with the EspINA software which allows faster semi-automated reconstructions (**i**). Notice that the overall quality of 3D reconstructions using Reconstruct or EspINA are similar. (**j**) EspINA software allows the segmentation and visualization of labelled structures in the three XYZ axes before and after segmentation (upper and lower rows, respectively). Scale bars are 10 μm in (**a**, **d**) 1 μm in (**e-f**, **g**, **h-i**) and 1 μm in the right panels of (**j**).

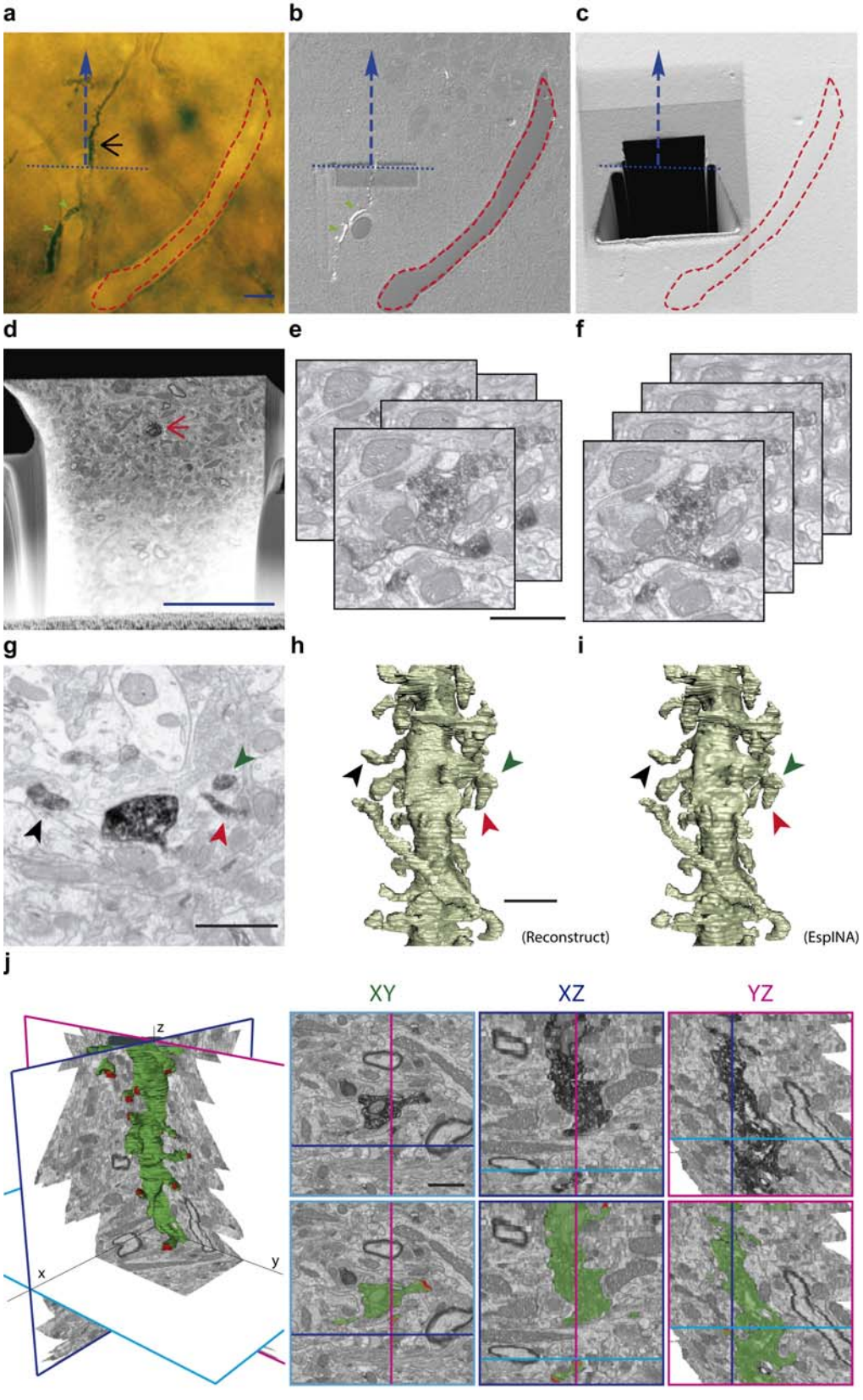
a
b
c
d
e
f
g
h
i
(Reconstruct)
(EspINA)
j
XY
XZ
YZ
z
x
y

Qualitative analyses of 3D reconstructions allowed the tracing of identified spines back to the parent dendrites, the study of the 3D architecture of synaptic interactions and the fine structural features of synapses and presynaptic elements (**Figs. r.4.2-6**). Thus, cell membranes, cytoskeletal components and organelles were clearly identifiable. Hence, DAB-labeled dendrites, and the spines arising from them, were recognizable, as were the unlabeled presynaptic boutons filled with synaptic vesicles and establishing synaptic contacts with DAB-traced profiles (**Fig. r.4.3a-b**). Postsynaptic densities and organelles present in both axonal (unlabelled) and postsynaptic (GFP-labeled) elements were clearly identifiable, including spine apparatus arranged in stacks, ER cisternae and mitochondria (**Fig. r.4.3c**). We conclude that FIB/SEM technology is a reliable and straightforward procedure which allows high-throughput, semi-automated 3D analyses of identified neuron-to-neuron synaptic interactions at the ultrastructural level with high resolution.

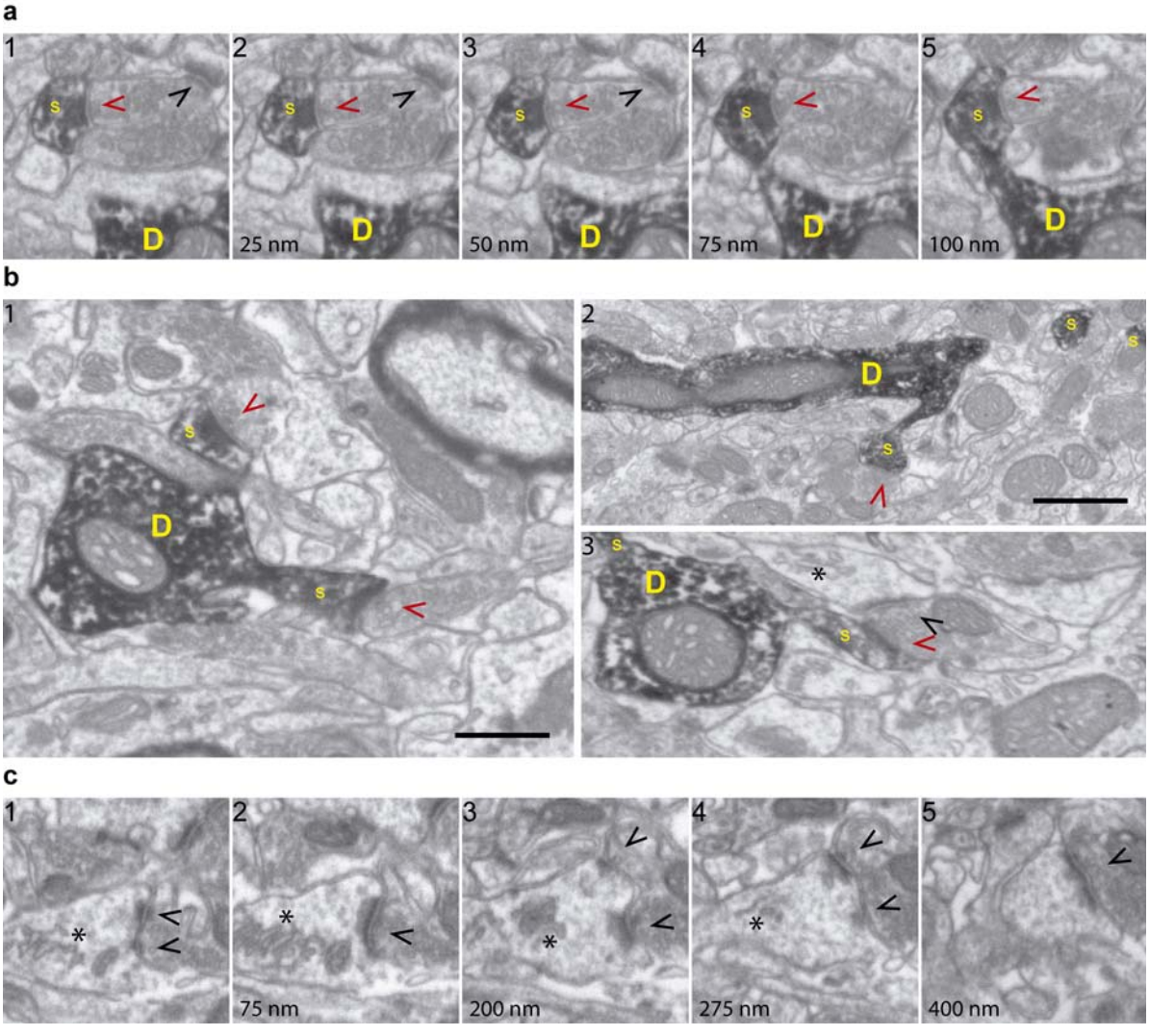

Figure r.4.3 FIB/SEM microscopy allows high resolution fine ultrastructural analysis of identified synapses.
(**a**) Five consecutive serial images (spaced 25 nm each) demonstrating high fine structural resolution of GFP/DAB stained dendrites, in both the XY and Z axes. The sequence shows a dendritic spine (s) emerging from the parent dendrite (D) and a presynaptic terminal forming synapse with the labeled spine (red arrowhead) and with an unlabeled spine (black arrowhead). Note that 25 nm thick Z-axis harvesting allows efficient and repeti-

tive visualization of structures of interest such as synapses and spine necks. (**b**) FIB/SEM images demonstrating overall ultrastructural quality and the unambiguous identification of dendrites (D), spines (s) and axon terminals establishing synapses with either labelled (red arrowhead) or unlabeled (black arrowhead) profiles. (**c**) Selected serial/correlative images (spaced 75-125 nm) showing different features in a single unlabeled dendritic spine, including spine apparatus (asterisk) and a perforated synapse (black arrowheads). Scale bar in (**b1**) is 0,5 µm and is applicable to all panels except for (**b2**). Scale bar in (**b2**) is 1 µm.

FIB/SEM analysis of input synapses onto mature adult-generated granule cells.

We applied FIB/SEM technology to the analysis of synaptogenesis on adult GCs. We first focused on neurons aged 8-9 weeks, when adult-generated GCs are considered to reach maturity (Zhao et al., 2006). Six dendritic segments were analyzed allowing the 3D reconstruction of up to 271 dendritic spines, of which 226 were fully reconstructed. A qualitative evaluation revealed that most spines were contacted by a single presynaptic bouton, although three spines (1%) were reported to receive both an excitatory contact on the head and a second synapse on the spine neck, which were established by different presynaptic boutons. A small percentage of dendritic spines, however, were found to lack synaptic contacts (asynaptic spines, 2%, N=5) (**Fig. r.4.4**), with all the remaining spines bearing exclusively asymmetric synaptic contacts. The majority of synapses were established on the spine heads, whereas a 3% (N=7) received synaptic input on the spine neck.

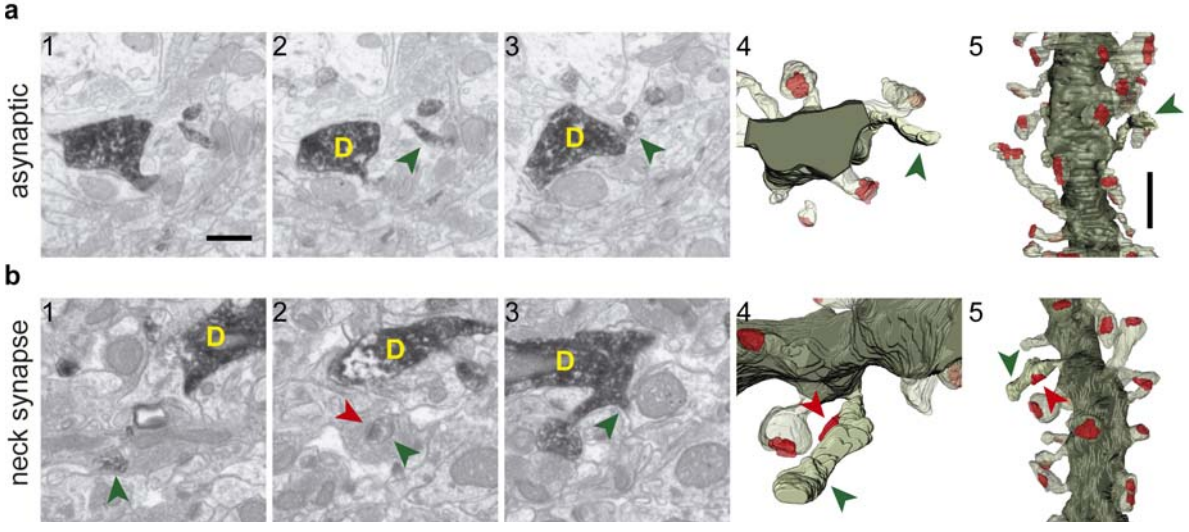

Figure r.4.4 Infrequent types of dendritic spines in 8 week-old GFP/DAB labeled GCs as reconstructed with FIB/SEM microscopy.
Examples show an asynaptic spine (**a**) and a dendritic spine receiving synaptic contact in the neck (**b**). The left images show 3 selected serial planes of the spines depicting the head (green arrowheads), neck and synaptic contact (red arrowheads), and the right 3D reconstructions show the labelled dendritic spines in two different orientations. Dendritic shaft (D) is colored solid dark green, the spine of interest in solid pale green and its synapse in solid red. Neighboring spines and synapses are colored in transparent pale green and red, respectively. Scale bar in (**a1**) is 0,5 µm and is applicable to (**a1-4**, **b1-4**); scale bar in (**a5**) is 1 µm and is applicable to (**a5**, **b5**).

The shapes and sizes of dendritic spines were highly variable. We noticed extremely large dendritic spines (1.8E8 nm3, around 0.60 µm diameter) and dendritic spines with small heads (1.7E6 nm3, around 0.25µm diameter). Although some large spines were apparently contacted by boutons form-

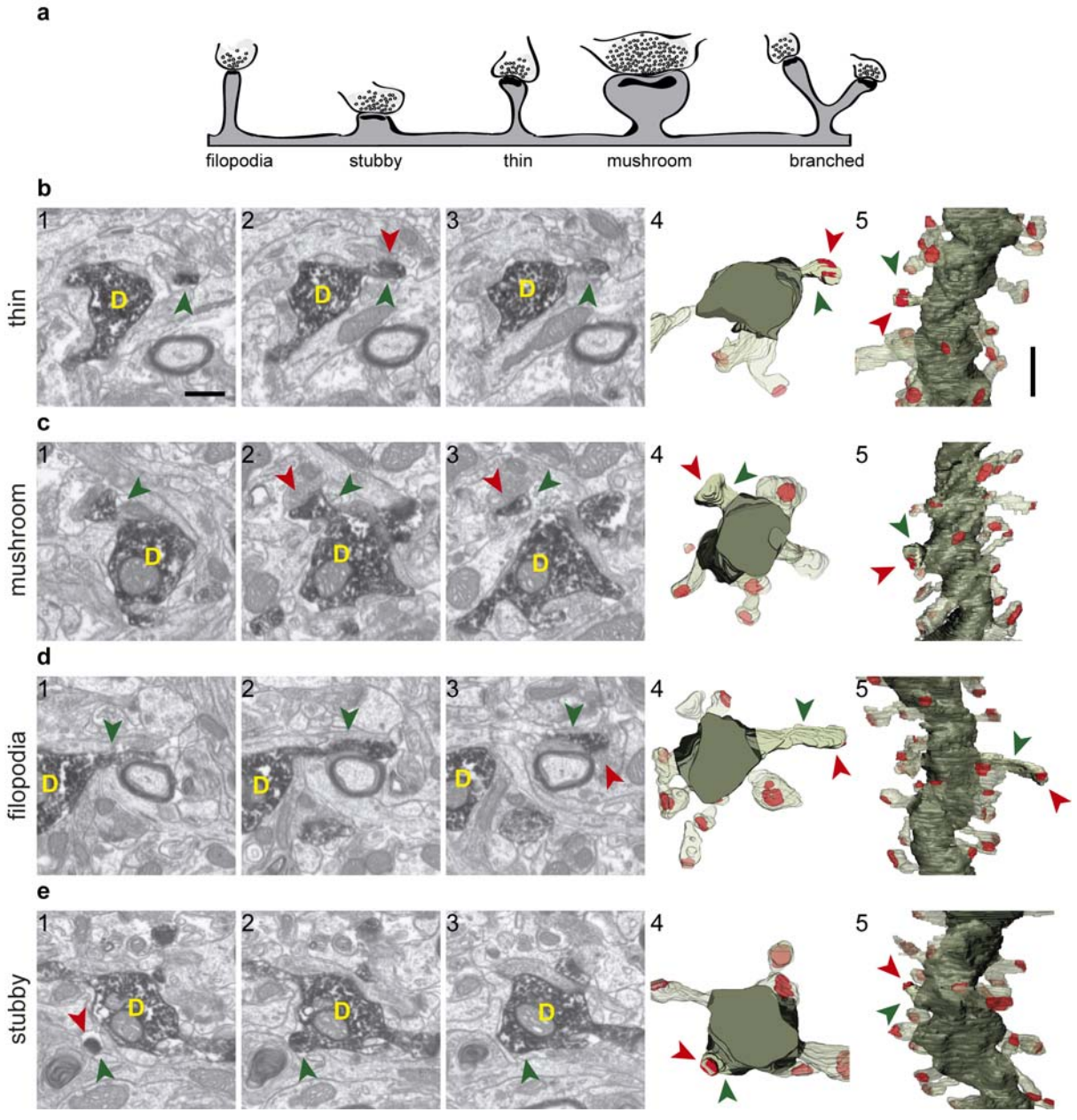

Figure r.4.5 Types of dendritic spines arising from 8 week-old GFP/DAB labeled GCs as reconstructed with FIB/SEM microscopy.

(**a**) Schematic representation of the 5 types of dendritic spines defined in the present study. Examples of thin (**b**), mushroom (**c**), filopodial (**d**) and stubby (**e**) dendritic spines arising from their parent dendrite (D). The 3 left images show selected serial planes of the spines depicting the head (green arrowheads), neck and synaptic contact (red arrowheads). The right 3D reconstructions show the labelled dendritic spines in two different orientations. Dendritic shaft (D) is colored solid dark green, the spine of interest in solid pale green and its synapse in solid red. Neighboring spines and synapses are colored in transparent pale green and red, respectively. Scale bar in (**b1**) is 0,5 μm and is applicable to (**b1-4**, **c1-4**, **d1-4**, **e1-4**). Scale bar in (**b5**) is 1 μm and is applicable to (**b5**, **c5**, **d5**, **e5**).

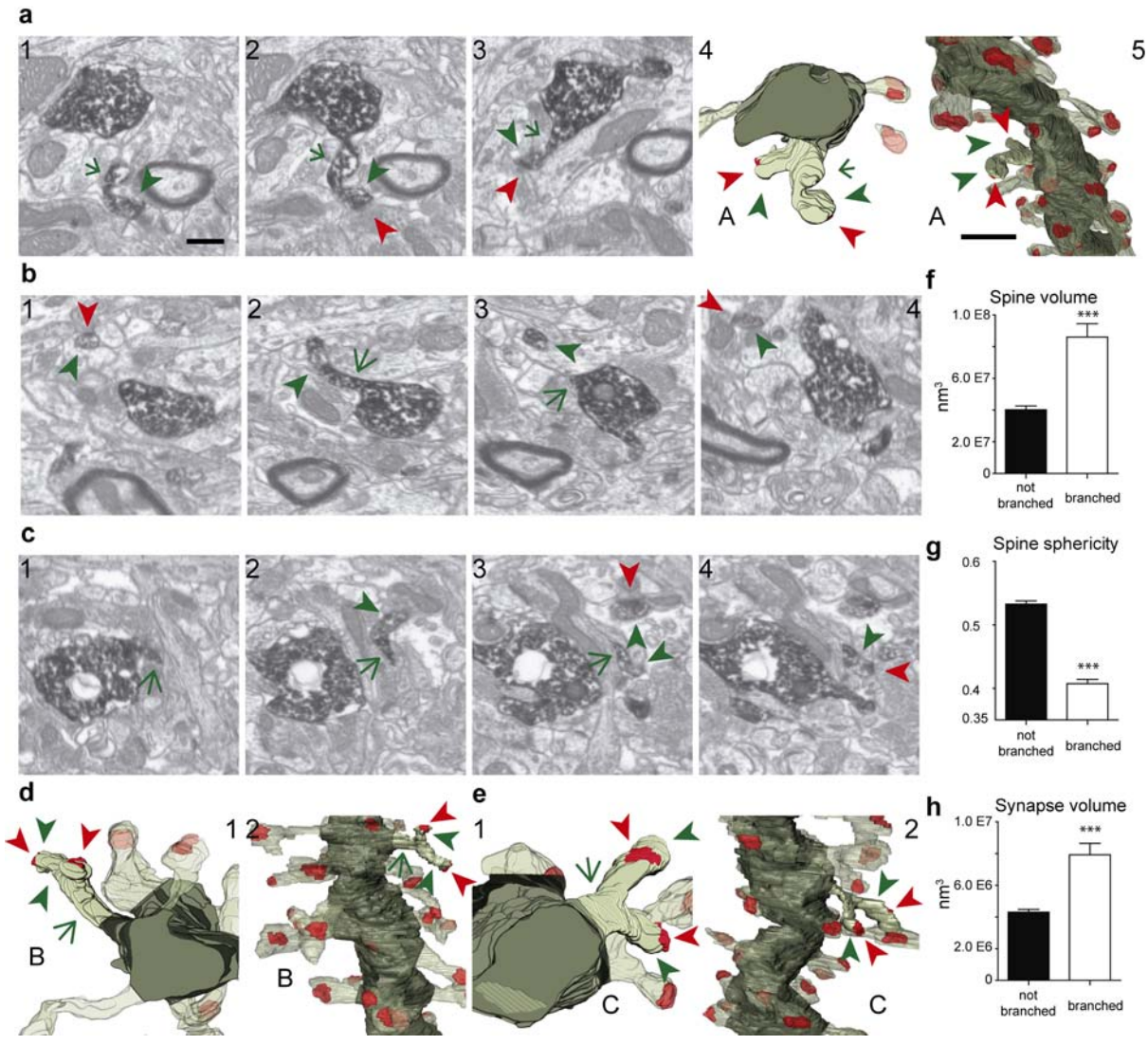

Figure r.4.6 FIB/SEM images and the corresponding 3D reconstructions illustrating branched spines in 8 week-old GCs.

(**a-e**) Three examples of branched spines. The FIB/SEM images in **a1-3**, **b1-4**, **c1-4** show selected serial planes of the dendritic spines A, B and C, and the parent dendrite. The corresponding 3D reconstructions are shown in two different orientations in panels **a4,5** (spine A), **d1,2** (spine B) and **e1,2** (spine C). Labeling of synaptic contacts are as in **Fig. r.4.5**. The spine heads are pointed by green arrowheads, the shared neck by a green arrow and their synaptic contacts by red arrowheads. The 3D reconstructions are colored as follows: the dendritic shaft in solid dark green, the spine of interest in solid pale green and its synapses in solid red. Neighboring spines and synapses are colored in transparent pale green and red, respectively. (**f-h**) Histograms show average spine volume (**f**), spine sphericity (**g**) and synapse volume (**h**) of non-branched and branched spines. Data represent mean ± SEM; *p < 0.05; **p < 0.01; ***p < 0.001; Mann-Whitney test. Scale bar in (**a1**) is 0.5 μm and is applicable to (**a1-4**, **b1-4**, **c1-4**, **d1**, **e1**). Scale bar in (**a5**) is 1 μm and is applicable to (**a5**, **d2**, **e2**).

ing 2 or more synaptic specializations, systematic analysis of serial image stacks revealed that virtually all these complex synapses were composed by a single U-shaped PSD (**Fig. r.4.3c**). 3D reconstructions allowed us to classify dendritic spines into 5 main types: thin (spines with small necks tipped by round-shaped heads), filopodia (thin and long spines with a point-shaped PSD with similar diameters in the neck and head), stubby (thick and short spines with no size differences between neck and head and spine length similar to neck width), mushroom (spines tipped by large heads typically displaying slightly concave invaginations invaded by the presynaptic bouton), and branched (spines with more than 1 head arising from a single neck) (**Fig. r.4.5**) (Peters and Kaiserman-Abramof, 1970; Harris et al., 1992; Bourne and Harris, 2008).

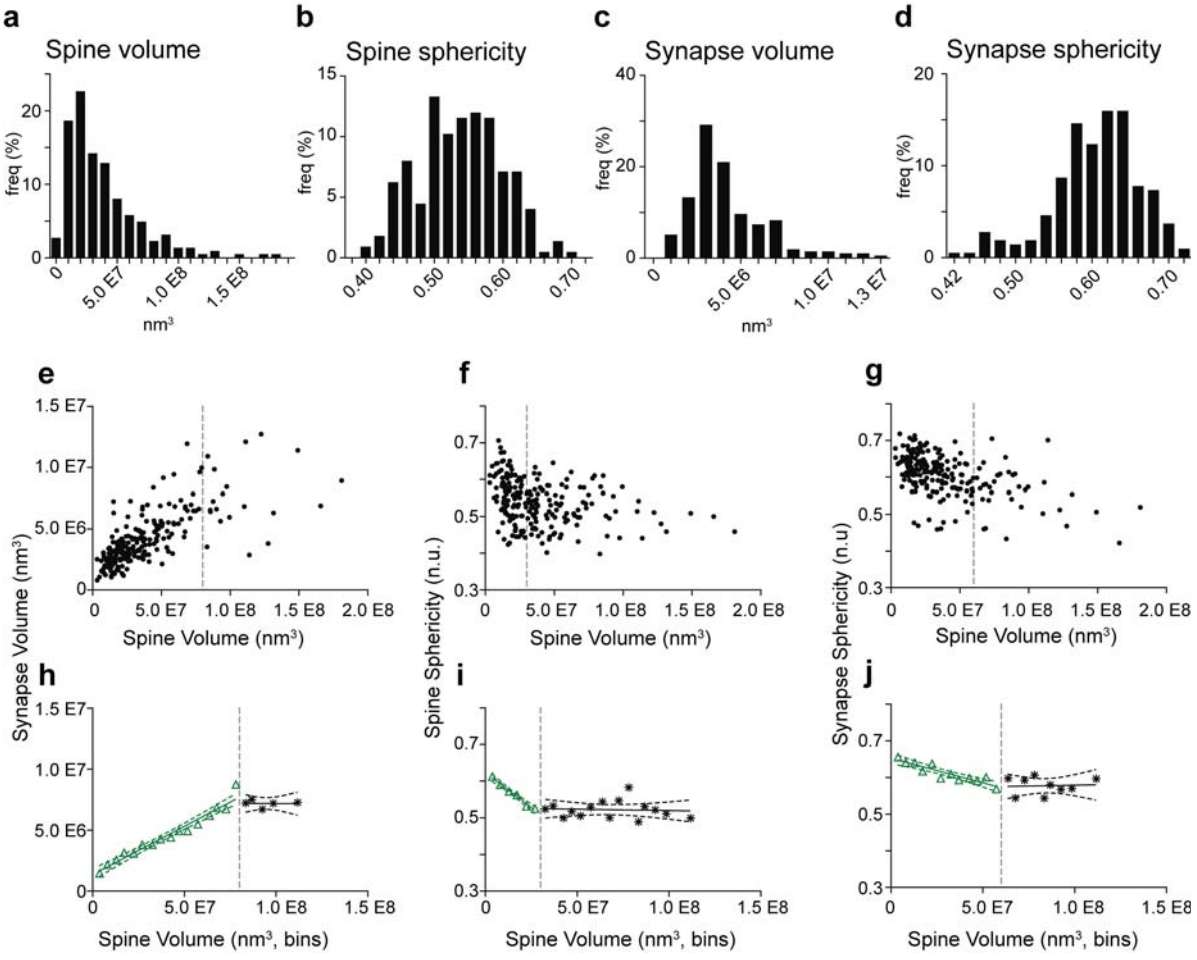

Figure r.4.7 Quantitative correlations of spine volumes with other morphological parameters of spines and synapses from 8 week-old GCs.

(**a-d**) Frequency histograms show the distribution of the different morphometric parameters analyzed, comprising spine volume (**a**), spine sphericity (**b**), synapse volume (**c**) and synapse sphericity (**d**). Note that all distributions display a continuous range of values. (**e-g**) Plots showing the correlation of individual spine volumes with synapse volume (**e**), spine sphericity (**f**) and synapse sphericity (**g**). (**h-j**) Binned analysis of the data shown in (**e-g**) revealing linear regressions between synaptic volume (**h**), spine sphericity (**i**) and synapse sphericity (**j**) with spine volume below (green) and above (black) defined spine volume thresholds (dashed gray lines). Dashed green and black lines represent the 95% confidence intervals for these fits. The data shows that the three parameters evolve linearly with spine volumes until a certain threshold, after which the three parameters remain constant. Note in (**e-g**) that above these thresholds these parameters no longer correlate. Abbreviations: *n.u.*, no units.

The largest proportion of dendritic spines corresponded to the thin and mushroom categories (43% and 20%, respectively). Lower percentages were found for filopodial and stubby categories (17% and 5%, respectively). Further, up to a 15% of dendritic spines were branched. Usually, such complex spines had two side branches (**Fig. r.4.6**) but we also noticed highly complex spines displaying up to 3 distinct tips. Virtually all the extensions that arose from these branched spines were tipped by synapses, which were established by different presynaptic terminals, indicating that these spines are poly-innervated. We also classified as above the single spine heads present in branched spines. Interestingly, the percentage of spine types (filopodia, thin, mushroom and stubby) in branched spines was similar to that of the whole population of dendritic spines (**Fig. r.4.8c**), indicating both individual heterogeneity in branched spines and robust conservation of spine categories. To our knowledge this is the first study reporting ramified, branched spines in adult generated GCs.

We next measured morphological parameters of both the dendritic spines and the synapses received by them. Overall spine and synapse volumes were significantly larger in branched spines, compared to single spines, whereas the sphericity was lower in branched spines, thus reflecting their complexity (**Fig. r.4.6f-h**). Among individualized spines, the distribution of all the morphometric parameters analyzed showed a continuous profile. Spine and synapse volumes distributed with a left-skewed curve, whereas sphericities distributed symmetrically around the mean (**Fig. r.4.7a-d**).

When analyzing relationships between the different parameters of a given single spine-synapse couple, we found that the spine volume correlated positively with the synapse volume and negatively with the spine and synapse's sphericities (**Fig. r.4.7e-g**). Spine volume bins of constant width were created for each comparison and the pooled points inside each bin were averaged (**Fig. r.4.7h-j**). In all cases, the dependent variable evolved linearly with increasing spine volume until a certain threshold, upon which it appeared to remain constant. This threshold was different in each comparison. More interestingly, individual values showed no correlation for data points above the defined threshold (**Fig. r.4.7e-g**, **Tables r4.1-2**).

Table r.4.1 Correlation analysis of spine volume against other variables.

	All spines		Spine Volume Threshold	Spines < threshold		Spines > threshold	
	P [(a)]	Spearman r		P	Spearman r	P	Spearman r
Spine Sphericity	***	-0.3566	3 E7 nm^3	***	-0.3782	ns	(-0.07636)
Synapse Volume	***	0.7414	8 E7 nm^3	***	0.7065	ns	(0.1654)
Synapse Sphericity	***	-0.5016	6 E7 nm^3	***	-0.4303	ns	(-0.2987)

[(a)] *p < 0.05; **p < 0.01; ***p < 0.001; Spearman test

Table r.4.2 Regression analysis of binned spine volume against other variables (below threshold) for 8-9 week-old GCs.

	R^2	P[(a)]	Slope	Y-interceipt
Spine Sphericity	0.9809	***	-3.815 E-9	0.6235
Synapse Volume	0.9529	***	0.07926	1.351 E6
Synapse Sphericity	0.8275	***	-1.341 E-9	0.6526

[a)] *p < 0.05; **p < 0.01; ***p < 0.001; test whether slopes are significantly non-zero.

Taken together, the present FIB/SEM analyses highlights the complex synaptic architecture of dendritic spines in mature GCs and has allowed us the description of vacant spines, branched spines, as well as a correlation of spine and synaptic sizes and sphericities.

Developmental analysis of input synapses onto adult-generated GCs.

To investigate how dendritic spines develop in adult generated GCs, we performed 3D reconstructions of dendritic segments in neurons aged 3- 4 weeks. We found 8 spines in 2 dendritic segments of 3-week-old GCs, and 20 spines in 6 segments of 4-week-old GCs, of which 22 were fully reconstructed (**Table r4.3**, **Fig. r.4.8**). As illustrated by our 3D reconstructions, the overall shapes of dendritic spines at 3-4 weeks were similar to those described for 8-9 week-old GCs (**Fig. r.4.8b**). To deeply characterize developing GC dendritic spines we pooled together data from 3 and 4 week-old neurons (**Table r3.5**). We did not find asynaptic spines at these ages, and all synaptic contacts were on the spine heads. The vast majority of spines bore one single synapse, but we found two spines (7%) receiving more than one synaptic contact on its head, a feature not found in mature GCs. One of these multi-innervated spines (MIS) received two contacts from different boutons, while the other MIS identified received three different excitatory synapses, two of them stablished by the same bouton. When considering the shapes of dendritic spines, 48% were thin, 24% mushroom and 24% filopodial. We also found one branched spine (4%) with three branch tips, but stubby spines were not found at 3-4 weeks (**Fig. r.4.8c**, **Table r.4.4**).

A comparison of spine types at 3-4 and 8 weeks revealed similar percentages of asynaptic, thin and mushroom spines at both ages, and slightly less filopodial spines at 3/4 weeks (**Fig. r.4.8c**). Moreover, in addition to the lack of stubby spines, branched spines were underrepresented at 3-4 weeks. These data show that while thin, mushroom and filopodial types are constant, ramified and stubby types are a preferential feature of mature GCs.

Table r.4.3 Data imaged for the analysis of WT, new-born GCs

	Animals	Dendritic segments	Depth imaged		Volume imaged (μm^3)
			Sections	µm	
3 week-old GCs	1	2	697	17.43	759.4
4 week-old GCs	2	6	920	23.00	1000.7
8-9 week-old GCs	2	6	1436	35.90	1564.5
Sum	5	14	3053	76.33	3324.5

Figure r.4.8 Comparative analysis of dendritic spines in 3-4 and 8-9 weeks old GCs.
(**a**) Examples of thin, filopodial and mushroom dendritic spines arising from their parent dendrite (D) in 3/4 week old GCs. The 3 left images show selected serial planes of the spines depicting the head (green arrowheads), neck and synaptic contact (red arrowheads). The 3D reconstructions are shown to the right. (**b**) 3D reconstructions allowing comparison of dendritic segments and spines at 3-4 and 8-9 weeks. Color code is the same as previously described. (**c**) Histograms showing the percentages of the different types of spines at 3-4 and 8-9 weeks; spine type percentages are also shown for branched spines (right). (**d**) Histograms showing spine volumes, spine sphericity, synapse volume and synapse sphericity at both ages. Data represent mean ± SEM. *$p < 0.05$; **$p < 0.01$; ***$p < 0.001$; Mann-Whitney test. Scale bar in (**a**) is 0.5 µm and is applicable to all panels in (**a**). Scale bar in (**b**) is 1 µm and applies to all panels in (**b**).

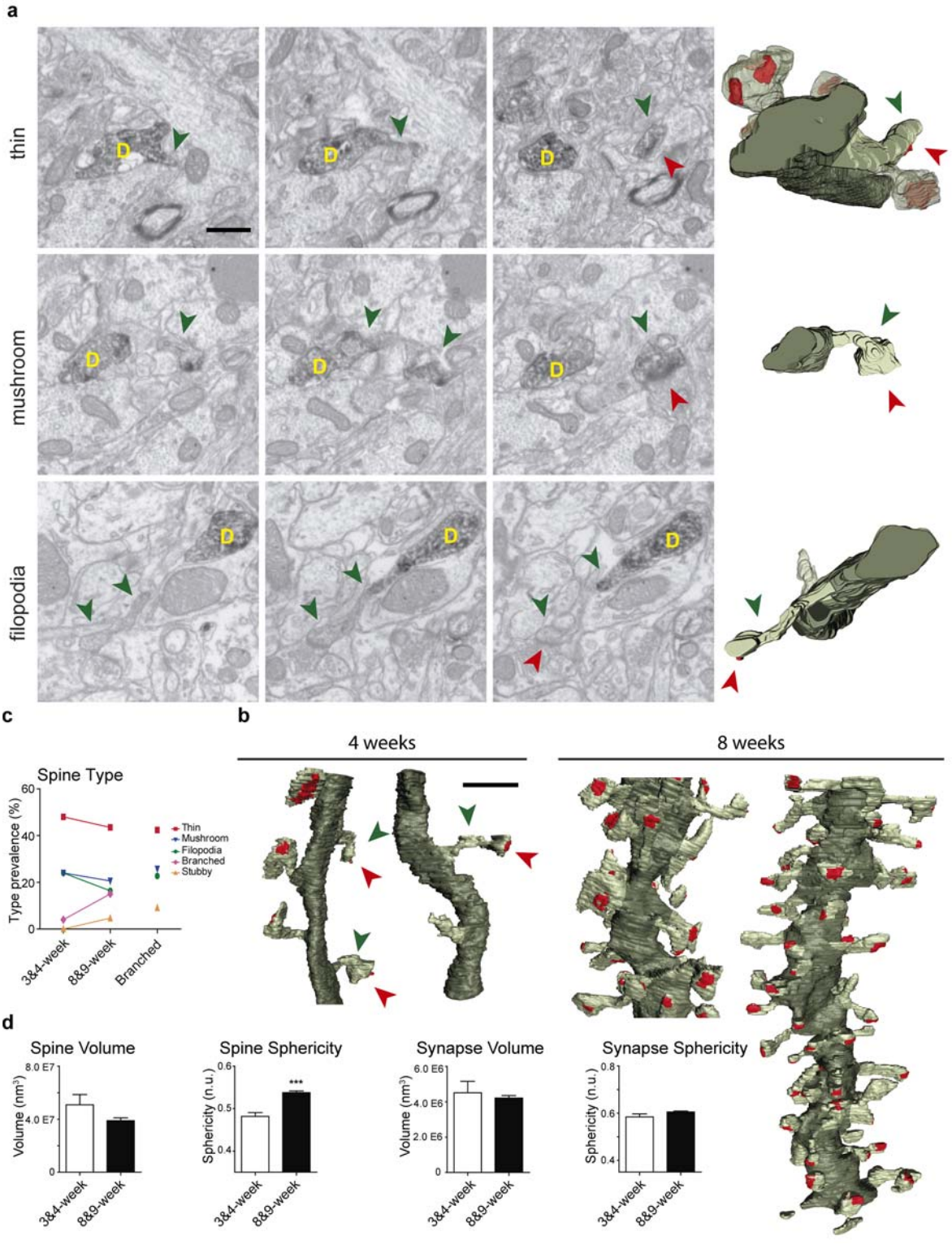
a
thin
mushroom
filopodia
D
c
Spine Type
Type prevalence (%)
60
40
20
0
Thin
Mushroom
Filopodia
Branched
Stubby
3&4-week
8&9-week
Branched
b
4 weeks
8 weeks
d
Spine Volume
Volume (nm³)
8.0 E7
4.0 E7
0
3&4-week
8&9-week
Spine Sphericity
Sphericity (n.u.)
0.6
0.5
0.4
***
Synapse Volume
Volume (nm³)
6.0 E6
4.0 E6
2.0 E6
Synapse Sphericity
Sphericity (n.u.)
0.8
0.6
0.4

Table r.4.4 Number of analyzed features in WT new-born GCs

a) Identified items		WT young	WT mature	ALL	"ND" meaning
Synapses	**#**	**27**	**244**	**271**	existence not clear
Spines	**#5-type** (a)	**26**	**235**	261	SpType not clear
	#4-type (b)	**28**	**271**	**299**	
	4T full 3D-#	22	226	248	
	4T full 3D-%	78.6%	83.4%	82.9%	
	5T-"nd", #	1	20	21	
	5T-"nd", %	3.8%	8.5%	8.0%	
	4T-"nd", #	2	22	24	
	4T-"nd", %	7.1%	8.1%	8.0%	
Assynaptic heads	**#**	0	5	5	No ND - only tagged if defined
	%	0.0%	1.8%	1.7%	
Presynaptic	**SB, #**	27	244	271	SBi not clear
	"nd", #	2	19	21	
	"nd", %	7.4%	7.8%	7.7%	
	NOT ND:				
	SB, #	25	225	250	
	MSB, #	19	162	181	
	MSB, %	76.0%	72.0%	72.4%	
	SSB, %	24.0%	28.0%	27.6%	
	SpType in SBs:				No ND - only pooled if defined: Spine Type is clear AND synapse existence is clear AND SBi is clear
	Spine 5T-# (no NDs)	25	221	246	
	Spine 4T-# (no NDs)	24	221	245	
	SSB SpType:				
	Spine 5T-# (no NDs)	6	63	69	
	Spine 4T-# (no NDs)	6	63	69	
	MSB SpType:				
	Spine 5T-# (no NDs)	19	158	177	
	Spine 4T-# (no NDs)	18	158	176	
b) Full 3D-reconstructed items					
Synapses	**4T**	**23**	**220**	243	No ND - only pooled if defined
	5T-all	22	189	211	
	5T-nonBranched	22	163	185	
Spines	***5-Type Spines:***				No ND - only pooled if defined: SpType clear
	All Spines	**20**	**191**	211	
	Spines with only one synapse	17	183	200	
	All Branched Spines	0	26	26	
	Branched spines with at least one synapse	0	26	26	
	All Non-Branched Spines	20	165	185	
	Non-Branched Spines with only one synapse/head	17	157	174	
	4-Type Spines:				
	All Spines	**22**	**226**	248	
	Spines with only one synapse	18	214	232	
Presynaptic	SSB + MSB spines (full 3D)	21	210	231	No ND - 2D ok AND full_3D available
	SSB-spines (full 3D)	4	59	63	
	MSB-spines (full 3D)	17	151	168	

(a) 5-type spines refers to all spines that enter classification into filopodia, thin, stubby, mushroom and branched.
(b) 4-type spines refers to all individualized spines that enter classification into filopodia, thin, stubby and mushroom

We also found that developing dendritic spine's volumes correlated positively with synaptic sizes, and negatively with spine's sphericity. Again, the relationship between a spine's volume and its synapse's volume exhibited a two-regime behavior: spines bigger than the threshold previously determined for the 8-9 week-old population did no longer exhibit correlation between spine volume and synapse volume (**Table r.4.5**). When compared to 8-9 week-old GCs, spines at 3/4 weeks were less spherical and tended to be larger (**Fig. r.4.8d**). Taken together, our data show that though there is a remarkable robustness in most morphological and morphometric parameters at both ages, stubby and branched spines are clearly a characteristic feature of mature GCs, and spines decrease in size and complexity with age.

Table r.4.5 Correlation analysis of young neuron's spine volume against other variables for 8-9 week-old GCs

	All spines		Spine Volume Threshold	Spines < threshold		Spines > threshold	
	P	Spearman r		P	Spearman r	P	Spearman r
Spine Sphericity	**	-0.6718	--	--	--	--	--
Synapse Volume	***	0.8060	8 E7 nm3	***	0.7607	ns	(0.50)
Synapse Sphericity	ns	(-0.29)	--	--	--	--	--

[(a)] *p < 0.05; **p < 0.01; ***p < 0.001; Spearman test

Spines from adult-generated GCs are preferentially innervated by multi-synaptic axon terminals.

We next investigated the features of axon terminals that were presynaptic to labeled GCs. We analyzed the connectivity of the 271 bouton terminals innervating the previously identified spines. At 8 weeks, about one fourth (28%) of presynaptic boutons established synapses exclusively onto the GFP-labeled dendritic spine (Single Synaptic Boutons, SSBs). The remaining axon terminals (72%) formed synapses with both the labeled identified spine and with one or more additional postsynaptic elements, the majority of them being also dendritic spines (Multiple Synaptic Boutons, MSBs) (**Fig. r.4.9g**). All the synapses were asymmetric. The majority of these MSBs established synapse with one to three unlabeled spines, in addition to the GFP-positive spine (**Fig. r.4.9b-f, h-i**). Interestingly, up to 26% of axon terminals were involved in complex synaptic configurations establishing simultaneous synapses with four or more spines, in addition to the identified spine (**Fig. r.4.9i**). Some MSBs in fact (8%) exhibited very complex configurations and established synapses with 7-10 different postsynaptic elements (**Fig. r.4.9c**, **f**). Finally, the SSB/MSB ratio was similar for all spine types (**Fig. r.4.10a**) and spines which are postsynaptic to either SSBs or MSBs did not differ in their morphological properties (**Fig. r.4.10b-e**).

At 3-4 weeks, 6 out of 25 axon terminals established a single synapse exclusively with the GFP-labeled spine (SSB), whereas 11 established contact with one additional element, and 8 boutons formed synapses with 2-3 unlabeled spines, in addition to the GFP-traced spine. Terminals establishing synapses with 5 or more spines were not found at 3-4 weeks. Thus, whereas the percentage of MSBs was similar at both ages, the average of synapses established by these boutons increased at 8 weeks (**Fig. r.4.9h**).

We conclude that although the innervation of developing GC spines by MSBs is a common feature of developing and adult spines, the complexity of synaptic multi-innervation increases in mature GCs.

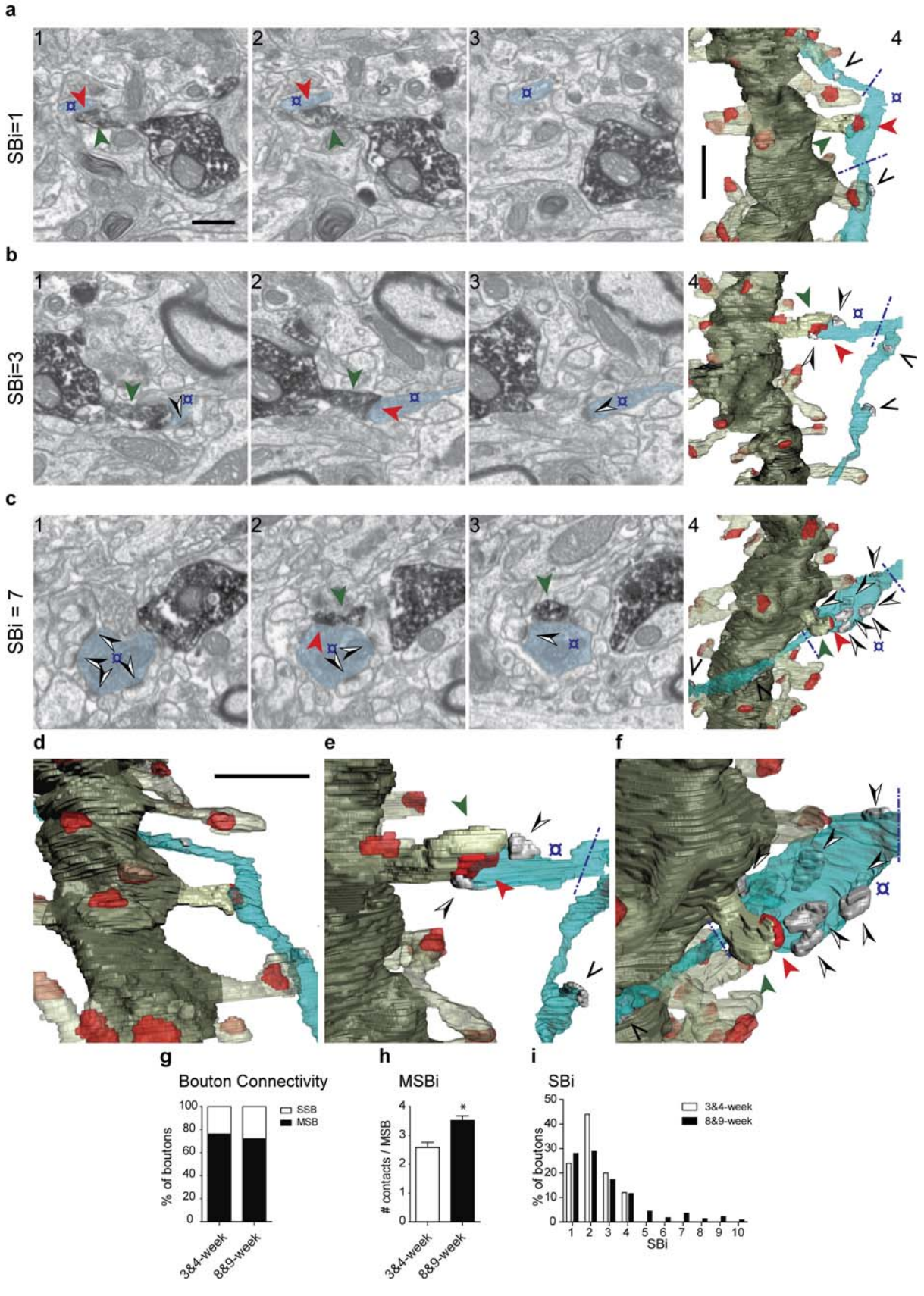
a
SBi=1
1
2
3
4
b
SBi=3
1
2
3
4
c
SBi = 7
1
2
3
4
d
e
f
g
Bouton Connectivity
% of boutons
100
80
60
40
20
0
SSB
MSB
3&4-week
8&9-week
h
MSBi
contacts / MSB
4
3
2
1
0
*
3&4-week
8&9-week
i
SBi
% of boutons
50
40
30
20
10
0
3&4-week
8&9-week
1 2 3 4 5 6 7 8 9 10
SBi

Figure r.4.9 Characteristics of presynaptic innervation of GC dendritic spines at 3-4 and 8-9 weeks.
(**a-c**) Three different examples of synaptic configurations, including a presynaptic bouton (o) contacting (red arrowhead) exclusively the DAB-labeled spine (green arrowhead) (**a**) and axon terminals forming complex synaptic configurations contacting both the labeled spine and unlabeled dendritic spines (black and white arrowheads) (**b**, **c**). The left FIB/SEM images show selected serial planes of the dendritic spines and presynaptic boutons. The corresponding 3D reconstructions are shown to the right (**a4**, **b4**, **c4**) as well as in a tilted orientation in **d**, **e** and **f**, respectively. Note that only the varicosities were analyzed, not the entire axon (varicosities delimited by blue dashed lines in the 3D panels). The axons may stablish other synapses elsewhere, not analyzed (black arrowheads in the 3D panels). The example shown in (**b**) illustrates a multisynaptic bouton establishing a total of 3 synapses and the example illustrated in (**c**) establishes 7 synapses. Color code is the same as previously described. Additionally, axon is transparent blue, and synapses established by the axon onto non-labeled spines are solid gray. (**g**) Percentage of single-synaptic (SSB) and multi-synaptic (MSB) boutons in 3-4 and 8-9 weeks-old dendritic spines. (**h**) Average number of synaptic contacts established by multi-synaptic boutons at 3-4 and 8-9 weeks. Data represent mean ± SEM. *p < 0.05; **p < 0.01; ***p < 0.001; Mann-Whitney test. (**i**) Histogram showing the frequency of synaptic contacts established by axon terminals at 3-4 and 8-9 weeks. Scale bar in (**a1**) is 0.5 µm and is applicable to panels (**a1-3**, **b1-3**, **c1-3**). Scale bar in (**a4**) is 1 µm and applies panels (**a4**, **b4**, **c4**). Scale bar in (**d**) is 1 µm and applies panels (**d**, **e**, **f**).

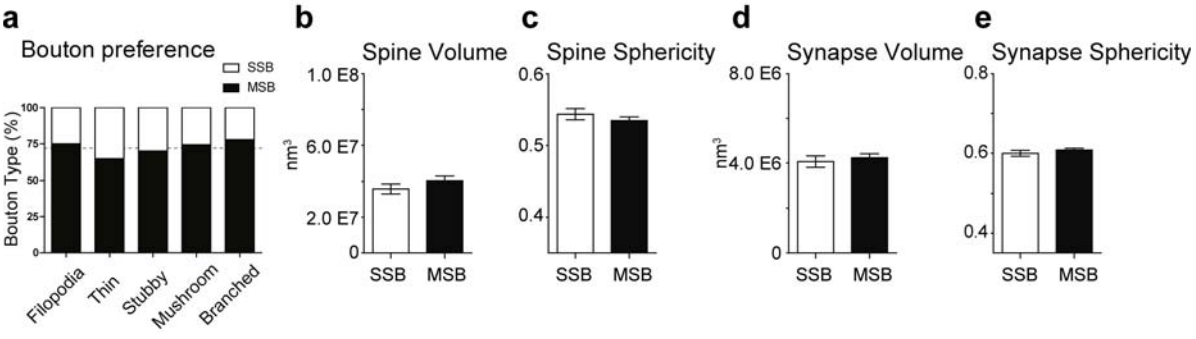

Figure r.4.10 Multisynaptic boutons innervate equally all spine types and morphologies.
(**a**) Percentage of single-synaptic (SSB) and multi-synaptic (MSB) boutons in different types of dendritic spines in 8-9-weeks old neurons; the dashed line indicates the overall percentage of SSBs and MSBs. (**b-e**) Histograms showing spine volumes (**b**), spine sphericity (**c**), synapse volume (**d**) and synapse sphericity (**e**) of spines innervated by either SSBs or MSBs in 8-9 week-old neurons. Grey dashed line shows the average percentage of MSB in the overall population. Data represent mean ± SEM. *p < 0.05; Mann-Whitney test.

5. Role of Reelin signaling in the synaptic integration of developing new-born granule cells in the adult hippocampus.

Introduction to Chapter 5: Reelin and adult neurogenesis.

Adult neurogenesis in the dentate gyrus is essential for learning and memory and it has been implicated in major neurodegenerative and psychiatric diseases (Zhao et al., 2008; Deng et al., 2010). Whereas recent studies have identified key factors for the regulation and proliferation rates of neuroprogenitor cells (Lie et al., 2005; Jessberger et al., 2008; Lagace et al., 2008; Gao et al., 2009; Karalay et al., 2011; Vadodaria and Gage, 2014), much less is known about the mechanisms that control synaptogenesis of adult-generated GCs and their recruitment into adult circuits (Toni et al., 2007). Interestingly, spatial learning training has been shown to accelerate the integration of adult-generated neurons, dendritic spine formation in adult-born GCs is impaired in mouse models of Alzheimer's disease and adult neurogenesis has been associated with forgetting established memories (Sun et al., 2009; Lemaire et al., 2012; Akers et al., 2014).

Recently, studies from colleagues found that Reelin signalling is involved in the migratory and maturation processes of adult-generated neurons. Adult Reelin-OE mice displayed decreased BrdU incorporation in the granule cell layer of the olfactory bulb, whereas new-born neurons in the DG located further from the subgranular zone (SGZ) (Pujadas et al., 2010). Other studies demonstrated that the Reelin pathway dramatically regulates GC adult neurogenesis in a cell-autonomous manner: whereas overexpression of Reelin accelerates dendritic maturation, disruption of the Reelin pathway results in the development of aberrant basal dendrites and in a defective growth of the dendritic arbor (Teixeira et al., 2012).

In this chapter we addressed the impact of the Reelin pathway in the synaptogenic process of adult-generated GCs by using retroviral tracing and FIB/SEM technology.

Reelin role on new-born GCs can be assessed by a correlative light microscopy-FIB/SEM imaging protocol.

We wanted to characterize the role of Reelin in the integration of new-born GCs into the preexisting DG circuitry. The critical period for new-born GCs extends from 4 to 6 weeks-old neurons and most physiological and branching features appear as mature at 8-9 week-old ones. To analyze whether this process would suffer alterations at the ultrastructural level under different Reelin signaling scenarios, we defined two timepoints for analysis: 4 weeks and 8-9 weeks post-infection.

We applied the same correlative light microscopy – FIB/SEM approach described on **chapter 4** to acquire high-resolution 3D images of dendritic segments of prelabeled new-born granule cells. This time, the experimental approach allowed the imaging of new-born GCs in both a gain and a loss-of-function scenario of Reelin signaling: Reelin-OE mice present exogenously Reelin-expressing GCs and the molecular layer bears higher levels of extracellular Reelin which is overexpressed by entorhinal pyramidal neurons. In contrast, infection with Cre recombinase-expressing retroviruses (RV-Cre-GFP) to flDab1 mice labeled new-born GCs with a cell-specific escision of the Dab1 gene (Dab1-KO cells), whereas the surrounding tissue displayed normal architecture and gene expression.

We acquired dendrites of both experimental groups additionally to the corresponding controls. The latter constitute the joint WT group analyzed in **chapter 4** and are also pooled together in the analysis presented in this chapter. For Reelin-OE and Dab1-KO cells, we imaged 9 and 5 dendritic segments that represented more than 1500 μm^3 and 1100 μm^3 of bulk tissue imaged, respectively. These dendrites corresponded either to 4 weeks (+880 μm^3 and +550 μm^3 in Reelin-OE and Dab1-KO cells respectively) and 8-9 weeks-old (+620 μm^3 and +570 μm^3) GCs (**Table r.5.1**). The systematic image analysis, annotation and segmentation of these acquisitions led to the identification of 161 and 84 dendritic spines in Reelin-OE and Dab1-KO cells. Together with the control group, the study contemplates a total of 544 identified dendritic spines, of which 433 were completely reconstructed and analyzed in 3D (**Table r.5.2**).

Table r.5.1 Data imaged for the analysis of Reelin-OE and Dab1-KO new-born GCs

		Animals	Dendritic segments	Depth imaged		Volume imaged (μm^3)
				Sections	µm	
Reelin-OE	4 week-old GCs	1	7	881	21.72	887.8
	8-9 week-old GCs	1	2	254	6.35	622.6
	Sum	2	9	1135	28.07	1510.4
Dab1-KO	4 week-old GCs	1	2	513	12.83	558.9
	8-9 week-old GCs	1	3	532	13.30	579.6
	Sum	2	5	1045	26.13	1138.5
All groups (with WT)	Sum	9	28	5233	130.52	5973.5

Table r.5.2 Number of analyzed features in Reelin-OE and Dab1-KO new-born GCs

a) Identified items		Reelin-OE young	Reelin-OE mature	Dab1-KO young	Dab1-KO mature	All ages R-OE	All ages Dab1-KO	All groups (with WT)
Synapses	#	**50**	**79**	**32**	**44**	129	76	**476**
Neck Synapses	#	0	1	0	1	1	1	9
	%	0.0%	3.1%	0.0%	2.3%	0.8%	1.3%	1.9%
Head Synapses	#	50	78	32	43	128	75	467
	%	100.0%	243.8%	40.5%	97.7%	99.2%	98.7%	98.1%
Spines	**#5-type** (a)	**57**	**90**	**30**	**44**	147	74	482
	#4-type (b)	**60**	**101**	**34**	**50**	161	84	**544**
	4T full 3D-#	45	82	27	41	127	68	443
	4T full 3D-%	75.0%	81.2%	79.4%	82.0%	78.9%	81.0%	81.4%
	5T-"nd", # (c)	8	6	2	2	14	4	39
	5T-"nd", %	14.0%	6.7%	6.7%	4.5%	9.5%	5.4%	8.1%
	4T-"nd", #	8	6	2	2	14	4	42
	4T-"nd", %	13.3%	5.9%	5.9%	4.0%	8.7%	4.8%	7.7%
Assynaptic heads	#	0	5	1	3	5	4	14
	%	0.0%	5.0%	2.9%	6.0%	3.1%	4.8%	2.6%
Presynaptic	**SB, #**	50	79	32	44	129	76	476
	"nd", #	14	21	3	4	35	7	63
	"nd", %	28.0%	26.6%	9.4%	9.1%	27.1%	9.2%	13.2%
	NOT ND:							
	SB, #	36	58	29	40	94	69	413
	MSB, #	23	31	20	19	54	39	274
	MSB, %	63.9%	53.4%	69.0%	47.5%	57.4%	56.5%	66.3%
	SSB, %	36.1%	46.6%	31.0%	52.5%	42.6%	43.5%	33.7%
	SpType in SBs:							
	Spine 5T-# (no NDs)	34	57	28	40	91	68	405
	Spine 4T-# (no NDs)	34	57	28	40	91	68	404
	SSB SpType:							
	Spine 5T-# (no NDs)	11	26	8	21	37	29	135
	Spine 4T-# (no NDs)	11	26	8	21	37	29	135
	MSB SpType:							
	Spine 5T-# (no NDs)	23	31	20	19	54	39	270
	Spine 4T-# (no NDs)	23	31	20	19	54	39	269

b) Full 3D-reconstructed items								
Synapses	**4T**	**41**	**68**	**28**	**40**	109	68	420
	5T-all	39	59	25	37	98	62	371
	5T-nonBranched	36	52	21	34	88	55	328
Spines	***5-Type Spines:***							
	All Spines	**42**	**69**	**23**	**37**	111	60	382
	Spines with only one synapse	37	59	19	30	96	49	345
	All Branched Spines	3	8	4	3	11	7	44
	Branched spines with at least one synapse	3	7	4	3	10	7	43
	All Non-Branched Spines	39	61	19	34	100	53	338
	Non-B.Sp with only one synapse/head	34	52	15	27	86	42	302
	4-Type Spines:							
	All Spines	**45**	**82**	**27**	**41**	127	68	443
	Spines with only one synapse	39	68	22	33	107	55	394
Presynaptic	SSB + MSB spines (full 3D)	32	52	26	38	84	64	379
	SSB-spines (full 3D)	11	25	6	21	36	27	126
	MSB-spines (full 3D)	21	27	20	17	48	37	253

(a) 5-type spines refers to all spines that enter classification into filopodia, thin, stubby, mushroom and branched.
(b) 4-type spines refers to all individualized spines that enter classification into filopodia, thin, stubby and mushroom
(c) non-determined ("nd") criteria are the same as stated in **Table r.4.4**.

Mature new-born granule cells exhibit structural alterations upon both up- and down-regulation of the Reelin signaling pathway.

We imaged dendritic segments of both Reelin-OE and Dab1-KO 8-9 week-old new-born GCs. From these, we identified 101 and 50 dendritic spines, of which 82 and 41 were imaged and reconstructed completely in 3D (**Table r.5.2**). Most of these spines bore a single excitatory synaptic contact on the spine head. However, 5 spines of Reelin-OE (5 %) and 3 of Dab1-KO cells (6%) were devoid of any postsynaptic density and presynaptic partner. Besides, 1 excitatory synapse on the spine neck was found in both genotypes (3% and 2%, respectively). Furthermore, in Dab1-KO GCs, we found 2 spines (4%) bearing 2 and 3 excitatory synapses on their head. In the latter, all three synapses were performed by the same presynaptic bouton, whereas in the former two independent boutons performed the two synapses identified. Likewise, in this same group we found 1 spine (2%) bearing two synapses –one at the head and one at the neck – performed by different boutons.

We next performed a 2-dimensional assessment of spine type prevalence according to the previously defined criteria. We were able to identify spines of all described types in both experimental groups analyzed. In Reelin-OE samples, spine type proportions were roughly similar to those found previously in WT, except for a 40% increase in the presence of "mushroom"-shaped spines. Dab1-KO GCs exhibited a similar prevalence of thin, branched and stubby spines, but presented 2.1 times more filopodia and only a 47% of the mushroom spines detected in control samples (**Fig. r.5.1 a-c**).

In order to further evaluate morphological features of these spines and synapses we segmented and isolated 3D reconstructions of all the fully imaged dendritic spines. Spine and synaptic volumes distributed in a left-skewed curve, whereas sphericity values distributed symmetrically around the mean, and all parameters measured displayed a continuum in their values distribution. Similarly to what was previously observed in the control samples, spine volumes exhibited a huge variability ranging across

Figure r.5.1 Comparative analysis of dendritic spines in 3-4 and 8-9 weeks-old GCs of Reelin-OE mice and Dab1-KO GCs.
(**a**) 3D reconstructions of dendritic segments from 4 and 8-9 week-old GCs of Reelin-OE, WT and Dab1-KO GCs. Color code is dark green for the dendritic shaft, pale green for the dendritic spines and red for the synapses. (**b-c**) Histograms showing the percentages of the different types of spines at 3-4 and 8-9 week-old GCs of the experimental groups described (**b**) and illustration of the spine type proportional representation in a putative dendritic segment containing 5 spines (**c**), based on a closed list d'Hondt method approach (spine designs as in **Fig. r.4.5a**) (**d-g**) Quantification of morphological features of dendritic spines. (**d-e**) Spine volume (**d**) and sphericity (**e**) of developing new-born GCs under different Reelin signaling paradigms. (**f**) Cumulative frequency distribution of spine volumes of 8-9 week-old GCs. Note that Reelin-OE spines show a bias from the WT curve for spine volumes above a given threshold (green dashed line). (**g**) Comparison of the spine volumes for spines above the threshold. (**h-l**) Quantification of morphological features of synapses received by new-born GCs. (**h-i**) Synapse volume (**h**) and sphericity (**i**) of synapses received by developing new-born GCs under different Reelin signaling paradigms. (**j**) Cumulative frequency distribution of synaptic volumes of 8-9 week-old GCs. Note that Reelin-OE synapses show a bias from the WT curve for synaptic volumes above a given threshold (green dashed line), whereas Dab1-KO GCs exhibit different synaptic volumes for synapses below a given threshold (red dashed line). (**k**) Comparison of the synaptic sizes of Dab1-KO and WT synapses smaller than the defined threshold (red dashed line). (**l**) Comparison of the synaptic sizes of WT and Reelin-OE synapses larger than the defined threshold (green dashed line). Data represent mean ± SEM. *$p < 0.05$; **$p < 0.01$; ***$p < 0.001$. Comparisons between two groups were assessed by Mann-Whitney test. Comparisons between three groups were assessed by Kruskal-Wallis test and post hoc Dunns test. When this analysis failed to determine significance between two individual groups, these were isolated and further compared by Mann-Whitney test (dashed lines). Scale bar in (**a**) is 1 μm and applies to all reconstructions.

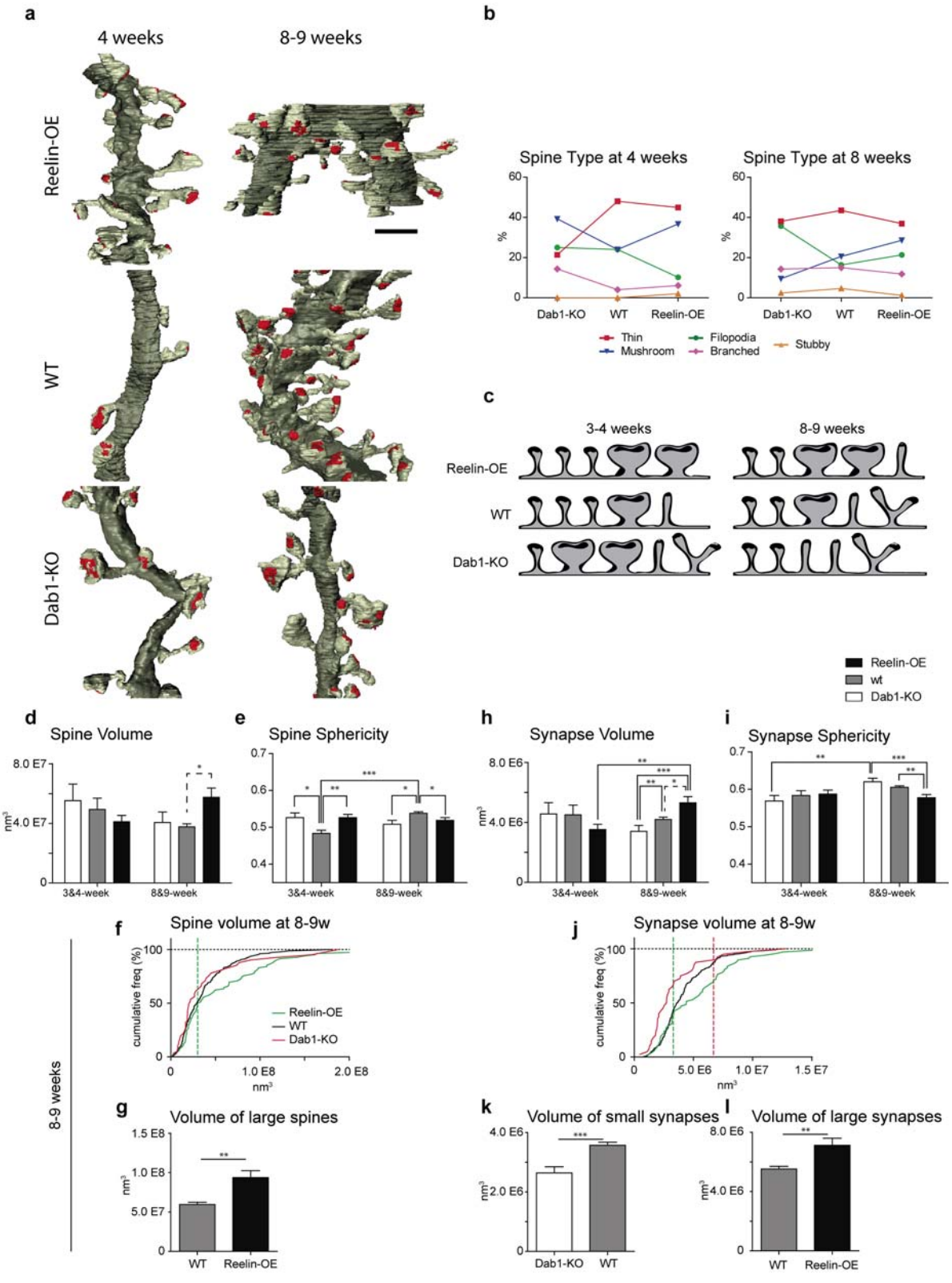
a
4 weeks
8-9 weeks
Reelin-OE
WT
Dab1-KO
b
Spine Type at 4 weeks
Spine Type at 8 weeks
%
Dab1-KO
WT
Reelin-OE
Thin
Mushroom
Filopodia
Branched
Stubby
c
3-4 weeks
8-9 weeks
Reelin-OE
WT
Dab1-KO
Reelin-OE
wt
Dab1-KO
d
Spine Volume
nm3
3&4-week
8&9-week
e
Spine Sphericity
h
Synapse Volume
i
Synapse Sphericity
8-9 weeks
f
Spine volume at 8-9w
cumulative freq (%)
Reelin-OE
WT
Dab1-KO
j
Synapse volume at 8-9w
g
Volume of large spines
k
Volume of small synapses
l
Volume of large synapses

Table r.5.3 Spine and synapse maximal records found for morphological parameters.

a) 3-4 week-old GCs

	Spine				Synapse			
	Volume		Sphericity		Volume		Sphericity	
	min	max	min	max	min	max	min	max
Reelin- OE	6.25E+06	1.43E+08	0.40	0.65	8.90E+05	1.19E+07	0.40	0.71
WT	7.60E+06	1.23E+08	0.41	0.56	6.85E+05	1.25E+07	0.44	0.70
Dab1KO	3.96E+06	1.89E+08	0.41	0.68	6.22E+05	1.95E+07	0.37	0.70

b) 8-9 week-old GCs

	Spine				Synapse			
	Volume		Sphericity		Volume		Sphericity	
	min	max	min	max	min	max	min	max
Reelin- OE	1.75E+06	3.00E+08	0.39	0.67	1.02E+06	1.86E+07	0.43	0.73
WT	1.68E+06	1.81E+08	0.40	0.71	7.94E+05	1.27E+07	0.42	0.72
Dab1KO	2.35E+06	1.88E+08	0.34	0.63	4.83E+05	1.28E+07	0.43	0.71

two orders of magnitude: 8-9 week Dab1-KO GCs presented spines with volumes comprised between 2.35E+06 to 1.88E+08 nm^3, and Reelin-OE spine volumes were found between 1.75E+06 and 3.00E+08 nm^3 (**Table r.5.3**). Interestingly, the biggest spine in Reelin-OE was 1.7 times larger than the largest one found in the control group (1.81E+008 nm^3). Likewise, 8-9 week GCs exhibited larger spines in Reelin-OE than in WT samples (**Fig. r.5.1d**), a phenotype that was specific to large spines (**Fig. r.5.1f-g**).

Spine sphericity values in 8-9 week GCs were comprised between 0.39 and 0.67 in Reelin-OE and between 0.34 and 0.63 in Dab1-KO cells (**Table r.5.3**). Spine sphericities of both Dab1-KO and Reelin-OE GCs were lower than the control group (**Fig. r.5.1d**). Therefore, spines of 8-9 week adult-born GCs exhibit larger sizes in Reelin-OE mice, and less compact morphologies in both Reelin-OE and Dab1-KO GCs.

Segmentations of synaptic areas including the postsynaptic density and the presynaptic membrane adjacent to the synaptic cleft gave rise to accurate 3D reconstructions, allowing for a similar morphometric analysis. Despite smaller sizes, synaptic volume values displayed a great variability, similar to the one found in control samples. Once more, the largest synapse was found in the Reelin-OE group (1.86E+07 nm^3) (**Table r.5.3**), although smaller synapses were as frequent as in control samples (**Fig. r.5.1j**). Indeed, synaptic volume seemed to increase with Reelin dosage: synapses of Reelin-OE GCs were larger than both controls and Dab1-KO GCs, which exhibited in average the smallest synapses (**Fig. r.5.1h**). More interestingly, when splitting the analysis between large and small synapses, we found that large (but not small) Reelin-OE synapses were larger than controls (**Fig. r.5.1l**), and that small (but not large) Dab1-KO synapses were smaller (**Fig. r.5.1k**). Furthermore, Reelin-OE GCs exhibited synapses less spherical than the ones found at control and Dab1-KO GCs (**Fig. r.5.1i**).

Altogether, we found an increase in synaptic complexity concomitant to Reelin dosage: Reelin-OE GCs bore larger and less compact synapses, whereas Dab1-KO GCs exhibited smaller and rounder synaptic contacts.

We previously described a correlation between the morphometric values of a given spine-synapse couple in the WT group (**chapter 3**). We wondered whether alterations in Reelin-mediated signaling could disrupt those correlations. When plotting the synaptic volume and the sphericities of the spine and the synapse against the volume of the synapse, we found that the correlations described were largely

conserved in both Reelin-OE and Dab1-KO GCs (**Fig. r.5.2**, **Table r.5.4**). Thus, volume and sphericity of a spine and its synapse appear to be highly correlated parameters, and this relationship is preserved upon modulations of Reelin signaling.

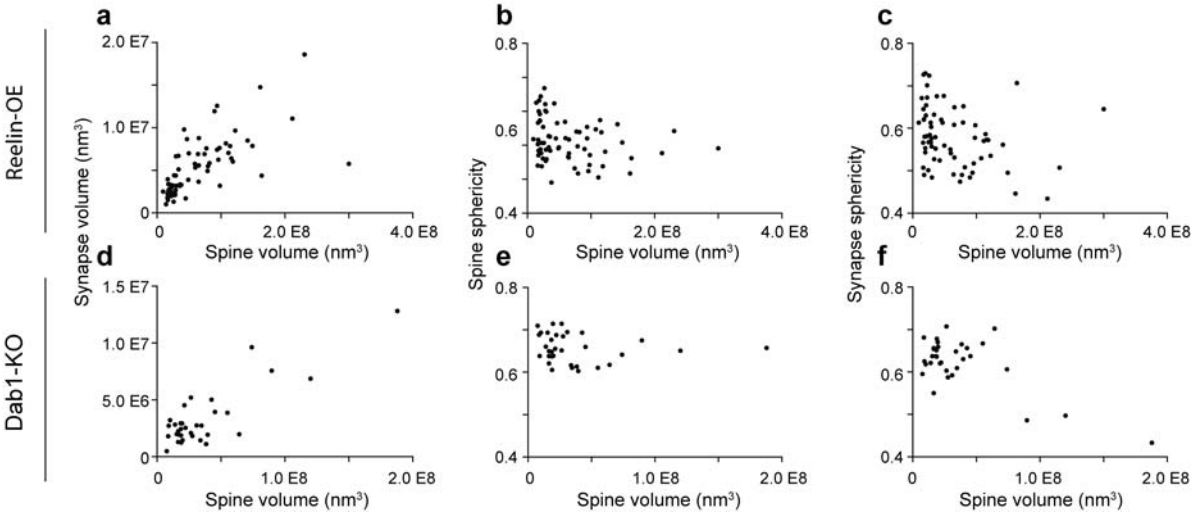

Figure r.5.2 Correlations of spine volumes with other morphological parameters of spines and synapses in Reelin-OE and Dab1-KO 8-9 week-old GCs.
(**a-c**) Plots showing the correlation of individual Reelin-OE spine volumes with synapse volume (**a**), spine sphericity (**b**) and synapse sphericity (**c**). (**d-f**) Plots showing the correlation of individual Dab1-KO spine volumes with synapse volume (**d**), spine sphericity (**e**) and synapse sphericity (**f**).

Table r.5.4 Correlation analysis of spine volume against other variables in Reelin-OE and Dab1-KO new-born GCs.

		Synapse Volume		Spine Sphericity		Synapse sphericity	
		P [a]	r [b]	P	r	P	r
Reelin-OE	4 week-old GCs	***	0.71	ns	- 0.20	**	- 0.44
	8-9 week-old GCs	***	0.85	*	- 0.46	**	- 0.60
Dab1-KO	4 week-old GCs	***	0.72	*	- 0.27	**	- 0.34
	8-9 week-old GCs	**	0.46	ns	- 0.24	***	- 0.69

[a] Two-tailed P values are represented as follows: P < 0.001 as ***; P < 0.01 as **; P < 0.05 as *; P > 0.05 as "ns".
[b] Spearman test r value

Developmental analysis of input synapses onto adult-generated GCs under gain and loss-of-function paradigms of Reelin signaling

We sought to determine to which extent Reelin signaling could affect the developmental process underlying afferent synapse formation and maturation on new-born GCs. We analyzed synapses and spines of dendrites of 4-week-old Reelin-OE and Dab1-KO GCs. We reconstructed 7 and 2 dendritic segments of Reelin-OE and Dab1-KO GCs, respectively which occupied an imaged volume of +880 and +550 μm³ (**Table r.5.1**). Detailed analysis of these dendritic segments allowed the identification of

60 and 34 dendritic spines, of which 45 and 27 were fully imaged and 3D-reconstructed (**Table r.5.2**). As in the control group, all synapses identified on 4-week GCs were located on the spine head. Once again, most spines received a single excitatory contact, but some exceptional features were noticed. We found one asynaptic dendritic spine, corresponding to a Dab1-KO GC. Besides, some spines were found to receive more than one synaptic contact on the head. In the Reelin-OE group, 1 spine (2%) exhibited two synapses, which were established by different presynaptic boutons. Likewise, two spines (6%) of Dab1-KO GCs exhibited two synapses each on their head established by the same bouton. Interestingly, a spinule was identified on each of the two Dab1-KO MIS mentioned.

Spine classification into the aforementioned types revealed substantial differences with respect to the previously characterized control group (**chapter 4**). In Reelin-OE 4-week new-born GCs, prevalence of thin, branched and stubby spines resembled those found in controls. By contrast, they exhibited only a 43% of the filopodia found in controls and a 53% increase in mushroom spines. On the other hand, spines on Dab1-KO immature GCs displayed a different pattern. Here, frequency of stubby and filopodia spine types was similar to control group. However, abundance of mushroom and branched spines was 1.6 and 3.5 folds the ones found in controls, respectively, whereas presence of thin spines represented a mere 45% of the control prevalence (**Fig. r.5.1a-c**). Altogether, spine types exhibited numerous structural alterations in immature GCs under modifications in the Reelin signaling pathway, and the abundance of mushroom spines was enhanced by almost a 50% in both Reelin-overexpressing and Reelin-unresponsive scenarios.

We next analyzed the morphological properties of individualized spines after 3D-reconstruction. Similarly to previously described, volumes of both spines and synapses presented very diverse values, ranging through two orders of magnitude in all experimental groups. Besides, sphericity values of either spines or synapses were found not lower than 0.40 nor bigger than 0.70. This range was slightly narrower than the one found in mature GCs (0.34 to 0.73) (**Table r.5.3**). Dendritic spines of both Reelin-OE and Dab1-KO 4-week GCs displayed similar average volumes but increased sphericity than controls (**Fig. r.5.1d-e**). Moreover, spine sphericities in 4-week GCs were similar to the ones found in 8-9 week GCs, whereas control spines increased their sphericity during maturation. Synapses in 4 week GCs were similar across genotypes in terms of both volume and sphericity, but synapses of immature Reelin-OE GCs exhibited lower sphericities than the ones found in mature Reelin-OE GCs (**Fig. r.5.1h-i**). Similarly, Dab1-KO GCs presented an increase in synapse sphericity during cell development that was not found in other genotypes (**Fig. r.5.1i**). Altogether, spines of both Reelin-OE and Dab1-KO 4-week GCs were more spherical than the control spines. However, their maturation did not imply any modification in their sphericities, in spite of the increase observed in control spines. In the other side, development of Reelin-OE new-born GCs came along with an increase in synapse volume and in Dab1-KO with an increase in synaptic sphericity.

We next wanted to analyze the relationship between morphometric parameters inside a given spine-synapse couple in Reelin-OE and Dab1-KO 4-week GCs. Interestingly, all three correlations reported were conserved and displayed the same sense in Dab1-KO samples, and Reelin-OE GCs exhibited correlation in the most robust relationships: spine volume correlated positively with synapse volume and negatively with synapse sphericity (**Table r.5.4**).

In sum, structural development of dendritic spines and synapses on new-born GCs was found to be affected by Reelin signaling in a number of ways. Mushroom spines were more frequent in both up- and down-regulation scenarios of Reelin signaling, whereas other spine types showed specific regulations to one of the experimental groups. Interestingly, abundance of branched spines in Dab1-KO GCs at early stages was found to be as high as in the mature population. Whereas control spines became

more spherical with cell maturation, any of the experimental groups displayed this phenotype. Synaptic morphology exhibited delays in the acquisition of maturity, since whereas parameters in 4-week control group were indistinguishable from 8-9 week ones, in the same period of time Reelin-OE and Dab1-KO GCs were found to evolve in synaptic volume and sphericity, respectively. Finally, previously characterized correlations between spine and synaptic morphometric parameters were conserved in both experimental situations.

Reelin signaling regulates presynaptic multiinnervation of spines of developing new-born GCs

We next analyzed the presynaptic element of the synapses established onto Reelin-OE and Dab1-KO developing GCs. Systematic analysis and annotation of the imaged dendrites allowed the identification of 129 and 76 presynaptic boutons establishing synapses with spines of Reelin-OE and Dab1-KO GCs. Together with the control group a total of 476 presynaptic boutons were identified, of which in 413 we could retrieve connectivity information (**Table r.5.2**).

At 8-9 weeks, about half (47% and 53%) of the presynaptic boutons innervating Reelin-OE and Dab1-KO GCs established a single synaptic contact onto the new-born GC (single synapse bouton, SSB), which represented a 29% and 69% increase with respect to the SSB population in the respective 4-week GCs. The amount of SSBs in the 8-9 week groups was substantially higher than the one found in the control group (28%). The remaining boutons established additional synapses onto non-labeled dendritic spines (multiple synapses bouton, MSB) and were present in both Reelin-OE and Dab1-KO samples (**Fig. r.5.3a-f**). We annotated the number of synapses established by every synaptic bouton (synaptic bouton index and MSB index, SBi and MSBi). In 8-9 week GCs, boutons innervating both Reelin-OE and Dab1-KO GCs established only a half (58% and 60%) of the number of synapses established of boutons onto control 8-9 week GCs. This reduced connectivity was also evident when analyzing only MSBs (62% and 69% of control MSBi average values, respectively). Accordingly, we found only 2 and 1 cases (2% and 3%) of MSBs with an index of 4, and none beyond, in either Reelin-OE or Dab1-KO respective analyses. More interestingly, boutons innervating 3-4 week GCs of both genotypes exhibited connectivity indexes similar to control ones (**Fig. r.5.3a-b**, **g-h**). Therefore, connectivity of the boutons establishing synapses onto developing GCs was unaltered in Reelin-OE and Dab1-KO cases, whereas it showed a 34% increase in control MSBs.

To analyze whether MSB identity of a bouton correlated to any particular spine morphology of the developing neuron when the Reelin signaling pathway was modified, we recovered both the type and morphometric parameters of the 8-9 week spines being contacted by either SSBs or MSBs. Overall, boutons contacting both Reelin-OE and Dab1-KO spines exhibited similar preferences for each of the spine types as for the global population in that genotype (**Fig. r.5.4a-b**). Nevertheless, SSBs establishing synapses on Dab1-KO filopodia were 22% more abundant than expected according to their frequency in the general Dab1-KO spine population (**Fig. r.5.4b**). Moreover, volumes and sphericities of synapses and new-born GC spines associated to these boutons showed no preference for the degree of connectivity of the presynaptic bouton in neither Reelin-OE nor Dab1-KO cases (**Fig. r.5.4c-d**).

Thus, modifications in the Reelin pathway do not provoke notable preferences between MSBs and a particular spine phenotype on the developing GC. In all, Reelin was shown to regulate the connectivity of boutons establishing synapses with developing GCs, but the individual connectivity of these boutons was not found to be associated to any particular postsynaptic morphology.

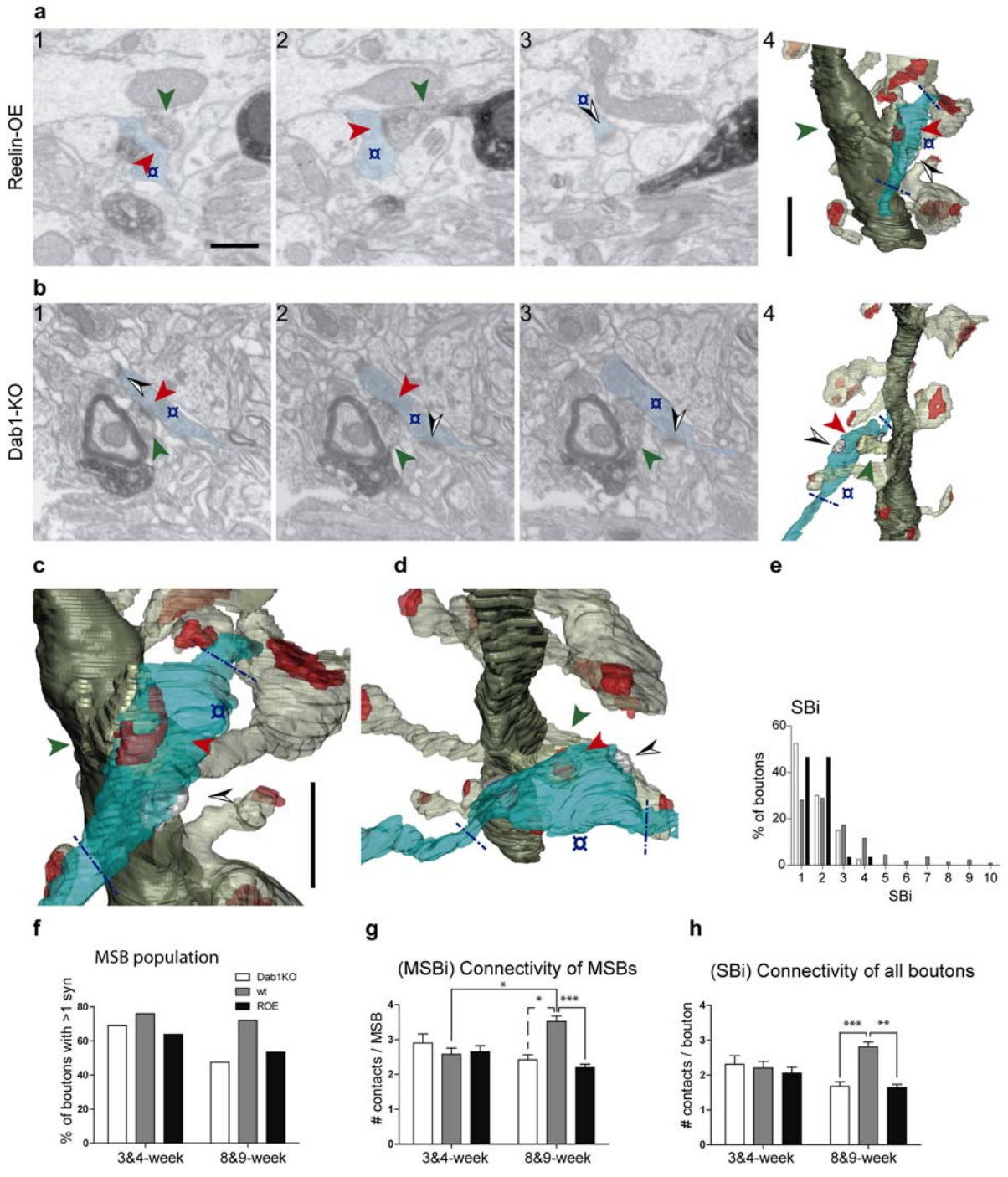

Figure r.5.3 Characteristics of presynaptic innervation of Reelin-OE and Dab1-KO GC dendritic spines at 3-4 and 8-9 weeks.

(**a**-**b**) Examples of presynaptic boutons (o) contacting (red arrowheads) the DAB-labeled spine (green arrowheads) and a second unlabeled spine (black and white arrowheads) in both Reelin-OE (**a**) and Dab1-KO (**b**) 8-9 week-old new-born GCs. The left FIB/SEM images show selected serial planes of the dendritic spines and presynaptic boutons. The corresponding 3D reconstructions are shown to the right (**a4, b4**) as well as in a tilted orientation in **c** and **d**, respectively. Note that only the varicosities were analyzed, not the entire axon (varicosities delimited by blue dashed lines in the 3D panels). Color code is the same as previously described. Additionally,

axon is transparent blue, and synapses established by the axon onto non-labeled spines are solid gray. (**e**) Histogram showing the frequency of synaptic contacts established by axon terminals at 3-4 and 8-9 weeks. (**f**) Percentage of multi-synaptic (MSB) boutons in 3-4 and 8-9 weeks-old dendritic spines of the different groups analyzed. (**g**) Average number of synaptic contacts established by multi-synaptic boutons at 3-4 and 8-9 weeks. (**h**) Average number of synaptic contacts established by all boutons pooled together. Data represent mean ± SEM. *p < 0.05; **p < 0.01; ***p < 0.001. Comparisons between two groups were assessed by Mann-Whitney test. Comparisons between three groups were assessed by Kruskal-Wallis test and post hoc Dunns test. When this analysis failed to determine significance between two individual groups, these were isolated and further compared by Mann-Whitney test (dashed lines). Scale bar in (**a1**) is 0.5 µm and is applicable to panels (**a1-3**, **b1-3**). Scale bar in (**a4**) is 1 µm and applies panels (**a4**, **b4**). Scale bar in (**c**) is 1 µm and applies panels (**c**, **d**).

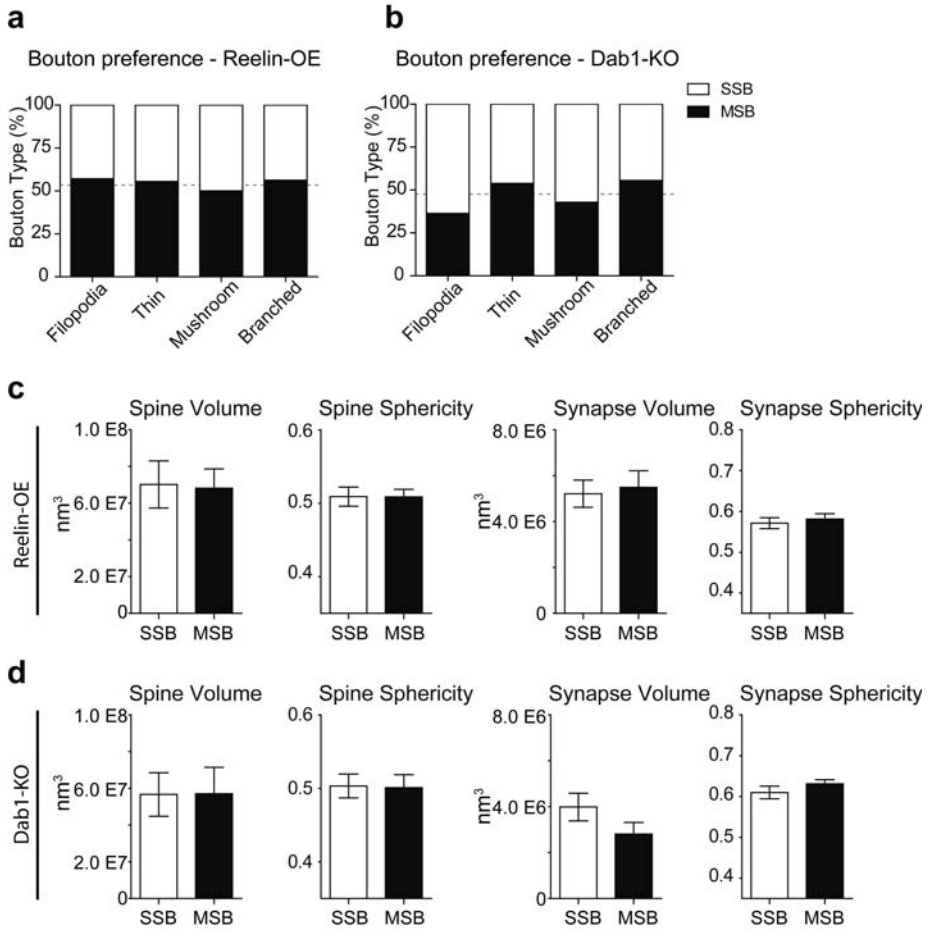

Figure r.5.4 Multisynaptic boutons innervate equally all spine types and morphologies in Reelin-OE and Dab1-KO assays.

(**a**-**b**) Percentage of single-synaptic (SSB) and multi-synaptic (MSB) boutons in different types of dendritic spines in 8-9-weeks old neurons of either Reelin-OE (**a**) or Dab1-KO (**b**) samples; the dashed line indicates the overall percentage of SSBs and MSBs. (**c**-**d**) Histograms showing spine volume, spine sphericity, synapse volume and synapse sphericity of spines innervated by either SSBs or MSBs in 8-9 week-old neurons of either Reelin-OE (**c**) or Dab1-KO (**d**) samples. Data represent mean ± SEM. *p < 0.05; Mann-Whitney test.

Discussion

1. Presynaptic plasticity in the hippocampus of Reelin-OE mice

Reelin protein has been proposed as an important regulator of synaptic plasticity in the adult hippocampus (Pujadas et al., 2010; Rogers et al., 2011; Rogers et al., 2013). Moreover, some presynaptic-compartment associated physiological recordings and molecular studies have shown implications of the Reelin signaling pathway in the function of the axon terminal. Hippocampal neurons from Reelin-OE mice were shown to fail to shift from paired-pulse facilitation (PPF) to paired-pulse depression (PPD) at high stimulating intensities, which could be an indicator of apparent absence or delay in the appearance of presynaptic fatigue typically observed after hyperstimulation protocols (Pujadas et al., 2010). Besides, *reeler* mice exhibit reduced levels of the SNARE protein SNAP-25 in hippocampal membrane fractions, boutons in RAD of these mice are filled with reduced numbers of synaptic vesicles, and both features display values similar to controls when recombinant Reelin is added (Hellwig et al., 2011).

We found that presynaptic boutons innervating all hippocampal layers were larger in Reelin-OE mice, and those present in layers RAD and OR exhibited less compact morphologies. Remarkably, these layers are heavily innervated by Schaffer collaterals of CA3 pyramidal neurons, and represent the major input to CA1 pyramidal cells (Ishizuka et al., 1990; Li et al., 1994). In the other side, mice with inhibited transgene expression showed a recovery of control bouton area in all layers. These mice presented circularity values similar to controls in the previously mentioned layers, while bouton circularity was found increased in OML and SLM. In the latter, tuft dendrites from CA1 pyramidal cells receive synaptic contacts from boutons of axons coming from entorhinal and thalamic afferences (Andersen et al., 2007; Spruston, 2008), whereas OML synapses are mainly composed by entorhinal afferences contacting dendritic spines from DG granule cells (Amaral et al., 2007). Therefore, structure of all hippocampal boutons showed responsiveness to Reelin signaling, while some phenotypes seemed restricted to chronic modifications or to particular synaptic partners. Furthermore, both bouton density and the amount of multisynaptic boutons were found increased all over the hippocampus of Reelin-OE mice. The abundance of multisynaptic boutons in the CA1 is increased after both LTP and associative learning paradigms (Toni et al., 1999; Geinisman et al., 2001). In the other hand, bouton size correlates both with the probability of neurotransmitter release and with the size of the active zone (Holderith et al., 2012). Therefore, our results suggest an increased presynaptic function in the hippocampus of Reelin-OE mice. Altogether, it could explain the previously reported resilience to presynaptic fatigue of these synapses (Pujadas et al., 2010). Since bouton size has also been correlated to the number of synaptic

vesicles in it (Adams and Jones, 1982; Knott et al., 2006), these results would also outline the involvement of Reelin protein in the regulation of presynaptic structural plasticity (Hellwig et al., 2011).

The presynaptic terminal function during synaptic activity involves a Ca^{2+}-dependent synaptic vesicle fusion and recycling process. A group of proteins interacting with N-ethylmaleimide sensitive fusion protein (NSF) attachment proteins (SNAP) were identified as key regulators of this process, and named as SNAP receptors (SNAREs). This group comprises VAMP, which is a vesicle-associated protein or v-SNARE, and two membrane (target) t-SNAREs, SNAP-25 and syntaxin1. Their clustering and recycling process drives the synaptic vesicle priming, fusion and recycling (Sudhof and Rizo, 2011). We did not find differences in the expression pattern nor in synaptosomal levels of SNAP-25, which hippocampal distribution coincides with its previously described pattern (Oyler et al., 1989). Moreover, isolated trials with the other two SNARE proteins did not reveal any changes in Reelin-OE mice, and by directed search of their gene expression in a whole-genome analysis performed with these mice by collaborators, these proteins revealed similar hippocampal expression levels across the experimental groups described (data not shown).

So, despite recent findings showed diminished values of this protein in *reeler* mice (but not in Dab1-KO mice) and that acute Reelin increase could also modify its levels (Hellwig et al., 2011), our findings indicate a presynaptic resilience to molecular changes upon chronic increases in Reelin expression. Interestingly, modifications of SNAP-25 expression or function trigger impaired synaptic plasticity and this protein has been associated to some psychiatric disorders such as schizophrenia and attention deficit and hyperactivity disorder (ADHD) (Thompson et al., 1998; Barr et al., 2000; Antonucci et al., 2013). Since Reelin-triggered increase in spontaneous neurotransmitter release is dependent on SNAP-25 function (Bal et al., 2013), preventing misregulations of this SNARE's expression in a sustained Reelin up-regulation scenario could prevent the appearance of synaptic pathologies. Similarly, we did not find evidences of molecular or expression pattern changes in another presynaptic marker, synapsin. This protein is a presynaptic terminal phosphoprotein whose most known function involves regulation of synaptic vesicle fusion with plasma membranes by reversal binding of synaptic vesicles to the actin cytoskeleton, although they have been also reported to exert functions in other steps of the synaptic vesicle recycling process (Fournier et al., 2009; Cesca et al., 2010). In this case, our results complement studies performed on hippocampal synaptosomal or membrane extracts from both *reeler* and Dab1-deficient mice, which found no differences in synapsin expression upon *in vivo* persistent modifications of the Reelin signaling pathway (Hellwig et al., 2011; Trotter et al., 2013).

Altogether, our results point to a clear effect of sustained Reelin *in vivo* overexpression on the presynaptic hippocampal bouton structural plasticity. However, key proteins in synaptic transmission such as Synapsins or SNAREs appear unmodified in Reelin-OE mice, despite the expression of the latter is reported to respond to acute Reelin treatments, or to the absence of Reelin. Therefore, synaptic homeostatic mechanisms might operate at mid-term processes, preserving key synaptic function regulators expression (and consequently the synaptic function integrity itself).

2. Postsynaptic plasticity in the hippocampus of Reelin-OE mice

Reelin confers unique structural properties to adult hippocampal dendritic spines.

Although there is consistent evidence in *reeler*/mDab1-KO mice and in *in vitro* systems that Reelin regulates the formation and maturation of dendritic spines in the developing brain (Liu et al., 2001; Niu et al., 2008; Ventruti et al., 2011), our results reflected that Reelin overexpression in adult mice does not alter the number of dendritic spines in the hippocampus but does affect their structural properties. These results are supported by studies in a postnatal, forebrain-specific Dab1 depletion model, which report reduced spine size but conserved density on apical dendrites of CA1 pyramidal cells (Trotter et al., 2013). Several mechanisms could explain this discrepancy. First, both *reeler* and *HRM* have increased Dab1 levels (Rice et al., 1998). It is therefore likely that application of Reelin to *reeler* neurons leads to hyperactivation of the Reelin signaling pathway. By contrast, Dab1 protein levels are slightly and severely reduced in both Reelin-OE mice and in the Dab1 conditional KO mouse model above mentioned, respectively (Pujadas et al., 2010; Trotter et al., 2013). Second, it is also possible that normal Reelin levels are required to achieve standard numbers of dendritic spines, and that above a certain threshold of activation, Reelin overexpression is not sufficient to modify these numbers. Third, it is also possible that adult neurons, by homeostatic physiological regulation, are specified to develop a maximum number of dendritic spines.

Besides, our results show that Reelin overexpression promotes hypertrophy of dendritic spines. We found that hippocampi of Reelin-OE mice exhibit larger dendritic spines and a lower spine head circularity index (which corresponds to an increased morphological complexity) in all layers, including the molecular layer of the DG. These observations thus support that these effects are a general consequence of the Reelin cascade in adult neurons. Enlargement of dendritic spines is a characteristic feature of synaptic plasticity events, including LTP (Toni et al., 2001; Popov et al., 2004; Yang et al., 2008; Hill and Zito, 2013), and is believed to confer a greater postsynaptic strength (Yuste and Majewska, 2001a; Matsuzaki et al., 2004; Bourne and Harris, 2008; Lee et al., 2009; O'Donnell et al., 2011). In fact, Reelin-OE mice exhibit increased LTP responses *in vivo* (Pujadas et al., 2010). Moreover, synaptic plasticity is associated with changes in the proportion of dendritic spine types (Medvedev et al., 2010). We found that Reelin overexpression in mice doubles the percentage of type III dendritic spines —which most likely represent the mushroom type population of dendritic spines—again in all layers. In contrast to

thin dendritic spines, mushroom spines are considered to be the most mature spines, acting as stable ”memory” spines (Kasai et al., 2003; Matsuzaki et al., 2004; Bourne and Harris, 2007; Yasumatsu et al., 2008; Yang et al., 2009; Kasai et al., 2010a). Moreover, recent studies report that LTP increases the proportion of mushroom spines (Medvedev et al., 2010). Finally, we found a substantial increase in the percentage of spines bearing SAs and in the size of the SAs themselves in Reelin-OE mice. The SA is a Ca^{2+}-sequestering organelle that regulates spine Ca^{2+} signaling, synaptic efficacy, and protein post-translational modifications, among other processes, and that is enriched in mushroom spines (Gray, 1959; Fifkova et al., 1983; Spacek and Harris, 1997; Fiala et al., 2002b; Nimchinsky et al., 2002; Vlachos et al., 2009). This finding again reinforces the notion that Reelin promotes the formation and stabilization of physiologically more efficient dendritic spines.

Reelin increases postsynaptic glutamatergic responses and LTP (Weeber et al., 2002; Beffert et al., 2005; Qiu et al., 2006b; Qiu et al., 2006a; Groc et al., 2007; Pujadas et al., 2010; Rogers et al., 2011; Rogers et al., 2013). Moreover, infusion of Reelin enhances cognitive performance in wild-type mice (Rogers et al., 2011), while overexpression fully rescues cognitive deficits in mouse models of Alzheimer's disease and during normal ageing (Pujadas et al., 2014). Together with these findings, the present data suggest that one of the mechanisms by which Reelin enhances cognitive performance in a range of conditions, as well as potentiating glutamatergic neurotransmission, is by forming more stable and complex, mushroom-type dendritic spines, thus enabling stronger postsynaptic responses. Finally, the finding that dendritic spine phenotypes were dramatically reversed when the Reelin transgene was switched off supports the notion that the structural changes observed were effectively caused by the activation of the Reelin cascade.

Reelin levels do not regulate postsynaptic protein expression levels but do determine their synaptic/extrasynaptic distribution.

Here we show that Reelin levels do not regulate the levels of distinct postsynaptic proteins, including glutamatergic receptor subunits and postsynaptic scaffolding, cytoskeletal, and signaling proteins. Although the Reelin pathway is believed to activate the CREB transcription factor pathway (Rogers et al., 2011) and gene expression alterations have been described in *reeler* mice (Kuvbachieva et al., 2004) our results support the notion that Reelin does not control the expression of target genes coding for synaptic proteins.

Recent studies show that Reelin increases synaptic activity through altering NMDA and AMPA receptor activation and surface trafficking activity *in vitro* (Beffert et al., 2005; Chen et al., 2005; Qiu et al., 2006a; Groc et al., 2007; Qiu and Weeber, 2007; Campo et al., 2009). Furthermore, some studies have pointed to a counteracting function of Reelin on the 2B subunit prevalence in the NMDA receptor configuration with implications on Reelin-triggered physiological and structural phenotypes. Notably, blockade of NR2B activity restored spine numbers and LTP in *HRM* (Iafrati et al., 2013) whereas LTP paradigms in Reelin-OE mice exhibited resilience to 2B subunit blockade (Teixeira et al., 2011). This would suggest that NMDA receptor function in *HRM* is NR2b-dependent, whereas Reelin overexpression leads to a downregulation of NR2b-mediated transmission. Similarly, *in vitro* studies showed a Reelin-mediated regulation of synaptic maturation towards NR2a-bearing synapses (Groc et al., 2007). Besides, previous studies of the same group described that 2A-2B subunit composition plasticity is triggered by lateral mobility of 2B subunit-containing receptors (Groc et al., 2006). Our results in the adult hippocampus *in vivo* support these observations by showing that Reelin induces a decrease in NR2a/b postsynaptic subunits, concomitant with an increase in extrasynaptic and cytosolic NR2a/b

content. Again, this Reelin-dependent localization was reversed after blocking Reelin transgene expression for one week, thereby suggesting that the Reelin pathway promotes both the lateral diffusion and internalization of these proteins *in vivo* in an acute manner. The mechanisms by which Reelin regulates NMDAR trafficking are still poorly understood, although they may include receptor subunit phosphorylation and the modulation of scaffolding and signaling proteins. It has been proposed that Reelin activates LIMK1, which phosphorylates Cofilin at serine residues (Arber et al., 1998; Yang et al., 1998; Meng et al., 2004; Chai et al., 2009), which in turn stabilizes the actin cytoskeleton in dendritic spines (Shi et al., 2009) and increases AMPAR surface trafficking (Gu et al., 2010; Wang et al., 2013). Although we did not detect differences in LIMK1 and Cofilin phosphorylation levels in Reelin-OE mice, we did observe Reelin-dependent changes in p-Cofilin distribution that mimicked those of NMDA receptor subunits.

However, spine structural phenotypes provoked by Reelin overexpression could be also explained by an alternative mechanism. Synaptic structural plasticity is activity-dependent (Yasumatsu et al., 2008). The spine cytoskeleton is mainly composed by actin (Matus et al., 1982; Kaech et al., 1997), which is further compartmentalized in three functionally different and spatially segregated pools (Honkura et al., 2008), which in turn correspond to the spatial segregation of specific actin binding proteins (Bramham, 2008; Racz and Weinberg, 2008, 2013). Since current injected at the synapse is related to the number of receptors and to the size of the PSD (Nusser and Somogyi, 1997; Nusser et al., 1998) and Reelin signaling has been involved in synaptic plasticity mechanisms (Pujadas et al., 2010; Teixeira et al., 2011; Rogers et al., 2013), much of our interest was focused on deciphering molecular mechanisms that localized near the synaptic active zone. The analyzed PSD-95, Cofilin and CaMKII proteins are confined to this zone (Racz and Weinberg, 2013). However, synaptic contact length and PSD-95 levels were largely conserved in Reelin-OE mice, as well as overall NMDA receptor levels. Moreover, overexpression of PSD-95 in mice develops a multiinnervated, abnormally excentric spine phenotype (Nikonenko 2008) which was never observed in our samples.

Therefore, a different actin pool could be responsible for the Reelin-triggered net increase in spine size. The so-called enlargement pool is located at the spine core and appears during activity-induced spine enlargement processes (Honkura et al., 2008). This pool requires a higher concentration of actin monomers, and is thought to provide the force needed for spine enlargement. It generates a highly cross-linked actin gel whose confinement in the spine head is necessary for persistent activity-triggered spine head growth (Kasai et al., 2010b). An important actin branching promoter and nucleator factor is Arp2/3, which is located in the core of dendritic spines (Bramham, 2008; Racz and Weinberg, 2008). The activity of this seven-protein complex is mediated by both ATP and a series of nucleation promoting factors (NPF) (Boczkowska et al., 2014), and the impairment of its function through the depletion of one of its NPFs, WAVE-1, leads to subtle alterations in dendritic spine morphology (Hazai et al., 2013).

Interestingly, Reelin signaling pathway has been shown to regulate Arp2/3 function through another of its NPFs: N-WASP. Activation of N-WASP involves a conformational modification that enables binding and further activation of Arp2/3. N-WASP activation can be attained by Cdc42, which is a downstream target of the Reelin/PI3K pathway. However, Dab1 also binds N-WASP to a sequence nearby to that of Cdc42, and Dab1-N-WASP can initiate Arp2/3 complex activation independently of other WASP activators (Suetsugu et al., 2004; Winder, 2004). Thus, Reelin overexpression could be enhancing the activity of the enlargement pool by a hyper-activation of the N-WASP – Arp2/3 pathway, leading to an increase in spine size. This pathway could be promoted either through PI3K – Cdc42 – N-WASP or directly through Dab1 – N-WASP, or both. The latter, though, would be consistent with conserved values of Cofilin, since this protein is also affected by Cdc42 activity (Leemhuis and Bock, 2011). Overall, this

mechanism could underlie a misregulation in the dendritic spine morphological dynamics, driving to an abnormally large spine population in a similar way as found in some psychiatric disorders (Kasai et al., 2010a). However, to confirm this hypothesis future experiments should be performed, testing both the levels of Arp2/3 and other candidate actin branching promoter proteins in Reelin-OE spines, as well as the dynamic properties of the different actin pools in dendritic spines that exhibit Reelin-triggered increases in size.

Altogether, the present findings in adult Reelin-OE mice support that, rather than inducing changes in the expression of synaptic protein components, Reelin signaling modulates glutamatergic neurotransmission by regulating post-translational mechanisms, including the trafficking and assembly of receptor subunits, Ca^{2+}-dependent neurotransmitter release, and structural modifications of pre- and postsynaptic spine components.

Is there a layer-specific synaptic responsiveness to Reelin?

Most of the pre- and postsynaptic alterations reported here in Reelin transgenic mice (including pre- and postsynaptic areas, bouton and multisynaptic bouton density, length of contacts, area of SA and percentage of spines containing SA) were more dramatic in the SLM, OML, and MML layers. These three layers correspond to principal cell dendrites receiving entorhinal input, in contrast to the SR, SO, and inner molecular layer (IML), which receive commissural/associational input. These differences could be explained by a differential, layer-specific distribution of Reelin signaling components or of Reelin itself. However, neither transgenic Reelin levels in our mice nor the expression of APOER2/VLDL receptors or mDab1 showed similar layer-specific distributions (Borrell et al., 2007; Pujadas et al., 2010; Trotter et al., 2013). Nevertheless, we cannot exclude that other signaling components are enriched in particular dendritic domains of pyramidal and granule cell neurons.

Perhaps the most dramatic layer-specific synaptic alteration reported here refers to the Reelin-dependent distribution of synaptopodin. An actin-binding protein tightly associated with SA, Synaptopodin is critical for the formation of this organelle, which has been linked to the structural and physiological properties of dendritic spines (Freire, 1978; Deller et al., 2000; Deller et al., 2003; Deller et al., 2006; Okubo-Suzuki et al., 2008; Vlachos et al., 2009; Vlachos et al., 2013; Zhang et al., 2013). Interestingly, synaptopodin expression parallels hippocampal development, precedes the appearance of LTP and its levels do not decline with aging (Czarnecki et al., 2005). Moreover, according to its subcellular location, its layered expression pattern has been proposed to reflect dendritic layers. Accordingly, synaptopodin expression pattern becomes disrupted in these areas in models with disrupted layering such as the *reeler* mouse (Deller et al., 2002). Further, when the hippocampal connectivity was injured by either an entorhinal cortex lesion or by kainic acid-induced epilepsy, the protein levels of synaptopodin in the molecular layers of the DG, but not in other hippocampal layers, were altered (Roth et al., 2001; Deller et al., 2006).

Here we found that Reelin induces a dramatic shift in synaptopodin distribution, with it being enriched in the SLM while decreasing in the dentate molecular layer. These alterations in distribution were not accompanied by changes in gene or protein expression in hippocampal fractions. Although entorhino-hippocampal connectivity varies between layers in the anteroposterior plane, in any case it coincides with a SLM/ML interphase, and hippocampi from Reelin-OE mice exhibited the same synaptopodin layering at different hippocampal planes. Further, one week of transgene inactivation in Reelin-OE-DOX mice generated an intermediate phenotype, suggesting an activity-dependent regula-

tion. Therefore, the synaptopodin phenotype on Reelin-OE mice might be provoked by an intermediate agent in the hippocampal synaptic circuitry.

Since another factor that presents a clear layering in the hippocampus is the distribution of specific interneuron arbors, some interneuronal cell type might exert an influence to the synaptopodin expression pattern limits detected. Parvalvumin-positive stratum oriens-lacunosum moleculare (O-LM) interneurons have their cell bodies in the OR and axons in the SLM. Enhanced presynaptic stimulation in the OR of Reelin-OE mice could develop hyperactivation of these cells, whose firing-triggered effects would be confined to the SLM. Besides, molecular layer perforant path-associated (MOPP) and hilar perforant path-associated (HIPP) interneurons receive excitatory inputs from the perforant path projection, and their axons innervate the MML and OML, whereas hilar commissural/association pathway-associated (HICAP) cells receive inputs from the commissural/association pathway (Freund and Buzsaki, 1996; Andersen et al., 2007). Hypothetically, a Synaptopodin expression-promoting activity from O-LM cells and a repressive activity from HICAP and MOPP and/or HIPP cells would reproduce the observed phenotype in a Reelin-enriched scenario. However, our results do not allow us to offer a mechanistic explanation for these findings, and furher experiments should be performed to determine its actors. Overall, our results support the notion that Reelin modulates synaptic structure and function differentially in distinct dendritic domains of the same neuron and that this modulation is correlated with the type of afferent synaptic input.

In conclusion, our results highlight the participation of Reelin in the structural modulation of synaptic terminals and dendritic spines *in vivo* in adult mice. Importantly, they support the idea that, in addition to modulating presynaptic terminals, Reelin promotes the appearance of large, mushroom-type dendritic spines with large SAs and increased extrasynaptic NMDA receptors. These data provide the structural basis to unravel the contribution of Reelin to normal neurotransmission and synaptic facilitation/LTP forms of plasticity and also to pathological conditions.

3. Reelin-triggered spine plasticity in pyramidal cells

Since principal or pyramidal cells are the predominant neuronal type for excitatory transmission in the brain (Cajal, 1904, 1933; Defelipe, 2011), we analyzed the role of Reelin signaling on the dendritic spines of these cells. We performed an analysis of the dendritic spine densities and morphologies in two pyramidal cell types: the hippocampal CA1 pyramidal cell and the S1BF layer 5 pyramidal cell. We further chose different dendritic areas of interest. In hippocampal CA1 pyramidal cells we analyzed their basal dendrites in OR and their apical oblique thin dendrites in RAD. In cortical Layer 5 pyramidal cells we focused on both trunk dendrites passing by layer 4 and in tuft dendrites in layers 2-3. Finally we modulated the levels of the Reelin signaling pathway in both directions, always using *in vivo*, sustained approaches: Reelin-OE mice provided a model of chronic Reelin upregulation, with confirmed exogenous expression in both areas defined (Pujadas et al., 2010). Besides, flDab1-Cre mice allowed the analysis of an adult long-term deployment of Reelin responsiveness in its endogenous locations (Pramatarova et al., 2008; Teixeira et al., 2014).

Reelin overexpression effect on dendritic spines of pyramidal cells

For CA1 pyramidal cells we report increasing spine density in basal dendrites with distance to the soma, whereas dendritic segments further than 50 μm away from the soma exhibit a constant spine density. Since average density is lower than the density attained in this plateau, our results point to the importance of a correct dendritic sampling when performing spine analysis from isolated dendritic segments. Further, this distribution pattern of dendritic spines reproduces the previously described patterns in other basal trees of pyramidal neurons (Benavides-Piccione et al., 2005; Ballesteros-Yanez et al., 2006; Benavides-Piccione et al., 2013). We found that spine density in basal and apical dendrites was conserved in Reelin-OE mice. This finding matches our previous ultrastructural analysis of the hippocampus of these mice reporting similar spine densities across all layers (**chapter 2**) (Pujadas et al., 2010). Interestingly, *HRM* CA1 pyramidal cells showed no changes in spine density neither upon Reelin supplementation (Rogers et al., 2013). In contrast, in WT mice only 5 days-long exposure to enhanced Reelin levels led to increased densities of spines in apical dendrites, whereas very acute treatments (3 hours) did not exert any effect (Rogers et al., 2011). However, the experimental methodology

used by these authors did not allow for the analysis of longer-term phenotypes, which most probably are the ones reflected in our experiments. Of more interest, these studies suggest that sustained increase in Reelin levels *in vivo* might exert different functions upon acute or chronic exposures. In accordance with this view, we previously showed that exogenous Reelin acute depletion in Reelin-OE mice caused loss of spines (**chapter 2**) (Pujadas et al., 2010). Therefore, Reelin might be able to regulate hippocampal dendritic spines *in vivo* in different ways depending on the length of the variation in Reelin signaling. Short (hours) exposures would have no effects on spines (Rogers et al., 2011), whereas acute (days) exposures might be able to trigger spine density modifications (Pujadas et al., 2010; Rogers et al., 2011). Finally, long-term modifications in Reelin upregulation would no longer affect the density of dendritic spines (Pujadas et al., 2010).

Basal dendrites from CA1 pyramidal cells exhibited spines of similar sizes and sphericities than their control counterparts. This is in accordance with previous ultrastructural analyses in these mice (**chapter 2**), that revealed similar spine sizes in the OR, taking into account that most spines in hippocampal OR belong to basal dendrites from CA1 pyramidal neurons (Andersen et al., 2007). Analysis of dendritic spine morphology in apical oblique dendrites in stratum radiatum revealed that these spines were of similar size and sphericity in Reelin-OE mice. This result differs from what was observed in the previous chapter, where Reelin-OE RAD showed larger, less circular dendritic spines, increased density of morphologically complex spine heads and randomly reconstructed trunk apical dendrites showed hypertrophic spines. At least three different arguments could explain this divergence.

One, the confocal microscopy analysis clearly relates to apical oblique dendrites. Besides, the ultrastructural analysis reflects the overall dendritic spine population in this layer. Since most spines in RAD belong to CA1 pyramidal neurons this discrepancy could suggest a differential effect of Reelin in spine morphology in apical oblique branches and dendritic trunk dendrites. Oblique branches and primary apical trunk dendrites might account for different physiological functions. Indeed, a single dendritic branch might represent a major signaling unit in pyramidal cells, since it could offer the physical support for local compartmentalization of a number of functions, from electrical integration to local plasticity events, including localized protein synthesis and the regulation of neurotransmitter and modulator release (Branco and Hausser, 2010). Indeed, different functions have been proposed to apical oblique dendrites of CA1 pyramidal cells compared to the trunk apical dendrite (Migliore et al., 2005). However, in order to extract conclusions in that sense, further experiments specifically comparing these two spine populations should be addressed.

Two, the distribution of sizes of dendritic spines might not be uniform in these apical oblique branches. Indeed, the threshold for dendritic spike generation varies with the distance to the branching point (Ferrante et al., 2013). Since spine synaptic strength is related to spine volume (Matsuzaki et al., 2001; Kopec et al., 2007; O'Donnell et al., 2011) spines near the branching point might be smaller. Our analysis of the apical oblique dendrites was based on pooling all the spines in these branches, and therefore the spines located in these initial segments could mask a size phenotype occurring in mid dendritic segments. However, other authors found no differences in the spine head distribution in these branches (Konur et al., 2003).

And/or three, the technical procedure employed for spine labeling and imaging might underestimate spine size morphology. Specifically, these cells were injected with Alexa 594 phluorophore and the signal was imaged directly without any previous amplification step. Despite this same protocol was used in similar samples and reported physiological changes in spine morphologies in previous studies (Knafo et al., 2009a; Knafo et al., 2009b), the amplitude of the change in spine size provoked by Reelin overexpression might be below its resolution limits. To overcome this possible caveat, in further simi-

lar studies in the flDab1 pyramidal neurons an improved protocol was used, consisting in a Lucifer Yellow-filling of the cells followed by immunohistochemical signal amplification before image acquisition (Benavides-Piccione et al., 2005; Knafo et al., 2012; Merino-Serrais et al., 2013).

In any case, regarding Reelin-OE apical dendrites of CA1 pyramidal cells, we face the dichotomy of what effect does sustained *in vivo* Reelin overexpression trigger in our samples. In this situation, since ultrastructural studies provide much stronger lateral resolution than confocal ones, their conclusions referring the analysis of spine morphologies should be more accurate. In this scenario, altogether our results prove that *in vivo* Reelin chronic overexpression does not affect spine density in hippocampal CA1 pyramidal cells. Besides, it promotes spine hypertrophy in their apical dendritic branches only, leading to a cell domain-specific effect.

Our analysis on layer 5 pyramidal cells show lower spine densities than in CA1 pyramidal cells, as previously reported (Konur et al., 2003). Moreover, Reelin-OE mice showed decreased spine densities in both dendritic zones analyzed. Similarly, studies on layer 2/3 pyramidal neurons of the same cortical region reported that enhanced maternal care provoked reduced spine density and enhanced Reelin protein levels in cortical extracts of adult offspring (Smit-Rigter et al., 2009). Since this model mimics early adverse childhood events that are associated to increased risk of onset of psychopathologies in more adult stages, our results support the notion of Reelin as factor providing resilience to such diseases (Teixeira et al., 2011). Further, these spines showed larger and less spherical morphologies, both associated with stronger synaptic contacts (Harris and Stevens, 1989; Matsuzaki et al., 2001; O'Donnell et al., 2011).

Downregulation of Reelin signaling effect on dendritic spines of pyramidal neurons

Analysis of dendritic spines in hippocampal CA1 pyramidal cells of adult Dab1-depleted mice showed that, again, Reelin signaling did not affect the spine density of basal dendrites. Moreover, our results show that these spines have smaller average volumes and a more spherical shape. Our results support analysis performed on apical oblique dendrites of CA1 pyramidal cells of a different mouse model for conditional deletion of Dab1 in the adult hippocampal circuitry (Trotter et al., 2013), revealing that downregulation of Reelin signaling in that model did not alter the spine density of these dendrites, but dendritic spines exhibited smaller areas. We should highlight, though, that these results are not coincident with observations in the *reeler* mouse brain. There, spine density of CA1 pyramidal cells decays with Reelin dose (Niu et al., 2008; Ventruti et al., 2011).

Moreover, constitutive Dab1 KO mice exhibit a dose-response reduction of spine density in tuft apical dendrites (Niu et al., 2008). By comparing these results, we could argue that the effect on spine density of hippocampal CA1 pyramidal neurons appears dependent on the onset of the Reelin signaling deployment: whereas constitutive suppression of Reelin signaling drives to reduced spine densities (Niu et al., 2008; Ventruti et al., 2011), adult-specific downregulation leaves spine density unaltered (Trotter et al., 2013). Developmental deficiencies in Reelin signaling lead to large abnormalities in cortical cytoarchitecture that last until adulthood (Sheldon et al., 1997; D'Arcangelo and Curran, 1998; Trommsdorff et al., 1999; Katsuyama and Terashima, 2009; Cremer et al., 2011). Therefore, conditional strategies of Reelin signaling modifications offer a much more interesting tool to decipher precise phenotypes promoted by Reelin in a healthy brain.

Finally, analysis of cortical Layer 5 pyramidal cell apical dendrites showed again lower spine densities

than the ones found in the hippocampus, as found by other authors (Konur et al., 2003). These cells showed larger spine densities in flDab1-Cre+TAM mice, showing an opposite phenotype than the observed in Reelin-OE mice. Therefore, our results show that Reelin signaling counteracts dendritic spine density on apical dendrites of Layer 5 pyramidal cells in S1BF. As stated before, mice receiving more maternal care showed less spine density and more Reelin expression levels (Smit-Rigter et al., 2009). Thus, these results further point to the protective role of Reelin aginst the onset of psychiatric disorders. We found, in the other side, that dendritic spines were larger and less spherical in flDab1-Cre mice, in a phenotype similar to that one found in Reelin-OE mice. This supports the general idea that different mechanisms might account for spine generation and spine enlargement processes (Knott et al., 2006; Cingolani and Goda, 2008; Yasumatsu et al., 2008). Since larger spines are associated with stronger synaptic inputs, together with the increased spine density reported we should expect an overall dendritic hyperactivity in these neurons. Further analyses should clarify whether this situation leads to a more active circuitry, or by contrast it reflects a compensating strategy of these cells to compensate for other deficiencies in signal transmission.

Reelin regulates spine plasticity in a cell-specific and dendritic domain-specific way

Altogether, our results show that Reelin signaling modulates spine density and morphology of pyramidal cells, and therefore it is implicated in synaptic plasticity mechanisms. Moreover, our results describe a range of effects that are pyramidal cell type-specific and even dendritic domain-specific.

Despite both being excitatory pyramidal cells, hippocampal CA1 and cortical Layer V pyramidal cells differ in a number of ways. First, dendritic receptive field of Layer V pyramidal cells is much larger than CA1 pyramidal cells. Indeed, Layer V pyramidal cells are the largest neurons of the cerebral cortex (Major et al., 2013). Second, the local connectivity of both cell types is also different. CA1 pyramidal cells receive entorhinal and thalamic inputs to their distal apical dendrites and commissural inputs to their proximal apical and basal dendrites (Andersen et al., 2007). Similarly, layer 5 connectivity reflects an arrangement of local inputs to basal and proximal apical dendrites and distant afferences to their distal apical dendritic branches. However, its specific innervations differ depending on the cortical zone, and exhibit an increased complexity. In particular, layer V neurons of barrel field columns receive contacts of different local and distal origins, mainly involving inputs from layer 4, 6 and 2-3 neurons and distal thalamic regions (Feldmeyer et al., 2013). Third, synaptic scaling evidences have been found in hippocampal CA1 pyramidal cells. These include an increased number of perforated PSDs at mid and distal apical dendrites, and an enhanced presence of AMPA-type glutamate receptors at mid, but not tuft, dendrites (Magee and Cook, 2000; Nicholson et al., 2006; Spruston, 2008). By contrast, synaptic scaling structural mechanisms would not be sufficient in the larger Layer V pyramidal cells to counteract passive dendritic attenuation phenomena and are not found in these cells (Williams and Stuart, 2002; Spruston, 2008). Fourth, the subcellular distribution of some voltage-gated cation channels (VGCC) differs between cell types. Specifically, A-type K^+ channels display higher levels at more distal dendrites of CA1 pyramidal neurons (Hoffman et al., 1997; Migliore et al., 2005). Conversely, the distribution of these channels is uniform in Layer V ones (Bekkers, 2000; Korngreen and Sakmann, 2000). Fifth, since one of the most important functions of VGCCs involves the regulation of back-propagated action potentials (Spruston, 2008), the presence and impact of these might vary between the two cell types. And sixth, dendritic spikes originated by synaptic inputs to tuft dendrites of CA1 pyramidal cells are unable to propagate to the soma. Spatiotemporal coincidence with more proximal dendritic spikes, originated by Schaffer collateral synapses, is needed to ensure proper propagation of these dendritic spikes (Jarsky et al., 2005). Conversely, somatic potentials can be triggered by tuft

stimulation in Layer 5 pyramidal neurons (Schiller et al., 1997; Stuart et al., 1997). However, in this case moderate inputs also need to be synchronized with backpropagating action potentials to ensure the propagation of the distally originated dendritic spike. These backpropagating action potentials would be induced by proximal synapses in an *in vivo* situation (Stuart and Hausser, 2001).

In the other side, we also report that Reelin regulation of dendritic spine morphology and density might vary depending on the dendritic domain of the pyramidal cell. Neuronal domain-specific differences might emerge from the above-mentioned different input synaptic partners. Besides, apical and basal dendritic trees exhibit largely different structures. Since signal propagation in dendrites is largely affected by branching events (Vetter et al., 2001; Schaefer et al., 2003), both dendritic domains might experience different synaptic integration processes. Considering that different dendritic domains also extend in different layers, domain-specific phenotypes could contribute to the emergence of some of the previously described layer-dependent phenotypes (**chapter 2**). Other authors have reported asymmetries in spine alterations in the CA1 pyramidal cells. In particular, a mouse model for Alzheimer 's disease showed reduced neck length but constant head size in basal dendrites in OR, whereas apical oblique dendrites in RAD exhibited similar neck length but reduced head size compared to controls (Merino-Serrais et al., 2011). Moreover, spine density was only reduced when these dendrites colocalized with APP deposits, but was maintained in transgenic mice in plaque-free dendritic segments. Further, Reelin overexpression in a different mouse model for Alzheimer's Disease prevented the disease-triggered spine loss in apical dendrites from CA1 pyramidal cells, and further demonstrated that Reelin might delay the polymerization of Aβ oligomers into fibrils (Pujadas et al., 2014).

In sum, our results show that Reelin signaling regulates spine plasticity in pyramidal neurons of different cortical regions, and that might do so by different mechanisms depending on the pyramidal cell identity and on the dendritic domain. Both of these features reflect particular synaptic circuitries and integrative strategies. Therefore, the adoption of different spine phenotypes under a similar Reelin signal suggests that specific response to Reelin in the synaptic zone is modulated according to local circuit requisites. Furthermore, it points Reelin signaling role close to the cortical synaptic plasticity regulation and mainteinance in the adult brain.

4. Imaging adult neurogenesis with a FIB/SEM microscope

Hippocampal adult neurogenesis is a biological process conserved in several species, including humans (Eriksson et al., 1998; Gage, 2000). It has recurrently been related to associative memory formation (Deng et al., 2010), and lately also to forgetting events (Frankland et al., 2013; Akers et al., 2014). Besides, several cognitive deficits and neurodegenerative and psychiatric disorders have been shown to present altered adult neurogenic patterns (Zhao et al., 2008). The fine description of the integration of a new-born granule cell in the preexisting synaptic circuitry is of great relevance for the understanding of the agents that regulate it, and therefore to discern the underlying mechanisms of high cognitive processes in health and disease.

Retroviral vector-based labeling approaches of new-born GCs have provided an extremely useful tool to visualize GCs of defined postmitotic ages and therefore to describe the morphological changes undergone during their development (Zhao et al., 2006; Ge et al., 2007; Sun et al., 2013). In our hands, this technique allowed successful labeling of new-born GC neurons, and PSD-95 positive dendritic spines were localized from 3 week-old GCs onwards, therefore reproducing the consensus in literature (Zhao et al., 2006; Deng et al., 2010). These constructs have also shown utility to analyze the synaptic integration of these cells at the ultrastructural level (van Praag et al., 2002; Toni et al., 2007; Toni et al., 2008). However, conventional serial-section electron microscopy-based approaches (Harris et al., 2006) involve such an amount of time and expertise that make high-throughput analyses very difficult or unfeasible. By contrast, recent development of combined scanning electron microscopes (SEM) with a variety of automated mechanisms to perform ultrathin sections represent a revulsive for the state-of-the-art of the technique (Helmstaedter et al., 2008; Knott et al., 2008; Merchan-Perez et al., 2009; Briggman and Bock, 2012; Helmstaedter, 2013; Knott and Genoud, 2013; Merchan-Perez et al., 2013).

We developed for the first time a correlative OM-FIB/SEM protocol combining immunohistochemical DAB labeling of the cells of interest and the complete 3D acquisition of labeled dendritic segments of interest with a FIB/SEM microscope. Targeted imaging and analysis of prelabeled samples helped to focus the course of the study and facilitated the analysis and data revision by independent investigators. Besides, DAB-positive neurites facilitated enormously the segmentation task. For instance, remote electrondense spines could be easily traced to their parent dendrite, since neurite continuity could be

inferred from the staining alone (Helmstaedter et al., 2008). But DAB labeling offered advantages in much earlier steps: since DAB deposits are visible during SEM imaging with backscattered electron detector, our approach allowed continued visualization of the dendrite of interest during the whole image acquisition process. Therefore, it ensured optimal framing of the imaged dendrite all over the acquired stack, thereby increasing the efficiency of the overall process. A recent study reported a correlative OM-FIB/SEM protocol based on fluorescence only (Maco et al., 2014). Despite feasible, blind imaging during FIB/SEM acquisition forces less optimal acquisition parameters, which balances DAB-stained samples as a better option to drive high-throughput analyses. Finally, the protocol used for tissue staining, contrasting and embedding was essentially the same as conventionally used for TEM purposes. Imaging with a lateral pixel size of 3.7 nm combined with z-spacings of 25 nm provided image datasets with enough resolution for a proper circuit reconstruction analysis (Briggman and Bock, 2012), while acquisition speed allowed the imaging of large tissue volumes of up to 11 μm in depth. We used and contributed to the development of the EspINA software for image segmentation (Morales et al., 2011), a multiplatform package that can be freely downloaded by the global public. Reconstructions from dendrite segmentations with both this software and Reconstruct (Fiala, 2005) were undistinguishable from each other, while semi-automated segmentation in EspINA hugely accelerated the segmentation steps. The relevance of this fact sets in that the reconstruction task is a bottleneck in the performance of electron-microscopy-based connectomics analysis (Helmstaedter, 2013). Therefore, the protocol we describe offers a reliable, high-throughput approach for the imaging of pre-labeled samples with a FIB/SEM microscope, and could be suitable to potentially any EM-processed biological tissue, both new and in stock.

Postsynaptic structures in developing new-born GCs

We performed a conventional classification of dendritic spines according to their morphological parameters and discriminated 5 different spine types: filopodia, stubby, thin, mushroom and branched spines (Harris et al., 1992; Harris and Weinberg, 2012; Rochefort and Konnerth, 2012). Our analysis in 8-9 week GCs reports a predominance of thin spines, a paired presence of mushroom and filopodia, a 15% of branched spines and very few stubby-like spines. These proportions are reflected by previous analyses of spine morphology in DG mature GCs (Harris et al., 1992; Woolley et al., 1996; Popov and Stewart, 2009). However, our results complement these studies in several ways.
First, the number of sampled spines outnumbers the previous attempts. To our knowledge, the results shown represent the most extensive analysis to date, comprising 235 spines with 271 identified spine heads. Second, the quality of the image datasets, both in terms of z-resolution (25 nm) and integrity (the technique overcomes ssTEM common artifacts such as loss or folding of slices) allowed a recurrent identification of each spine and synaptic contact in successive sequential images. Significantly, some authors recently claimed that stubby spines had been traditionally over-reported due to limited spatial resolution (Tonnesen et al., 2014), which reinforces our findings. Third, the sampled dendritic spines belong to GCs with a known date of birth, which permitted to analyze developmental features in spine morphology.

We detected a remarkable increase in the branched spine population in 8-9 week GCs compared to 3-4 week GCs. Interestingly, branched spines are known to exist in GCs, and their heads are innervated by independent presynaptic boutons (Geinisman et al., 1989; Trommald et al., 1996; Trommald and Hulleberg, 1997; Popov and Stewart, 2009). Moreover, branched spine population in the DG is increased after perforant path LTP (Trommald et al., 1996), as well in other cortical areas in response to either LTP or conditioning learning paradigms (Johansson and Belichenko, 2002; Sanders et al., 2012),

suggesting a particular role for this spine configuration in memory processes. Actually, some authors have suggested that the appearance of branched spines would underlie synaptic maturation events and have implications in synaptic efficacy (Rusakov et al., 1996; Sorra et al., 1998; Toni et al., 1999). Although some have hypothesized that both heads would receive inputs from the same synaptic bouton (Sorra et al., 1998; Toni et al., 1999), according to our observations synapses on the heads of a branched spine were always established by independent boutons. Also, we observed that spine types were conserved between the individual heads of branched spines and the overall spine population. Altogether, it suggests that mature, active and/or resource-rich spines might promote the emergence of new protrusions from their necks. These protrusions, however, should behave as newly generated spines (Kasai et al., 2010b) and therefore grow and find a presynaptic partner in the neighboring neuropil. Since spine types are conserved, the eventual splitting of a branched spine into individual spines would not affect the overall weight of spine morphological prevalences, although spine splitting is not thought to take place in response to LTP (Fiala et al., 2002a). In sum, our qualitative and quantitative description of branched spines presence in developing new-born granule cells represents a novel contribution to the comprehension of this particularly complex spine type.

Quantitative analysis of spine morphologies in developing new-born GCs

Dendritic spines exhibit a wide range of morphologies, and their classification into predefined spine types does not completely reflect their dynamic diversity. Early studies reflected such variety in shapes, and alternative, richer classification paradigms were proposed (Jones and Powell, 1969; Spacek and Hartmann, 1983). However, the finding that spine morphological parameters displayed a unimodal distribution prompted some authors to suggest that dendritic spine morphological diversity was instead a continuum of shapes (Trommald et al., 1996; Trommald and Hulleberg, 1997). A more recent exhaustive ultrastructural analyisis of 144 fully-reconstructed dendritic spines from mouse visual cortex layer 2/3 pyramidal neurons further supported this hypothesis (Arellano et al., 2007a). Moreover, an extensive confocal microscopy analysis of 8900 human dendritic spines from layer III pyramidal neurons in the cingulate cortex described that spine size distribution was skewed to the left and could be fitted by a gamma function (Benavides-Piccione et al., 2013). In our hands, the analysis of 226 fully-reconstructed spines of 8-9 week GCs revealed a unimodal, left-skewed distribution of the volumes of both the spines and the synapses received by these, whereas sphericities described a continuous distribution of values symmetrically scattered around the mean. Therefore, our results support the notion that dendritic spine morphologies exhibit a continuum of shapes.

Through a quantitative analysis of developmental changes in spine morphology we showed that development of new-born GCs is accompanied by an increase in the sphericity, or compactness, of their spines. This is consistent with the finding that newborn spines on pyramidal neurons exhibit a reduction in their surface-to-volume ratio, an equivalent of the sphericity parameter, concomitant with spine maturation (Knott et al., 2006). Revisiting the dynamic processes that underlie activity-triggered spine enlargement, spine growth involves an intermediate, unstable stage characterized by the activation of its actin enlargement pool. It is during this stage that the spine size increases in response to activity. Following this stage, stable pool of F-actin grows (since its presence is proportional to the spine size), thereby ensuring the persistence of the spine enlargement (Honkura et al., 2008; Yasumatsu et al., 2008; Kasai et al., 2010a). Therefore, the evolution from the enlargement to the stable state involves the change of the cytoskeletal motor force defining the spine shape: from the enlargement pool to the stable and dynamic actin pools combined. Interestingly, spines in the enlargement phase exhibit more excentric (less circular or spherical) morphologies than later on, even though their size is maintained

(Honkura et al., 2008). Hence, this schema could explain the phenotypes observed in our samples.

Moreover, since our results emerged from spines belonging to the overall spine population of new-born GCs, they suggest a synchronized process of spine maturation in these cells. In this scenario, 3-4 week GCs' spines would be in the enlargement phase, whereas 8-9 week GCs' spines would have already stabilized their morphology and increase in size, displaying a stable phase state. This hypothesis fits in the described developmental process of these cells, since no spines can be found in 2 week GCs, almost all protrusions are present at 6 weeks and 8 week GCs are assumed to exhibit spine features of an already mature GC (Zhao et al., 2006). Further, this hypothesis would point the actin cytoskeletal dynamics inside the spinoskeleton as a central element in this synchronic synaptic integrative process. The fine description and further mechanisms underlying this process, though, will require future insights and experiments. In sum, our results show that spine population of developing new-born GCs experience a synchronic structural maturation, which consists in the acquisition of a more spherical morphology at mature stages.

Correlation of paired morphological measurements inside a spine-synapse couple

Since spine structure is closely related to the spine function (Yuste and Majewska, 2001a; Bourne and Harris, 2008; Cingolani and Goda, 2008; Tonnesen et al., 2014), it is not surprising that different morphological parameters of either the spine or its synapse might be related. A number of articles have described correlations for paired measurements of different synapse-related parameters, delinating two main structural governance blocks with close, although different, functions: On one hand, the volume of the dendritic spine head is associated to the average reliablility and strength of the synapse (Arellano et al., 2007a). Accordingly, spine head volume correlates with its stable F-Actin pool and with its total actin load (Honkura et al., 2008), with the size of the PSD (Harris and Stevens, 1989; Schikorski and Stevens, 1997; Trommald and Hulleberg, 1997; Schikorski and Stevens, 1999; Arellano et al., 2007a; Holderith et al., 2012) and with the glutamate sensitivity of the spine (Matsuzaki et al., 2001), but also with the total number and docked fraction of presynaptic vesicles (Harris and Stevens, 1989; Schikorski and Stevens, 1997, 1999). On the other hand, spine neck structure and geometry regulates the strength of the synapse by determining the properties of its Ca^{2+}-dependent learning rules (O'Donnell et al., 2011; Gulledge et al., 2012). Consequently, the length of the spine neck correlates with the time constant of Ca^{2+} compartmentalization (Majewska et al., 2000b; Yuste et al., 2000; Sabatini et al., 2002; Noguchi et al., 2005) and with spine filtering properties of electron potentials (Svoboda et al., 1996; Araya et al., 2006).

Our results reproduced the correlation between total spine volume and PSD size (Lisman and Harris, 1993; Knott et al., 2006; Arellano et al., 2007a; Nikonenko et al., 2008; Cane et al., 2014). Moreover, we described for the first time that the compactness or sphericity of the spine and the synapse correlate with the volume of the dendritic spine. Furthermore, binned analysis of these data showed a linear relationship between those variables under certain thresholds, and more interestingly paired correlations no longer existed for data points above the thresholds defined. Altogether, these observations allow us to consider how these parameters might be co-regulated in the dynamic spine population.

First, despite sizes of dendritic spines depict a huge variability of two orders of magnitude, their values are still constrained in a range, and the left-skewed distribution ensures a major population of similarly medium-sized spines. This is, big spines are scarce, and therefore little and medium-sized spines are the only ones that might be able to grow. This is in accordance with the fact that activity-dependent spine enlargement occurs preferentially on small-sized spines (Matsuzaki et al., 2004). Similar distributions

and conjectures were observed and could be arisen for the synaptic volume and the respective sphericities. As a result, the growth of an initially small spine would trigger an enlargement of its synapse. However, once the synapse becomes 'big', it would stop increasing, irrespectively of the spine volume. Similarly, the growth of the spine would involve the acquisition of a less spherical shape, and once attained, spine sphericity would no longer be reduced by increased spine growth. Finally, and in the same direction, the growth of the spine would ensure the attainment of a less compact synapse, and once attained, synapse compactness would no longer be regulated by spine growth. This view would ensure that the growth of an initially small spine would provide a larger, less spherical spine bearing a larger, less compact synapse. More important, this view would ensure that the morphological parameters of the grown spine would be physiologically functional, conferring this spine a greater synaptic strength. Note that individual nascent spines on dendrites from mature new-born GCs might undergo the same process. However, spinogenesis in mature GCs would no longer be a synchronic process, and therefore average measurements from the global spine population would reflect the predominant feature, which are stable spines.

Second, our results show a near-lineal evolution of these parameters. Indeed, the extrapolation of these fits with a 95% confidence interval would give rise to the assumption that the smallest spine that could exist would be a round spine with a sphericity of 0.61 to 0.64, bearing a compact, small synapse of 8.83E+05 to 1.81E+06 nm^3 that would have an sphericity of 0.64 to 0.67. However, very early stages of spine generation may require a specific approach. A study analyzing the morphological and synaptic development of newborn spines in pyramidal cells at the ultrastructural level imaged as young as 1.5 days-old spines, and concluded that spine growth precedes synapse formation (Knott et al., 2006). In this study, the youngest spines exhibited small volumes of 1.7E+07 to 9.7E+07 nm^3, and those bearing synapses had PSDs with surface areas comprised between 6.0E+03 to 9.3E+04 nm^2. Assuming from our data that initial synaptic mean sphericity should be 0.652 ± 0.007, and using the formula defining the sphericity from a particle's surface and volume (**methods** (**1**)) (Wadell, 1935), the PSDs in their youngest spines would present an estimate volume of 2.30E+04 ± 3.7E+02 to 1.40E+06 ± 2.3 E+04 nm^3. Mainly, these volumes match inside the predicted range arisen from our results.

Therefore, our results describe a robust linear relationship between the volume and the sphericity of both the spine and the synapse of mature new-born GCs, which might be also applicable to other spine populations. In particular, our analyses describe linear relationships for paired spine and synapse morphometric values under specific thresholds, which are mainly conserved in young GCs.

Presynaptic innervation of newborn GCs

Boutons stablishing synapses with more than one postsynaptic partner have been described innervating different cortical areas (Sorra and Harris, 1993; Toni et al., 1999; Geinisman et al., 2001; Knott et al., 2006). Their presence was shown to increase 60 minutes after LTP induction, and was preceded by a transient increase in the abundance of perforated synapses (Toni et al., 1999). Interestingly, estradiol, associative learning paradigms and new-born dendritic spine formation showed to promote the appearance of these boutons (Woolley et al., 1996; Geinisman et al., 2001; Knott et al., 2006). These findings support the notion that multisynaptic boutons (MSBs) would represent an intermediate element in the process of spine integration in the preexisting circuitry (Knott et al., 2006). This is, that new spines would establish synapses with existing boutons, thereby generating MSBs, and subsequent competition steps would drive the pruning of the least active, leading to a final status of SSB.

MSB population in pyramidal cells has been reported to be around 20% on a control situation, whereas they represent the presynaptic partner of almost the 70% of the new spines (Knott et al., 2006). In new-born GCs from the DG, MSB population has also been related to the maturation of these cells. Whereas in mature GCs MSBs represent almost a 40% of the presynaptic partners, 4-week-old GCs receive contacts from MSBs in more than a 75% of their spines (Toni et al., 2007). Similarly, our analysis depicted a MSB prevalence of a 76% in 3-4 week-old and of a 72% in 8-9 week-old GC synapses. In the other hand, we showed that MSBs innervating spines from 8-9 week-old GCs establish a 34% more synapses. When some authors noticed an increase in CA1 MSB prevalence after LTP, their presence was associated with increased number synaptic contacts with the same dendrite (Toni et al., 2001). However, we did not find any example of a MSB innervating twice the labeled new-born GC.

In more wide terms, both situations might be compatible. Assuming that MSB emergence responds to the activation of a bouton-spine couple, this situation can be triggered by both sides. After LTP, hyperstimulation of a given synapse comes from the presynaptic side. A given hyperstimulated SSB might therefore be activated irrespectively of the previous physiological input received by its coupled dendrite, and would promote its synapse, giving rise to a MSB contacting multiple times with the same dendrite. In the case of a new-born GC willing to become integrated in the preexistent circuitry, it is the postsynaptic GC that drives the hyperexcitability the influenced circuits. Since to become integrated each spine will have to compete with other spines for a given bouton, prompting this bouton to establish more contacts would serve as a way for facilitating the success of this synaptic competition.

Besides, paralleled studies involving hippocampal LTP found that, at 2 hours post-stimulation, there was a reduction in the percentage of small spines (Bourne and Harris, 2011) and a reduction in the percentage of SSBs (Bourne et al., 2013), in concordance with the previous finding that hippocampal SSBs were preferentially associated to SSB boutons (Woolley et al., 1996). To decipher such relationship, we analyzed the properties of spines contacted by either SSBs or MSBs, and found that neither the spine type nor any morphological parameter related to the spine or the synapse exhibited a preference for the bouton type. Therefore, the identity of a SSB or MSB is unrelated to the morphological characteristics of the integrating GC spine.

Altogether, we found that the integration of new-born GCs occurred concomitantly with an increase of connectivity of presynaptic MSBs, and that the presynaptic identity was unrelated to the postsynaptic morphology. Some evidences point to the fact that developing new-born GCs preferentially integrate onto preexisting circuits rather than promoting the generation of new pre- and postsynaptic partners and that this competitive process is specific for the adult brain (Toni and Sultan, 2011). Therefore, unveiling the fine mechanism regulating this competitive process might shed light onto the understanding of the functional role of adult hippocampal neurogenesis.

5. Reelin signaling and hippocampal adult neurogenesis

Hippocampal adult neurogenesis is affected by Reelin-triggered signaling. Dab1 deficits have been shown to regulate both the dendritic growth and dendritic branch orientation of new-born GCs in the DG (Teixeira et al., 2012), and Reelin overexpression leads to mispositioning these cells in the granular layer (Pujadas et al., 2010). Moreover, Reelin signaling has been shown to regulate events related to synaptic plasticity (Qiu et al., 2006a; Qiu and Weeber, 2007; Niu et al., 2008; Pujadas et al., 2010; Rogers et al., 2011; Rogers et al., 2013).

We used a retroviral infection strategy to selectively image new-born granule cells of a known age in Reelin-OE mice. In the other side, simultaneous Cre recombinase expression in these retroviruses allowed the generation of new-born GC-specific depletion of Dab1 in flDab1 mice, and therefore a cell-specific disruption of the responsiveness to Reelin signaling (Zhao et al., 2006; Teixeira et al., 2012). Taking advantage of the previous development of a high-throughput ultrastructural reconstruction imaging protocol based on FIB/SEM microscopy (**chapter 4**), we proceeded to an exhaustive ultrastructural analysis to unravel fine mechanisms by which Reelin signaling might regulate the integration of developing new-born GCs in the preexisting DG circuitry.

Dendrites from 3-4 and 8-9 week-old new-born GCs from both Reelin-OE mice and Dab1-KO cells were imaged with a lateral resolution of 3,7 nm and a z-spacing of 25 nm, in addition to their relative controls. In sum, the detailed analysis of an imaged volume of +5900 μm^3 containing 28 dendritic segments of interest led to the identification of 476 synapses, 544 spines and 476 presynaptic boutons, and to the complete 3D reconstruction of 443 dendritic spines with their respective synaptic specializations. This dataset provided complete structural information of both the labeled items and the surrounding neuropil, thereby reinforcing the feasibility of the previously defined imaging method for the analysis of targeted subcellular regions of interest in the nanoscopic scale.

Reelin signaling in dendritic spines of developing new-born GCs

We identified dendritic spines of all types in all the experimental groups except for stubbies, which were not found neither in WT nor in Dab1-KO 3-4 week GCs. Indeed, the relative presence of spine types and synaptic arrangements exhibited punctual variations across ages and genotypes. Despite the most common feature was one spine – one synapse, in some cases other arrangements were found.

In 8-9 week Reelin-OE GCs we identified five spines (5%) without a clear PSD specialization nor any presynaptic partner, accounting for previously defined vacant or asynaptic dendritic spines (Arellano et al., 2007b). Besides, we found two multi-innervated spines (MIS) in 8-9 week-old Dab1-KO GCs, whereas any of the other groups exhibited such spine type at mature stages. Interestingly, MIS formation has been shown to be a process promoted by nitric oxide (NO) signaling. It occurs in an activity-dependent manner triggered by the recruitment of neuronal NO synthase (nNOS) at the synapse by PSD-95 (Ishii et al., 2006; Nikonenko et al., 2008). Since NO has been shown to promote the generation of presynaptic varicosities (Nikonenko et al., 2003), this molecule has been proposed to act as a retrograde messenger that would promote the generation of new synapses (Hardingham et al., 2013). This is, local diffusion of NO secreted by new protrusions would stimulate the differentiation of a neighboring axon into a varicosity, thereby facilitating the establishment of a synapse. Notably, deficiency for nNOS in mice has been associated to impaired fear conditioning (Kelley et al., 2009) and impaired LTP (Kelley et al., 2011), as well as increased levels of cAMP response element-binding protein (CREB) phosphorylation. Moreover, studies with KO mice for selective receptors of NO revealed that its signaling is required for LTP in such a way that suggests a possible dual pre- and postsynaptic contribution (Taqatqeh et al., 2009). Finally, nNOS protein in the cortex and hippocampus localizes to the cytoplasm of a small population of GABAergic cells whereas in a larger population of excitatory neurons its localization is restricted to the spine head (Aoki et al., 1997; Hardingham et al., 2013). Notably, NO signaling is related to Reelin signaling in a number of ways.

First, CREB is a transcription factor for Reelin (Chen et al., 2002) and Reelin injections increase its activation and enhance dendritic spine density in the CA1 (Rogers et al., 2011). Moreover, CREB phosphorylation has also been related to synapse formation stages (O'Connell et al., 2000; Aguado et al., 2009), whereas lack of CREB activity leads to decreased expression of Dab1 and developmental cortical layering defects (Diaz-Ruiz et al., 2008). Second, crosstalk between NO and Reelin signaling pathways takes place in the olfactory bulb. There, interneurons expressing ApoER2 and nNOS innervate Reelin-expressing periglomerular cells that are sensitive to NO signaling. In turn, *reeler* mice exhibit reduced protein levels of nNOS in the olfactory bulb (Herrmann et al., 2008). And third, interneurons expressing nNOS and Reelin are found in the hippocampus and Reelin deficiency in *HRM* is associated with a loss of these neurons specifically in the DG ML and sub-granular zone (SGZ) (Romay-Tallon et al., 2010).

This could suggest that, in new-born GCs, generation of MIS could be jointly regulated by Reelin and NO: whereas synaptic integration in young GCs could involve the formation of MIS through NO activity, Reelin signaling in mature GCs could prevent this process. Otherwise, lack of Reelin in Dab1-KO cells would leave an immature phenotype to last longer, leading to abnormal MIS presence in 8-9 week-old GCs. This mechanism, though, should be confirmed by specific experiments.

Interestingly, our analysis of the dendritic spine morphology depicted different phenotypes that suggest an abnormal development of Dab1-KO new-born GCs. By contrast with the above-mentioned presence of MIS at mature stages, branched spine presence showed a premature abundance in these

cells, whereas spine type classification depicted a disrupted spine pattern at early stages. Besides, the presence of mushroom-like spines in 8-9 week-old GCs showed a direct dependence on Reelin signaling levels. These results are in accordance with previous experiments showing increased complex spines in Reelin-OE mice (**chapters 2**, **3**).

Our results also showed that in mature GCs Reelin overexpression is associated with larger large spines and bigger, less spherical synapses. Besides, lack of Reelin signaling was found associated with a reduced size of the synapse, whose morphology depicted less mature (more spherical) shapes at 8-9 weeks than at 4 weeks. Moreover, both up- and downregulation of the Reelin signaling disrupted the developmental increase in spine sphericity observed in control situations. Spines exhibit a great variability in their sizes and shapes, and both spontaneous and activity-triggered volume fluctuations occur in a mechanism ultimately related to the actin cytoskeleton (Cingolani and Goda, 2008; Racz and Weinberg, 2008). As stated above, spine enlargement strictly depends on a specific actin pool, characterized by a highly ramified structure (Honkura et al., 2008; Kasai et al., 2010b). The actin nucleator and ramification-promoting complex Arp2/3 is a marker of this actin pool (Bramham, 2008; Racz and Weinberg, 2013). Depletion of Arp2/3 levels leads to spine loss, reduced LTP-triggered spine enhancement and reduced spine circularity, and leads to an abnormally high amount of filopodia-like spines (Kim et al., 2013). Interestingly, mice deficient for WAVE-1, a regulator of this complex, exhibit synaptic deficiencies that to a certain extent mimic those found in our models of modified Reelin expression. The hippocampal stratum radiatum of WAVE-1 KO mice presents increased bouton size, as well as a reduction in spine circularity and enhanced presence of MIS, always consisting of two synaptic contacts established by the same axon (Hazai et al., 2013), whereas these mice show deficits in spatial learning, memory and anxiety-related tests (Soderling et al., 2003). Since these effects are potentially due to the activation of Arp2/3, similar phenotypes could be hypothesized through its activation via N-WASP. The latter can be directly activated by Dab1 or through Cdc42 (Suetsugu et al., 2004; Winder, 2004), which is also a downstream effector of the Reelin-PI3K signaling pathway (Leemhuis and Bock, 2011).

Therefore, modifications in the Reelin signaling pathway could lead to a misregulation of the spine cytoskeleton through N-WASP. Our results suggest that normal enlarged spine maturation is no longer evident in both up- and downregulation models for Reelin signaling. Moreover, previous observations of reconstructed spines of CA1 pyramidal cells (**chapter 2**) showed similarly hypertrophic dendritic spines. It is known that larger spines live longer whereas small spines exhibit a more motile behavior (Korkotian and Segal, 2001; Konur and Yuste, 2004; Matsuzaki et al., 2004; Yasumatsu et al., 2008). In dendritic spines of Reelin-OE 8-9 week GCs, increased spine volume compared to controls was restricted to the large spine population. This would add up in the above-mentioned hypothesis, since small spines would be devoid of the enlargement pool regulated by Arp2/3 (Honkura et al., 2008; Racz and Weinberg, 2013) and therefore should not exhibit morphological deficits. Further experiments should be addressed to clarify this mechanism. Altogether, our results show that proper spine development in new-born GCs requires Reelin signaling in a functional level, and that both excess and shortage of its function leads to abnormally excentric spine and synaptic morphologies.

Reelin signaling in the presynaptic innervation to developing new-born GCs

Boutons innervating dendritic spines of developing new-born GCs exhibited less synaptic contacts when the Reelin signaling pathway was altered. This was due to two factors: first, these mature GCs displayed less numbers of presynaptic boutons establishing multiple synapses (MSBs) than control

GCs. Second, these MSBs performed less than 4 synapses each, whereas in control GCs this number raised up to 10. Therefore, synaptic connectivity of presynaptic boutons innervating new-born GCs appeared to be both dependent on defective Reelin signaling occurring in these cells and on enhanced Reelin expression in the DG.

Deciphering the fine mechanism by which Reelin signaling triggers these effects would be of outstanding interest, since the proper integration of new-born granule cells is needed to exert their function (Aimone et al., 2006, 2009; Aimone et al., 2011). From our samples, two scenarios might be considered: Reelin-OE experiment is based on mice overexpressing Reelin exogenously in a sustained manner, in which we should expect increased levels of extracellular Reelin in the DG (Pujadas et al., 2010). Therefore, phenotypes observed in new-born GCs or their presynaptic partners can both be triggered by increased responses to Reelin signaling. Besides, our Dab1-KO approach is cell-specific. Here, labeling new-born GCs involved the escision of the Dab1 gene in these cells, but not in their neighborhood (Zhao et al., 2006; Teixeira et al., 2012). In this case, we should expect a defective response to Reelin in these cells, but not in their presynaptic partners, which remained genetically unaltered. Although the mechanisms should be different, we observed similar phenotypes in both models. Therefore, either both mechanisms converged in the same phenotype, or both models triggered a common pathway.

Our experiments do not resolve this question. However, we could argue that the simplest way to get twice the same phenotype is having a common mechanism. In our samples, this could only be possible if the presynaptic innervation phenotype was triggered by the new-born GC. If this was the case, in Reelin-OE mice new-born GCs would experience an enhanced Reelin signaling. Accordingly, their spines should trigger an enhanced retrograde signaling towards its bouton. In the other side, Dab1-KO new-born GCs would experience a defective response to Reelin signaling, and we should expect a lowered retrograde signaling from their spines to the relative presynaptic boutons. In this situation, our results would suggest that both enhanced and lowered retrograde spine-bouton signaling would result in defective developmentally-induced hyperconnectivity of the presynaptic MSBs innervating new-born GCs. A number of molecules regulating presynaptic synaptogenesis might be suitable for this mechanism, and multiple signaling arrangements could respond for this on-off effect too. Taking into account the previously mentioned MIS phenotype, we could propose the involvement of the NO signaling system, which is known to induce presynaptic plasticity (Nikonenko et al., 2003; Hardingham et al., 2013) and is postsynaptically-secreted (Nikonenko et al., 2008) and whose defects in signaling have been reported in psychiatric diseases similar to those associated to Reelin dysfunction, such as depression, Parkinson's disease and Alzheimer's disease (Zhou and Zhu, 2009).

Altogether with the observations regarding spine and synaptic morphologies, our results show that proper integration of new-born GCs in the preexisting circuitry might be disrupted upon insults in the regulation of the Reelin pathway. These findings are in accordance with previous studies reporting that both subthreshold levels and chronic excess of Reelin would be deleterious: the former would delay the normal development of excitatory synapses (Trotter et al., 2013) whereas the latter would promote circuitry alterations based on spine morphology and number (Pujadas et al., 2010; Rogers et al., 2013). Also, our results complement previous observations showing that new-born GCs exhibited abnormal, although different, dendritic arborization patterns in both Reelin signaling up- and downregulation strategies (Teixeira et al., 2012).

A correct integration of new-born granule cells in the preexisting circuitry is essential for their correct function (Deng et al., 2010; Aimone et al., 2011). Since young GCs have been shown to exert different functions than old GCs in the DG (Nakashiba et al., 2012; Akers et al., 2014), our results suggest that Reelin signaling might be an important factor in the regulation the DG function. Adult hippocampal

neurogenesis impairment has been associated to multiple cognitive disorders. In particular, some antidepressant treatments have shown to promote adult neurogenesis, and this process has been therefore pointed as a candidate mechanism for the etiology of depression (Sahay and Hen, 2007). Moreover, schizophrenia models based on maternal immune activation have been shown to damage both prenatal and postnatal hippocampal neurogenesis. Furthermore, in these models a developmental insult leads to a persistent impairment in brain function that might underlie future schizophrenia-associated phenotypes (Meyer, 2013). Further, the global hippocampal function has been shown to be associated to the pathophysiology of schizophrenia, which is partially dependent on the processes regulated by new-born GCs (Tamminga et al., 2010), besides of being also related to other cognitive and mood disorders.

Hence, our results suggest that the Reelin signaling pathway might exert a structural role in the synaptic plasticity mechanisms that take place during the integration of new-born GCs in the adult hippocampus. The striking relevance of this process in the pathophysiology of different cognitive and psychiatric disorders suggests a high importance of this signaling pathway in the overall mechanisms underlying such diseases.

Conclusions

The results obtained in this study allow us to raise the following conclusions:

1. Sustained *in vivo* Reelin over-expression triggers increased structural complexity of presynaptic boutons in the adult hippocampus

2. Sustained *in vivo* Reelin over-expression gives rise to dendritic spine hypertrophy in the adult hippocampus

3. Reelin modulates the complexity of the spine apparatus and the presence of synaptopodin in a lamina-specific manner in the adult hippocampus

4. Reelin regulates the synaptic-extrasynaptic distribution of NMDA receptor subunits 2A and 2B and of p-cofilin molecules in the stratum radiatum of the adult hippocampus.

5. Sustained *in vivo* Reelin over-expression triggers reduced dendritic spine density in dendrites of S1BF layer 5 but maintained in CA1 pyramidal cells, and spine hypertrophy in dendrites of S1BF layer 5 pyramidal cells.

6. Conditional adult Dab1 depletion in Cre/flDab1+TAM mice provokes an increase in the density of spines in dendrites from S1BF layer 5 but not in CA1 pyramidal cells, spine hypertrophy in dendrites of S1BF layer 5 pyramidal cells and spine shrinkage on basal dendrites from CA1 pyramidal cells.

7. The correlative OM-FIBSEM method described represents a reliable, high-throughput procedure for obtaining high-resolution 3D images of pre-labeled dendritic segments.

8. Thin spines are the most frequent type in developing new-born granule cells in the dentate gyrus (DG). Most synaptic contacts on dendritic spines are located on the spine head.

9. Developing new-born DG granule cells (GCs) bear branched spines. These spines are larger and less spherical than non-branched and display more synaptic volume. Spine heads from branched spines receive synaptic contacts from independent presynaptic boutons.

10. Morphometric parameters of spines and synapses of adult new-born DG GCs display a continuum of values. Spine volume correlates positively with synapse volume and negatively with spine sphericity and synapse sphericity. These pairs of magnitudes exhibit linear relationships for spines below a certain volume threshold.

11. Spines of developing new-born DG granule cells are more spherical at 8-9 weeks than at 3-4 weeks.

12. Spines from adult-generated GCs are preferentially innervated by multisynaptic boutons (MSBs). MSBs contacting 8-9 week-old GCs establish more synapses than MSBs contacting 3-4 week-old GCs.

13. 8-9 week-old new-born granule cells exhibit structural alterations upon both up- and down-regulation of the Reelin signaling pathway. 8-9 week GCs display spine and synapse hypertrophy upon Reelin overexpression and smaller synapses upon Dab1 depletion.

14. Spines from both Reelin-OE and Dab1-KO new-born GCs are preferentially contacted by MSBs. MSBs contacting both Reelin-OE and Dab1-KO 8-9 week-old GCs establish less synapses than MSBs contacting WT GCs of the same age.

Materials and Methods

Materials

Animals

Mice were housed in groups (2-6 mice per cage) and maintained in a 12-h light-dark cycle with access to food and water *ad libitum*. All experiments were conducted blind and in compliance with the protocols approved by local ethics committee and with the European guidelines.

The double transgenic mouse line *pCaMKIIα-tTA* / *tetO-rlM* (Reelin-OE) overexpresses Reelin under the calcium–calmodulin-dependent kinase IIa promoter through a tTA transactivator. Littermates lacking one of the two transgenes (+/*tetO-rlM*; *pCaMKIIα*/+ or +/+) do not exhibit any transgene expression according to previous characterization experiments, and were used as controls. Feeding for one week with doxycycline-containing feed (Bio-Serv, 200 mg per kg) successfully blocks the transgene expression (Pujadas et al., 2010).

Transgenic reporter line *B6.Cg-Tg(Thy1-YFPH)2Jrs/J* (Thy1H) was purchased from Jackson (Feng et al., 2000) and maintained on a *C57BL/6J* background. We generated a triple heterozygote transgenic mouse line *pCaMKIIα* / *tetO-rlM* / *Thy1H* (Thy/Reelin-OE) in our laboratory. Littermates lacking one of the two transgenes necessary for Reelin overexpression (+/*tetO-rlM* / *Thy1H*; *pCaMKIIα*/+ / *Thy1H* or +/+/ *Thy1H*) were used as controls in the respective experiments.

Floxed *dab1* mice (flDab1) (Pramatarova et al., 2008) and *Ubiquitous CreER^{T2}* mice (UbiCre, Jackson, *B6.Cg-Tg(UBC-cre/ESR1)1Ejb/J*) were maintained on a *C57BL/6J* background, and flDab1 mice were backcrossed for five generations to ensure strain purity.

Double transgenic mice *UbiCre$^{+/-}$* / *dab1$^{flox/flox}$* (Cre/flDab1) were generated by maintaining the Cre line in heterozygosis. Conditional escision of the *dab1* gene by means of intraperitoneal injection of tamoxifen (TAM) generated a conditional *dab1* knock-out (KO) model (Cre/flDab1+TAM) (Teixeira et al., 2014).

Chemicals

Common chemicals and reagents were purchased from Sigma-Aldrich and Panreac. Specifically, electron microscopy fixatives, alcohols and special reagents used were: activated charchoal Norit pellets from Sigma, Ethanol and Paraformaldehyde from Panreac, Osmium Tetroxide and Glutaraldehyde from Electron Microscopy Sciences and Uranyl Acetate from Fluka (Sigma-Aldrich). For animal treatment protocols, tamoxifen (TAM) and sunflower oil were purchased from Sigma. For intracellular labeling techniques, 4',6-Diamidino-2-phenylindole dihydrochloride (DAPI) and Lucifer Yellow were purchased from Sigma-Aldrich and Alexa 594 fluorophore from Invitrogen. For the generation of a point-spread function suitable for experimental deconvolution procedures, yellow-green beads of 110 nm diameter were purchased from Molecular Probes.

Antibodies

Anti-Lucifer Yellow (Rabbit polyclonal "poly", developed at Instituto Cajal) was gently provided by Javier deFelipe). Commercial antibodies used were actin (mouse monoclonal "mAb" clone C4, Millipore); synapsin (rabbit poly, Synaptic Systems); synapsin 2 (rabbit poly, Stressgen Bioreagents); SNAP25 (mouse mAb clone SMI-81, Becton-Dickinson); synaptopodin (rabbit poly, Synaptic Systems); NR2a (rabbit poly, Millipore); NR2b (rabbit poly, Millipore); p-cofilin on serine 3 (rabbit poly, Santa Cruz); NR1 (mouse mAb clone 54.1, BD Biosciences); GluR1 (rabbit mAb clone C3T, Millipore); GluR2/3 (rabbit poly, Chemicon); PSD-95 (mouse mAb clone 7E3-1B8, Millipore); CaMKII (mouse mAb clone 6G9, Affinity Bioreagents); LIMK-1 (rabbit poly, Santa Cruz); p-LIMK1 (Thr508)/LIMK2 (Thr505) (rabbit poly, Cell Signaling Technology); Cofilin (rabbit poly; 1/500; Millipore) and GFP (rabbit poly, Life Technologies).
For immunogold analyses, primary antibodies used were the following: NR2a (rabbit poly, Millipore); NR2b (rabbit poly, Novus Biologicals); p-cofilin on serine 3 (rabbit mAb clone 77G2, Cell Signaling Technology). Secondary 18-nm gold-tagged polyclonal antibodies goat-anti-rabbit were purchased from British Biocell International.

Software

Softwares used for general image analysis and quantification were Fiji (Schindelin et al., 2012) (distribution of ImageJ – Wayne Rasband, NIH – freely downloadable at http://fiji.sc/Fiji); Imaris (Bitplane); Autodeblur (Autoquant, Media Cybernetics) and Metamorph (Molecular Devices). Additional sofwares used specifically in the FIB/SEM approaches were EspINA (Morales et al., 2011) (Cajal Blue Brain Project); Reconstruct (Fiala, 2005) (freely downloadable at http://synapses.clm.utexas.edu/tools/reconstruct/reconstruct.stm) and Photoshop (Adobe Systems). To quantify the signal density in Western Blot bands we used GelPro (Media Cybernetics). Statistical analyses were performed in GraphPad Prism (GraphPad Software) and Igor Pro (Wavemetrics) and Excel (Microsoft). Bibliograhpy managing in manuscripts was handled with EndNote (Thomson Reuters).

Methods

Tamoxifen Injection

In order to obtain temporally-controlled, ubiquitous Cre-mediated recombination in Cre/flDab1 mice, we administered TAM injections (30 mg/ml in 1:10 alcohol:sunflower oil). Seven week-old mice received daily intraperitoneal injections of 180 mg/kg for 3 days, at least 5 weeks before any experimental assay.

Retroviral (RV) tracing

To label new-born granule cells in control and Reelin-OE mice and to generate cell-specific escision of the *dab1* gene in flDab1 mice, we used a RV CAG-GFP-IRESCRE stock encoding for GFP and Cre-recombinase (Zhao et al., 2006). The plasmids used for the production of GFP-expressing RVs were a generous gift from Fred H. Gage. To visualize PSD-95 clusters in new-born granule cells we used the retroviral vector MRSVPSD95g developed previously in C. Lois group (Kelsch et al., 2008). RVs were produced by transient transfection of the 293 cell line as described previously (Zhao et al., 2006). RV stocks were concentrated by ultracentrifugation to working titers of $1x10^7$-$2x10^8$ pfu/ml. Adult mice (7–8 weeks old) were anesthetized and placed in a stereotaxic frame. The scalp was incised, and holes were drilled in the skull. Targets with coordinates (in mm) relative to bregma in the anteroposterior, mediolateral, and dorsoventral planes were as follows: DG [-2.0, 1.4, 2.2]. In experimental animals, 1.5µl per DG of virus solution was infused at 0.2µl/min via glass micropipette, leaving the micropipettes in place an additional 5 min to ensure diffusion.

Synaptosome extracts

Hippocampal synaptosome-enriched protein extracts were obtained following a protocol described elsewhere (Niu et al., 2008). Briefly, adult mice were sacrificed by decapitation, brains were removed from the skull, and hippocampi were dissected in ice-cold dissection buffer and pooled (4 hippocampi

per sample). Hippocampi were homogenized in 1.5 ml of SP buffer (0.32M sucrose with protease and phosphatase inhibitors –see lysis buffer) with an Eppendorf tissue grinder. A 150-µl aliquot of homogenate was kept for validation purposes. The homogenate was centrifuged twice at 800g for 5 min at 4ºC in a F45-24-11 rotor on an Eppendorf 5415R centrifuge, and pellets were discarded. The cleaned supernatant was then centrifuged at 5769g for 11 min at 4ºC in a TLA-55 rotor on a Beckmann OPTIMA TLX ultracentrifuge. The supernatant was then carefully removed, and the pellet was resuspended in 250 µl of lysis buffer (Hepes 50mM pH 7.5, NaCl 150mM, $MgCl_2$ 1.5mM, EGTA 1mM, Glicerol 10%, Triton X100 1%; protease inhibitor: Complete protease inhibitor from Roche; phosphatase inhibitors: NaF 10mM, Na_3VO_4 0.2 mM, $Na_2H_2P_2O_7$ 10mM).

Western Blots

Western blots against various proteins of interest were performed following conventional procedures (Pujadas et al., 2010). Briefly, samples were resolved in SDS-polyacrylamide gels and transferred to nitrocellulose membranes. Blots were incubated in primary antibody diluted in TBST-5% non-fat milk for 2h at room temperature or overnight at 4ºC. After incubation with a secondary antibody for 1h at room temperature, membranes were developed with the ECL+ system (GE Healthcare). We used the following primary antibodies: actin (1:100000; Millipore), synapsin 2 (1:500; Stressgen Bioreagents), SNAP25 (1:750; Becton-Dickinson), synaptopodin (1:750; Synaptic Systems), NR2a (1:500; Millipore), NR2b (1:500; Millipore), p-cofilin on serine 3 (1:100; Santa Cruz), NR1 (1:1000; BD Biosciences), GluR1 (1:500; Millipore), GluR2/3 (1:1000; Chemicon), PSD-95 (1:1000; Millipore), CaMKII (1:2000; Affinity Bioreagents), LIMK-1 (1:100; Santa Cruz), p-LIMK1 (Thr508)/LIMK2 (Thr505) (1:500; Cell Signaling Technology) and cofilin (1:500; Millipore). Densitometric analyses of three different blots each containing two bands per experimental group were pooled for statistical analysis of every antibody quantified.

Immunohistochemistry and mean intensity measurements

Five-month-old Reelin-OE mice (n=3), control littermates (n=3), and Reelin-OE treated with doxycycline (DOX) for 7 days (n=3) were anesthetized and perfused with 4% paraformaldehyde in 0.1 M Phosphate buffer. Brains were removed, post-fixed overnight in the same solution, cryoprotected, and frozen. They were then were coronally sectioned at 30 µm, distributed into 10 series, and maintained at −20ºC in PB-30% and glycerol-30% ethylene glycol. For the immunodetection of Synaptopodin, sections were blocked for 2h at RT with PBS containing 10% of normal goat serum (NGS) and 0.2% of gelatin and then incubated with rabbit anti-synaptopodin (1:500, Synaptic Systems) overnight at 4°C with PBS–5% NGS. Next, they were incubated with goat anti-rabbit fluorochrome-labeled secondary antibodies (1:700, Molecular Probes), mounted in Mowiol, and stored at −20°C. Sections were viewed in a Leica SP2 confocal scanning laser microscope. The acquisition of confocal stacks of 3–5 dorsal hippocampi was achieved in a Leica SP2 microscope. Images were taken at a 20x magnification with a z-spacing of 2 µm. To allow comparison between all the animal groups, sections were immunolabeled in bulk and photographed in identical conditions. Acquisition x- and y-resolution was set at 1.46 µm/px. From each stack, the intensity of 2 to 3 confocal slices was z-projected. Regions of interest (ROIs) were defined across various layers (5 to 10 ROIs per layer), avoiding histological artifacts such as vessels or cell nuclei from which grey values were recorded. Intensities were normalized to average slice intensity to retrieve a local contrast index comparable across acquisitions. A similar procedure was applied for the analyisis of the hippocampal expression pattern of synapsin (1:1000, Synaptic Systems)

and SNAP-25 (1:1000, Becton-Dickinson) by using a minimum of 3 animals per experimental group.

Intracellular injections of fluorophore

Individual labeling of pyramidal cells on fixed tissue was performed as described elsewhere (Knafo et al., 2009a). Briefly, mice were anesthetized with isofluorane and transcardially perfused with 4% paraformaldehyde in 0.1M phosphate buffer. The brains were post-fixed in the same fixative for 24h, and coronal sections (150 μm) were cut with a vibratome and prelabeled with DAPI. Pyramidal neurons in the hippocampal CA1 pyramidal layer of Reelin-OE mice and control littermates were injected individually with Alexa 594 by passing a steady hyperpolarizing current through the electrode (0.5 to -1.0 nA). The current was applied until the distal tips of each neuron fluoresced brightly.

To image CA1 and cortical S1BF layer 5 pyramidal cells in experiments involving Cre/flDab1+TAM mice, a different fluorophore was used (Benavides-Piccione et al., 2005). There, samples from either flDab1 mice or flDab1+TAM mice were injected with Lucifer Yellow (8% in 0.1M T ris buffer, pH 7.4) in a similar way as described above. After injecting the neurons, the sections were processed for immunohistochemistry as previously described with an antibody to Lucifer Yellow (1:400000, gently provided by Javier deFelipe) and revealed by 488 nm excitation wavelength fluorophore-conjugated secondary antibody (Alexa fluor 488, Life Technologies).

Deconvolution

For spine morphology confocal analyzes, high-resolution 12 bit image stacks were acquired in a Leica SP5 confocal microscope (63x oil objective NA1.4; 1.75x zoom; 2048x2048 pixel resolution; final voxel size x, y = 68.8 nm, z =125.9 nm), with a line averaging of 3 iterations. Laser intensity and gain were set so as less than 1% of saturated pixels were found inside spine heads during live visualization. No offset was applied to ensure optimal performance of the deconvolution procedure.

For both Lucifer Yellow-labeled cells and YFP-positive cells immunostained with Alexa fluor 488, confocal image stacks were processed with an experimental deconvolution procedure using Fiji platform (Schindelin et al., 2012). An experimental point-spread function (PSF) was first generated by acquiring in a Leica SP5 microscope optimal-resolution image stacks comprising 110 nm beads (Molecular Probes). Up to 6 stacks were centered, averaged, background-substracted and scaled to match the same voxel size of the experimental stacks. Next, this PSF was used to deconvolve the confocal acquisitions of labeled dendrites. Briefly, we used the 3D Parallel Iterative Deconvolution plugin available on the Fiji platform. We applied the Wiener Filter Preconditioned Landweber (WPL) method with a filter gamma of 0.001 for a maximum of 50 iterations or until mean change was below 0.01%. The deconvolution step was performed in batch for all the stacks jointly analyzed. This was attained through a custom-made ImageJ Macro language script. Similar scripts were also generated to automatize previous and subsequent confocal image stack processing steps.

For Alexa 594-labeled cells, these same procedures were slightly different. The acquisition was performed on a Leica SP5 microscope (63x glycerol objective NA 1.3; 3.2x zoom; 1024x1024; final voxel size x, y = 75.1 nm, z = 136.4 nm). These confocal image stacks were processed with a 3D blind deconvolution algorithm (Autodeblur; Autoquant, Media Cybernetics) for ten iterations to reduce the out-of-focus signal.

Spine density

For hippocampal CA1 pyramidal cell spine density measurements, maximal intensity z-projections of confocal acquisitions of the dendrites of interest were used. Sholl analyses were performed by dividing the length of the dendritic segment by the number of spines in this distance for every 10 μm distance from the soma. The average of all segments analyzed provided the average spine density reported.

For cortical Layer 5 pyramidal cell spine density measurements, two approaches were performed. In experiments concerning Reelin-OE mice, *a visum* counts of spine puncta were performed for dendritic segments whose length was further measured live with Metamorph software. Previous DAPI staining of the tissue slices allowed the proper identification of the cortical layers, and the further selection of the dendrites of interest. In experiments concerning Cre/flDab1+TAM mice, we performed maximal intensity z-projections of confocal acquisitions of dendritic segments of interest. Further counts of the number of spines identified in 10 μm-long dendritic segments were performed.

For most spine density analyses, a minimum of 4 animals, 10 cells per animal and 3 dendritic segments per cell in each experimental group were counted and averaged. In the following cases sample sizes were below this limit: In experiments involving Cre/flDab1+TAM mice, hippocampal CA1 analyis was based in a sample size of 3 mice, 36 cells and +380 segments in each group and cortical S1BF Layer 5 pyramidal cell analysis was based in a sample size of 2 to 4 animals, 7-11 cells and +50 dendritic segments in each group.

Spine morphological analysis from confocal stacks

Spine head englobing surfaces were obtained from deconvolved confocal stacks of dendritic segments with Imaris software using a protocol similar to previously reported (Knafo et al., 2009a). Briefly, images were opened with Imaris software (Bitplane) and smoothened. Smooth radius chosen was 1 pixel for injected cells and 2 pixels for Thy1H-positive cells, according to an empirical output optimization procedure. Surfaces were manually added using the Marching Cubes tool. When necessary, the surface was further optimized by cutting surface surplus. For each spine an optimal surface that matched the contours of the head was created. The image of each dendrite was rotated in three dimensions and examined to assure that the solid surface selected for each spine head was correct. Finally, the volumes, sphericities and surface areas of all the spines in every stack were exported, pooled and analyzed. Spine sphericity was automatically calculated by the software with the formula described previously (Wadell, 1935). The sphericity, Ψ, of a particle is the ratio of the surface area of a sphere (with the same volume as the given particle) to the surface area of the particle. It can be expressed as:

$$(1)\ \Psi = \frac{\pi^{\frac{1}{3}}(6V_p)^{\frac{2}{3}}}{A_p}$$

Where V_p is the volume of the particle and A_p is the surface area of the particle.

For most spine morphology analyses, a minimum of 4 animals, 5 cells and +1500 spines were pooled and averaged in each experimental group. In the following cases sample sizes were below this limit: Basal CA1spine morphology analysis in experiments involving Reelin-OE mice was based on a sample

size of at least 3 mice, 12 cells and +300 spines per group. In experiments involving Cre/flDab1+TAM mice, hippocampal CA1 analyis was based in a sample size of 3 mice, 14 cells and +1500 spines in each group and cortical S1BF Layer 5 pyramidal cell analysis was based in a sample size of 2 animals, 13-16 cells and +750 spines in each group.

Electron microscopy

For conventional EM analyses, adult Reelin-OE mice (n=3), control littermates (n=3), and Reelin-OE mice treated with DOX for 7 days (n=3) were perfused with 2% glutaraldehyde-2% paraformaldehyde in 0.12 M phosphate buffer. After post-fixation in the same solution overnight, tissue slices were transferred to 2% osmium tetroxide, stained with 2% uranyl acetate, dehydrated, and embedded with araldite. Ultrathin sections were then obtained and stained with lead citrate. Electron micrographs (at 25,000x) of each hippocampal layer were randomly taken, and the area, circularity index and phenotype of spines receiving at least one synaptic contact were determined (n=112–161 spines for each layer and group). Moreover, the density of dendritic spines showing spine apparatus (n=30–70 electron micrographs analyzed per layer and group) and the area of this organelle (n=44–83 spine apparatuses) were calculated. Finally, we analyzed the area and circularity index of axon terminals and the length of their synaptic contacts (n=92–171 synaptic terminals for each layer and group).

Post-embedding immunogold immunohistochemistry

For post-embedding immunostaining analysis, adult Reelin transgenic mice (n=2), control littermates (n=2) and Reelin transgenic mice treated with DOX for 7 days (n=2) were perfused with 0.1% glutaraldehyde-4% paraformaldehyde in 0.12 M phosphate buffer and processed. After removal, brains were cryoprotected gradually in sucrose and cryofixed by immersion in liquid propane. Freeze substitution was performed at −90°C for 3 days in an "Automatic Freeze Substitution System" (AFS, Leica), using methanol containing 0.5% uranyl acetate as substitution medium. Brains were infiltrated in Lowicryl HM20 at −50°C and then polymerized with UV lamps. Ultrathin sections were collected and processed for post-embedding immunostaining. Samples were incubated with either rabbit anti-NR2a (1:5, Millipore), rabbit anti-NR2b (1:5, Novus Biologicals), or rabbit anti-p-cofilin (1:5, Cell Signaling Technology) antiserum. Sections were then incubated with goat anti-rabbit 18-nm gold-tagged antibody (1:20; British Biocell International). These sections were then counterstained with uranyl acetate and lead citrate. Electron micrographs (30,000x) were obtained in the stratum radiatum (SR) of the hippocampus CA1 region, and the number of dots per dendritic spine was counted in those spines that contained at least one gold particle (n=32–50 spines per group).

Pre-embedding electron microscopy

Animals were anaesthetized by isofluorane inhalation and were intracardially perfused with 4% paraformaldehyde and 0.1% glutaraldehyde in 0.12M phosphate buffer. The brain was then extracted from the skull and postfixed overnight in 4% paraformaldehyde. Vibratome slices were processed for GFP immunostaining (1:1000) and developed with diaminobenzidine (DAB). Staining was then postfixed with 1% glutaraldehyde. Afterwards, slices were osmified in 2% osmium tetroxide, incubated in 2% uranyl acetate and flat-embedded in Araldite.

Araldite-embedded slices containing DAB labeled cells were glued on the top of araldite blocks and studied under an optical widefield microscope (OM). Three criteria were used to select the dendritic segments to be sampled later by FIB/SEM (i) They were located at 40 to XX μm from the soma, where dendritic spines are numerous in adult GC dendrites. (ii) The dendritic tree was intensely and homogeneously labeled with DAB. (iii) Relatively straight segments that coursed parallel to the surface of the block where chosen. Although dendrites coursing in any direction can be sampled, this optimal orientation permits the acquisition of long series of images without the need to displace the field of view of the FIB/SEM on the run.

Once the dendritic segment has been selected, the exposed surface of the block was devastated using an Ultracut microtome until the selected dendrite was 3 to 5 μm below the surface, so it was readily accessible for imaging by the FIB/SEM. We finally acquired images of the surface of the final devastated sample with the OM at different magnifications.

Three-dimensional electron microscopy using FIB/SEM technology

Previously prepared samples on top of araldite blocks were treated as required to be imaged by FIB/SEM microscope (Merchán-Pérez et al., 2009). They were glued onto a sample stub using a conductive adhesive tab. To avoid charge artifacts all surfaces of the block except the sample were painted with colloidal silver paint and dried in a vacuum chamber overnight. The blocks were then sputter-coated with gold/palladium for 15 seconds to facilitate charge dissipation.

Three-dimensional brain tissue samples were obtained using a dual-beam microscope that combines a focused ion beam (FIB) and a a high resolution field emission scanning electron microscope (SEM) (Crossbeam® Neon40 EsB, Carl Zeiss NTS GmbH, Oberkochen, Germany). This instrument uses a focused gallium ion beam which can mill the sample surface, removing thin layers of material on a nanometer scale.

The samples were introduced in the column and low magnification images of the whole surface of the block were acquired with the secondary-electron detector of the SEM column (**Fig. r.4.2b**).

In order to accurately locate the selected dendritic segment for FIB/SEM acquisition we used the pair of OM and SEM microphotographs that were taken from the same tissue block. These two images were matched and overlaid using Photoshop. The block borders, surface impurities or exposed DAB precipitates were both visible in the OM and SEM images, so they were used as landmarks to correctly superpose both images. As a result, the exact position of the selected dendritic segment (only visible in OM images) could be traced on the SEM microphotograph (**Fig. r.4.2a-b**).

The sample was then precisely oriented inside the column so as the viewing direction matched the preferred direction of the dendritic segment. A first coarse cross-section was milled with the FIB with a 10 nA gallium beam as a viewing channel for SEM observation at the appropriate location (**Fig. r.4.2c**). Exploration of the exposed surface helped to identify the target dendrite and to choose the final framing. Next, fine milling of the exposed surface was performed with the FIB, using a beam current of 750 pA that removes a thin layer of material. After removing each slice, the milling process was paused and the freshly exposed surface was imaged with a 1.9 kV acceleration potential using the in-column energy selective backscattered electron detector. The milling and imaging processes were sequentially repeated and long series of images were acquired through a fully automated procedure, thus obtain-

ing a stack of images that represented a three-dimensional sample of the tissue (Merchán-Pérez et al., 2009). Image resolution in the xy plane was set to 3.7 nm/pixel. Resolution in the z axis —equivalent to the thickness of the layer of material removed by the FIB in each cycle— was 25 nm.

A total of 5 mice were processed for the control group analysis detailed in **chapter 4** (1 for the 3 week group, 2 for each of the 4 and 8-9week group) and 4 more animals were processed for the Reelin-OE and single cell Dab1-KO analysis (1 for the 4 week group and 1 for the 8-9 week group for each genotype). 2 to 6 acquisitions were obtained from each group, each acquisition comprising a tissue volume from 53 to 481 μm^3 (mean 213 μm^3). The total volume of tissue analyzed surpassed 750 μm^3 in the 3 week group, 1000 μm^3 in the 4 week group and 1500 μm^3 in the 8-9 week group in control mice. Similarly, it surpassed 880 μm^3 and 600 μm^3 in 4-week and 8-9 week group of Reelin-OE mice, and was above 550 μm^3 in both groups regarding Dab1-KO granule cells (**Table r.4.3**).

Connectomics analysis

Automatic alignment (registration) of the stacks of images and signal normalization across slices was performed with Fiji (Schindelin et al., 2012). Exploratory navigation through the stacks of images was performed either with Fiji or with Espina software.

Different spine protrusions were identified and catalogued in a database and information related to spine morphology, synapse presence and location, and innervating bouton connectivity were carefully annotated and reviewed by at least 3 independent specialized scientists.

To assess spine morphology classification upon visualization of the EM image stacks, a criterion based on previous classification studies (Harris et al., 1992) was applied. Accordingly, spines were classified between classical, stubby, mushroom and branched. In addition, a new index was recorded to every spine regarding its PSD morphology: if it was a circular –no differentiated head-PSD, was defined as index = 1. Finally, "classical" spines were subdivided between filopodia ("classical"; index = 1) and thin ("classical"; index = else). Therefore, we ended up with 5 different spine types: filopodia, thin, stubby, mushroom and branched.

Image segmentation and quantitative morphometric analysis

Three-dimensional (3D) reconstruction of the labeled dendritic segments and synaptic contacts was carried out intensively with EspINA software (Morales et al., 2011). Briefly, aligned and normalized stacks were further distorted with a Gaussian blurr with a 10 pixel radius. The former 'clean' stack was used for user-based segmentation, whereas the 'blurred' stack served for automatic, seed-based segmentation purposes. By combining both features, DAB-labeled dendrites and their spines were completely segmented along the stack. Further, their synaptic specializations were manually segmented, by performing close contours in each slide, which included both the PSD and the apposed presynaptic membrane. Each segmented item was independently identified.

We exported the image segmentation binary files into the Imaris platform. There, we generated surfaces that mimicked the segmentations by an absolute intensity and maximal thresholding approach, without any smooth step. Next, all spines were cut from their parent dendritic shaft through the base of their neck in a 3D optimal orientation. Branched spines were duplicated and saved apart for separate

analysis, and further cut into individual spines by their shared neck istmus. Volume and sphericity of the final surfaces generated was annotated. By comparing connectomics annotations with the 3D segmentations, we matched and named each spine and synapse with our register in the database, updating both the database and the segmentations. This allowed us to retrieve volumes and sphericities of the previously identified spines in the connectomics analysis.

Image segmentation with the Reconstruct software (Fiala, 2005) was performed for evaluation purposes only. 6 dendritic segments belonging to different experimental groups (3 control 8-9 weeks, 1 Dab1-KO 4 weeks, 2 Reelin-OE 8 weeks) were segmented with this software, in addition to the previously described segmentation with EspINA. Briefly, dendritic contours of the DAB-labeled dendrite were outlined in each slice. We next imported the binary files supporting this segmentation into the Imaris platform and a surface was generated as previously described. Surfaces of the same dendrite being reconstructed through both softwares by the same user were overlaid, visualized simultaneously and rotated in three dimensions to evaluate possible mismatches (**Fig. r.4.2h-i**). This evaluation served the investigators to determine that EspINA software-based segmentations reached the quality offered by Reconstruct segmentation toolkit.

ImageJ-based custom-made scripts were developed to automatize the different image processing steps described.

For paired analysis of different parameters of spine-synapse couples, a database was generated that included both each spine and synapse paired identifiers as well as the different morphometric values (volume and sphericity) associated to each item. Spines analyzed corresponded to 8-9 week GCs, fully 3D-reconstructed individualized spines establishing a single synaptic contact (214 spine-synapse couples in the wt group; 68 in the Reelin-OE; 33 in the Dab1-KO). Correlation was statistically analyzed by nonparametric, two-tailed Spearman test. Binned analysis in the 8-9 week GC wt group was performed by further pooling and averaging of these data inside bins of constant width. We chose optimal bin widths of spine volume that allowed both maximal number of values per bin while giving a maximal number of bins in the different analyisis. Bins including a single data point were excluded from analysis. Bin width used was 5.0E+06 nm3 for all analysis, including spine volume – synapse volume analysis (n = 21 bins; n' = 16 bins in the lower range), spine volume – spine sphericity analysis (n = 21; n' = 6) and spine volume – synapse sphericity analysis (n = 21; n' = 12). Linear regressions were performed by best-fit approaches, and were statistically tested to be different from zero with the statistical software Graphpad. Thresholds were determined by optimizing the goodness of fit (R^2) of these regressions in the data points inside the lower range.

Resum

Introducció

Formació de les sinapsis durant el desenvolupament del sistema nerviós

El sistema nerviós central és una estructura altament compartimentalitzada des d'un punt de vista anatòmic, fisiològic i funcional. Els mecanismes que en regulen la formació presenten protagonistes altament conservats evolutivament, i a grans trets s'organitzen en successives interaccions inductives. Aquestes donaran lloc a diferents onades de senyalització que regularan processos diferents però intrínsecament relacionats amb el funcionament final del sistema, com són la generació i supervivència de cèl·lules neurals, o els processos de guia axonal que permetran la precisa connexió de cèl·lules distants. La formació de sinapsis és el pas que tanca el procés de cablejat, donant lloc a una estructura prou estable com per durar una vida sencera, i alhora prou plàstica com per permetre modificacions – i fins i tot l'eliminació – en base a experiències sensitives.

Certs requeriments governen aquest procés. Primer, el terminal axònic ha d'abastar la cèl·lula diana a la regió adient de la membrana. Aquesta regió esdevindrà la membrana postsinàptica, i ha de ser sensible al neurotransmissor alliberat pel terminal. Segon, les membranes pre- i postsinàptica han de posicionar-se perfectament, permetent que les respostes a l'alliberament de senyal es donguin en el rang del mil·lisegon. I tercer, l'estructura resultant ha de presentar alhora robustesa i mal·leabilitat, permetent modificacions en funció de l'activitat sinàptica que hi tingui lloc.

Diferents estratègies tenen lloc en el cervell que faciliten la primera premissa. Una d'elles és l'establiment de sinapsis concretes en llocs determinats (**Fig. i.1.1**). Així, regions delimitades com les capes corticals són sovint escenari de la delimitació espacial de sinapsis entre determinats axons i arbres dendrítics. Aquesta ordenació, juntament amb la intervenció de mecanismes finals de reconeixement mutu a nivell molecular, suposa un mecanisme recurrent per l'establiment de les connexions adients. En concret, les cèl·lules piramidals de la CA1 de l'hipocamp presenten aquesta segregació sinàptica, rebent diferents aferències en diferents zones del seu arbre dendrític (**Fig. i.1.2**). Així, axons comissurals provinents de cèl·lules piramidals de la CA3 innerven les seves dendrites basals a l'stratum oriens (SO) i segments dendrítics proximals al soma de l'arbre apical a l'stratum radiatum (SR), mentre que les dendrites apicals llunyanes situades a l'stratum lacunosum-moleculare (SLM) reben sinapsis d'axons provinents de

l'escorça entorhinal, en l'anomenada via perforant (Andersen et al., 2007). Aquest confinament espaial de les aferències presinàptiques proporciona a aquestes cèl·lules l'habilitat d'integrar en la cèl•lula receptora impulsos provinents de diferents zones del sistema nerviós (Chadderton et al., 2014).

El desenvolupament de les sinapis comporta un intercanvi de comunicacions entre els compartiments pre- i postsinàptic. Vies de senyalització anterògrades i retrògrades asseguren una correcta organització de la maquinària sinàptica, garantint així el producte final sigui una sinapsi funcional. La maquinària sinàptica concreta presenta certa especificitat al neurotransmissor majoritari involucrat en la sinapsi, que alhora defineix químicament la neurona presinàptica.

Els neurotransmissors acostumen a ser molècules de baix pes molecular, tot i que alguns pèptids poden actuar com a missatgers a les sinapsis. No obstant, l'efecte precís d'un determinat neurotransmissor depèn en major mesura del receptor involucrat. Al seu torn, els receptors es classifiquen en ionotròpics o metabotròpics, depenent de si ells mateixos conformen un canal iònic que s'obre en resposta a l'associació a neurotransmissor, o si pel contrari es tracta de proteïnes que senyalitzen l'obertura de canals iònics a través de missatgers secundaris, respectivament. Així, una reduïda gamma de neurotransmissors principals combinada amb una rica varietat de receptors permet una gran diversitat d'efectes possibles.

Al sistema nerviós central (CNS), les sinapsis poden ser excitatòries o inhibitòries en funció dels canals iònics que hi intervinguin. Tot i que un mateix neurotransmissor pot generar respostes de tots dos tipus, generalment un determinat neurotransmissor s'associa a un tipus de sinapsi concreta. Així, les sinapsis excitatòries s'associen al neurotransmissor Glutamat, i els seus receptors s'associen a canals permeables a Na^+ i Ca^{2+}. Igualment, les sinapsis inhibitòries estan mediades pels neurotransmissors GABA o Glicina, que promouen l'obertura de canals de Cl^-.

Les sinapsis excitatòries i inhibitòries presenten estructures diferents morfològicament. El seu anàlisi per mitjà de tècniques de microscòpia electrònica va portar a classificar-les respectivament en Gray Tipus I o asimètriques i Gray Tipus II o simètriques (**Fig. i.1.3**) (Gray, 1959). Les Tipus I presenten vesícules circulars i una regió més electrodensa adjacent a la membrana postsinàptica, que es coneix com densitat postsinàptica (PSD). Les Tipus II presenten vesícules més ovalades i zones més electrodenses adjacents a les membranes pre- i postsinàptiques.

Els receptors ionotròpics de les sinapsis glutamatèrgiques es classifiquen en tres grups segons el seu agonista farmacològic: AMPA, Kainat o NMDA. Tots ells són permeables a Na^+ i K^+, però a més el receptor NMDA és permeable a Ca^{2+}. El seu porus es veu bloquejat en repòs per Mg^{2+} i es desbloqueja de manera sensible a despolaritzacions de la membrana postsinàptica. Així, doncs, el receptor NMDA funciona com un detector de coincidència entre l'activitat pre- i postsinàptica, la qual cosa el situa en un important lloc en la regulació de la plasticitat sinàptica (**Fig. i.1.4**).

Finalment, les sinapsis es poden classificar en axodendrítiques, asosomàtiques o axoaxòniques, depenent del domini neuronal involucrat en l'element pre- i postsinàptic, respectivament. En les últimes, la sinapsi controla l'alliberament de neurotransmissor per part de l'axó innervat, afectant indirectament a la seva neurona postsinàptica. Els contactes axosomàtics són freqüents en sinapsis inhibitòries, donat que la inhibició és més efectiva quan se situa prop del segment inicial de l'axó. Els contactes axodendrítics poden tenir lloc al tronc dendrític o sobre les espines dendrítiques. Aquests últims representen la majoria de contactes excitatoris en les neurones corticals (Colonnier, 1968).

Espines dendrítiques

Les espines dendrítiques són petites protrusions que emergeixen de les dendrites de multitud de neurones, i són l'estructura postsinàptica de la major part dels contactes excitatoris en el cervell (Gray, 1959). Pràcticament totes elles reben sinapsis, mentre que les vacants presenten una morfologia filopodial (Arellano et al., 2007b). Les espines presenten una gran variabilitat de formes i mides, i tot i que la seva existència i relació amb les connexions sinàptiques i l'aprenentatge estan documentades des d'un segle ençà per Santiago Ramon y Cajal (**Fig. i.1.5**), la seva funció concreta és encara avui motiu de debat (Cajal, 1888; Yuste and Majewska, 2001b).

El seu rol s'ha associat a múltiples factors. En primer lloc, a una extensió de la superfície receptiva de la dendrita, en un paral·lelisme als microvil·lis intestinals (Cajal, 1891). Tot i descartada (la gran part del tronc dendrític no rep sinapsis), aquesta hipòtesi va donar lloc a la suposició de que les espines engrandeixen l'espai receptiu en el què una dendrita pot rebre sinapsis (Peters and Kaiserman-Abramof, 1970; Swindale, 1981).

En segon lloc, les espines poden actuar com a unitats de processament de senyal anàlogues a portes lògiques (Shepherd, 1996). El fet que potencials d'acció retropropagats durant fenòmens com la LTP podrien dotar les espines abastades de certa capacitat de predisposició per la senyalització. En la mateixa direcció, diferents evidències han apuntat a que les espines posseeixen certa capacitat de filtrat i amplificació de senyal (Shepherd et al., 1985; Svoboda et al., 1996; Araya et al., 2006).

Una tercera hipòtesi descriu les espines dendrítiques com un compartiment bioquímic, aïllat de la dendrita pel coll dendrític. La seva geometria conforma un impediment a la lliure difusió de molècules (Majewska et al., 2000a). Aquesta compartimentalització presenta implicacions en la dinàmica d'ions de Ca^{2+} entre l'espina i la dendrita (Majewska et al., 2000a; Noguchi et al., 2005), que al seu torn regula i enllaça els fenòmens de plasticitat sinàptica i estructural (Yuste and Majewska, 2001b). És remarcable que la concentració de Ca^{2+} a l'espina pot ésser modulada per diferents efectors moleculars, com també per canvis en la mida i forma de l'espina. Així, doncs, la funció de les espines dendrítiques pot ser la implementació de lleis d'aprenentatge local basades en dinàmiques de calci i específiques de l'activitat rebuda (Yuste and Majewska, 2001b; Yuste, 2011).

Durant el desenvolupament del cervell, la formació de sinapsis comporta la generació d'espines dendrítiques. La sinaptogènesi i l'espinogènesi, per tant, apareixen en aquesta etapa com processos altament relacionats (tot i que diferents). La seva observació en diferents models va donar lloc a hipòtesis diferents sobre la seva regulació (**Fig. i.1.6a-c**). En les cèl·lules de Purkinje del cerebel l'espinogènesi apareix com un fenomen intrínsec a la neurona, que no depèn d'activitat sinàptica (Sotelo, 1975, 1978; O'Brien and Unwin, 2006) D'altra banda, en altres models tots dos processos apareixen més íntimament lligats (Yuste and Bonhoeffer, 2004).

La diversitat morfològica de les espines dendrítiques ha suscitat la suposició de l'existència d'una paral·lela diversitat funcional (Yuste and Majewska, 2001b). Així, doncs, tot i que paràmetres concrets de la seva morfologia mostren distribucions contínues (Trommald and Hulleberg, 1997; Arellano et al., 2007a; Tonnesen et al., 2014), el seu estudi morfològic sovint s'ha basat en una classificació en tipus concrets. La distinció més típica inclou les classes fil·lopodi (*filopodia*), taló (*stubby*), prima (*thin*) i bolet (*mushroom*) (**Fig. i.1.6d**) (Peters and Kaiserman-Abramof, 1970; Tashiro and Yuste, 2003; Rochefort and Konnerth, 2012). Alguns estudis van suggerir que alguns tipus d'espina podien ser més abundants en etapes tempranes que madures, i viceversa (Trachtenberg et al., 2002). En la mateixa línia, uns altres autors vàren proposar un mecanisme pel qual la maduració d'una espina comportés un pas per tots aquests tipus. Començaria amb una sinapsi a *shaft* per part de l'axó, que s'especialitzaria com a tipus

stubby per acabar desenvolupant-se en *thin* i madurant a *mushroom* (Miller and Peters, 1981). Aquesta hipòtesi ha estat en part desacreditada a partir d'estudis ultrastructurals, en el que s'observen estructures sinàptiques difícilment assolibles per aquest mitjà (Knott et al., 2006).

Per últim, el model filopodial proposa que la generació espontània de fil·lopodis donaria lloc posteriorment a una especialització en espina dendrítica en una forma depenent d'activitat sinàptica (Dailey and Smith, 1996; Ziv and Smith, 1996), i és el que gaudeix d'una més àmplia acceptació en el conjunt de les sinapsis corticals.

Plasticitat sinàptica i d'espina en el cervell adult

Les espines dendrtítiques presenten una gran plasticitat morfològica durant la vida d'un individu, tant a nivell estructural com molecular i fisiològic. Aquesta plasticitat s'ha assenyalat com el principal correlat físic dels processos d'aprenentatge i memòria. El procés global enllaçant els canvis morfològics amb els fisiològics han estat àmpliament discutits, però recentment han estat resumits en una sèrie de regles que conjuntament descriuen el procés de generació espontània, selecció i enfortiment de les espines (**Fig. i.2.1**) (Kasai et al., 2010b).

A nivell global, la generació de noves espines seria un procés espontani i fins a cert punt lent (Nagerl et al., 2004), mentre que l'augment de la mida en resposta a activitat sinàptica seria un procés molt més ràpid, que podria reflectir més fàcilment l'adquisició de noves memòries.

Conjuntament, aquest model prediu el següent mecanisme: Els fil·lopodis emergeixen de forma espontània i aquells que troben un terminal formen sinapsis silencioses. Les espines resultants que es vegin estimulades experimentaran un increment de mida depenent d'activitat i s'integraran en el circuit, persistint més temps. Les que no, seran eliminades. Les espines persistents poden estabilitzar-se i enfortir-se, tant per mecanismes depenents d'activitat sinàptica com per mitjà de fluctuacions intrínseques, essent capaces de persistir al llarg d'una vida.

El manteniment de les espines dendrítiques està altament regulat per conjunts compartimentalitzats d'actina en la pròpia espina (Honkura et al., 2008). En repòs, dos conjunts són evidents: El conjunt dinàmic es localitza a l'àpex de l'espina i polimeritza més ràpid en espines més grans, generant contínuament la força expansiva necessària per mantenir el volum de l'espina. El conjunt estable se situa a prop del coll, la seva presència és major en espines més grans i la seva mida determina l'amplitud de les fluctuacions espontànies de volum. Per últim, el conjunt d'eixamplament està composat per fibres entrelligades de F-actina que es comporten com un gel. La difusió d'aquest gel pel coll de l'espina provoca que l'espina engrandida reverteixi la seva mida a la dimensió original més petita, i no es pot engrandir a continuació. Per això se l'anomena també "gel de memòria". Aquest genera la força necessària per augmentar la mida de les espines. L'estabilització de l'espina engrandida dependrà aleshores dels dos primers conjunts descrits.

Efectors moleculars en la plasticitat sinàptica

Multitud d'efectors i vies de senyalització intervenen en la regulació de la plasticitat sinàptica. En concret, revisarem els principals agents afectant la dinàmica de Ca^{2+}, el citosquelet d'actina i la funció glutamatèrgica.

Les dinàmiques locals de Ca^{2+} es poden veure regulades per dos grans mecanismes: influx i eflux (**Fig.**

i.2.2) (Yuste and Majewska, 2001b). En primer lloc, l'"influx local es pot donar per la regulació de canals permeables a calci, com els receptors NMDA i alguns AMPA. També pot donar-se per l'obertura de canals de Ca^{2+} sensibles a voltatge presents en l'espina en resposta a potencials d'acció retropropagats. En tercer lloc, el Ca^{2+} pot ser alliberat d'estructures internes d'emmagatzematge, com els aparells d'espina. Aquest és una forma especialitzada de reticle endoplasmàtic composat de piles i es troba en espines madures del tipus *mushroom* (Gray, 1959; Spacek and Harris, 1997; Jedlicka et al., 2008). La Sinaptopodina és una proteïna que s'uneix a actina que localitza a l'aparell d'espina i la funció de la qual és determinant per la plasticitat d'espina depenent d'activitat (Vlachos et al., 2009; Segal et al., 2010; Vlachos et al., 2013). S'expressa en neurones piramidals i granulars de l'hipocamp, descrivint un patró laminat (Mundel et al., 1997; Deller et al., 2000; Roth et al., 2001; Bas Orth et al., 2005). En segon lloc, l'extrusió de Ca^{2+} es pot assolir per mitjans actius o bé passius. La presència de bombes de calci a la membrana plasmàtica (PMCAs) i a la superfície de magatzems interns (bombes SERCA) poden dirigir el transport de Ca^{2+} a l'espai extracel·lular o a l'aparell d'espina, respectivament. D'altra banda, el Ca^{2+} de l'espina pot difondre al tronc dendrític a través del coll de l'espina, la geometria del qual afectarà les dinàmiques d'aquest flux (Majewska et al., 2000b; Noguchi et al., 2005).

La morfologia de l'espina està altament regulada pel citosquelet d'actina, el qual és el major component del citosquelet de l'espina (Matus et al., 1982; Kaech et al., 1997). Les fibres d'actina formen feixos en el coll de l'espina, mentre que en el cap interaccionen amb la membrana plasmàtica i la PSD pels extrems barbats. Distints microdominis de l'espina es caracteritzen per la presència de determinades proteïnes d'unió a actina (ABPs) (**Fig. i.2.3**). A l'àpex de l'espina la major funció consisteix en l'estabilització dels receptors de neurotransmissor en la PSD. L'enllaç amb els receptors NMDA pot tenir lloc a través d'α-actinina, mentre que l'enllaç amb els AMPA és mediat per proteïnes bastida com PSD-95, Abp1, PICK1 i neurabina (Racz and Weinberg, 2013). Alhora, α-actinina interacciona bioquímica i funcionalment amb CaMKII. Finalment, α-actinina s'associa a Sinaptopodina. Sota la superfície de l'espina se situa cofilina, un enzim proteolític que s'inactiva per fosforilació, senyalitzada a través de les quinases LIMK i Slingshot. Se situa a la regió dinàmica de l'espinosquelet i localitza també a la PSD. Per sota d'aquesta zona, la ramificació dels filaments d'actina ve regulada pel complex Arp2/3, que alhora presenta diferents vies de modulació. Al core de l'espina hi ha situat el conjunt d'actina estable (Honkura et al., 2008), al qual s'associen les ABPs cortactina, profilina i drebrina. La cortactina està relacionada amb processos de nucleació i ramificació de filaments d'actina, i pot activar el complex Arp2/3. Les profilines regulen l'enlongació de filaments facilitant l'addició de monòmers d'actina a l'extrem barbat, i en processos d'LTP poden ser reclutades des del tronc dendrític cap a l'espina (Ackermann and Matus, 2003). Finalment, la drebrina pot inhibir la interacció dels filaments d'actina amb tropomiosina i α-actinina, i regula l'expansió i estabilització dels filaments (Racz and Weinberg, 2013).

Per últim, la morfologia de l'espina i la mida de la seva PSD correlacionen amb el contingut i distribució de receptors de neurotransmissor (Nusser et al., 1998), així com amb el corrent injectat durant la sinapsi i la sensibilitat a glutamat de l'espina (Matsuzaki et al., 2001). Alhora, canvis ràpids en la distribució de subunitats de receptors de glutamat i el seu tràfic són fenòmens regulats per activitat sinàptica (Greger and Esteban, 2007), oferint un enllaç entre reorganitzacions moleculars i plasticitat sinàptica. Els receptors AMPA són els responsables dels primers esdeveniments despolaritzants en el procés sinàptic. La seva fosforilació en modifica la conductància, variant-ne l'activitat (Derkach et al., 1999; Kristensen et al., 2011). Una gamma de quinases estan involucrades en aquest procés, com CaMKII, PKA i PKC, entre d'altres (Huganir and Nicoll, 2013). El procés està regulat per activitat de manera bidireccional: la LTP promou la fosforilació mentre que la LTP la disminueix (Barria et al., 1997; Lee et al., 1998). D'altra banda, els receptors AMPA presenten un elevat tràfic per membrana. Les sinapsis sense receptors AMPA s'anomenen "silencioses" (Gomperts et al., 1998), i la seva activació depèn del reclutament d'aquests receptors, bé per exo- i endocitosi (Park et al., 2004; Greger and Esteban, 2007)

o bé per difusió lateral en la membrana (Opazo et al., 2012).

Els nivells de proteïna de receptor NMDA són independents de la quantitat de F-actina a l'espina o de la mida de la PSD (Kasai et al., 2003) o de l'activitat sinàptica (Gardoni et al., 2009). No obstant, el tràfic de subunitats específiques i la fosforilació d'aquestes sí que es veuen regulats per activitat (**Fig. i.2.4**) (Tovar and Westbrook, 2002; Yashiro and Philpot, 2008; Paoletti et al., 2013). Alhora, els receptors NMDA són necessaris per LTP i LTD (Liu et al., 2004; Foster et al., 2010), i per l'espinogènesi desencadenada per LTP tardana (Maletic-Savatic, 1999; Gambrill and Barria, 2011). Alhora, les subunitats GluN2 2A i 2B confereixen propietats particulars al receptor. En concret, la maduració de les sinapsis en el cervell neonatal comporta un canvi de 2B a 2A (Paoletti et al., 2013). Una maduració similar té lloc en les sinapsis adultes, i el canvi es dóna mitjançant la migració lateral de subunitats 2A (Barria and Malinow, 2002; Groc et al., 2006). Tot i que l'abundància relativa de subunitats 2A i 2B confereix propietats diferents a la sinapsi, la relació de cadascuna amb tipus concrets de plasticitat és motiu de cert debat (Yashiro and Philpot, 2008; Brigman et al., 2010). Recentment s'ha proposat que les respectives cues C-terminals poden jugar un paper clau en el mecanisme fi desencadenat per aquestes proteïnes (Ryan et al., 2013).

Funcions de la Reelina en el sistema nerviós

La Reelina és una proteïna de la matriu extracel·lular que juga un paper clau tan en processos del desenvolupament del sistema nerviós com en plasticitat sinàptica. Es va descobrir a partir de la mutació espontània en ratolí que generà la línia *reeler* (Goffinet and Dernoncourt, 1991; Miao et al., 1994; Bar et al., 1995). L'absència de la proteïna Reelina es va identificar com la causant del fenotip (D'Arcangelo et al., 1995). La identificació del gen *RELN* en humans (DeSilva et al., 1997) va permetre detectar individus on no s'expressava correctament, generant lissencefàlia amb hipoplàsia cerebel·lar (LCH), un fenotip amb trets característics semblants als del ratolí *reeler* (Hong et al., 2000).

El gen *reln* de ratolí es troba al cromosoma 5 i s'extén al llarg de 450 Kb (Royaux et al., 1997). Conté 65 exons, diferents llocs de poliadenilació, 3 potencials llocs d'inici de transcripció, i presenta diferents variants d'mRNA fruit d'empalmament alternatiu. El gen *RELN* en humans està localitzat a 7q22, i presenta llocs d'unió per diversos factors de transcripció (Chen et al., 2002; Levenson et al., 2008). D'altra banda, l'expressió de Reelina pot regular-se epigenèticament per mitjà de metilacions en nombroses illes CpG que presenta el seu promotor. L'mRNA complet és el més freqüent, i consta de 11673 parells de bases.

La proteïna completa conté 3461 aminoàcids (D'Arcangelo et al., 1997), i un cop glicosilada i secretada té un pes aparent de 427 kDa, tot i que la previsió és inferior (D'Arcangelo et al., 1997; Tissir and Goffinet, 2003). Presenta una estructura modular, amb el pèptid senyal per secreció a l'N-terminal seguit d'una regió crucial pel seu funcionament i dimerització que reconeix i inhibeix l'anticòs monoclonal CR-50 (**Fig. i.3.1**) (Del Rio et al., 1997). La zona central presenta vuit repeticions, i el conservat extrem C-terminal és necessari per la senyalització (Derer et al., 2001; Nakano et al., 2007). La Reelina és proteolitzada en dos punts després de ser secretada, generant cinc fragments proteolítics (Jossin et al., 2004; Knuesel, 2010), dels quals el central és capaç d'unir-se a receptors i permet recuperar el fenotip control en mostres *reeler* (Jossin et al., 2004; Jossin and Goffinet, 2007).

La senyalització de Reelina transcorre principalment a través de la binarització i unió als receptors VLDLR i ApoER2, que al seu torn promouen el reclutament i fosforilació de la proteïna citoplasmàtica

Dab1 per quinases de la família Src (**Fig. i.3.2**) (Howell et al., 1999; Arnaud et al., 2003b; Kuo et al., 2005). El patró d'expressió de Dab1 és força complementari al de Reelina (Rice et al., 1998; Borrell et al., 2007) i la seva absència promou l'aparició de fenotips semblants al *reeler* (Sheldon et al., 1997). L'activació de Dab1 dóna lloc a la divergència de la via en diferents cascades intracel·lulars de senyalització, incloent la via de les ERK (Simo et al., 2007), la de PI3K/Akt (Beffert et al., 2002; Gonzalez-Billault et al., 2005) i la Crk/CrkL-C3G (Ballif et al., 2004; Matsuki et al., 2008; Feng and Cooper, 2009), totes elles arribant als citosquelets d'actina i tubulina.

Reelina al desenvolupament del sistema nerviós

Durant el desenvolupament del sistema nerviós, l'expressió de Reelina té lloc per mitjà de les cèl·lules Cajal-Retzius (CR) al cervell anterior i en precursors granulars del cerebel, tot i que també s'expressa en menor mesura en altres zones (Alcantara et al., 1998). Les cèl·lules CR són una població cel·lular transient que se situa a la zona marginal de l'escorça i l'hipocamp, i que pràcticament desapareix a les dues setmanes del naixement (Cajal, 1891; Retzius, 1893; Meyer et al., 2002; Soriano and Del Rio, 2005). Les cèl•lules CR secreten Reelina a partir de E10 a la zona marginal (Derer et al., 2001), en un procés clau per la migració neuronal en la formació de la placa cortical i en la migració de les cèl·lules piramidals de l'hipocamp (**Fig. i.3.3**) (Del Rio et al., 1997; Super et al., 1998). La secreció de Reelina per les cèl•lules CR de la capa molecular externa (OML) del gir dentat (DG) es dóna al llarg de la vida, regulant així la migració de neurones de nova generació en el DG (Forster et al., 2006). D'altra banda, la pèrdua de Reelina està relacionada amb la dispersió de les cèl·lules granulars del DG tant en humans com en ratolins (Haas et al., 2002; Duveau et al., 2011).

D'altra banda, la funció de Reelina en el desenvolupament també està relacionada amb el creixement axonal i dendrític. A l'hipocamp, els axons entrant per la via perforant a l'stratum lacunosum-moleculare (SLM) i OML se senten atrets per la Reelina secretada per les cèl·lules CR locals, la qual en promou la sinaptogènesi (Del Rio et al., 1997; Borrell et al., 1999; Borrell et al., 2007). Igualment, en diferents zones la Reelina s'ha vist involucrada en processos d'enlongació i ramificació dendrtítica (Niu et al., 2004; Olson et al., 2006; Nichols and Olson, 2010).

Conjuntament, la Reelina juga diversos papers clau en el desenvolupament del sistema nerviós. Regula la migració radial de neurones piramidals en les estructures corticals, i està també involucrada en processos de creixement axonal en la formació de l'hipocamp, així com en els processos de sinaptogènesi temprana d'aquests axons. Finalment, també regula el desenvolupament de l'arbre dendrític en nombrosos tipus neuronals.

Reelina en el cervell adult

L'expressió de Reelina pateix un canvi important d'expressió un cop acabada l'etapa de migració neuronal. Les zones marginals esdevenen capa 1 en la neoescorça i SLM i OML a l'hipocamp (Frotscher, 1998). La població de cèl·lules CR desapareix progressivament durant les primeres setmanes postnatals, tot i que algunes cèl·lules s'han trobat en etapes adultes (Abraham and Meyer, 2003). Al mateix temps, la Reelina passa a ser expressada per interneurones GABAèrgiques situades al llarg de la neoescorça i l'hipocamp, en cèl·lules mitrals del bulb olfactiu, en cèl·lules granulars del cerebel i en cèl·lules piramidals de capa 2 de les escorces piriforme i entorhinal (Alcantara et al., 1998; Pesold et al., 1998; Abraham and Meyer, 2003; Pappas et al., 2003; Herz and Chen, 2006; Ramos-Moreno et al., 2006). Aquest canvi d'expressió suggereix l'existència d'una nova funció per la Reelina en el cervell postnatal i adult.

La intervenció de la via de Reelina en processos sinaptogènics en el desenvolupament tardà de l'hipocamp (Borrell et al., 1999), així com l'aparició d'alteracions en la circuiteria de la retina de ratolins amb deficiències en la senyalització de Reelina (Rice et al., 2001; Trotter et al., 2011) varen fer suposar

que aquest nou rol tenia a veure amb la plasticitat sinàptica (**Fig. i.3.4**).

Els ratolins hemizigots per la mutació *reeler* (*HRM*) presenten una citoarquitectura histològica conservada amb alhora una menor expressió de Reelina (Liu et al., 2001; Badea et al., 2007; Katsuyama and Terashima, 2009), oferint un model més adient que els propis *reeler*. Ratolins deficients en Reelina presenten deficiències en LTP (Qiu et al., 2006b; Rogers et al., 2011), mentre que la perfusió de Reelina a cultius *reeler* o la injecció en cervells de *HRM* en promouen la millora (Weeber et al., 2002; Rogers et al., 2013). En concret, es va veure que la regulació de la LTP per Reelina depèn de l'ensamblatge alternatiu d'un exó d'ApoER2 (Beffert et al., 2005), en un mecanisme que involucra la receptors NMDA. La Reelina promou la fosforilació de les subunitats 2A i 2B dels receptors NMDA a través de la via de Dab1 (Chen et al., 2005; Qiu et al., 2006a). L'activitat NMDA modula la interacció entre ApoER2 i PSD-95 (Hoe et al., 2006; Qiu et al., 2006a), mentre que Reelina promou la mobilitat de les subunitats 2B dels receptors NMDA, induïnt l'enriquiment de les sinapsis en receptors amb subunitats 2A (Sinagra et al., 2005; Groc et al., 2007; Qiu and Weeber, 2007). Conjuntament, Reelina regula positivament la resposta NMDA. La plasticitat induïda per Reelina està mediada també per receptors AMPA, però per vies diferents. Concretament, Reelina promou l'activitat AMPA regulant-ne la presència de receptors en superfície senyalitzant a través de PI3K (Qiu et al., 2006a; Qiu and Weeber, 2007).

La Reelina regula també la plasticitat de les espines dendrítiques. Concretament, els ratolins *reeler* presenten menor densitat d'espines i una reduïda complexitat d'aquestes en diferents zones corticals (Liu et al., 2001). La densitat d'espines en neurones piramidals d'hipocamp de ratolins *reeler* mostra una reducció d'acord al nivell d'expressió de Reelina, i extractes de sinaptosomes d'hipocamp mostren nivells reduïts de PSD-95 i subunitat 2A de receptor NMDA (Niu et al., 2008; Ventruti et al., 2011). Animals deficients en Dab1 mostren fenotips similars, consistents amb reduccions en la densitat d'espines en piramidals de CA1 i nivells més reduïts de PSD-95 i NR2A en sinaptosomes d'hipocamp. En el terminal presinàptic, botons d'hipocamp d'animals *reeler* presentaven més vesícules, i extractes de membrana d'hipocamp mostraven nivells reduïts de la proteïna SNARE SNAP-25, mentre que la suplementació de Reelina en permetia la recuperació.

Per últim, l'ús d'un model de deleció específica de Dab1 en neurones excitatòries en l'adult va permetre fer un estudi de la via de Reelina en una citoarquitectura intacta. Aquest cop, però, no es van observar canvis en la densitat d'espines dendrítiques a l'hipocamp, tot i que sí en la mida d'aquestes, sent més petites en els animals deficients en Dab1. Els nivells de proteïnes associades a la presinapsi i postsinapsi en aquests animals van mostrar també nivells similars als controls. La deficiència en Dab1 es va veure associada a un defecte en la LTP, així com també es van detectar anomalies en processos de memòria associativa a llarg termini.

Reelina i patologies del sistema nerviós

La Reelina duu a terme papers clau tant en el desenvolupament del cervell com en la seva funció en l'adult. Per tant, irregularitats en el funcionament d'aquesta proteïna són susceptibles d'estar relacionats amb un rang divers de desordres neurològics, tant psiquiàtrics com neurodegeneratius.

Així, doncs, s'han reportat abnormalitats en l'expressió de Reelina en pacients d'esquizofrènia, trastorn bipolar, autisme i depressió (Impagnatiello et al., 1998; Fatemi et al., 2000; Guidotti et al., 2000; Costa et al., 2001; Persico et al., 2001; Knable et al., 2004; Abdolmaleky et al., 2005; Knuesel, 2010; Folsom and Fatemi, 2013). La involucració de Reelina en aquests desordres s'ha vist tant activa com passiva, en consonància amb la hipòtesi de doble cop: Abnormalitats en el desenvolupament augmenten la vulnerabilitat de l'individu a la manifestació de la malaltia, i la Reelina pot participar en diverses de les possibles abnormalitats. D'altra banda, una senyalització deficient de Reelina promou una disfunció

cognitiva. D'altra banda, Reelina s'ha vist també relacionada amb epilèpsia (Haas et al., 2002; Haas and Frotscher, 2010), essent-ne un marcador la dispersió de cèl•lules granulars del DG, present també en ratolins *reeler*.

La regulació epigenètica de l'expressió de Reelina per mitjà de la metilació del promotor s'ha proposat com un mitjà viable per reduir-ne l'expressió (Dong et al., 2007), i alhora se n'han vist evidències en mostres post-mortem de pacients d'esquizofrènia (Veldic et al., 2004; Abdolmaleky et al., 2005; Guidotti et al., 2007). No obstant, altres mecanismes poden ser decisius en la generació d'expressions aberrants d'aquesta proteïna (Folsom and Fatemi, 2013).

Per últim, la senyalització de Reelina s'ha vist relacionada cada cop més amb la patofisiologia de la malaltia d'Alzheimer (Knuesel, 2010) a través de nombroses evidències: En primer lloc, una isoforma d'ApoE és el major factor de risc per la malaltia d'Alzheimer. Aquesta promou la neteja de dipòsits de β-amiloide (Aβ) (Schmechel et al., 1993; Tsai et al., 1994; Urosevic and Martins, 2008), i ho fa a través d'ApoER2 i VLDLR (Herz and Chen, 2006). A més els dipòsits Aβ colocalitzen amb Reelina i el seu precursor APP interacciona amb Reelina i Dab1 (Trommsdorff et al., 1998; Homayouni et al., 1999; Hoe et al., 2009; Doehner et al., 2010) mentre que Reelina pot contrarestar la disfunció sinàptica induïda per Aβ (Durakoglugil et al., 2009). En segon lloc, la fosforilació de la proteïna estabilitzadora de microtúbuls Tau es veu regulada per Reelina (Hiesberger et al., 1999; Beffert et al., 2002; Gonzalez-Billault et al., 2005). Alhora, mostres de pacients d'Alzheimer han presentat nivells alterats d'expressió i glicosilació de Reelina (Botella-Lopez et al., 2006; Chin et al., 2007; Botella-Lopez et al., 2010), així com s'han associat alguns polimorfismes de Reelina a la patologia d'Alzheimer (Seripa et al., 2008; Kramer et al., 2011). Conjuntament, la disminució en la senyalització de Reelina a causa de l'edat (Knuesel et al., 2009) podria promoure una fosforilació anòmala de Tau i empitjorar la neteja de pèptids Aβ. Això facilitaria l'aparició de madeixes neurofibril•lars i promouria l'amiloidogènesi, respectivament, la qual cosa podria ser la base de l'empitjorament en habilitats cognitives present en la malaltia d'Alzheimer (Pujadas et al., 2014).

Models animals per l'estudi del paper de la via de Reelina en el cervell adult

El ratolí Reelin-OE és una línia Tet-OFF composada per dos transgens que sobreexpressen Reelina sota el control de *pCaMKIIα* (**Fig. i.3.5**). El promotor de CaMKIIα dirigeix l'expressió del transactivador regulat per tetraciclina (*tTA*), permetent així una regulació temporal (a partir de P5) i cel.lular (simulant l'expressió de CaMKIIα) de l'expressió del transgen. El segon trangsgen codifica per un promotor induïble pel transactivador tTA que condueix l'expressió del gen exògen de Reelina. En ratolins dobles transgènics *pCaMKIIα-tTA* / *tetO-rlM* (Reelin-OE), la sobreexpressió de Reelina es pot reprimir mitjançant l'administració de doxiciclina (Pujadas et al., 2010). Els animals Reelin-OE presenten expressió exògena en nombroses cèl·lules piramidals de l'escorça i hipocamp, així com també en cèl·lules granulars del DG, entre altres conjunts cel·lulars. Aquests animals presenten una sobreexpressió de tres cops els nivells de proteïna a escorça i hipocamp, i fins a set cops en estriat, mentre que els nivells de Dab1 estan lleugerament disminuïts. Els ratolins Reelin-OE s'ha vist que presenten una major LTP *in vivo* a l'hipocamp, conjuntament amb alteracions puntuals de paràmetres relacionats amb la neurogènesi. Per tant, el model Reelin-OE, que presenta una laminació cortical normal, permet l'examinació específica de les funcions de Reelina en el cervell anterior adult.

El ratolí floxed Dab1 (flDab1) és un model knock-in amb l'exó III (codificant pels residus 23-69) del locus de *dab1* flanquejat per seqüències *loxP* (Pramatarova et al., 2008; Teixeira et al., 2014). Animals

adults homozigots flDab1 presenten alteracions estructurals permanents que inclouen una disminució en la mida del cerebel, cèl•lules piramidals ectòpiques en les CA1 i CA3 de l'hipocamp, una desestructuració lleu de la capa 2 de l'escorça i la presència de neurones ectòpiques en la capa 1 (**Fig. i.3.6c**). D'altra banda, aquest ratolí presenta alguns fenotips de comportament associats a esquizofrènia que es veuen incrementats per factors associats a increments de risc.

El creuament d'aquest ratolí amb una línia Ubiquitina $CreER^{T2}$, el model resultant (Cre/flDab1) permet la supressió de l'expressió de Dab1 a través de l'administració de tamoxifè (TAM) (**Fig. i.3.6a-b**). Els defectes de malposicionament cel·lular observats en el model flDab1 no es veuen influenciats per la inactivació en adult de l'expressió del gen (Teixeira et al., 2014).

Per últim, l'injecció estereotàxica de retrovirus Cre-GFP (Zhao et al., 2006) al DG d'animals flDab1 adults permet la inactivació localitzada de la sensibilitat a la via de Reelina en neurones de nova generació del DG, oferint alhora la possibilitat de traçar l'edat exacta de la cèl·lula infectada (**Fig. i.3.6d**) (Teixeira et al., 2012).

Conjuntament, aquests models animals han estat de gran utilitat per l'estudi del paper de la Reelina en l'establiment i manteniment de sinapsis en el cervell adult. Aquestes qüestions delimiten els objectius que s'han volgut assolir en el present treball.

Resultats i discussió

Plasticitat presinàptica en l'hipocamp de ratolins Reelin-OE

La Reelina s'ha vist involucrada recentment en diversos fenòmens de plasticitat sinàptica especialment relacionats amb el terminal presinàptic (Pujadas et al., 2010; Hellwig et al., 2011). Vàrem trobar que els botons presinàptics de l'hipocamp d'animals Reelin-OE presentaven mides més grans, i aquells situats en les capes RAD i OR mostraven morfologies menys compactes, mentre que la inactivació del transgen permetia observar mides i circularitats semblants al grup control i per sobre d'aquest en les capes OML i SLM (**Fig. r.1.1d-e**). Aquestes capes estan innervades per aferències entorhinals i talàmiques, mentre que les RAD i OR estan innervades per col·laterals de Schaffer provinents de cèl·lules piramidals de la CA3 (Andersen et al., 2007). Per tant, l'estructura dels botons a l'hipocamp presenta sensibilitat a la senyalització per Reelina, però l'efecte concret sobre determinats fenotips apareix condicionat per la circuiteria inherent a la capa. Altres fenotips, com la densitat de botons o l'abundància de botons multisinàptics, es van trobar augmentats arreu de l'hipocamp (**Fig. r.1.1a-b**). Per tant els nostres resultats suggereixen l'existència d'una major activitat presinàptica en l'hipocamp d'animals Reelin-OE.

D'altra banda, l'anàlisi de diferents marcadors presinàptics en extractes de sinaptosomes d'hipocamp va mostrar que els nivells de proteïnes com la SNARE SNAP-25 ni la fosfoproteïna sinapsina estaven alterats en els animals Reelin-OE (**Fig. r.1.2a-b**). Més enllà, un anàlisi immunohistoquímic de la seva distribució tampoc en va revelar canvis en el patró d'expressió a l'hipocamp (**Fig. r.1.2c-d**). En el cas de SNAP-25, s'ha vist que els seus nivells d'expressió estan disminuïts en animals *reeler*, i la suplementació de Reelina en permet recuperar els nivells. És interessant, alhora, remarcar que el mateix estudi no va detectar-ne valors disminuïts en animals Dab1-KO ni en dobles mutants dels receptors ApoER2 i VLDLR (Hellwig et al., 2011). L'increment d'alliberació de neurotransmissor en resposta a Reelina depèn de la funció d'SNAP-25 (Bal et al., 2013), i alhora canvis en l'expressió d'aquesta proteïna s'han vist relacionats amb nombrosos desordres psiquiàtrics com esquizofrènia i ADHD (Thompson et al., 1998; Barr et al., 2000; Antonucci et al., 2013). Els nostres resultats mostren una resiliència presinàptica a canvis d'expressió de SNAP-25 en resposta a un augment crònic de l'expressió de Reelina. Aquest fenomen podria prevenir de l'aparició de les esmentades patologies sinàptiques que depenen dels nivells sostinguts d'expressió d'SNAP-25. En el cas de la sinapsina, els nostres resultats recolzen troballes

prèvies d'altres grups, donat que no presenta tampoc valors alterats ni en animals *reeler* ni en animals deficients en Dab1 (Hellwig et al., 2011; Trotter et al., 2013).

Conjuntament, els nostres resultats apunten a que l'augment sostingut dels nivells de Reelina té un clar efecte sobre la plasticitat estructural presinàptica en l'hipocamp. Alhora, suggereixen l'existència de mecanismes d'homeostasi sinàptica per canvis crònics en l'expressió de Reelina, que preservarien l'expressió de reguladors clau de la funció presinàptica, i en conseqüència preservarien la integritat de la mateixa funció presinàptica.

Plasticitat postsinàptica en l'hipocamp d'animals Reelin-OE

La Reelina regula la plasticitat estructural de les espines dendrítiques en l'hipocamp adult

Els nostres resultats reflecteixen que la sobreexpressió de Reelina a l'adult no altera el número d'espines dendrítiques a l'hipocamp, però sí regula les seves propietats estructurals (**Fig. r.2.1**). Aquests resultats estan en consonància amb l'observat en un model de deleció adulta del gen Dab1 en neurones del cervell anterior, en el qual van veure disminucions de la mida de les espines però no de la densitat d'aquestes en neurones piramidals de la CA1 (Trotter et al., 2013). D'altra banda, però, models de deleció constitutiva de la via de senyalització de Reelina i assaigs *in vitro* han reportat que Reelina influencia la formació de noves espines (Liu et al., 2001; Niu et al., 2008; Ventruti et al., 2011). Aquestes discrepàncies es poden donar per diversos motius. En primer lloc, els nivells de Dab1 estan reduïts en els ratolins Reelin-OE i condicional deficient en Dab1 mencionats anteriorment (Pujadas et al., 2010; Trotter et al., 2013). En canvi, els ratolins *reeler* i *HRM* presenten nivells augmentats de Dab1 (Rice et al., 1998), per la qual cosa podríem suposar que l'aplicació de Reelina en aquestes neurones pot provocar una resposta major. En segon lloc, és possible que la senyalització per Reelina garantitzi l'obtenció d'un nivell estàndard d'espines dendrítiques, i que un cop assolit no promogués majors efectes en aquest sentit. En tercer lloc, és possible que les neurones en el cervell adult presentin mecanismes homeostàtics dirigits a frenar l'aparició d'espines dendrítiques més enllà de cert llindar fisiològic.

Alhora, mostrem que la sobreexpressió de Reelina promou la hipertròfia de les espines dendrítiques. En concret, els hipocamps dels animals Reelin-OE presentaven espines més grans i menys circulars en totes les capes (**Fig. r.2.1c-d**). L'eixamplament de les espines es dóna en diversos fenòmens de plasticitat sinàptica, com la LTP, i es relaciona amb una major força postsinàptica (Toni et al., 2001; Yuste and Majewska, 2001b; Matsuzaki et al., 2004; Bourne and Harris, 2008; O'Donnell et al., 2011; Hill and Zito, 2013). Alhora, els animals Reelin-OE mostren una major LTP hippocampal *in vivo* (Pujadas et al., 2010). Mostrem també que les espines del tipus III – les més complexes, associades doncs al tipus *mushroom* – eren més abundants en totes les capes (**Fig. r.2.1h**). Les espines tipus *mushroom* estan considerades ser més madures i estables, i se les ha proposat com el suport físic de processos de memòria (Kasai et al., 2003; Matsuzaki et al., 2004; Bourne and Harris, 2007; Yasumatsu et al., 2008; Yang et al., 2009; Kasai et al., 2010a). Alhora, una reconstrucció basada en talls seriats mostrà una abundant població d'espines hipertròfiques en el stratum radiatum dels animals Reelin-OE (**Fig. r.2.6**).

Per últim, reportem també un increment de la densitat d'espines amb aparell d'espina (SA) i en la mida d'aquest orgànul en els animals Reelin-OE (**Fig. r.2.2b-c**). El SA està involucrat en l'emmagatzematge de Ca^{2+} i el seu tràfic, en processos relacionats amb la plastitcitat sinàptica i està present principalment en espines del tipus *mushroom* (Gray, 1959; Fifkova et al., 1983; Spacek and Harris, 1997; Fiala et al., 2002b; Nimchinsky et al., 2002; Vlachos et al., 2009). Per últim, la inactivació de l'expressió del transgen reverteix els fenotips descrits (**Fig. r.2.1**, **Fig. r.2.2**). Conjuntament, els nostres resultats suggereixen que Reelina promou la formació i l'estabilització d'espines fisiològicament més eficients.

Els nivells de Reelina no regulen l'expressió de proteïnes postsinàptiques però sí la seva distribució sinàptica-extrasinàptica

Els nostres resultats mostren que l'expressió de diferents proteïnes associades a la postsinapsi no es veu afectada en els animals Reelin-OE, incloent subunitats de receptors de glutamat, proteïnes bastida postsinàptiques, proteïnes associades al citosquelet i proteïnes de senyalització intracel·lular (**Figs. r.2.3**, **r.2.4a-b**, **r.2.5a**). Aquesta observació concorda amb experiments no publicats de col·legues que indiquen que l'expressió de gens associats a la sinapsi en l'hipocamp d'animals Reelin-OE no es veu

alterada, i amb el fet que l'ablació de la senyalització de Reelina específicament en adult tampoc comporti canvis en l'expressió d'aquestes proteïnes (Trotter et al., 2013). En canvi, l'administració aguda de Reelina provoca l'activació de CREB (Rogers et al., 2011). En conjunt, els nostres resultats suporten la idea de que Reelina no controla l'expressió de gens codificant per proteïnes de la sinapsi.

Estudis recents mostren que Reelina promou l'activitat sinàptica a través de modificacions en l'activació i tràfic en superfície de receptors d'AMPA i NMDA (Beffert et al., 2005; Chen et al., 2005; Qiu et al., 2006a; Groc et al., 2007; Qiu and Weeber, 2007; Campo et al., 2009). Més enllà, alguns estudis han apuntat a que Reelina actua promovent la presència de la subunitat 2A envers de la 2B en la població de receptors NMDA, amb implicacions tant fisiològiques com estructurals (Groc et al., 2007; Teixeira et al., 2011; Iafrati et al., 2013). Alhora, s'ha vist que la plasticitat en la composició 2A-2B de la població de receptors NMDA es regula mitjançant la mobilitat lateral dels receptors amb subunitats 2B (Groc et al., 2006). En aquesta línia, els nostres resultats mostren que Reelina promou una disminució de les subunitats NR2a/2b a la postsinapsi (**Fig. r.2.4c-j**), concomitant amb un augment de la seva presència extrasinàptica i citosòlica. Alhora, aquest efecte es va revertir mitjançant el bloqueig de l'expressió de Reelina exògena durant 1 setmana, indicant que canvis ràpids en l'expressió de Reelina promouen la migració d'aquests receptors.

Per últim, s'ha vist que Reelina promou l'estabilització del citosquelet d'actina per mitjà de la regulació de la fosforilació de cofilina a través de LIMK (Arber et al., 1998; Yang et al., 1998; Meng et al., 2004; Chai et al., 2009), la qual cosa podria explicar l'estabilització de les espines dendrítiques (Shi et al., 2009) i els canvis en el tràfic de receptors AMPA (Gu et al., 2010; Wang et al., 2013). Tot i que els nivells de p-LIMK1 i p-cofilina no estaven alterats en animals Reelin-OE (**Figs. r.2.3f**, **r.2.5a-b**) , vàrem trobar canvis en la distribució de p-cofilina que seguien el patró observat amb les subunitats de receptors NMDA (**Fig. r.2.5c-f**).

Els efectes derivats de la sobreexpressió de Reelina són dependents de capa

Gran part de les alteracions pre- i postsinàptiques reportades pels animals Reelin-OE presentaven fenotips més accentuats a les capes SLM, OML i MML, incloent mides dels botons i espines, densitat de botons i abundància de botons multisinàptics, llargada del contacte, àrea del SA i fracció d'espines amb SA. Aquestes capes es corresponen amb les capes innervades per l'aferència entorhinal a l'hipocamp per la via perforant. Cal remarcar, però, que la distribució de Reelina en els animals sobreexpressants o el de distribució de Dab1 en l'adult no mostren paral·lelismes amb el patró laminat descrit (Borrell et al., 2007; Pujadas et al., 2010; Trotter et al., 2013). No obstant, no podem excloure que altres molècules rellevants presentin enriquiments locals en dominis dendrítics específics de neurones piramidals i granulars.

En aquest sentit, el fenotip més clar és el referent a l'expressió de sinaptopodina. Aquesta proteïna és crucial per l'existència de l'SA i s'ha relacionat amb la plasticitat de l'espina dendrítica (Freire, 1978; Deller et al., 2000; Deller et al., 2003; Deller et al., 2006; Okubo-Suzuki et al., 2008; Vlachos et al., 2009; Vlachos et al., 2013; Zhang et al., 2013). La seva expressió laminar s'ha associat a la distribució de capes dendrítiques (Deller et al., 2002), i presenta canvis en situacions d'estrès sinàptic com lesions a l'escorça entorhinal o episodis epilèptics induïts per àcid kaínic (Roth et al., 2001; Deller et al., 2006). Hem vist que la sobreexpressió de Reelina provoca un canvi notable en la distribució de sinaptopodina a l'hipocamp, consistent en un enriquiment a l'SLM i una disminució a les capes moleculars del DG, tots dos efectes veient-se parcialment revertits pel bloqueig de l'expressió del transgen (**Fig. r.2.2f-i**). Els nostres resultats indiquen, doncs, que Reelina modula l'estructura i funció sinàptica de manera diferencial en diferents dominis dendrítics d'una mateixa neurona, i que aquesta modulació presenta correlacions amb el tipus d'innervació aferent.

La Reelina promou la plasticitat d'espina en neurones piramidals

Efectes de la sobreexpressió de Reelina sobre espines dendrítiques de neurones piramidals

En cèl·lules piramidals de la CA1 mostrem que la densitat d'espines en les dendrites basals augmenta a mesura que les dendrites s'allunyen del soma, fins estabilitzar-se a partir d'una distància de 50 µm, de manera similar a l'observat en altres estudis (Benavides-Piccione et al., 2005; Ballesteros-Yanez et al., 2006; Benavides-Piccione et al., 2013). Vàrem trobar que la densitat d'espines en dendrites basals i apicals estava conservada en els animals Reelin-OE (**Fig. r.3.1c-d**, **g-h**), reforçant els resultats dels anàlisis basats en microscòpia electrònica obtinguts prèviament (**capítol 2**) (Pujadas et al., 2010). Conjuntament amb diferents experiments analitzant el paper de la via de Reelina sobre l'espinogènesi *in vivo*, una possible conclusió seria que un augment sostingut de Reelina *in vivo* provocaria fenotips diferents depenent de la durada d'aquest. Així, exposicions curtes (hores) a nivells elevats de Reelina no provocarien canvis en la densitat d'espines (Rogers et al., 2011), mentre que canvis aguts (dies) en els nivells de senyalització serien capaços de desencadenar canvis en la densitat d'espines (Pujadas et al., 2010; Rogers et al., 2011). Per últim, modificacions cròniques dels nivells de Reelina no tindrien efectes sobre la densitat d'espines (Pujadas et al., 2010).

Les espines de les dendrites basals de cèl·lules piramidals de la CA1 presenten espines de mides i esfericitats similars a les observades en el grup control (**Fig. r.3.1e-f**). Això és coherent amb l'observat en els anàlisis ultrastructurals, que presentaven espines de mida semblant a l'OR, si tenim en compte que la majoria d'espines a l'OR corresponen a dendrites basals de neurones piramidals de la CA1 (Andersen et al., 2007). D'altra banda, l'anàlisi de la morfologia de les espines en dendrites apicals obliqües al RAD va mostrar mides i esfericitats semblants als controls (**Fig. r.3.1i-j**). En aquest cas, però, els resultats difereixen de l'observat anteriorment. Havent d'escollir entre els resultats emanats de l'anàlisi confocal o de microscòpia electrònica, en tant que els anàlisis d'ultrastructura gaudeixen d'una major resolució lateral, les conclusions d'aquests referents a l'anàlisi de morfologies d'espina haurien de ser més acurades.

Per tant, conjuntament els nostres resultats mostren que la sobreexpressió crònica *in vivo* de Reelina no afecta la densitat d'espines en neurones piramidals de CA1 però promou una hipertròfia d'espines dendrítiques localitzada a l'arbre dendrític apical.

L'anàlisi de les dendrites de neurones piramidals de capa 5 de l'escorça S1BF va mostrar densitats d'espines inferiors que els registres d'hipocamp (**Fig. r.3.2c**, **f**), concordant amb experiments d'altres autors (Konur et al., 2003). A més, els animals Reelin-OE presenten disminucions en la densitat d'espines en tots dos trams apicals analitzats. De manera similar, uns estudis en neurones piramidals de capa 2/3 de la mateixa zona cortical varen mostrar que nounats que havien rebut millors atencions maternes presentaven alhora menys densitat d'espines i increments en l'expressió de Reelina ja en l'etapa adulta (Smit-Rigter et al., 2009). Aquests tipus d'experiments repliquen el fet de que events adversos durant etapes infantils es correlacionen amb un major risc de desenvolupar malalties psiquiàtriques en l'etapa adulta. En aquest sentit, els nostres resultats suporten la idea que Reelina seria un factor promovent la resiliència a aquests desordres (Teixeira et al., 2011). Alhora, aquestes espines eren més grans i menys esfèriques en animals Reelin-OE (**Fig. r.3.2d-e**, **g-h**), fenotips associats amb contactes sinàptics més eficients (Harris and Stevens, 1989; Matsuzaki et al., 2001; O'Donnell et al., 2011).

Efectes de la disrupció de la via de senyalització de Reelina sobre espines dendrítiques de neurones piramidals

L'estudi en cèl·lules piramidals de la CA1 de l'hipocamp d'animals en els quals s'havia suprimit l'expressió de Dab1 en adult va mostrar que la densitat d'espines en les dendrites basals no es veu afectada per Reelina (**Fig. r.3.3c-d**). Més enllà, vàrem veure que aquestes presentaven volums més petits i majors esfericitats (**Fig. r.3.3e-f**). Aquests resultats estan en concordància amb l'observat en un altre model diferent de depleció de Dab1 en adult (Trotter et al., 2013). Contràriament, en models de basats en la disrupció constitutiva de la senyalització de Reelina sí que s'observen canvis en la densitat d'espina (Niu et al., 2008; Ventruti et al., 2011). Davant d'aquesta controvèrsia, cal tenir en compte que la deficiència de Reelina en el desenvolupament comporta greus deficiències en la citoarquitectura cortical que es conserven en l'adult (Sheldon et al., 1997; D'Arcangelo and Curran, 1998; Trommsdorff et al., 1999; Katsuyama and Terashima, 2009; Cremer et al., 2011). Per tant, les estratègies basades en la modificació condicional de la senyalització de Reelina són eines força més interessants per desxifrar els fenotips concrets que desencadena Reelina en un cervell sa.

En últim lloc, les espines de la dendrita apical de neurones piramidals de capa 5 eren més abundants en ratolins flDab1/Cre+TAM (**Fig. r.3.4c**). Aquest fenotip és diametralment oposat en l'observat anteriorment en ratolins Reelin-OE. Per tant, els nostres resultats suggereixen que Reelina regula negativament la densitat d'espines en dendrites apicals de neurones piramidals de capa 5 a l'escorça S1BF. En línia amb l'argumentat anteriorment, aquest resultat suggereix un rol protectiu de Reelina enfront l'aparició de malalties psiquiàtriques. D'altra banda, les espines dels animals deficients en Dab1 eren més grans i menys esfèriques (**Fig. r.3.4d-e**), un fenotip similar a l'observat en ratolins Reelin-OE. Aquesta troballa recolza la idea genèrica de que la generació i l'engrandiment-estabilització de les espines són dos processos que poden estar regulats diferentment (Knott et al., 2006; Cingolani and Goda, 2008; Yasumatsu et al., 2008), i conjuntament amb la dada de densitat suggereix que aquestes neurones en els animals deficients en Dab1 presenten una hiperexcitabilitat a nivell postsinàptic.

En resum, els nostres resultats mostren que la senyalització de Reelina modula la densitat i la morfologia de les espines dendrítiques de les neurones piramidals. Alhora, els nostres resultats descriuen un ampli rang d'efectes que presenten especificitat pel tipus de cèl·lula piramidal i/o per un domini dendrític concret, suggerint que l'efecte desencadenat per Reelina s'adequa a les necessitats locals. Conjuntament, situen la via de senyalització de Reelina en processos de regulació i manteniment de la plasticitat sinàptica cortical en el cervell adult.

Anàlisi de la neurogènesi adulta per microscòpia FIB/SEM

La neurogènesi adulta a l'hipocamp és un procés biològic conservat en nombroses espècies, entre elles els humans (Eriksson et al., 1998; Gage, 2000). S'ha relacionat aquest procés amb la formació de memòries associatives (Deng et al., 2010), així com a processos d'oblit (Frankland et al., 2013; Akers et al., 2014). Alhora, nombrosos dèficits cognitius, neurodegeneratius i psiquiàtrics s'han vist associats a patrons alterats de neurogènesi (Zhao et al., 2008). La descripció acurada de la integració de les neurones granulars (GCs) de nova generació en la circuiteria preexistent és de gran rellevància per la comprensió dels agents que la regulen, i per tant per poder desxifrar els mecanismes que governen processos cognitius avançats.

Hem desenvolupat per primer cop un protocol de microscòpia correlativa OM-FIB/SEM combinant un marcatge de diaminobenzidina (DAB) obtingut per tècniques immunohistoquímiques i l'adquisició exhaustiva en tres dimensions en un microscopi FIB/SEM de segments dendrítics d'interès marcats (**Figs. r.4.2**, **r.4.3**). El fet de dirigir el procés a unes mostres prèviament marcades ha ajudat enormement a focalitzar l'adquisició i l'anàlisi, així com també n'ha facilitat en gran mesura la supervisió i revisió per investigadors independents. La tasca de segmentació s'ha vist també millorada en tractar-se d'estructures electrodenses gràcies al marcatge de DAB (**Fig. r.4.2g-j**) (Helmstaedter et al., 2008). Recentment s'ha descrit un mètode de correlació OM-FIB/SEM basat únicament en fluorescència (Maco et al., 2014). Tot i que viable, el procés d'adquisició en el microscopi FIB/SEM és en aquest cas a cegues. D'altra banda, en el nostre protocol la dendrita d'interés roman visible durant tot el procés d'adquisició d'imatges (**Fig. r.4.2d**), assegurant un enquadrat perfecte al llarg de tota la pila d'imatges, i revertint en una millor eficiència general. Els paràmetres usats en l'adquisició, una resolució lateral de 3.7 nm i en profunditat de 25 nm, asseguren prou resolució per la reconstrucció d'una circuiteria neuronal (Briggman and Bock, 2012) permetent alhora l'obtenció de dades de grans volums de teixit, de fins a 11 μm de profunditat. Hem usat i contribuït al desenvolupament del programari de lliure distribució EspINA per la segmentació (**Fig. r.4.2i-j**) (Morales et al., 2011). La comparativa de les reconstruccions obtingudes a partir d'aquest programa són indistingibles de les obtingudes amb el tradicional Reconstruct (**Fig. r.4.2h**) (Fiala, 2005), però a canvi permet certa automatització del procés, accelerant la fase de segmentació. Conjuntament, el protocol que descrivim ofereix una aproximació fiable, factible i eficient per a l'obtenció d'imatges d'alta resolució en 3D per microscòpia FIB/SEM de mostres prèviament marcades. Alhora, permet l'aplicació potencial per a qualsevol teixit biològic ja preparat per microscòpia electrònica pels mètodes convencionals.

Estructures postsinàptiques en noves GCs en desenvolupament

Una classificació de les espines dendrítiques en els cinc tipus convencionals (**Fig. r.4.5**) va revelar que les GCs de nova generació de 8-9 setmanes presenten predominantment espines *thin*, seguides de les *mushroom* i *filopodia*, un 15% d'espines *branched* i molt poques del tipus *stubby* (**Fig. r.4.8c**). Aquestes proporcions quadren a grans trets en l'observat per GCs madures del DG (Harris et al., 1992; Woolley et al., 1996; Popov and Stewart, 2009). Els nostres resultats aporten tres principals novetats a aquest anàlisi: En primer lloc, l'anàlisi es basa en 235 espines amb 271 caps identificats, essent el més extens a dia d'avui (**Taula r.4.4**). En segon lloc, la qualitat, integritat i resolució dels conjunts d'imatges (**Taula r.4.3**) permet la identificació recurrent de cada espina i sinapsi en successives imatges seqüencials (**Fig. r.4.3a**), permetent una major objectivitat en els processos d'identificació i classificació. En tercer lloc, coneixem l'edat de les neurones analitzades, permetent així fer un anàlisi de l'evolució de certs paràmetres relacionats amb la morfologia de l'espina al llarg del desenvolupament d'aquestes cèl·lules (**Fig. r.4.8b-d**).

Hem trobat un augment remarcable de la població d'espines *branched* en les GCs de 8-9 setmanes comparades amb les de 3-4. S'ha vist que aquesta població augmenta en el DG resposta a a LTP de la via perforant (Trommald et al., 1996), així com també en altres àrees del cervell en resposta a LTP o a paradigmes d'aprenentatge (Johansson and Belichenko, 2002; Sanders et al., 2012), suggerint un rol particular d'aquest tipus d'espina en processos de memòria. En paral•lel, altres autors l'han associat a una major eficàcia de la sinapsi (Rusakov et al., 1996; Sorra et al., 1998; Toni et al., 1999). Tots dos caps rebien contactes de botons independents, d'acord amb el reportat en estudis anteriors (Geinisman et al., 1989; Trommald et al., 1996; Trommald and Hulleberg, 1997; Popov and Stewart, 2009), i les morfologies dels caps individuals presentaven proporcions de tipus d'espina similars a la població general d'espines. En conjunt, la nostra descripció d'espines *branched* en GCs de nova generació del DG (**Figs. r.4.6**, **r.4.8c**) representa una nova contribució al coneixement d'aquest tipus particular d'espina.

Anàlisi quantitatiu de morfologies d'espina en el desenvolupament de GCs de nova generació

El desenvolupament de les GCs de nova generació està acompanyat d'un increment en l'esfericitat de les seves espines (**Fig. r.4.8d**). És interessant remarcar que un fet similar s'ha descrit que ocorre durant el desenvolupament de noves espines en neurones piramidals (Knott et al., 2006). El mecanisme que podria explicar aquest fet podria estar relacionat amb una maduració sincrònica de les espines d'aquestes cèl•lules. En l'estadi de 3-4 setmanes, aquestes espines presentarien una fase d'expansió, protagonitzada pel conjunt d'eixamplament del citosquelet d'actina (Honkura et al., 2008), mentre que a l'etapa de 8-9 setmanes el creixement ja s'hauria estabilitzat i la morfologia de l'espina vindria determinada per l'activitat dels conjunts d'actina de l'espina estable i dinàmic. Aquesta hipòtesi concorda amb la cronologia del desenvolupament d'aquestes cèl•lules, les quals no presenten espines a 2 setmanes, la densitat madura d'espines s'assoleix a les 6 setmanes, mentre que les cèl•lules de 8 setmanes presenten un fenotip de morfologia d'espina ja madura (Zhao et al., 2006). En resum, els nostres resultats mostren que la població d'espines de les GCs de nova generació en desenvolupament experimenten una maduració estructural sincrònica, que consisteix en l'adquisició d'una morfologia més esfèrica en estadis més madurs.

Correlació de mesures morfològiques aparellades de conjunts espina-sinapsi

Es coneix que l'ultrastructura dels diferents components de la sinapsi guarda una estreta relació intrínseca. En concret, el volum del cap de l'espina està associat amb la fiabilitat i força de la sinapsi (Arellano et al., 2007a), mentre que la morfologia del coll està relacionada amb la constant de temps de la compartimentalització del Ca^{2+} (Majewska et al., 2000b; Yuste et al., 2000; Sabatini et al., 2002; Noguchi et al., 2005) i amb les propietats de filtrat de potencials elèctrics per part de l'espina (Svoboda et al., 1996; Araya et al., 2006).

Els nostres resultats reprodueixen la correlació reportada prèviament entre volum d'espina i mida de la PSD (**Fig. r.4.7e**) (Lisman and Harris, 1993; Knott et al., 2006; Arellano et al., 2007a; Nikonenko et al., 2008; Cane et al., 2014). Alhora, descrivim per primer cop que l'esfericitat de l'espina i la sinapsi correlacionen amb el volum de l'espina (**Fig. r.4.7f-g**). Un anàlisi per classes ens ha permès veure, a més, que aquests parells de variables esmentats guarden relacions gairebé lineals per sota de determinats llindars de volum d'espina (**Fig. r.4.7h-j**), i que les dades per sobre d'aquests llindars ja no mostren correlació (**Taules r.4.1-2**). Conjuntament, els nostres resultats mostren que el volum de l'espina, el volum de la sinapsi i l'esfericitat de tots dos elements són paràmetres que es veuen en certa manera regulats de forma coordinada. La presència d'aquests llindars suggereixen, alhora, que aquesta regulació té lloc dins d'un marc fisiològic, assegurant la formació en tot cas d'estructures efectives des d'un punt de vista estructural i funcional. Per últim, la descripció d'aquests llindars i les relacions obtingudes són consistents amb dades provinents d'estudis independents en altres zones de l'escorça (Knott et al., 2006)

i es reprodueixen a grans trets en una mostra més petita com és el grup de 3-4 setmanes (**Taula r.4.5**). Per tant, les relacions lineals mostrades suposen una robusta aproximació a la interrelació d'aquestes variables morfològiques per espines dendrítiques en desenvolupament, aplicables a les cèl·lules d'estudi però també molt probablement a altres tipus neuronals del cervell.

Innervació presinàptica de GCs de nova generació

S'ha proposat que els botons presinàptics que estableixen sinapsis amb múltiples parelles postsinàptiques (botons multisinàptics, MSBs) s'identifiquen amb un element transitori en el procés d'integració de noves espines en un circuit preexistent (Knott et al., 2006). Aquests representen el 20% en una situació estable, mentre que la seva presència puja fins al 70% quan es miren exclusivament els companys presinàptics d'espines noves (Knott et al., 2006). En GCs del DG, suposen el 75% en GCs de 4 setmanes i el 40% en el cas de GCs madures (Toni et al., 2007). En aquesta línia, el nostre anàlisi ha mostrat que suposen el 76% de la inervació presinàptica de noves GCs de 3-4 setmanes, i el 72% a les 8-9 setmanes (**Fig. r.4.9g**). Alhora, mostrem que els MSBs innervant espines de noves GCs de 8-9 setmanes estableixen un 34% més de sinapsis (**Fig. r.4.9h**).

L'anàlisi de la morfologia de les espines dendrítiques de la nova GC innervades per botons MSB o SSB va mostrar que en cap cas el tipus de botó es correlacionava amb un tipus d'espina concret (**Fig. r.4.10a**). Més enllà, tampoc es van observar diferències en la mida ni esfericitat d'aquestes espines ni de les sinapsis establertes (**Fig. r.4.10b-e**). Aquest fet contrasta amb estudis recents, que veient una reducció de l'abundància de botons SSB i una pèrdua (no directament relacionada) d'espines de mida petita van suggerir la possibilitat de que tots dos tipus d'especialitzacions estiguessin associats (Bourne and Harris, 2011; Bourne et al., 2013).

Conjuntament, mostrem que la integració de les noves GCs té lloc simultàniament amb un augment de la connectivitat dels MSBs que les innerven, i que les espines de les noves GCs contacten amb aquests botons o amb SSBs indistintament del tipus d'espina o de la morfologia i mida d'aquesta o la sinapsi. Donat que aquest procés integratiu conté un important factor de competició (Toni and Sultan, 2011), desxifrar el mecanisme concret pel qual es dóna pot ser de gran interès per comprendre el rol funcional de la neurogènesi adulta a l'hipocamp.

La Reelina en la neurogènesi adulta a l'hipocamp

La neurogènesi adulta en l'hipocamp presenta cert grau de regulació per la via de Reelina. La pèrdua de Dab1 ocasiona dèficits en el creixement i arborització de l'arbre dendrític de noves GCs del DG (Teixeira et al., 2012), i la sobreexpressió de Reelina provoca un mal posicionament d'aquestes cèl·lules en la capa granular (Pujadas et al., 2010).

Aprofitant l'estratègia d'adquisició d'imatges en un microscopi FIB/SEM descrita en el **capítol 4**, hem dut a terme un estudi de l'efecte de canvis en l'activitat de la via de Reelina en el procés d'integració sinàptica de noves GCs del DG. Conjuntament, hem fet ús d'un mètode de traçat d'aquestes cèl·lules per mitjà de vectors retrovirals i dels models animals Reelin-OE i flDab1. Això ens ha permès l'estudi de la neurogènesi adulta al DG de en escenaris de sobreexpressió generalitzada de Reelina i de disrupció de Dab1 (Dab1-KO) específicament en la nova GC. El volum d'imatges analitzat, conjuntament amb els respectius grups control, suposa +5900 μm^3 (**Taula r.5.1**), conté 28 segments dendrítics d'interès i comprèn la identificació de 476 sinapsis, 544 espines i 476 botons presinàptics, i la reconstrucció completa en 3D de 443 espines amb les respectives especialitzacions sinàptiques (**Taula r.5.2**). Aquest conjunt de dades ha proporcionat informació estructural completa tant dels elements traçats com del neuropil adjacent. Això reforça la utilitat del mètode correlatiu OM-FIB/SEM d'adquisició d'imatges prèviament descrit per l'anàlisi dirigit de regions subcel·lulars d'interès a l'escala nanoscòpica.

Reelina i les espines de noves GCs en desenvolupament

Espines de tots els tipus excepte les poc freqüents stubby vàren ser identificades en totes les mostres analitzades. No obstant, es van observar canvis concrets en l'abundància de certes classes depenent de l'edat de la cèl·lula i del grup experimental. Tot i que el fenomen més abundant eren espines dendrítiques amb una única sinapsi, es varen detectar altres estructures: Es van trobar 5 espines sense sinapsi (5%) en GCs de 8-9 setmanes de ratolins Reelin-OE (**Taula r.5.2**), que es correspondrien amb les descrites com espines asinàptiques (Arellano et al., 2007b). D'altra banda, es vàren detectar dues espines multiinnervades (MIS) en GCs Dab1-KO de 8-9 setmanes. Aquest tipus d'espina no es va observar en cap altre grup a l'etapa de 8-9 setmanes. S'ha vist que la formació de MIS es veu promoguda per la via de senyalització de l'òxid nítric (NO), en una forma depenent d'activitat que inclou el reclutament de la sintasa neuronal de NO (nNOS) a la sinapsi per PSD-95 (Nikonenko et al., 2003; Ishii et al., 2006; Nikonenko et al., 2008). És interessant remarcar que la via de NO presenta certes relacions amb la de Reelina, com és que totes dues vies poden involucrar l'expressió de CREB (Chen et al., 2002; Aguado et al., 2009; Kelley et al., 2011), la descripció de parells cel·lulars mútuament sensibles a Reelina i nNOS al bulb olfactiu (Herrmann et al., 2008) o la presència a l'hipocamp d'una població d'interneurones que expressen nNOS i Reelina (Romay-Tallon et al., 2010). En aquest sentit, una regulació combinada per part de nNOS i Reelina de la formació de MIS en les noves GCs del DG podria explicar que neurones insensibles a Reelina presentin aquestes espines en estadis anormalment tardans. No obstant, aquest possible mecanisme necessita experiments específics per tal de ser confirmat.

Altres fenotips, com una abundància prematura d'espines *branched* en neurones Dab1-KO o una abundància d'espines *mushroom* en GCs de 8-9 setmanes que és major a major nivell de senyalització de Reelina (**Fig. r.5.1a-c**) suporten la idea de la regulació de Reelina de la morfologia de les espines dendrítiques de GCs de nova generació.

Alhora, en GCs de 8-9 setmanes, major Reelina es va veure associada amb una major mida de les espines més grans (**Fig. r.5.1d**), i una reducció de l'esfericitat de les sinapsis (**Fig. r.5.1h**). En sentit contrari, l'augment o l'absència de senyalització de Reelina es va veure associat amb un increment o

reducció de la mida de la sinapsi, respectivament (**Fig. r.5.1h**). En tercer lloc, en cap dels dos escenaris experimentals es va observar el procés d'augment d'esfericitat d'espina associat a maduració que s'havia descrit prèviament pel grup control (**Fig. r.5.1e**). Aquests resultats suggereixen que l'engrandiment sincronitzat de les espines durant el desenvolupament de les noves GC no té lloc quan es desregula l'expressió de Reelina. Un actor important en l'etapa immadura d'eixamplament d'espina és la proteïna promotora de la ramificació d'actina Arp2/3 (Bramham, 2008). Un regulador d'aquesta, N-WASP, es veu activat directament per Dab1 o per via de Cdc42, un efector de la via de Reelina per sota de PI3K (Suetsugu et al., 2004; Winder, 2004; Leemhuis and Bock, 2011). Una desregulació d'aquesta via podria impedir la correcta maduració de les espines, donant lloc a espines hipertròfiques, en consonància amb observacions anteriors en altres cèl·lules (**capítol 2**) (Pujadas et al., 2010). No obstant, seran necessaris més experiments per definir de manera precisa aquest mecanisme. Els nostres resultats mostren que el desenvolupament adient de les espines de noves GCs requereix nivells funcionals de senyalització de Reelina, i que tant l'excés com la mancança d'aquesta via dóna lloc a morfologies atípiques d'espines i sinapsis, menys esfèriques que l'esperat en situacions control.

Reelina i la innervació presinàptica a noves GCs en desenvolupament

La integració de les noves GCs en el circuit sinàptic és clau per la pròpia funció de la neurogènesi adulta a l'hipocamp (Aimone et al., 2006, 2009; Aimone et al., 2011). Desxifrar el mecanisme concret pel qual es regula aquest procés és doncs de gran rellevància.

Alteracions en la via de Reelina es van veure associades amb canvis en el nombre de sinapsis que estableixen els botons presinàptics a noves GCs. Dos factors varen contribuir a aquest fet: En primer lloc, aquestes GCs presentaven menys botons presinàptics del tipus MSB (**Fig. r.5.3f**). En segon lloc, aquests MSBs establien un màxim de 4 sinapsis, mentre que en GCs control aquest número ascendia a 10 (**Fig. r.5.3e**, **g**). Per tant, la connectivitat dels botons innervant noves GCs es va veure afectada tant per la sobreexpressió generalitzada de Reelina com per la interrupció d'aquesta senyalització en la nova GC (**Fig. r.5.3h**).

Observant els nostres resultats, el mateix fenotip final s'ha pogut assolir bé per mitjans independents per tots dos grups experimentals, o bé per una via comuna. Els nostres experiments no permeten resoldre aquesta pregunta, però podríem argumentar que la manera més senzilla d'obtenir dos cops el mateix resultat és anant per un mecanisme comú. En el nostre cas, això només seria possible si el fenotip d'innervació presinàptica estigués provocat per la nova GC. Això suggeriria que tant un augment com una reducció del senyal de Reelina en la nova GC provocaria una senyalització retrògrada al botó presinàptic que s'interpretaria de la mateixa manera. Tot i que nombrosos mecanismes podrien explicar aquest funcionament, per coincidència amb l'anterior fenotip de MIS podríem proposar la involucració de la via de NO. Aquesta molècula s'ha proposat que funciona com un missatger retrògrad a la sinapsi, potenciant la diferenciació a varicositat dels axons presinàptics (Nikonenko et al., 2003; Nikonenko et al., 2008; Hardingham et al., 2013). Alhora, defectes en la senyalització d'aquesta via s'han vist reportats en malalties psiquiàtriques similars a les associades amb disfuncions de Reelina, com depressió, malaltia de Pàrquinson i malaltia d'Alzheimer (Zhou and Zhu, 2009).

Conjuntament amb les observacions referents a la morfologia de les sinapsis i les espines, els nostres resultats mostren que la integració adient de les noves GCs al circuit preexistent pot veure's alterada per insults en la via de Reelina. Aquest concepte és coherent amb estudis previs reportant que tant la manca com l'excés crònic de Reelina poden ser nocius: el primer retardaria el normal desenvolupament de les sinapsis (Trotter et al., 2013) mentre que el segon promouria alteracions en els circuits sinàptics basades en el nombre i morfologia de les espines (Pujadas et al., 2010; Rogers et al., 2013). Explícitament en noves neurones del DG, treballs paral·lels de col·legues han mostrat que totes dues modificacions

provoquen defectes específics en l'arborització dendrítica d'aquestes cèl·lules (Teixeira et al., 2012). En tant que les noves GCs tenen un paper específic en el funcionament del DG (Nakashiba et al., 2012; Akers et al., 2014), els nostres resultats suggereixen que la senyalització de Reelina és un factor important en la regulació de la funció del DG. La desregulació de la neurogènesi adulta en l'hipocamp s'ha vist relacionada amb múltiples desordres cognitius, com la depressió o l'esquizofrènia (Sahay and Hen, 2007; Meyer, 2013).

En resum, els nostres resultats suggereixen que la via de Reelina juga un paper estructural en mecanismes de plasticitat sinàptica que tenen lloc durant la integració de noves GCs a l'hipocamp adult. La rellevància d'aquest procés en la patofisiologia de diferents dolències cognitives i psiquiàtriques suggereix una elevada importància d'aquesta via de senyalització en la regulació dels mecanismes subjacents.

Conclusions

Els resultats obtinguts en aquesta tesi permeten extreure les següents conclusions:

1. La sobreexpressió *in vivo* sostinguda de Reelina desencadena una major complexitat estructural dels botons presinàptics de l'hipocamp adult

2. La sobreexpressió *in vivo* sostinguda de Reelina provoca una hipertròfia de les espines dendrítiques a l'hipocamp adult

3. La Reelina modula la complexitat de l'aparell d'espina i la presència de sinaptopodina d'una manera específica de capa en l'hipocamp adult

4. La Reelina regula la distribució sinàptica-extrasinàptica de les subunitats 2A i 2B de receptors NMDA i de molècules de p-cofilina a l'stratum radiatum de l'hipocamp adult.

5. La sobreexpressió *in vivo* sostinguda de Reelina desencadena una menor densitat d'espines en dendrites de neurones piramidals de capa 5 de S1BF però no en piramidals de CA1, i hipertròfia d'espines dendrítiques en neurones piramidals de capa 5 de S1BF.

6. La escissió condicional de Dab1 en adult en ratolins Cre/flDab1+TAM desencadena una major densitat d'espines en neurones piramidals de capa 5 de S1BF però no en piramidals de CA1, una hipertròfia d'espines en piramidals de S1BF i un encongiment d'espines en piramidals de la CA1.

7. El mètode descrit de microscòpia correlativa OM-FIB/SEM ofereix una aproximació fiable i eficient per a l'obtenció d'imatges d'alta resolució en 3D de dendrites prèviament marcades.

8. Les espines thin representen el tipus més freqüent d'espina en neurones granulars (GCs) de nova generació del gir dentat (DG). La majoria de contactes sinàptics rebuts per aquestes espines tenen lloc sobre el cap de l'espina.

9. Les GCs de nova generació en desenvolupament presenten espines branched. Aquestes espines són més grans, més esfèriques i presenten més volum sinàptic que les no-branched. Els caps d'una espina branched reben sinapsis de botons presinàptics independents.

10. Els paràmetres morfomètrics de les espines i sinapsis de GCs de nova generació del DG presenten una distribució contínua de valors. El volum de l'espina correlaciona positivament amb el volum de la sinapsi i negativament amb l'esfericitat de l'espina i l'esfericitat de la sinapsi. Aquests parells de magnituds mostren relacions lineals per espines amb volums per sota d'un cert llindar.

11. Les espines de GCs de nova generació en desenvolupament són més esfèriques a 8-9 setmanes que a 3-4 setmanes.

12. Les espines de GCs de nova generació estan innervades preferentment per botons multisinàptics (MSBs). Els MSBs que contacten GCs de 8-9 setmanes estableixen més sinapsis que els MSBs que contacten GCs de 3-4 setmanes.

13. Les GCs de nova generació de 8-9 setmanes presenten alteracions estructurals a raó tant de la sobreexpressió com de la depleció de la via de Reelina. Les GCs de 8-9 setmanes presenten hipertròfia d'espina i de sinapsi en casos de sobreexpressió de Reelina, i sinapsis més petites en casos de depleció de Dab1.

14. Les espines de GCs de nova generació en desenvolupament Reelin-OE i Dab1-KO estan innervades preferentment per MSBs. Els MSBs que contacten GCs de 8-9 setmanes tant d'animals Reelin-OE com cèl·lules Dab1-KO estableixen menys sinapsis que els MSBs que contacten GCs WT de la mateixa edat.

References

Abdolmaleky HM, Cheng KH, Russo A, Smith CL, Faraone SV, Wilcox M, Shafa R, Glatt SJ, Nguyen G, Ponte JF, Thiagalingam S, Tsuang MT (2005) Hypermethylation of the reelin (RELN) promoter in the brain of schizophrenic patients: a preliminary report. Am J Med Genet B Neuropsychiatr Genet 134B:60-66.

Abraham H, Meyer G (2003) Reelin-expressing neurons in the postnatal and adult human hippocampal formation. Hippocampus 13:715-727.

Ackermann M, Matus A (2003) Activity-induced targeting of profilin and stabilization of dendritic spine morphology. Nat Neurosci 6:1194-1200.

Adams I, Jones DG (1982) Quantitative ultrastructural changes in rat cortical synapses during early-, mid- and late-adulthood. Brain Res 239:349-363.

Aguado F, Diaz-Ruiz C, Parlato R, Martinez A, Carmona MA, Bleckmann S, Urena JM, Burgaya F, del Rio JA, Schutz G, Soriano E (2009) The CREB/CREM transcription factors negatively regulate early synaptogenesis and spontaneous network activity. J Neurosci 29:328-333.

Aimone JB, Wiles J, Gage FH (2006) Potential role for adult neurogenesis in the encoding of time in new memories. Nat Neurosci 9:723-727.

Aimone JB, Wiles J, Gage FH (2009) Computational influence of adult neurogenesis on memory encoding. Neuron 61:187-202.

Aimone JB, Deng W, Gage FH (2011) Resolving new memories: a critical look at the dentate gyrus, adult neurogenesis, and pattern separation. Neuron 70:589-596.

Akers KG, Martinez-Canabal A, Restivo L, Yiu AP, De Cristofaro A, Hsiang HL, Wheeler AL, Guskjolen A, Niibori Y, Shoji H, Ohira K, Richards BA, Miyakawa T, Josselyn SA, Frankland PW (2014) Hippocampal neurogenesis regulates forgetting during adulthood and infancy. Science 344:598-602.

Alcantara S, Ruiz M, D'Arcangelo G, Ezan F, de Lecea L, Curran T, Sotelo C, Soriano E (1998) Regional and cellular patterns of reelin mRNA expression in the forebrain of the developing and adult mouse. J Neurosci 18:7779-7799.

Allegra Mascaro AL, Cesare P, Sacconi L, Grasselli G, Mandolesi G, Maco B, Knott GW, Huang L, De Paola V, Strata P, Pavone FS (2013) In vivo single branch axotomy induces GAP-43-dependent sprouting and synaptic remodeling in cerebellar cortex. Proc Natl Acad Sci U S A 110:10824-10829.

Amaral DG, Scharfman HE, Lavenex P (2007) The dentate gyrus: fundamental neuroanatomical organization (dentate gyrus for dummies). Prog Brain Res 163:3-22.

Andersen P, Morris RG, Amaral D, Bliss TV, O'Keefe J (2007) The Hippocampus Book. New York: Oxford University Press.

Antonucci F, Corradini I, Morini R, Fossati G, Menna E, Pozzi D, Pacioni S, Verderio C, Bacci A, Matteoli M (2013) Reduced SNAP-25 alters short-term plasticity at developing glutamatergic synapses. EMBO Rep 14:645-651.

Aoki C, Rhee J, Lubin M, Dawson TM (1997) NMDA-R1 subunit of the cerebral cortex co-localizes with neuronal nitric oxide synthase at pre- and postsynaptic sites and in spines. Brain Res 750:25-40.

Araya R, Jiang J, Eisenthal KB, Yuste R (2006) The spine neck filters membrane potentials. Proc Natl Acad Sci U S A 103:17961-17966.

Arber S, Barbayannis FA, Hanser H, Schneider C, Stanyon CA, Bernard O, Caroni P (1998) Regulation of actin dynamics through phosphorylation of cofilin by LIM-kinase. Nature 393:805-809.

Arellano JI, Benavides-Piccione R, Defelipe J, Yuste R (2007a) Ultrastructure of dendritic spines: correlation between synaptic and spine morphologies. Front Neurosci 1:131-143.

Arellano JI, Espinosa A, Fairen A, Yuste R, DeFelipe J (2007b) Non-synaptic dendritic spines in neocortex. Neuroscience 145:464-469.

Arnaud L, Ballif BA, Cooper JA (2003a) Regulation of protein tyrosine kinase signaling by substrate degradation during brain development. Mol Cell Biol 23:9293-9302.

Arnaud L, Ballif BA, Forster E, Cooper JA (2003b) Fyn tyrosine kinase is a critical regulator of disabled-1 during brain development. Curr Biol 13:9-17.

Assadi AH, Zhang G, Beffert U, McNeil RS, Renfro AL, Niu S, Quattrocchi CC, Antalffy BA, Sheldon

M, Armstrong DD, Wynshaw-Boris A, Herz J, D'Arcangelo G, Clark GD (2003) Interaction of reelin signaling and Lis1 in brain development. Nat Genet 35:270-276.

Badea A, Nicholls PJ, Johnson GA, Wetsel WC (2007) Neuroanatomical phenotypes in the reeler mouse. Neuroimage 34:1363-1374.

Bal M, Leitz J, Reese AL, Ramirez DM, Durakoglugil M, Herz J, Monteggia LM, Kavalali ET (2013) Reelin mobilizes a VAMP7-dependent synaptic vesicle pool and selectively augments spontaneous neurotransmission. Neuron 80:934-946.

Ballesteros-Yanez I, Benavides-Piccione R, Elston GN, Yuste R, DeFelipe J (2006) Density and morphology of dendritic spines in mouse neocortex. Neuroscience 138:403-409.

Ballif BA, Arnaud L, Arthur WT, Guris D, Imamoto A, Cooper JA (2004) Activation of a Dab1/CrkL/C3G/Rap1 pathway in Reelin-stimulated neurons. Curr Biol 14:606-610.

Bar I, Lambert De Rouvroit C, Royaux I, Krizman DB, Dernoncourt C, Ruelle D, Beckers MC, Goffinet AM (1995) A YAC contig containing the reeler locus with preliminary characterization of candidate gene fragments. Genomics 26:543-549.

Barr CL, Feng Y, Wigg K, Bloom S, Roberts W, Malone M, Schachar R, Tannock R, Kennedy JL (2000) Identification of DNA variants in the SNAP-25 gene and linkage study of these polymorphisms and attention-deficit hyperactivity disorder. Mol Psychiatry 5:405-409.

Barria A, Malinow R (2002) Subunit-specific NMDA receptor trafficking to synapses. Neuron 35:345-353.

Barria A, Muller D, Derkach V, Griffith LC, Soderling TR (1997) Regulatory phosphorylation of AMPA-type glutamate receptors by CaM-KII during long-term potentiation. Science 276:2042-2045.

Bas Orth C, Vlachos A, Del Turco D, Burbach GJ, Haas CA, Mundel P, Feng G, Frotscher M, Deller T (2005) Lamina-specific distribution of Synaptopodin, an actin-associated molecule essential for the spine apparatus, in identified principal cell dendrites of the mouse hippocampus. J Comp Neurol 487:227-239.

Baude A, Nusser Z, Roberts JD, Mulvihill E, McIlhinney RA, Somogyi P (1993) The metabotropic glutamate receptor (mGluR1 alpha) is concentrated at perisynaptic membrane of neuronal subpopulations as detected by immunogold reaction. Neuron 11:771-787.

Beffert U, Morfini G, Bock HH, Reyna H, Brady ST, Herz J (2002) Reelin-mediated signaling locally regulates protein kinase B/Akt and glycogen synthase kinase 3beta. J Biol Chem 277:49958-49964.

Beffert U, Weeber EJ, Durudas A, Qiu S, Masiulis I, Sweatt JD, Li WP, Adelmann G, Frotscher M, Hammer RE, Herz J (2005) Modulation of synaptic plasticity and memory by Reelin involves differential splicing of the lipoprotein receptor Apoer2. Neuron 47:567-579.

Bekkers JM (2000) Distribution and activation of voltage-gated potassium channels in cell-attached and outside-out patches from large layer 5 cortical pyramidal neurons of the rat. J Physiol 525 Pt 3:611-620.

Benavides-Piccione R, Ballesteros-Yanez I, DeFelipe J, Yuste R (2002) Cortical area and species differences in dendritic spine morphology. J Neurocytol 31:337-346.

Benavides-Piccione R, Fernaud-Espinosa I, Robles V, Yuste R, DeFelipe J (2013) Age-based comparison of human dendritic spine structure using complete three-dimensional reconstructions. Cereb Cortex 23:1798-1810.

Benavides-Piccione R, Dierssen M, Ballesteros-Yanez I, Martinez de Lagran M, Arbones ML, Fotaki V, DeFelipe J, Elston GN (2005) Alterations in the phenotype of neocortical pyramidal cells in the Dyrk1A+/- mouse. Neurobiol Dis 20:115-122.

Binzegger T, Douglas RJ, Martin KA (2004) A quantitative map of the circuit of cat primary visual cortex. J Neurosci 24:8441-8453.

Blackstad TW (1965) Mapping of experimental axon degeneration by electron microscopy of Golgi preparations. Z Zellforsch Mikrosk Anat 67:819-834.

Blackwood DH, Fordyce A, Walker MT, St Clair DM, Porteous DJ, Muir WJ (2001) Schizophrenia and affective disorders--cosegregation with a translocation at chromosome 1q42 that directly disrupts brain-expressed genes: clinical and P300 findings in a family. Am J Hum Genet 69:428-433.

Bock DD, Lee WC, Kerlin AM, Andermann ML, Hood G, Wetzel AW, Yurgenson S, Soucy ER, Kim HS, Reid RC (2011) Network anatomy and in vivo physiology of visual cortical neurons. Nature 471:177-182.

Boczkowska M, Rebowski G, Kast DJ, Dominguez R (2014) Structural analysis of the transitional state of Arp2/3 complex activation by two actin-bound WCAs. Nat Commun 5:3308.

Borrell V, Pujadas L, Simo S, Dura D, Sole M, Cooper JA, Del Rio JA, Soriano E (2007) Reelin and mDab1 regulate the development of hippocampal connections. Mol Cell Neurosci 36:158-173.

Borrell V, Del Rio JA, Alcantara S, Derer M, Martinez A, D'Arcangelo G, Nakajima K, Mikoshiba K, Derer P, Curran T, Soriano E (1999) Reelin regulates the development and synaptogenesis of the layer-specific entorhino-hippocampal connections. J Neurosci 19:1345-1358.

Botella-Lopez A, Cuchillo-Ibanez I, Cotrufo T, Mok SS, Li QX, Barquero MS, Dierssen M, Soriano E, Saez-Valero J (2010) Beta-amyloid controls altered Reelin expression and processing in Alzheimer's disease. Neurobiol Dis 37:682-691.

Botella-Lopez A, Burgaya F, Gavin R, Garcia-Ayllon MS, Gomez-Tortosa E, Pena-Casanova J, Urena JM, Del Rio JA, Blesa R, Soriano E, Saez-Valero J (2006) Reelin expression and glycosylation patterns are altered in Alzheimer's disease. Proc Natl Acad Sci U S A 103:5573-5578.

Bouche E, Romero-Ortega MI, Henkemeyer M, Catchpole T, Leemhuis J, Frotscher M, May P, Herz J, Bock HH (2013) Reelin induces EphB activation. Cell Res 23:473-490.

Bourne J, Harris KM (2007) Do thin spines learn to be mushroom spines that remember? Curr Opin Neurobiol 17:381-386.

Bourne JN, Harris KM (2008) Balancing structure and function at hippocampal dendritic spines. Annu Rev Neurosci 31:47-67.

Bourne JN, Harris KM (2011) Coordination of size and number of excitatory and inhibitory synapses results in a balanced structural plasticity along mature hippocampal CA1 dendrites during LTP. Hippocampus 21:354-373.

Bourne JN, Chirillo MA, Harris KM (2013) Presynaptic ultrastructural plasticity along CA3-->CA1 axons during long-term potentiation in mature hippocampus. J Comp Neurol 521:3898-3912.

Boyle MP, Bernard A, Thompson CL, Ng L, Boe A, Mortrud M, Hawrylycz MJ, Jones AR, Hevner RF, Lein ES (2011) Cell-type-specific consequences of Reelin deficiency in the mouse neocortex, hippocampus, and amygdala. J Comp Neurol 519:2061-2089.

Bramham CR (2008) Local protein synthesis, actin dynamics, and LTP consolidation. Curr Opin Neurobiol 18:524-531.

Branco T, Hausser M (2010) The single dendritic branch as a fundamental functional unit in the nervous system. Curr Opin Neurobiol 20:494-502.

Briggman KL, Denk W (2006) Towards neural circuit reconstruction with volume electron microscopy techniques. Curr Opin Neurobiol 16:562-570.

Briggman KL, Bock DD (2012) Volume electron microscopy for neuronal circuit reconstruction. Curr Opin Neurobiol 22:154-161.

Brigman JL, Wright T, Talani G, Prasad-Mulcare S, Jinde S, Seabold GK, Mathur P, Davis MI, Bock R, Gustin RM, Colbran RJ, Alvarez VA, Nakazawa K, Delpire E, Lovinger DM, Holmes A (2010) Loss of GluN2B-containing NMDA receptors in CA1 hippocampus and cortex impairs long-term depression, reduces dendritic spine density, and disrupts learning. J Neurosci 30:4590-4600.

Bushby AJ, P'Ng K M, Young RD, Pinali C, Knupp C, Quantock AJ (2011) Imaging three-dimensional tissue architectures by focused ion beam scanning electron microscopy. Nat Protoc 6:845-858.

Cajal S (1888) Estructura de los centros nerviosos de las aves. Revista Trimestral de Histología Normal y Patológica 1:10.

Cajal S (1889) Conexión general de los elementos nerviosos. La Medicina Práctica 88:341-346.

Cajal S (1890) Textura de las circunvoluciones cerebrales de los mamíferos inferiores. Nota preventiva. . Gac Méd Catalana 1:22-31.

Cajal S (1891) Sur la structure de l'écorce cérébrale de quelques mammifères. La Cellule 7:51.

Cajal S (1904) La textura del sistema nervioso del hombre y los vertebrados. Madrid: Moya.

Cajal S (1911) Histologie du système nerveux de l'home et des vertébrés. Paris.

Cajal S (1917) Recuerdos de mi vida, Vol.2. Historia de mi labor científica. Madrid: Moya.

Cajal S (1933) ¿Neuronismo o reticularismo? Las pruebas objetivas de la unidad anatómica de las células nerviosas. Arch Neurobiol 13:1-144.

Campo CG, Sinagra M, Verrier D, Manzoni OJ, Chavis P (2009) Reelin secreted by GABAergic neurons regulates glutamate receptor homeostasis. PLoS One 4:e5505.

Cane M, Maco B, Knott G, Holtmaat A (2014) The Relationship between PSD-95 Clustering and Spine Stability In Vivo. J Neurosci 34:2075-2086.

Caviness VS, Jr. (1982) Neocortical histogenesis in normal and reeler mice: a developmental study based upon [3H]thymidine autoradiography. Brain Res 256:293-302.

Caviness VS, Jr., Sidman RL (1973) Time of origin or corresponding cell classes in the cerebral cortex of normal and reeler mutant mice: an autoradiographic analysis. J Comp Neurol 148:141-151.

Cesca F, Baldelli P, Valtorta F, Benfenati F (2010) The synapsins: key actors of synapse function and plasticity. Prog Neurobiol 91:313-348.

Cingolani LA, Goda Y (2008) Actin in action: the interplay between the actin cytoskeleton and synaptic efficacy. Nat Rev Neurosci 9:344-356.

Colgan LA, Yasuda R (2014) Plasticity of dendritic spines: subcompartmentalization of signaling. Annu Rev Physiol 76:365-385.

Colonnier M (1968) Synaptic patterns on different cell types in the different laminae of the cat visual cortex. An electron microscope study. Brain Res 9:268-287.

Cooper JA (2008) A mechanism for inside-out lamination in the neocortex. Trends Neurosci 31:113-119.

Costa E, Davis J, Grayson DR, Guidotti A, Pappas GD, Pesold C (2001) Dendritic spine hypoplasticity and downregulation of reelin and GABAergic tone in schizophrenia vulnerability. Neurobiol Dis 8:723-742.

Cremer CM, Lubke JH, Palomero-Gallagher N, Zilles K (2011) Laminar distribution of neurotransmitter receptors in different reeler mouse brain regions. Brain Struct Funct 216:201-218.

Czarnecki K, Haas CA, Bas Orth C, Deller T, Frotscher M (2005) Postnatal development of synaptopodin expression in the rodent hippocampus. J Comp Neurol 490:133-144.

Chadderton P, Schaefer AT, Williams SR, Margrie TW (2014) Sensory-evoked synaptic integration in cerebellar and cerebral cortical neurons. Nat Rev Neurosci 15:71-83.

Chai X, Forster E, Zhao S, Bock HH, Frotscher M (2009) Reelin stabilizes the actin cytoskeleton of neuronal processes by inducing n-cofilin phosphorylation at serine3. J Neurosci 29:288-299.

Chen Y, Sharma RP, Costa RH, Costa E, Grayson DR (2002) On the epigenetic regulation of the human reelin promoter. Nucleic Acids Res 30:2930-2939.

Chen Y, Beffert U, Ertunc M, Tang TS, Kavalali ET, Bezprozvanny I, Herz J (2005) Reelin modulates NMDA receptor activity in cortical neurons. J Neurosci 25:8209-8216.

Chin J, Massaro CM, Palop JJ, Thwin MT, Yu GQ, Bien-Ly N, Bender A, Mucke L (2007) Reelin depletion in the entorhinal cortex of human amyloid precursor protein transgenic mice and humans with Alzheimer's disease. J Neurosci 27:2727-2733.

D'Arcangelo G, Curran T (1998) Reeler: new tales on an old mutant mouse. Bioessays 20:235-244.

D'Arcangelo G, Miao GG, Chen SC, Soares HD, Morgan JI, Curran T (1995) A protein related to extracellular matrix proteins deleted in the mouse mutant reeler. Nature 374:719-723.

D'Arcangelo G, Nakajima K, Miyata T, Ogawa M, Mikoshiba K, Curran T (1997) Reelin is a secreted glycoprotein recognized by the CR-50 monoclonal antibody. J Neurosci 17:23-31.

D'Arcangelo G, Homayouni R, Keshvara L, Rice DS, Sheldon M, Curran T (1999) Reelin is a ligand for lipoprotein receptors. Neuron 24:471-479.

Dailey ME, Smith SJ (1996) The dynamics of dendritic structure in developing hippocampal slices. J Neurosci 16:2983-2994.

Defelipe J (2011) The evolution of the brain, the human nature of cortical circuits, and intellectual creativity. Front Neuroanat 5:29.

del Rio JA, Martinez A, Fonseca M, Auladell C, Soriano E (1995) Glutamate-like immunoreactivity and fate of Cajal-Retzius cells in the murine cortex as identified with calretinin antibody. Cereb Cortex 5:13-21.

Del Rio JA, Heimrich B, Borrell V, Forster E, Drakew A, Alcantara S, Nakajima K, Miyata T, Ogawa M, Mikoshiba K, Derer P, Frotscher M, Soriano E (1997) A role for Cajal-Retzius cells and reelin in the development of hippocampal connections. Nature 385:70-74.

Deller T, Merten T, Roth SU, Mundel P, Frotscher M (2000) Actin-associated protein synaptopodin in the rat hippocampal formation: localization in the spine neck and close association with the spine apparatus of principal neurons. J Comp Neurol 418:164-181.

Deller T, Bas Orth C, Vlachos A, Merten T, Del Turco D, Dehn D, Mundel P, Frotscher M (2006) Plasticity of synaptopodin and the spine apparatus organelle in the rat fascia dentata following entorhinal cortex lesion. J Comp Neurol 499:471-484.

Deller T, Haas CA, Deissenrieder K, Del Turco D, Coulin C, Gebhardt C, Drakew A, Schwarz K, Mundel P, Frotscher M (2002) Laminar distribution of synaptopodin in normal and reeler mouse brain depends on the position of spine-bearing neurons. J Comp Neurol 453:33-44.

Deller T, Korte M, Chabanis S, Drakew A, Schwegler H, Stefani GG, Zuniga A, Schwarz K, Bonhoeffer T, Zeller R, Frotscher M, Mundel P (2003) Synaptopodin-deficient mice lack a spine apparatus and show deficits in synaptic plasticity. Proc Natl Acad Sci U S A 100:10494-10499.

Deng W, Aimone JB, Gage FH (2010) New neurons and new memories: how does adult hippocampal neurogenesis affect learning and memory? Nat Rev Neurosci 11:339-350.

Derer P, Derer M, Goffinet A (2001) Axonal secretion of Reelin by Cajal-Retzius cells: evidence from comparison of normal and Reln(Orl) mutant mice. J Comp Neurol 440:136-143.

Derkach V, Barria A, Soderling TR (1999) Ca2+/calmodulin-kinase II enhances channel conductance of alpha-amino-3-hydroxy-5-methyl-4-isoxazolepropionate type glutamate receptors. Proc Natl Acad Sci U S A 96:3269-3274.

DeSilva U, D'Arcangelo G, Braden VV, Chen J, Miao GG, Curran T, Green ED (1997) The human reelin gene: isolation, sequencing, and mapping on chromosome 7. Genome Research 7:157-164.

Diaz-Ruiz C, Parlato R, Aguado F, Urena JM, Burgaya F, Martinez A, Carmona MA, Kreiner G, Bleckmann S, Del Rio JA, Schutz G, Soriano E (2008) Regulation of neural migration by the CREB/CREM transcription factors and altered Dab1 levels in CREB/CREM mutants. Mol Cell Neurosci 39:519-528.

Doehner J, Madhusudan A, Konietzko U, Fritschy JM, Knuesel I (2010) Co-localization of Reelin and proteolytic AbetaPP fragments in hippocampal plaques in aged wild-type mice. J Alzheimers Dis 19:1339-1357.

Dong E, Guidotti A, Grayson DR, Costa E (2007) Histone hyperacetylation induces demethylation of reelin and 67-kDa glutamic acid decarboxylase promoters. Proc Natl Acad Sci U S A 104:4676-4681.

Dong E, Caruncho H, Liu WS, Smalheiser NR, Grayson DR, Costa E, Guidotti A (2003) A reelin-integrin receptor interaction regulates Arc mRNA translation in synaptoneurosomes. Proc Natl Acad Sci U S A 100:5479-5484.

Duit S, Mayer H, Blake SM, Schneider WJ, Nimpf J (2010) Differential functions of ApoER2 and very low density lipoprotein receptor in Reelin signaling depend on differential sorting of the receptors. J Biol Chem 285:4896-4908.

Dulabon L, Olson EC, Taglienti MG, Eisenhuth S, McGrath B, Walsh CA, Kreidberg JA, Anton ES (2000) Reelin binds alpha3beta1 integrin and inhibits neuronal migration. Neuron 27:33-44.

Dumitriu D, Rodriguez A, Morrison JH (2011) High-throughput, detailed, cell-specific neuroanatomy of dendritic spines using microinjection and confocal microscopy. Nat Protoc 6:1391-1411.

Durakoglugil MS, Chen Y, White CL, Kavalali ET, Herz J (2009) Reelin signaling antagonizes beta-amyloid at the synapse. Proc Natl Acad Sci U S A 106:15938-15943.

Duveau V, Madhusudan A, Caleo M, Knuesel I, Fritschy JM (2011) Impaired reelin processing and secretion by Cajal-Retzius cells contributes to granule cell dispersion in a mouse model of temporal lobe epilepsy.

Hippocampus 21:935-944.

Egorov AV, Hamam BN, Fransen E, Hasselmo ME, Alonso AA (2002) Graded persistent activity in entorhinal cortex neurons. Nature 420:173-178.

Elston GN (2003) Cortex, cognition and the cell: new insights into the pyramidal neuron and prefrontal function. Cereb Cortex 13:1124-1138.

Elston GN, DeFelipe J (2002) Spine distribution in cortical pyramidal cells: a common organizational principle across species. Prog Brain Res 136:109-133.

Eriksson PS, Perfilieva E, Bjork-Eriksson T, Alborn AM, Nordborg C, Peterson DA, Gage FH (1998) Neurogenesis in the adult human hippocampus. Nat Med 4:1313-1317.

Fairen A (2005) Pioneering a golden age of cerebral microcircuits: the births of the combined Golgi-electron microscope methods. Neuroscience 136:607-614.

Fairen A, Peters A, Saldanha J (1977) A new procedure for examining Golgi impregnated neurons by light and electron microscopy. J Neurocytol 6:311-337.

Fatemi SH, Earle JA, McMenomy T (2000) Reduction in Reelin immunoreactivity in hippocampus of subjects with schizophrenia, bipolar disorder and major depression. Mol Psychiatry 5:654-663, 571.

Feldmeyer D, Brecht M, Helmchen F, Petersen CC, Poulet JF, Staiger JF, Luhmann HJ, Schwarz C (2013) Barrel cortex function. Prog Neurobiol 103:3-27.

Feng G, Mellor RH, Bernstein M, Keller-Peck C, Nguyen QT, Wallace M, Nerbonne JM, Lichtman JW, Sanes JR (2000) Imaging neuronal subsets in transgenic mice expressing multiple spectral variants of GFP. Neuron 28:41-51.

Feng L, Cooper JA (2009) Dual functions of Dab1 during brain development. Mol Cell Biol 29:324-332.

Feng L, Allen NS, Simo S, Cooper JA (2007) Cullin 5 regulates Dab1 protein levels and neuron positioning during cortical development. Genes Dev 21:2717-2730.

Ferrante M, Migliore M, Ascoli GA (2013) Functional impact of dendritic branch-point morphology. J Neurosci 33:2156-2165.

Fiala JC (2005) Reconstruct: a free editor for serial section microscopy. J Microsc 218:52-61.

Fiala JC, Allwardt B, Harris KM (2002a) Dendritic spines do not split during hippocampal LTP or maturation. Nat Neurosci 5:297-298.

Fiala JC, Spacek J, Harris KM (2002b) Dendritic spine pathology: cause or consequence of neurological disorders? Brain Res Brain Res Rev 39:29-54.

Fifkova E, Markham JA, Delay RJ (1983) Calcium in the spine apparatus of dendritic spines in the dentate molecular layer. Brain Res 266:163-168.

Folsom TD, Fatemi SH (2013) The involvement of Reelin in neurodevelopmental disorders. Neuropharmacology 68:122-135.

Forster E, Zhao S, Frotscher M (2006) Laminating the hippocampus. Nat Rev Neurosci 7:259-267.

Foster KA, McLaughlin N, Edbauer D, Phillips M, Bolton A, Constantine-Paton M, Sheng M (2010) Distinct roles of NR2A and NR2B cytoplasmic tails in long-term potentiation. J Neurosci 30:2676-2685.

Fournier NM, Darnbrough AL, Wintink AJ, Kalynchuk LE (2009) Altered synapsin I immunoreactivity and fear behavior in male and female rats subjected to long-term amygdala kindling. Behav Brain Res 196:106-115.

Frankland PW, Kohler S, Josselyn SA (2013) Hippocampal neurogenesis and forgetting. Trends Neurosci 36:497-503.

Freire M (1978) Effects of dark rearing on dendritic spines in layer IV of the mouse visual cortex. A quantitative electron microscopical study. J Anat 126:193-201.

Freund TF, Buzsaki G (1996) Interneurons of the hippocampus. Hippocampus 6:347-470.

Frotscher M (1998) Cajal-Retzius cells, Reelin, and the formation of layers. Curr Opin Neurobiol 8:570-575.

Gage FH (2000) Mammalian neural stem cells. Science 287:1433-1438.

Gambrill AC, Barria A (2011) NMDA receptor subunit composition controls synaptogenesis and synapse stabilization. Proc Natl Acad Sci U S A 108:5855-5860.

Gao Z, Ure K, Ables JL, Lagace DC, Nave KA, Goebbels S, Eisch AJ, Hsieh J (2009) Neurod1 is essential for the survival and maturation of adult-born neurons. Nat Neurosci 12:1090-1092.

Gardoni F, Mauceri D, Malinverno M, Polli F, Costa C, Tozzi A, Siliquini S, Picconi B, Cattabeni F, Calabresi P, Di Luca M (2009) Decreased NR2B subunit synaptic levels cause impaired long-term potentiation but not long-term depression. J Neurosci 29:669-677.

Ge S, Yang CH, Hsu KS, Ming GL, Song H (2007) A critical period for enhanced synaptic plasticity in newly generated neurons of the adult brain. Neuron 54:559-566.

Geinisman Y, Morrell F, deToledo-Morrell L (1989) Perforated synapses on double-headed dendritic spines: a possible structural substrate of synaptic plasticity. Brain Res 480:326-329.

Geinisman Y, Berry RW, Disterhoft JF, Power JM, Van der Zee EA (2001) Associative learning elicits the formation of multiple-synapse boutons. J Neurosci 21:5568-5573.

Goffinet AM (1983) The embryonic development of the cerebellum in normal and reeler mutant mice. Anat Embryol (Berl) 168:73-86.

Goffinet AM, Dernoncourt C (1991) Localization of the reeler gene relative to flanking loci on mouse chromosome 5. Mamm Genome 1:100-103.

Goldowitz D, Cushing RC, Laywell E, D'Arcangelo G, Sheldon M, Sweet HO, Davisson M, Steindler D, Curran T (1997) Cerebellar disorganization characteristic of reeler in scrambler mutant mice despite presence of reelin. J Neurosci 17:8767-8777.

Gomperts SN, Rao A, Craig AM, Malenka RC, Nicoll RA (1998) Postsynaptically silent synapses in single neuron cultures. Neuron 21:1443-1451.

Gonzalez-Billault C, Del Rio JA, Urena JM, Jimenez-Mateos EM, Barallobre MJ, Pascual M, Pujadas L, Simo S, Torre AL, Gavin R, Wandosell F, Soriano E, Avila J (2005) A role of MAP1B in Reelin-dependent neuronal migration. Cereb Cortex 15:1134-1145.

Gordon U, Polsky A, Schiller J (2006) Plasticity compartments in basal dendrites of neocortical pyramidal neurons. J Neurosci 26:12717-12726.

Gray EG (1959) Axo-somatic and axo-dendritic synapses of the cerebral cortex: an electron microscope study. J Anat 93:420-433.

Greger IH, Esteban JA (2007) AMPA receptor biogenesis and trafficking. Curr Opin Neurobiol 17:289-297.

Groc L, Choquet D, Stephenson FA, Verrier D, Manzoni OJ, Chavis P (2007) NMDA receptor surface trafficking and synaptic subunit composition are developmentally regulated by the extracellular matrix protein Reelin. J Neurosci 27:10165-10175.

Groc L, Heine M, Cousins SL, Stephenson FA, Lounis B, Cognet L, Choquet D (2006) NMDA receptor surface mobility depends on NR2A-2B subunits. Proc Natl Acad Sci U S A 103:18769-18774.

Gu J, Lee CW, Fan Y, Komlos D, Tang X, Sun C, Yu K, Hartzell HC, Chen G, Bamburg JR, Zheng JQ (2010) ADF/cofilin-mediated actin dynamics regulate AMPA receptor trafficking during synaptic plasticity. Nat Neurosci 13:1208-1215.

Guidotti A, Ruzicka W, Grayson DR, Veldic M, Pinna G, Davis JM, Costa E (2007) S-adenosyl methionine and DNA methyltransferase-1 mRNA overexpression in psychosis. Neuroreport 18:57-60.

Guidotti A, Auta J, Davis JM, Di-Giorgi-Gerevini V, Dwivedi Y, Grayson DR, Impagnatiello F, Pandey G, Pesold C, Sharma R, Uzunov D, Costa E (2000) Decrease in reelin and glutamic acid decarboxylase67 (GAD67) expression in schizophrenia and bipolar disorder: a postmortem brain study. Arch Gen Psychiatry 57:1061-1069.

Gulyas AI, Miles R, Hajos N, Freund TF (1993) Precision and variability in postsynaptic target selection of inhibitory cells in the hippocampal CA3 region. Eur J Neurosci 5:1729-1751.

Gulledge AT, Carnevale NT, Stuart GJ (2012) Electrical advantages of dendritic spines. PLoS One 7:e36007.

Haas CA, Frotscher M (2010) Reelin deficiency causes granule cell dispersion in epilepsy. Exp Brain Res 200:141-149.

Haas CA, Dudeck O, Kirsch M, Huszka C, Kann G, Pollak S, Zentner J, Frotscher M (2002) Role for reelin in the development of granule cell dispersion in temporal lobe epilepsy. J Neurosci 22:5797-5802.

Hardingham N, Dachtler J, Fox K (2013) The role of nitric oxide in pre-synaptic plasticity and homeostasis. Front Cell Neurosci 7:190.

Harris KM, Stevens JK (1989) Dendritic spines of CA 1 pyramidal cells in the rat hippocampus: serial electron microscopy with reference to their biophysical characteristics. J Neurosci 9:2982-2997.

Harris KM, Weinberg RJ (2012) Ultrastructure of synapses in the mammalian brain. Cold Spring Harb Perspect Biol 4.

Harris KM, Jensen FE, Tsao B (1992) Three-dimensional structure of dendritic spines and synapses in rat hippocampus (CA1) at postnatal day 15 and adult ages: implications for the maturation of synaptic physiology and long-term potentiation. J Neurosci 12:2685-2705.

Harris KM, Perry E, Bourne J, Feinberg M, Ostroff L, Hurlburt J (2006) Uniform serial sectioning for transmission electron microscopy. J Neurosci 26:12101-12103.

Hazai D, Szudoczki R, Ding J, Soderling SH, Weinberg RJ, Sotonyi P, Racz B (2013) Ultrastructural abnormalities in CA1 hippocampus caused by deletion of the actin regulator WAVE-1. PLoS One 8:e75248.

He Y, Janssen WG, Rothstein JD, Morrison JH (2000) Differential synaptic localization of the glutamate transporter EAAC1 and glutamate receptor subunit GluR2 in the rat hippocampus. J Comp Neurol 418:255-269.

Helmstaedter M (2013) Cellular-resolution connectomics: challenges of dense neural circuit reconstruction. Nat Methods 10:501-507.

Helmstaedter M, Briggman KL, Denk W (2008) 3D structural imaging of the brain with photons and electrons. Curr Opin Neurobiol 18:633-641.

Hellwig S, Hack I, Kowalski J, Brunne B, Jarowyj J, Unger A, Bock HH, Junghans D, Frotscher M (2011) Role for Reelin in neurotransmitter release. J Neurosci 31:2352-2360.

Herrmann G, Mishev G, Scotti AL (2008) Olfactory bulb interneurons releasing NO exhibit the Reelin receptor ApoEr2 and part of those targeted by NO express Reelin. J Chem Neuroanat 36:160-169.

Herz J, Chen Y (2006) Reelin, lipoprotein receptors and synaptic plasticity. Nat Rev Neurosci 7:850-859.

Hiesberger T, Trommsdorff M, Howell BW, Goffinet A, Mumby MC, Cooper JA, Herz J (1999) Direct binding of Reelin to VLDL receptor and ApoE receptor 2 induces tyrosine phosphorylation of disabled-1 and modulates tau phosphorylation. Neuron 24:481-489.

Hill TC, Zito K (2013) LTP-induced long-term stabilization of individual nascent dendritic spines. J Neurosci 33:678-686.

Hirotsune S, Takahara T, Sasaki N, Hirose K, Yoshiki A, Ohashi T, Kusakabe M, Murakami Y, Muramatsu M, Watanabe S, et al. (1995) The reeler gene encodes a protein with an EGF-like motif expressed by pioneer neurons. Nat Genet 10:77-83.

Hoe HS, Pocivavsek A, Chakraborty G, Fu Z, Vicini S, Ehlers MD, Rebeck GW (2006) Apolipoprotein E receptor 2 interactions with the N-methyl-D-aspartate receptor. J Biol Chem 281:3425-3431.

Hoe HS, Lee KJ, Carney RS, Lee J, Markova A, Lee JY, Howell BW, Hyman BT, Pak DT, Bu G, Rebeck GW (2009) Interaction of reelin with amyloid precursor protein promotes neurite outgrowth. J Neurosci 29:7459-7473.

Hoffman DA, Magee JC, Colbert CM, Johnston D (1997) K+ channel regulation of signal propagation in dendrites of hippocampal pyramidal neurons. Nature 387:869-875.

Hoffpauir BK, Pope BA, Spirou GA (2007) Serial sectioning and electron microscopy of large tissue volumes for 3D analysis and reconstruction: a case study of the calyx of Held. Nat Protoc 2:9-22.

Holderith N, Lorincz A, Katona G, Rozsa B, Kulik A, Watanabe M, Nusser Z (2012) Release probability of hippocampal glutamatergic terminals scales with the size of the active zone. Nat Neurosci 15:988-997.

Homayouni R, Rice DS, Sheldon M, Curran T (1999) Disabled-1 binds to the cytoplasmic domain of

amyloid precursor-like protein 1. J Neurosci 19:7507-7515.

Hong SE, Shugart YY, Huang DT, Shahwan SA, Grant PE, Hourihane JO, Martin ND, Walsh CA (2000) Autosomal recessive lissencephaly with cerebellar hypoplasia is associated with human RELN mutations. Nat Genet 26:93-96.

Honkura N, Matsuzaki M, Noguchi J, Ellis-Davies GC, Kasai H (2008) The subspine organization of actin fibers regulates the structure and plasticity of dendritic spines. Neuron 57:719-729.

Howell BW, Herrick TM, Cooper JA (1999) Reelin-induced tyrosine phosphorylation of disabled 1 during neuronal positioning. Genes Dev 13:643-648.

Huganir RL, Nicoll RA (2013) AMPARs and synaptic plasticity: the last 25 years. Neuron 80:704-717.

Iafrati J, Orejarena MJ, Lassalle O, Bouamrane L, Chavis P (2013) Reelin, an extracellular matrix protein linked to early onset psychiatric diseases, drives postnatal development of the prefrontal cortex via GluN2B-NMDARs and the mTOR pathway. Mol Psychiatry.

Ikeda Y, Terashima T (1997) Expression of reelin, the gene responsible for the reeler mutation, in embryonic development and adulthood in the mouse. Dev Dyn 210:157-172.

Impagnatiello F, Guidotti AR, Pesold C, Dwivedi Y, Caruncho H, Pisu MG, Uzunov DP, Smalheiser NR, Davis JM, Pandey GN, Pappas GD, Tueting P, Sharma RP, Costa E (1998) A decrease of reelin expression as a putative vulnerability factor in schizophrenia. Proc Natl Acad Sci U S A 95:15718-15723.

Ishii H, Shibuya K, Ohta Y, Mukai H, Uchino S, Takata N, Rose JA, Kawato S (2006) Enhancement of nitric oxide production by association of nitric oxide synthase with N-methyl-D-aspartate receptors via post-synaptic density 95 in genetically engineered Chinese hamster ovary cells: real-time fluorescence imaging using nitric oxide sensitive dye. J Neurochem 96:1531-1539.

Ishizuka N, Weber J, Amaral DG (1990) Organization of intrahippocampal projections originating from CA3 pyramidal cells in the rat. J Comp Neurol 295:580-623.

Izhikevich EM, Edelman GM (2008) Large-scale model of mammalian thalamocortical systems. Proc Natl Acad Sci U S A 105:3593-3598.

Jain V, Seung HS, Turaga SC (2010) Machines that learn to segment images: a crucial technology for connectomics. Curr Opin Neurobiol 20:653-666.

Jarsky T, Roxin A, Kath WL, Spruston N (2005) Conditional dendritic spike propagation following distal synaptic activation of hippocampal CA1 pyramidal neurons. Nat Neurosci 8:1667-1676.

Jedlicka P, Vlachos A, Schwarzacher SW, Deller T (2008) A role for the spine apparatus in LTP and spatial learning. Behav Brain Res 192:12-19.

Jessberger S, Toni N, Clemenson GD, Jr., Ray J, Gage FH (2008) Directed differentiation of hippocampal stem/progenitor cells in the adult brain. Nat Neurosci 11:888-893.

Johansson BB, Belichenko PV (2002) Neuronal plasticity and dendritic spines: effect of environmental enrichment on intact and postischemic rat brain. J Cereb Blood Flow Metab 22:89-96.

Jones EG, Powell TP (1969) Morphological variations in the dendritic spines of the neocortex. J Cell Sci 5:509-529.

Jossin Y, Goffinet AM (2007) Reelin signals through phosphatidylinositol 3-kinase and Akt to control cortical development and through mTor to regulate dendritic growth. Mol Cell Biol 27:7113-7124.

Jossin Y, Cooper JA (2011) Reelin, Rap1 and N-cadherin orient the migration of multipolar neurons in the developing neocortex. Nat Neurosci 14:697-703.

Jossin Y, Ignatova N, Hiesberger T, Herz J, Lambert de Rouvroit C, Goffinet AM (2004) The central fragment of Reelin, generated by proteolytic processing in vivo, is critical to its function during cortical plate development. J Neurosci 24:514-521.

Kaech S, Fischer M, Doll T, Matus A (1997) Isoform specificity in the relationship of actin to dendritic spines. J Neurosci 17:9565-9572.

Kandel ER, Schwartz JH, Jessell TM, Siegelbaum SA, Hudspeth AJ (2012) Principles of Neural Science, 5th Edition: Mc Graw Hill.

Karalay O, Doberauer K, Vadodaria KC, Knobloch M, Berti L, Miquelajauregui A, Schwark M, Jagasia

R, Taketo MM, Tarabykin V, Lie DC, Jessberger S (2011) Prospero-related homeobox 1 gene (Prox1) is regulated by canonical Wnt signaling and has a stage-specific role in adult hippocampal neurogenesis. Proc Natl Acad Sci U S A 108:5807-5812.

Kasai H, Matsuzaki M, Noguchi J, Yasumatsu N, Nakahara H (2003) Structure–stability–function relationships of dendritic spines. Trends in Neurosciences 26:360-368.

Kasai H, Fukuda M, Watanabe S, Hayashi-Takagi A, Noguchi J (2010a) Structural dynamics of dendritic spines in memory and cognition. Trends Neurosci 33:121-129.

Kasai H, Hayama T, Ishikawa M, Watanabe S, Yagishita S, Noguchi J (2010b) Learning rules and persistence of dendritic spines. Eur J Neurosci 32:241-249.

Katsuyama Y, Terashima T (2009) Developmental anatomy of reeler mutant mouse. Dev Growth Differ 51:271-286.

Kelsch W, Lin CW, Lois C (2008) Sequential development of synapses in dendritic domains during adult neurogenesis. Proc Natl Acad Sci U S A 105:16803-16808.

Kelley JB, Balda MA, Anderson KL, Itzhak Y (2009) Impairments in fear conditioning in mice lacking the nNOS gene. Learn Mem 16:371-378.

Kelley JB, Anderson KL, Altmann SL, Itzhak Y (2011) Long-term memory of visually cued fear conditioning: roles of the neuronal nitric oxide synthase gene and cyclic AMP response element-binding protein. Neuroscience 174:91-103.

Kim IH, Racz B, Wang H, Burianek L, Weinberg R, Yasuda R, Wetsel WC, Soderling SH (2013) Disruption of Arp2/3 results in asymmetric structural plasticity of dendritic spines and progressive synaptic and behavioral abnormalities. J Neurosci 33:6081-6092.

Knable MB, Barci BM, Webster MJ, Meador-Woodruff J, Torrey EF, Stanley Neuropathology C (2004) Molecular abnormalities of the hippocampus in severe psychiatric illness: postmortem findings from the Stanley Neuropathology Consortium. Mol Psychiatry 9:609-620, 544.

Knafo S, Alonso-Nanclares L, Gonzalez-Soriano J, Merino-Serrais P, Fernaud-Espinosa I, Ferrer I, DeFelipe J (2009a) Widespread changes in dendritic spines in a model of Alzheimer's disease. Cereb Cortex 19:586-592.

Knafo S, Venero C, Merino-Serrais P, Fernaud-Espinosa I, Gonzalez-Soriano J, Ferrer I, Santpere G, DeFelipe J (2009b) Morphological alterations to neurons of the amygdala and impaired fear conditioning in a transgenic mouse model of Alzheimer's disease. J Pathol 219:41-51.

Knafo S, Venero C, Sanchez-Puelles C, Pereda-Perez I, Franco A, Sandi C, Suarez LM, Solis JM, Alonso-Nanclares L, Martin ED, Merino-Serrais P, Borcel E, Li S, Chen Y, Gonzalez-Soriano J, Berezin V, Bock E, Defelipe J, Esteban JA (2012) Facilitation of AMPA receptor synaptic delivery as a molecular mechanism for cognitive enhancement. PLoS Biol 10:e1001262.

Knoth R, Singec I, Ditter M, Pantazis G, Capetian P, Meyer RP, Horvat V, Volk B, Kempermann G (2010) Murine features of neurogenesis in the human hippocampus across the lifespan from 0 to 100 years. PLoS One 5:e8809.

Knott G, Genoud C (2013) Is EM dead? J Cell Sci 126:4545-4552.

Knott G, Marchman H, Wall D, Lich B (2008) Serial section scanning electron microscopy of adult brain tissue using focused ion beam milling. J Neurosci 28:2959-2964.

Knott GW, Holtmaat A, Wilbrecht L, Welker E, Svoboda K (2006) Spine growth precedes synapse formation in the adult neocortex in vivo. Nat Neurosci 9:1117-1124.

Knuesel I (2010) Reelin-mediated signaling in neuropsychiatric and neurodegenerative diseases. Prog Neurobiol 91:257-274.

Knuesel I, Nyffeler M, Mormede C, Muhia M, Meyer U, Pietropaolo S, Yee BK, Pryce CR, LaFerla FM, Marighetto A, Feldon J (2009) Age-related accumulation of Reelin in amyloid-like deposits. Neurobiol Aging 30:697-716.

Konur S, Yuste R (2004) Imaging the motility of dendritic protrusions and axon terminals: roles in axon sampling and synaptic competition. Mol Cell Neurosci 27:427-440.

Konur S, Rabinowitz D, Fenstermaker VL, Yuste R (2003) Systematic regulation of spine sizes and densities in pyramidal neurons. J Neurobiol 56:95-112.

Kopec CD, Real E, Kessels HW, Malinow R (2007) GluR1 links structural and functional plasticity at excitatory synapses. J Neurosci 27:13706-13718.

Kopec CD, Li B, Wei W, Boehm J, Malinow R (2006) Glutamate receptor exocytosis and spine enlargement during chemically induced long-term potentiation. J Neurosci 26:2000-2009.

Korkotian E, Segal M (2001) Regulation of dendritic spine motility in cultured hippocampal neurons. J Neurosci 21:6115-6124.

Korngreen A, Sakmann B (2000) Voltage-gated K+ channels in layer 5 neocortical pyramidal neurones from young rats: subtypes and gradients. J Physiol 525 Pt 3:621-639.

Kramer PL, Xu H, Woltjer RL, Westaway SK, Clark D, Erten-Lyons D, Kaye JA, Welsh-Bohmer KA, Troncoso JC, Markesbery WR, Petersen RC, Turner RS, Kukull WA, Bennett DA, Galasko D, Morris JC, Ott J (2011) Alzheimer disease pathology in cognitively healthy elderly: a genome-wide study. Neurobiol Aging 32:2113-2122.

Kristensen AS, Jenkins MA, Banke TG, Schousboe A, Makino Y, Johnson RC, Huganir R, Traynelis SF (2011) Mechanism of Ca2+/calmodulin-dependent kinase II regulation of AMPA receptor gating. Nat Neurosci 14:727-735.

Kruger MT, Zhao S, Chai X, Brunne B, Bouche E, Bock HH, Frotscher M (2010) Role for Reelin-induced cofilin phosphorylation in the assembly of sympathetic preganglionic neurons in the murine intermediolateral column. Eur J Neurosci 32:1611-1617.

Kubo K, Mikoshiba K, Nakajima K (2002) Secreted Reelin molecules form homodimers. Neurosci Res 43:381-388.

Kuo G, Arnaud L, Kronstad-O'Brien P, Cooper JA (2005) Absence of Fyn and Src causes a reeler-like phenotype. J Neurosci 25:8578-8586.

Kuvbachieva A, Bestel AM, Tissir F, Maloum I, Guimiot F, Ramoz N, Bourgeois F, Moalic JM, Goffinet AM, Simonneau M (2004) Identification of a novel brain-specific and Reelin-regulated gene that encodes a protein colocalized with synapsin. Eur J Neurosci 20:603-610.

Lagace DC, Benavides DR, Kansy JW, Mapelli M, Greengard P, Bibb JA, Eisch AJ (2008) Cdk5 is essential for adult hippocampal neurogenesis. Proc Natl Acad Sci U S A 105:18567-18571.

Lee HK, Kameyama K, Huganir RL, Bear MF (1998) NMDA induces long-term synaptic depression and dephosphorylation of the GluR1 subunit of AMPA receptors in hippocampus. Neuron 21:1151-1162.

Lee SJ, Escobedo-Lozoya Y, Szatmari EM, Yasuda R (2009) Activation of CaMKII in single dendritic spines during long-term potentiation. Nature 458:299-304.

Leemhuis J, Bock HH (2011) Reelin modulates cytoskeletal organization by regulating Rho GTPases. Commun Integr Biol 4:254-257.

Lemaire V, Tronel S, Montaron MF, Fabre A, Dugast E, Abrous DN (2012) Long-lasting plasticity of hippocampal adult-born neurons. J Neurosci 32:3101-3108.

Levenson JM, Qiu S, Weeber EJ (2008) The role of reelin in adult synaptic function and the genetic and epigenetic regulation of the reelin gene. Biochim Biophys Acta 1779:422-431.

Li W, Zhou Y, Jentsch JD, Brown RA, Tian X, Ehninger D, Hennah W, Peltonen L, Lonnqvist J, Huttunen MO, Kaprio J, Trachtenberg JT, Silva AJ, Cannon TD (2007) Specific developmental disruption of disrupted-in-schizophrenia-1 function results in schizophrenia-related phenotypes in mice. Proc Natl Acad Sci U S A 104:18280-18285.

Li XG, Somogyi P, Ylinen A, Buzsaki G (1994) The hippocampal CA3 network: an in vivo intracellular labeling study. J Comp Neurol 339:181-208.

Liao D, Scannevin RH, Huganir R (2001) Activation of silent synapses by rapid activity-dependent synaptic recruitment of AMPA receptors. J Neurosci 21:6008-6017.

Lie DC, Colamarino SA, Song HJ, Desire L, Mira H, Consiglio A, Lein ES, Jessberger S, Lansford H, Dearie AR, Gage FH (2005) Wnt signalling regulates adult hippocampal neurogenesis. Nature 437:1370-1375.

Lisman JE, Harris KM (1993) Quantal analysis and synaptic anatomy--integrating two views of hippocampal plasticity. Trends Neurosci 16:141-147.

Lisman JE, Raghavachari S, Tsien RW (2007) The sequence of events that underlie quantal transmission at central glutamatergic synapses. Nat Rev Neurosci 8:597-609.

Liu L, Wong TP, Pozza MF, Lingenhoehl K, Wang Y, Sheng M, Auberson YP, Wang YT (2004) Role of NMDA receptor subtypes in governing the direction of hippocampal synaptic plasticity. Science 304:1021-1024.

Liu WS, Pesold C, Rodriguez MA, Carboni G, Auta J, Lacor P, Larson J, Condie BG, Guidotti A, Costa E (2001) Down-regulation of dendritic spine and glutamic acid decarboxylase 67 expressions in the reelin haploinsufficient heterozygous reeler mouse. Proc Natl Acad Sci U S A 98:3477-3482.

Lois C, Alvarez-Buylla A (1994) Long-distance neuronal migration in the adult mammalian brain. Science 264:1145-1148.

Maco B, Cantoni M, Holtmaat A, Kreshuk A, Hamprecht FA, Knott GW (2014) Semiautomated correlative 3D electron microscopy of in vivo-imaged axons and dendrites. Nat Protoc 9:1354-1366.

Maco B, Holtmaat A, Cantoni M, Kreshuk A, Straehle CN, Hamprecht FA, Knott GW (2013) Correlative in vivo 2 photon and focused ion beam scanning electron microscopy of cortical neurons. PLoS One 8:e57405.

Magee JC, Cook EP (2000) Somatic EPSP amplitude is independent of synapse location in hippocampal pyramidal neurons. Nat Neurosci 3:895-903.

Majewska A, Tashiro A, Yuste R (2000a) Regulation of spine calcium dynamics by rapid spine motility. J Neurosci 20:8262-8268.

Majewska A, Brown E, Ross J, Yuste R (2000b) Mechanisms of calcium decay kinetics in hippocampal spines: role of spine calcium pumps and calcium diffusion through the spine neck in biochemical compartmentalization. J Neurosci 20:1722-1734.

Major G, Larkum ME, Schiller J (2013) Active properties of neocortical pyramidal neuron dendrites. Annu Rev Neurosci 36:1-24.

Maletic-Savatic M (1999) Rapid Dendritic Morphogenesis in CA1 Hippocampal Dendrites Induced by Synaptic Activity. Science 283:1923-1927.

Matsuki T, Pramatarova A, Howell BW (2008) Reduction of Crk and CrkL expression blocks reelin-induced dendritogenesis. J Cell Sci 121:1869-1875.

Matsuzaki M, Honkura N, Ellis-Davies GC, Kasai H (2004) Structural basis of long-term potentiation in single dendritic spines. Nature 429:761-766.

Matsuzaki M, Ellis-Davies GC, Nemoto T, Miyashita Y, Iino M, Kasai H (2001) Dendritic spine geometry is critical for AMPA receptor expression in hippocampal CA1 pyramidal neurons. Nat Neurosci 4:1086-1092.

Matus A, Ackermann M, Pehling G, Byers HR, Fujiwara K (1982) High actin concentrations in brain dendritic spines and postsynaptic densities. Proc Natl Acad Sci U S A 79:7590-7594.

Medvedev NI, Popov VI, Rodriguez Arellano JJ, Dallerac G, Davies HA, Gabbott PL, Laroche S, Kraev IV, Doyere V, Stewart MG (2010) The N-methyl-D-aspartate receptor antagonist CPP alters synapse and spine structure and impairs long-term potentiation and long-term depression induced morphological plasticity in dentate gyrus of the awake rat. Neuroscience 165:1170-1181.

Meng Y, Takahashi H, Meng J, Zhang Y, Lu G, Asrar S, Nakamura T, Jia Z (2004) Regulation of ADF/cofilin phosphorylation and synaptic function by LIM-kinase. Neuropharmacology 47:746-754.

Merchan-Perez A, Rodriguez JR, Alonso-Nanclares L, Schertel A, Defelipe J (2009) Counting Synapses Using FIB/SEM Microscopy: A True Revolution for Ultrastructural Volume Reconstruction. Front Neuroanat 3:18.

Merchan-Perez A, Rodriguez JR, Gonzalez S, Robles V, Defelipe J, Larranaga P, Bielza C (2013) Three-Dimensional Spatial Distribution of Synapses in the Neocortex: A Dual-Beam Electron Microscopy Study. Cereb Cortex.

Merino-Serrais P, Knafo S, Alonso-Nanclares L, Fernaud-Espinosa I, DeFelipe J (2011) Layer-specific

alterations to CA1 dendritic spines in a mouse model of Alzheimer's disease. Hippocampus 21:1037-1044.

Merino-Serrais P, Benavides-Piccione R, Blazquez-Llorca L, Kastanauskaite A, Rabano A, Avila J, DeFelipe J (2013) The influence of phospho-tau on dendritic spines of cortical pyramidal neurons in patients with Alzheimer's disease. Brain 136:1913-1928.

Meyer G, Perez-Garcia CG, Abraham H, Caput D (2002) Expression of p73 and Reelin in the developing human cortex. J Neurosci 22:4973-4986.

Meyer U (2013) Developmental neuroinflammation and schizophrenia. Prog Neuropsychopharmacol Biol Psychiatry 42:20-34.

Miao GG, Smeyne RJ, D'Arcangelo G, Copeland NG, Jenkins NA, Morgan JI, Curran T (1994) Isolation of an allele of reeler by insertional mutagenesis. Proc Natl Acad Sci U S A 91:11050-11054.

Migliore M, Ferrante M, Ascoli GA (2005) Signal propagation in oblique dendrites of CA1 pyramidal cells. J Neurophysiol 94:4145-4155.

Miller M, Peters A (1981) Maturation of rat visual cortex. II. A combined Golgi-electron microscope study of pyramidal neurons. J Comp Neurol 203:555-573.

Mishchenko Y, Hu T, Spacek J, Mendenhall J, Harris KM, Chklovskii DB (2010) Ultrastructural analysis of hippocampal neuropil from the connectomics perspective. Neuron 67:1009-1020.

Miyata T, Nakajima K, Aruga J, Takahashi S, Ikenaka K, Mikoshiba K, Ogawa M (1996) Distribution of a reeler gene-related antigen in the developing cerebellum: an immunohistochemical study with an allogeneic antibody CR-50 on normal and reeler mice. J Comp Neurol 372:215-228.

Morales J, Alonso-Nanclares L, Rodriguez JR, Defelipe J, Rodriguez A, Merchan-Perez A (2011) Espina: a tool for the automated segmentation and counting of synapses in large stacks of electron microscopy images. Front Neuroanat 5:18.

Morimura T, Hattori M, Ogawa M, Mikoshiba K (2005) Disabled1 regulates the intracellular trafficking of reelin receptors. J Biol Chem 280:16901-16908.

Mundel P, Heid HW, Mundel TM, Kruger M, Reiser J, Kriz W (1997) Synaptopodin: an actin-associated protein in telencephalic dendrites and renal podocytes. J Cell Biol 139:193-204.

Nagerl UV, Eberhorn N, Cambridge SB, Bonhoeffer T (2004) Bidirectional activity-dependent morphological plasticity in hippocampal neurons. Neuron 44:759-767.

Nakano Y, Kohno T, Hibi T, Kohno S, Baba A, Mikoshiba K, Nakajima K, Hattori M (2007) The extremely conserved C-terminal region of Reelin is not necessary for secretion but is required for efficient activation of downstream signaling. J Biol Chem 282:20544-20552.

Nakashiba T, Cushman JD, Pelkey KA, Renaudineau S, Buhl DL, McHugh TJ, Rodriguez Barrera V, Chittajallu R, Iwamoto KS, McBain CJ, Fanselow MS, Tonegawa S (2012) Young dentate granule cells mediate pattern separation, whereas old granule cells facilitate pattern completion. Cell 149:188-201.

Nichols AJ, Olson EC (2010) Reelin promotes neuronal orientation and dendritogenesis during preplate splitting. Cereb Cortex 20:2213-2223.

Nicholson DA, Trana R, Katz Y, Kath WL, Spruston N, Geinisman Y (2006) Distance-dependent differences in synapse number and AMPA receptor expression in hippocampal CA1 pyramidal neurons. Neuron 50:431-442.

Nikonenko I, Jourdain P, Muller D (2003) Presynaptic remodeling contributes to activity-dependent synaptogenesis. J Neurosci 23:8498-8505.

Nikonenko I, Boda B, Steen S, Knott G, Welker E, Muller D (2008) PSD-95 promotes synaptogenesis and multiinnervated spine formation through nitric oxide signaling. J Cell Biol 183:1115-1127.

Nimchinsky EA, Sabatini BL, Svoboda K (2002) Structure and function of dendritic spines. Annu Rev Physiol 64:313-353.

Niu S, Yabut O, D'Arcangelo G (2008) The Reelin signaling pathway promotes dendritic spine development in hippocampal neurons. J Neurosci 28:10339-10348.

Niu S, Renfro A, Quattrocchi CC, Sheldon M, D'Arcangelo G (2004) Reelin Promotes Hippocampal Dendrite Development through the VLDLR/ApoER2-Dab1 Pathway. Neuron 41:71-84.

Noguchi J, Matsuzaki M, Ellis-Davies GC, Kasai H (2005) Spine-neck geometry determines NMDA receptor-dependent Ca2+ signaling in dendrites. Neuron 46:609-622.

Nusser Z, Somogyi P (1997) Compartmentalised distribution of GABAA and glutamate receptors in relation to transmitter release sites on the surface of cerebellar neurones. Prog Brain Res 114:109-127.

Nusser Z, Lujan R, Laube G, Roberts JD, Molnar E, Somogyi P (1998) Cell type and pathway dependence of synaptic AMPA receptor number and variability in the hippocampus. Neuron 21:545-559.

O'Brien J, Unwin N (2006) Organization of spines on the dendrites of Purkinje cells. Proc Natl Acad Sci U S A 103:1575-1580.

O'Connell C, Gallagher HC, O'Malley A, Bourke M, Regan CM (2000) CREB phosphorylation coincides with transient synapse formation in the rat hippocampal dentate gyrus following avoidance learning. Neural Plast 7:279-289.

O'Donnell C, Nolan MF, van Rossum MC (2011) Dendritic spine dynamics regulate the long-term stability of synaptic plasticity. J Neurosci 31:16142-16156.

Okubo-Suzuki R, Okada D, Sekiguchi M, Inokuchi K (2008) Synaptopodin maintains the neural activity-dependent enlargement of dendritic spines in hippocampal neurons. Mol Cell Neurosci 38:266-276.

Olson EC, Kim S, Walsh CA (2006) Impaired neuronal positioning and dendritogenesis in the neocortex after cell-autonomous Dab1 suppression. J Neurosci 26:1767-1775.

Opazo P, Sainlos M, Choquet D (2012) Regulation of AMPA receptor surface diffusion by PSD-95 slots. Curr Opin Neurobiol 22:453-460.

Oyler GA, Higgins GA, Hart RA, Battenberg E, Billingsley M, Bloom FE, Wilson MC (1989) The identification of a novel synaptosomal-associated protein, SNAP-25, differentially expressed by neuronal subpopulations. J Cell Biol 109:3039-3052.

Paoletti P, Bellone C, Zhou Q (2013) NMDA receptor subunit diversity: impact on receptor properties, synaptic plasticity and disease. Nat Rev Neurosci 14:383-400.

Pappas GD, Kriho V, Liu WS, Tremolizzo L, Lugli G, Larson J (2003) Immunocytochemical localization of reelin in the olfactory bulb of the heterozygous reeler mouse: an animal model for schizophrenia. Neurol Res 25:819-830.

Park M, Penick EC, Edwards JG, Kauer JA, Ehlers MD (2004) Recycling endosomes supply AMPA receptors for LTP. Science 305:1972-1975.

Persico AM et al. (2001) Reelin gene alleles and haplotypes as a factor predisposing to autistic disorder. Mol Psychiatry 6:150-159.

Pesold C, Impagnatiello F, Pisu MG, Uzunov DP, Costa E, Guidotti A, Caruncho HJ (1998) Reelin is preferentially expressed in neurons synthesizing gamma-aminobutyric acid in cortex and hippocampus of adult rats. Proc Natl Acad Sci U S A 95:3221-3226.

Peters A, Kaiserman-Abramof IR (1970) The small pyramidal neuron of the rat cerebral cortex. The perikaryon, dendrites and spines. Am J Anat 127:321-355.

Peters A, Palay SL (1996) The morphology of synapses. J Neurocytol 25:687-700.

Peters A, Palay SL, Webster H, DeFelipe J (1991) The fine structure of the nervous system. Neurons and their supporting cells., 3rd Edition. New York: Oxford University Press.

Popov VI, Stewart MG (2009) Complexity of contacts between synaptic boutons and dendritic spines in adult rat hippocampus: three-dimensional reconstructions from serial ultrathin sections in vivo. Synapse 63:369-377.

Popov VI, Davies HA, Rogachevsky VV, Patrushev IV, Errington ML, Gabbott PL, Bliss TV, Stewart MG (2004) Remodelling of synaptic morphology but unchanged synaptic density during late phase long-term potentiation (LTP): a serial section electron micrograph study in the dentate gyrus in the anaesthetised rat. Neuroscience 128:251-262.

Portera-Cailliau C, Pan DT, Yuste R (2003) Activity-regulated dynamic behavior of early dendritic protrusions: evidence for different types of dendritic filopodia. J Neurosci 23:7129-7142.

Pramatarova A, Chen K, Howell BW (2008) A genetic interaction between the APP and Dab1 genes

influences brain development. Mol Cell Neurosci 37:178-186.

Prybylowski K, Chang K, Sans N, Kan L, Vicini S, Wenthold RJ (2005) The synaptic localization of NR2B-containing NMDA receptors is controlled by interactions with PDZ proteins and AP-2. Neuron 47:845-857.

Pujadas L, Gruart A, Bosch C, Delgado L, Teixeira CM, Rossi D, de Lecea L, Martinez A, Delgado-Garcia JM, Soriano E (2010) Reelin regulates postnatal neurogenesis and enhances spine hypertrophy and long-term potentiation. J Neurosci 30:4636-4649.

Pujadas L, Rossi D, Andres R, Teixeira CM, Serra-Vidal B, Parcerisas A, Maldonado R, Giralt E, Carulla N, Soriano E (2014) Reelin delays amyloid-beta fibril formation and rescues cognitive deficits in a model of Alzheimer's disease. Nat Commun 5:3443.

Qiu S, Weeber EJ (2007) Reelin signaling facilitates maturation of CA1 glutamatergic synapses. J Neurophysiol 97:2312-2321.

Qiu S, Zhao LF, Korwek KM, Weeber EJ (2006a) Differential reelin-induced enhancement of NMDA and AMPA receptor activity in the adult hippocampus. J Neurosci 26:12943-12955.

Qiu S, Korwek KM, Pratt-Davis AR, Peters M, Bergman MY, Weeber EJ (2006b) Cognitive disruption and altered hippocampus synaptic function in Reelin haploinsufficient mice. Neurobiol Learn Mem 85:228-242.

Racz B, Weinberg RJ (2004) The subcellular organization of cortactin in hippocampus. J Neurosci 24:10310-10317.

Racz B, Weinberg RJ (2008) Organization of the Arp2/3 complex in hippocampal spines. J Neurosci 28:5654-5659.

Racz B, Weinberg RJ (2013) Microdomains in forebrain spines: an ultrastructural perspective. Mol Neurobiol 47:77-89.

Ramos-Moreno T, Galazo MJ, Porrero C, Martinez-Cerdeno V, Clasca F (2006) Extracellular matrix molecules and synaptic plasticity: immunomapping of intracellular and secreted Reelin in the adult rat brain. Eur J Neurosci 23:401-422.

Retzius G (1893) Die Cajal'schen Zellen der Grosshirnrinde beim Menschen und bei Säugethieren. Biologische Untersuchungen 5:1-8.

Rice DS, Sheldon M, D'Arcangelo G, Nakajima K, Goldowitz D, Curran T (1998) Disabled-1 acts downstream of Reelin in a signaling pathway that controls laminar organization in the mammalian brain. Development 125:3719-3729.

Rice DS, Nusinowitz S, Azimi AM, Martinez A, Soriano E, Curran T (2001) The reelin pathway modulates the structure and function of retinal synaptic circuitry. Neuron 31:929-941.

Rochefort NL, Konnerth A (2012) Dendritic spines: from structure to in vivo function. EMBO Rep 13:699-708.

Rogers JT, Rusiana I, Trotter J, Zhao L, Donaldson E, Pak DT, Babus LW, Peters M, Banko JL, Chavis P, Rebeck GW, Hoe HS, Weeber EJ (2011) Reelin supplementation enhances cognitive ability, synaptic plasticity, and dendritic spine density. Learn Mem 18:558-564.

Rogers JT, Zhao L, Trotter JH, Rusiana I, Peters MM, Li Q, Donaldson E, Banko JL, Keenoy KE, Rebeck GW, Hoe HS, D'Arcangelo G, Weeber EJ (2013) Reelin supplementation recovers sensorimotor gating, synaptic plasticity and associative learning deficits in the heterozygous reeler mouse. J Psychopharmacol 27:386-395.

Romay-Tallon R, Dopeso-Reyes IG, Lussier AL, Kalynchuk LE, Caruncho HJ (2010) The coexpression of reelin and neuronal nitric oxide synthase in a subpopulation of dentate gyrus neurons is downregulated in heterozygous reeler mice. Neural Plast 2010:130429.

Roth SU, Sommer C, Mundel P, Kiessling M (2001) Expression of synaptopodin, an actin-associated protein, in the rat hippocampus after limbic epilepsy. Brain Pathol 11:169-181.

Royaux I, Lambert de Rouvroit C, D'Arcangelo G, Demirov D, Goffinet AM (1997) Genomic organization of the mouse reelin gene. Genomics 46:240-250.

Rusakov DA, Stewart MG, Korogod SM (1996) Branching of active dendritic spines as a mechanism for controlling synaptic efficacy. Neuroscience 75:315-323.

Ryan TJ, Kopanitsa MV, Indersmitten T, Nithianantharajah J, Afinowi NO, Pettit C, Stanford LE, Sprengel R, Saksida LM, Bussey TJ, O'Dell TJ, Grant SG, Komiyama NH (2013) Evolution of GluN2A/B cytoplasmic domains diversified vertebrate synaptic plasticity and behavior. Nat Neurosci 16:25-32.

Sabatini BL, Oertner TG, Svoboda K (2002) The life cycle of Ca(2+) ions in dendritic spines. Neuron 33:439-452.

Sahay A, Hen R (2007) Adult hippocampal neurogenesis in depression. Nat Neurosci 10:1110-1115.

Sanai N, Nguyen T, Ihrie RA, Mirzadeh Z, Tsai HH, Wong M, Gupta N, Berger MS, Huang E, Garcia-Verdugo JM, Rowitch DH, Alvarez-Buylla A (2011) Corridors of migrating neurons in the human brain and their decline during infancy. Nature 478:382-386.

Sanders J, Cowansage K, Baumgartel K, Mayford M (2012) Elimination of dendritic spines with long-term memory is specific to active circuits. J Neurosci 32:12570-12578.

Schaefer AT, Larkum ME, Sakmann B, Roth A (2003) Coincidence detection in pyramidal neurons is tuned by their dendritic branching pattern. J Neurophysiol 89:3143-3154.

Schikorski T, Stevens CF (1997) Quantitative ultrastructural analysis of hippocampal excitatory synapses. J Neurosci 17:5858-5867.

Schikorski T, Stevens CF (1999) Quantitative fine-structural analysis of olfactory cortical synapses. Proc Natl Acad Sci U S A 96:4107-4112.

Schiller J, Schiller Y, Stuart G, Sakmann B (1997) Calcium action potentials restricted to distal apical dendrites of rat neocortical pyramidal neurons. J Physiol 505 (Pt 3):605-616.

Schindelin J, Arganda-Carreras I, Frise E, Kaynig V, Longair M, Pietzsch T, Preibisch S, Rueden C, Saalfeld S, Schmid B, Tinevez JY, White DJ, Hartenstein V, Eliceiri K, Tomancak P, Cardona A (2012) Fiji: an open-source platform for biological-image analysis. Nat Methods 9:676-682.

Schmechel DE, Saunders AM, Strittmatter WJ, Crain BJ, Hulette CM, Joo SH, Pericak-Vance MA, Goldgaber D, Roses AD (1993) Increased amyloid beta-peptide deposition in cerebral cortex as a consequence of apolipoprotein E genotype in late-onset Alzheimer disease. Proc Natl Acad Sci U S A 90:9649-9653.

Sdrulla AD, Linden DJ (2007) Double dissociation between long-term depression and dendritic spine morphology in cerebellar Purkinje cells. Nat Neurosci 10:546-548.

Segal M, Vlachos A, Korkotian E (2010) The spine apparatus, synaptopodin, and dendritic spine plasticity. Neuroscientist 16:125-131.

Sekine K, Kawauchi T, Kubo K, Honda T, Herz J, Hattori M, Kinashi T, Nakajima K (2012) Reelin controls neuronal positioning by promoting cell-matrix adhesion via inside-out activation of integrin alpha5beta1. Neuron 76:353-369.

Sentürk A, Pfennig S, Weiss A, Burk K, Acker-Palmer A (2011) Ephrin Bs are essential components of the Reelin pathway to regulate neuronal migration. Nature 478:274-274.

Senzaki K, Ogawa M, Yagi T (1999) Proteins of the CNR family are multiple receptors for Reelin. Cell 99:635-647.

Seripa D, Matera MG, Franceschi M, Daniele A, Bizzarro A, Rinaldi M, Panza F, Fazio VM, Gravina C, D'Onofrio G, Solfrizzi V, Masullo C, Pilotto A (2008) The RELN locus in Alzheimer's disease. J Alzheimers Dis 14:335-344.

Sheldon M, Rice DS, D'Arcangelo G, Yoneshima H, Nakajima K, Mikoshiba K, Howell BW, Cooper JA, Goldowitz D, Curran T (1997) Scrambler and yotari disrupt the disabled gene and produce a reeler-like phenotype in mice. Nature 389:730-733.

Shepherd GM (1996) The dendritic spine: a multifunctional integrative unit. J Neurophysiol 75:2197-2210.

Shepherd GM, Brayton RK, Miller JP, Segev I, Rinzel J, Rall W (1985) Signal enhancement in distal cortical dendrites by means of interactions between active dendritic spines. Proc Natl Acad Sci U S A 82:2192-2195.

Shi Y, Pontrello CG, DeFea KA, Reichardt LF, Ethell IM (2009) Focal adhesion kinase acts downstream of EphB receptors to maintain mature dendritic spines by regulating cofilin activity. J Neurosci 29:8129-8142.

Sik A, Penttonen M, Ylinen A, Buzsaki G (1995) Hippocampal CA1 interneurons: an in vivo intracellular labeling study. J Neurosci 15:6651-6665.

Silberberg G, Markram H (2007) Disynaptic inhibition between neocortical pyramidal cells mediated by Martinotti cells. Neuron 53:735-746.

Simo S, Cooper JA (2013) Rbx2 regulates neuronal migration through different cullin 5-RING ligase adaptors. Dev Cell 27:399-411.

Simo S, Jossin Y, Cooper JA (2010) Cullin 5 regulates cortical layering by modulating the speed and duration of Dab1-dependent neuronal migration. J Neurosci 30:5668-5676.

Simo S, Pujadas L, Segura MF, La Torre A, Del Rio JA, Urena JM, Comella JX, Soriano E (2007) Reelin induces the detachment of postnatal subventricular zone cells and the expression of the Egr-1 through Erk1/2 activation. Cereb Cortex 17:294-303.

Sinagra M, Verrier D, Frankova D, Korwek KM, Blahos J, Weeber EJ, Manzoni OJ, Chavis P (2005) Reelin, very-low-density lipoprotein receptor, and apolipoprotein E receptor 2 control somatic NMDA receptor composition during hippocampal maturation in vitro. J Neurosci 25:6127-6136.

Smalheiser NR, Costa E, Guidotti A, Impagnatiello F, Auta J, Lacor P, Kriho V, Pappas GD (2000) Expression of reelin in adult mammalian blood, liver, pituitary pars intermedia, and adrenal chromaffin cells. Proc Natl Acad Sci U S A 97:1281-1286.

Smit-Rigter LA, Champagne DL, van Hooft JA (2009) Lifelong impact of variations in maternal care on dendritic structure and function of cortical layer 2/3 pyramidal neurons in rat offspring. PLoS One 4:e5167.

Soderling SH, Langeberg LK, Soderling JA, Davee SM, Simerly R, Raber J, Scott JD (2003) Loss of WAVE-1 causes sensorimotor retardation and reduced learning and memory in mice. Proc Natl Acad Sci U S A 100:1723-1728.

Somogyi P, Hodgson AJ (1985) Antisera to gamma-aminobutyric acid. III. Demonstration of GABA in Golgi-impregnated neurons and in conventional electron microscopic sections of cat striate cortex. Journal of Histochemistry & Cytochemistry 33:249-257.

Somogyi P, Klausberger T (2005) Defined types of cortical interneurone structure space and spike timing in the hippocampus. J Physiol 562:9-26.

Sonomura T, Furuta T, Nakatani I, Yamamoto Y, Unzai T, Matsuda W, Iwai H, Yamanaka A, Uemura M, Kaneko T (2013) Correlative analysis of immunoreactivity in confocal laser-scanning microscopy and scanning electron microscopy with focused ion beam milling. Front Neural Circuits 7:26.

Soriano E, Del Rio JA (2005) The cells of cajal-retzius: still a mystery one century after. Neuron 46:389-394.

Sorra KE, Harris KM (1993) Occurrence and three-dimensional structure of multiple synapses between individual radiatum axons and their target pyramidal cells in hippocampal area CA1. J Neurosci 13:3736-3748.

Sorra KE, Fiala JC, Harris KM (1998) Critical assessment of the involvement of perforations, spinules, and spine branching in hippocampal synapse formation. J Comp Neurol 398:225-240.

Sotelo C (1975) Anatomical, physiological and biochemical studies of the cerebellum from mutant mice. II. Morphological study of cerebellar cortical neurons and circuits in the weaver mouse. Brain Res 94:19-44.

Sotelo C (1978) Purkinje cell ontogeny: formation and maintenance of spines. Prog Brain Res 48:149-170.

Sotelo C, Hillman DE, Zamora AJ, Llinas RR (1975) Climbing fiber deafferentation: Its action on Purkinje cell dendritic spines. Brain Research 98:7.

Spacek J, Hartmann M (1983) Three-dimensional analysis of dendritic spines. I. Quantitative observations related to dendritic spine and synaptic morphology in cerebral and cerebellar cortices. Anat Embryol (Berl) 167:289-310.

Spacek J, Harris KM (1997) Three-dimensional organization of smooth endoplasmic reticulum in hippocampal CA1 dendrites and dendritic spines of the immature and mature rat. J Neurosci 17:190-203.

Spalding KL, Bergmann O, Alkass K, Bernard S, Salehpour M, Huttner HB, Bostrom E, Westerlund I,

Vial C, Buchholz BA, Possnert G, Mash DC, Druid H, Frisen J (2013) Dynamics of hippocampal neurogenesis in adult humans. Cell 153:1219-1227.

Sprengel R, Suchanek B, Amico C, Brusa R, Burnashev N, Rozov A, Hvalby O, Jensen V, Paulsen O, Andersen P, Kim JJ, Thompson RF, Sun W, Webster LC, Grant SG, Eilers J, Konnerth A, Li J, McNamara JO, Seeburg PH (1998) Importance of the intracellular domain of NR2 subunits for NMDA receptor function in vivo. Cell 92:279-289.

Spruston N (2008) Pyramidal neurons: dendritic structure and synaptic integration. Nat Rev Neurosci 9:206-221.

Stevens JK, Davis TL, Friedman N, Sterling P (1980) A systematic approach to reconstructing microcircuitry by electron microscopy of serial sections. Brain Res 2:265-293.

Stuart G, Schiller J, Sakmann B (1997) Action potential initiation and propagation in rat neocortical pyramidal neurons. J Physiol 505 (Pt 3):617-632.

Stuart GJ, Hausser M (2001) Dendritic coincidence detection of EPSPs and action potentials. Nat Neurosci 4:63-71.

Sudhof TC, Rizo J (2011) Synaptic vesicle exocytosis. Cold Spring Harb Perspect Biol 3.

Suetsugu S, Tezuka T, Morimura T, Hattori M, Mikoshiba K, Yamamoto T, Takenawa T (2004) Regulation of actin cytoskeleton by mDab1 through N-WASP and ubiquitination of mDab1. Biochem J 384:1-8.

Sun B, Halabisky B, Zhou Y, Palop JJ, Yu G, Mucke L, Gan L (2009) Imbalance between GABAergic and Glutamatergic Transmission Impairs Adult Neurogenesis in an Animal Model of Alzheimer's Disease. Cell Stem Cell 5:624-633.

Sun GJ, Sailor KA, Mahmood QA, Chavali N, Christian KM, Song H, Ming GL (2013) Seamless reconstruction of intact adult-born neurons by serial end-block imaging reveals complex axonal guidance and development in the adult hippocampus. J Neurosci 33:11400-11411.

Super H, Martinez A, Del Rio JA, Soriano E (1998) Involvement of distinct pioneer neurons in the formation of layer-specific connections in the hippocampus. J Neurosci 18:4616-4626.

Svoboda K, Tank DW, Denk W (1996) Direct measurement of coupling between dendritic spines and shafts. Science 272:716-719.

Sweet HO, Bronson RT, Johnson KR, Cook SA, Davisson MT (1996) Scrambler, a new neurological mutation of the mouse with abnormalities of neuronal migration. Mamm Genome 7:798-802.

Swindale N (1981) Dendritic spines only connect. Trends Neurosci 4:2.

Szabadics J, Varga C, Molnar G, Olah S, Barzo P, Tamas G (2006) Excitatory effect of GABAergic axo-axonic cells in cortical microcircuits. Science 311:233-235.

Tamminga CA, Stan AD, Wagner AD (2010) The hippocampal formation in schizophrenia. Am J Psychiatry 167:1178-1193.

Taqatqeh F, Mergia E, Neitz A, Eysel UT, Koesling D, Mittmann T (2009) More than a retrograde messenger: nitric oxide needs two cGMP pathways to induce hippocampal long-term potentiation. J Neurosci 29:9344-9350.

Tashiro A, Yuste R (2003) Structure and molecular organization of dendritic spines. Histol Histopathol 18:617-634.

Teixeira CM, Masachs N, Muhaisen A, Bosch C, Perez-Martinez J, Howell B, Soriano E (2014) Transient downregulation of Dab1 protein levels during development leads to behavioral and structural deficits: relevance for psychiatric disorders. Neuropsychopharmacology 39:556-568.

Teixeira CM, Martin ED, Sahun I, Masachs N, Pujadas L, Corvelo A, Bosch C, Rossi D, Martinez A, Maldonado R, Dierssen M, Soriano E (2011) Overexpression of Reelin prevents the manifestation of behavioral phenotypes related to schizophrenia and bipolar disorder. Neuropsychopharmacology 36:2395-2405.

Teixeira CM, Kron MM, Masachs N, Zhang H, Lagace DC, Martinez A, Reillo I, Duan X, Bosch C, Pujadas L, Brunso L, Song H, Eisch AJ, Borrell V, Howell BW, Parent JM, Soriano E (2012) Cell-autonomous inactivation of the reelin pathway impairs adult neurogenesis in the hippocampus. J Neurosci 32:12051-12065.

Thompson PM, Sower AC, Perrone-Bizzozero NI (1998) Altered levels of the synaptosomal associated

protein SNAP-25 in schizophrenia. Biol Psychiatry 43:239-243.

Tissir F, Goffinet AM (2003) Reelin and brain development. Nat Rev Neurosci 4:496-505.

Toni N, Sultan S (2011) Synapse formation on adult-born hippocampal neurons. Eur J Neurosci 33:1062-1068.

Toni N, Buchs PA, Nikonenko I, Bron CR, Muller D (1999) LTP promotes formation of multiple spine synapses between a single axon terminal and a dendrite. Nature 402:421-425.

Toni N, Buchs PA, Nikonenko I, Povilaitite P, Parisi L, Muller D (2001) Remodeling of synaptic membranes after induction of long-term potentiation. J Neurosci 21:6245-6251.

Toni N, Laplagne DA, Zhao C, Lombardi G, Ribak CE, Gage FH, Schinder AF (2008) Neurons born in the adult dentate gyrus form functional synapses with target cells. Nat Neurosci 11:901-907.

Toni N, Teng EM, Bushong EA, Aimone JB, Zhao C, Consiglio A, van Praag H, Martone ME, Ellisman MH, Gage FH (2007) Synapse formation on neurons born in the adult hippocampus. Nat Neurosci 10:727-734.

Tonnesen J, Katona G, Rozsa B, Nagerl UV (2014) Spine neck plasticity regulates compartmentalization of synapses. Nat Neurosci 17:678-685.

Tovar KR, Westbrook GL (2002) Mobile NMDA receptors at hippocampal synapses. Neuron 34:255-264.

Trachtenberg JT, Chen BE, Knott GW, Feng G, Sanes JR, Welker E, Svoboda K (2002) Long-term in vivo imaging of experience-dependent synaptic plasticity in adult cortex. Nature 420:788-794.

Traynelis SF, Wollmuth LP, McBain CJ, Menniti FS, Vance KM, Ogden KK, Hansen KB, Yuan H, Myers SJ, Dingledine R (2010) Glutamate receptor ion channels: structure, regulation, and function. Pharmacol Rev 62:405-496.

Trommald M, Hulleberg G (1997) Dimensions and density of dendritic spines from rat dentate granule cells based on reconstructions from serial electron micrographs. J Comp Neurol 377:15-28.

Trommald M, Hulleberg G, Andersen P (1996) Long-term potentiation is associated with new excitatory spine synapses on rat dentate granule cells. Learn Mem 3:218-228.

Trommsdorff M, Borg JP, Margolis B, Herz J (1998) Interaction of cytosolic adaptor proteins with neuronal apolipoprotein E receptors and the amyloid precursor protein. J Biol Chem 273:33556-33560.

Trommsdorff M, Gotthardt M, Hiesberger T, Shelton J, Stockinger W, Nimpf J, Hammer RE, Richardson JA, Herz J (1999) Reeler/Disabled-like disruption of neuronal migration in knockout mice lacking the VLDL receptor and ApoE receptor 2. Cell 97:689-701.

Trotter J, Lee GH, Kazdoba TM, Crowell B, Domogauer J, Mahoney HM, Franco SJ, Muller U, Weeber EJ, D'Arcangelo G (2013) Dab1 is required for synaptic plasticity and associative learning. J Neurosci 33:15652-15668.

Trotter JH, Klein M, Jinwal UK, Abisambra JF, Dickey CA, Tharkur J, Masiulis I, Ding J, Locke KG, Rickman CB, Birch DG, Weeber EJ, Herz J (2011) ApoER2 function in the establishment and maintenance of retinal synaptic connectivity. J Neurosci 31:14413-14423.

Tsai MS, Tangalos EG, Petersen RC, Smith GE, Schaid DJ, Kokmen E, Ivnik RJ, Thibodeau SN (1994) Apolipoprotein E: risk factor for Alzheimer disease. Am J Hum Genet 54:643-649.

Urosevic N, Martins RN (2008) Infection and Alzheimer's disease: the APOE epsilon4 connection and lipid metabolism. J Alzheimers Dis 13:421-435.

Utsunomiya-Tate N, Kubo K, Tate S, Kainosho M, Katayama E, Nakajima K, Mikoshiba K (2000) Reelin molecules assemble together to form a large protein complex, which is inhibited by the function-blocking CR-50 antibody. Proc Natl Acad Sci U S A 97:9729-9734.

Vadodaria KC, Gage FH (2014) SnapShot: adult hippocampal neurogenesis. Cell 156:1114-1114 e1111.

van Praag H, Schinder AF, Christie BR, Toni N, Palmer TD, Gage FH (2002) Functional neurogenesis in the adult hippocampus. Nature 415:1030-1034.

Veldic M, Caruncho HJ, Liu WS, Davis J, Satta R, Grayson DR, Guidotti A, Costa E (2004) DNA-methyltransferase 1 mRNA is selectively overexpressed in telencephalic GABAergic interneurons of schizophrenia brains. Proc Natl Acad Sci U S A 101:348-353.

Ventruti A, Kazdoba TM, Niu S, D'Arcangelo G (2011) Reelin deficiency causes specific defects in the molecular composition of the synapses in the adult brain. Neuroscience 189:32-42.

Vetter P, Roth A, Hausser M (2001) Propagation of action potentials in dendrites depends on dendritic morphology. J Neurophysiol 85:926-937.

Vlachos A, Korkotian E, Schonfeld E, Copanaki E, Deller T, Segal M (2009) Synaptopodin regulates plasticity of dendritic spines in hippocampal neurons. J Neurosci 29:1017-1033.

Vlachos A, Ikenberg B, Lenz M, Becker D, Reifenberg K, Bas-Orth C, Deller T (2013) Synaptopodin regulates denervation-induced homeostatic synaptic plasticity. Proc Natl Acad Sci U S A 110:8242-8247.

Wadell H (1935) Volume, Shape and Roundness of Quartz Particles. Journal of Geology 43:250-280.

Wang Y, Dong Q, Xu XF, Feng X, Xin J, Wang DD, Yu H, Tian T, Chen ZY (2013) Phosphorylation of cofilin regulates extinction of conditioned aversive memory via AMPAR trafficking. J Neurosci 33:6423-6433.

Weeber EJ, Beffert U, Jones C, Christian JM, Forster E, Sweatt JD, Herz J (2002) Reelin and ApoE receptors cooperate to enhance hippocampal synaptic plasticity and learning. J Biol Chem 277:39944-39952.

Williams SR, Stuart GJ (2002) Dependence of EPSP efficacy on synapse location in neocortical pyramidal neurons. Science 295:1907-1910.

Winder SJ (2004) Filopodia formation and Disabled degradation downstream of Reelin. Biochem J 384:e1-2.

Woolley CS, Wenzel HJ, Schwartzkroin PA (1996) Estradiol increases the frequency of multiple synapse boutons in the hippocampal CA1 region of the adult female rat. J Comp Neurol 373:108-117.

Yang G, Pan F, Gan WB (2009) Stably maintained dendritic spines are associated with lifelong memories. Nature 462:920-924.

Yang N, Higuchi O, Ohashi K, Nagata K, Wada A, Kangawa K, Nishida E, Mizuno K (1998) Cofilin phosphorylation by LIM-kinase 1 and its role in Rac-mediated actin reorganization. Nature 393:809-812.

Yang Y, Wang XB, Frerking M, Zhou Q (2008) Spine expansion and stabilization associated with long-term potentiation. J Neurosci 28:5740-5751.

Yashiro K, Philpot BD (2008) Regulation of NMDA receptor subunit expression and its implications for LTD, LTP, and metaplasticity. Neuropharmacology 55:1081-1094.

Yasumatsu N, Matsuzaki M, Miyazaki T, Noguchi J, Kasai H (2008) Principles of long-term dynamics of dendritic spines. J Neurosci 28:13592-13608.

Yoneshima H, Nagata E, Matsumoto M, Yamada M, Nakajima K, Miyata T, Ogawa M, Mikoshiba K (1997) A novel neurological mutant mouse, yotari, which exhibits reeler-like phenotype but expresses CR-50 antigen/reelin. Neurosci Res 29:217-223.

Young-Pearse TL, Suth S, Luth ES, Sawa A, Selkoe DJ (2010) Biochemical and functional interaction of disrupted-in-schizophrenia 1 and amyloid precursor protein regulates neuronal migration during mammalian cortical development. J Neurosci 30:10431-10440.

Yuste R (2011) Dendritic spines and distributed circuits. Neuron 71:772-781.

Yuste R, Majewska A (2001a) Book Review: On the Function of Dendritic Spines. The Neuroscientist 7:387-395.

Yuste R, Majewska A (2001b) On the function of dendritic spines. Neuroscientist 7:387-395.

Yuste R, Bonhoeffer T (2004) Genesis of dendritic spines: insights from ultrastructural and imaging studies. Nat Rev Neurosci 5:24-34.

Yuste R, Majewska A, Holthoff K (2000) From form to function: calcium compartmentalization in dendritic spines. Nat Neurosci 3:653-659.

Zhang XL, Poschel B, Faul C, Upreti C, Stanton PK, Mundel P (2013) Essential role for synaptopodin in dendritic spine plasticity of the developing hippocampus. J Neurosci 33:12510-12518.

Zhao C, Deng W, Gage FH (2008) Mechanisms and functional implications of adult neurogenesis. Cell 132:645-660.

Zhao C, Teng EM, Summers RG, Jr., Ming GL, Gage FH (2006) Distinct morphological stages of dentate granule neuron maturation in the adult mouse hippocampus. J Neurosci 26:3-11.

Zhou L, Zhu DY (2009) Neuronal nitric oxide synthase: structure, subcellular localization, regulation, and clinical implications. Nitric Oxide 20:223-230.

Ziv NE, Smith SJ (1996) Evidence for a role of dendritic filopodia in synaptogenesis and spine formation. Neuron 17:91-102.

Appendix

Coauthored publications

1. Reelin regulates postnatal neurogenesis and enhances spine hypertrophy and long-term potentiation. J Neurosci. 2010 Mar 31;30(13):4636-49

Pujadas L, Gruart A, BOSCH C, Delgado L, Teixeira CM, Rossi D, de Lecea L, Martinez A, Delgado-Garcia JM, Soriano E.

4636 • The Journal of Neuroscience, March 31, 2010 • 30(13):4636 – 4649

Behavioral/Systems/Cognitive

Reelin Regulates Postnatal Neurogenesis and Enhances Spine Hypertrophy and Long-Term Potentiation

Lluís Pujadas,[1,2,3] **Agnès Gruart,**[4] **Carles Bosch,**[1,2,3] **Lídia Delgado,**[1,2,3] **Cátia M. Teixeira,**[1,2,3] **Daniela Rossi,**[1,2,3] **Luis de Lecea,**[5] **Albert Martínez,**[1,2,3] **José M. Delgado-García,**[4] **and Eduardo Soriano**[1,2,3]

[1]Developmental Neurobiology and Regeneration Laboratory, Institute for Research in Biomedicine, Barcelona, [2]Department of Cell Biology, University of Barcelona, and [3]Centro de Investigación en Red sobre Enfermedades Neurodegenerativas (CIBERNED-ISCIII), 08028 Barcelona, Spain, [4]Neurosciences Division, Faculty of Experimental Sciences, University Pablo de Olavide, 41013 Sevilla, Spain, and [5]Department of Molecular Biology, Department of Psychiatry and Behavioral Sciences, Stanford University, Palo Alto, California 94304

Reelin, an extracellular protein essential for neural migration and lamination, is also expressed in the adult brain. To unravel the function of this protein in the adult forebrain, we generated transgenic mice that overexpress Reelin under the control of the CaMKIIα promoter. Overexpression of Reelin increased adult neurogenesis and impaired the migration and positioning of adult-generated neurons. In the hippocampus, the overexpression of Reelin resulted in an increase in synaptic contacts and hypertrophy of dendritic spines. Induction of long-term potentiation (LTP) in alert-behaving mice showed that Reelin overexpression evokes a dramatic increase in LTP responses. Hippocampal field EPSP during a classical conditioning paradigm was also increased in these mice. Our results indicate that Reelin levels in the adult brain regulate neurogenesis and migration, as well as the structural and functional properties of synapses. These observations suggest that Reelin controls developmental processes that remain active in the adult brain.

Introduction

Reelin is an extracellular protein that is essential for neuronal migration and brain development (D'Arcangelo et al., 1995; Alcantara et al., 1998; Rice and Curran, 2001; Soriano and Del Rio, 2005; Cooper, 2008). Functions exerted by Reelin are mediated through the receptors apolipoprotein E receptor 2 (ApoER2) and very-low-density lipoprotein receptor (VLDLR), which trigger a complex signaling cascade involving members of the Src kinase family, the adaptor Dab1, the PI3K, Erk1/2 and GSK3β kinases, and CrkL, among others (Howell et al., 1997, 1999; Hiesberger et al., 1999; Beffert et al., 2002; Arnaud et al., 2003; Ballif et al., 2004; González-Billault et al., 2005; Simó et al., 2007).

In the adult brain, Reelin is expressed by subsets of neurons in the cerebral cortex, in particular by GABAergic interneurons (Alcantara et al., 1998). Although the role of Reelin in the adult brain is not well understood, it has been shown that this protein is expressed in synaptic contacts, and that neurons deficient in ApoER2 and VLDLR receptors have impaired long-term potentiation (LTP) (Pesold et al., 1998; Beffert et al., 2005). Recently, it has been demonstrated that Reelin participates in the composition, recruitment and traffic of NMDA receptor subunits (Chen et al., 2005; Qiu et al., 2006; Groc et al., 2007), in the generation of dendrites, and in the formation of dendritic spines (Matsuki et al., 2008; Niu et al., 2008). Furthermore, the lack of spines in cultured *reeler* neurons is recovered by incubation with Reelin (Matsuki et al., 2008; Niu et al., 2008). Altogether, these studies suggest that Reelin is involved in the correct formation and maintenance of synapses. This protein also acts as a detachment factor in the migration of subventricular zone (SVZ)-derived neurons in the rostral migratory stream (RMS) to the olfactory bulb (OB) (Hack et al., 2002). Moreover, deficits in Reelin levels and genetic variants have been associated with several psychiatric disorders (Impagnatiello et al., 1998; Persico et al., 2001), which, together with studies demonstrating altered Reelin levels in Alzheimer's disease, the localization of Reelin with β-amyloid deposits, and the importance of Reelin in neurodegeneration and β-amyloid-induced synaptic depression (Beffert et al., 2006; Botella-López et al., 2006; Durakoglugil et al., 2009; Knuesel et al., 2009), supports the notion that this protein participates in the pathogenesis of neurological diseases.

Most studies on Reelin functions in the adult brain have been based on analyses of the Reelin-deficient *reeler* mice and heterozygous *reeler* mice, as a model of Reelin haploinsufficiency. Studies in *reeler* mice are hampered by the dramatic defects in brain lamination and organization, which raises the question as to whether defects in *reeler* mouse function are secondary to the mispositioning of neurons. Moreover, transgenic mice expressing Reelin under the control of the Nestin promoter rescue the

Received Oct. 23, 2009; revised Jan. 19, 2010; accepted Feb. 18, 2010.

This project was supported by Grant BFU2008-3980 [Ministerio de Ciencia e Innovacion (MICINN), Spain] and grants from The "Marató de TV3" and "Caixa Catalunya-Obra Social" Foundations to E.S. and by Grants PI07/0715 (Fondo de Investigación Sanitaria) to A.M., BFU2008-03390/BMC (MICINN) to A.G., and BFU2008-00899 (MICINN) to J.M.D.-G. We thank Drs. M. Mayford (Scripps Research Institute, La Jolla, CA), J. A. Cooper (Fred Hutchinson Cancer Research Center, Seattle, WA), T. Curran (Joseph Stokes Jr. Research Institute, Philadelphia, PA), and A. M. Goffinet (Université Catholique de Louvain, Brussels, Belgium) for generously providing materials used in this study; M. Esteban for contributing to physiology experiments and providing technical assistance; C. Díaz-Ruiz, J. M. Ureña, and A. La Torre for scientific comments; B. Pintado, E. M. Pastor, and L. Brunso for technical assistance; and Tanya Yates for editorial help.

Correspondence should be addressed to either Lluís Pujadas or Eduardo Soriano, Developmental Neurobiology and Regeneration Laboratory (PS1-A1), Institute for Research in Biomedicine, Barcelona, Barcelona Science Park, Baldiri Reixac, 10, 08028 Barcelona, Spain, E-mail: lluis.pujadas@irbbarcelona.org or eduardo.soriano@irbbarcelona.org.

DOI:10.1523/JNEUROSCI.5284-09.2010

 0270-6474/10/304636-14$15.00/0

2. Overexpression of Reelin prevents the manifestation of behavioral phenotypes related to schizophrenia and bipolar disorder. Neuropsychopharmacology. 2011 Nov;36(12):2395-405.

Teixeira CM, Martín ED, Sahún I, Masachs N, Pujadas L, Corvelo A, BOSCH C, Rossi D, Martinez A, Maldonado R, Dierssen M, Soriano E.

Neuropsychopharmacology (2011), 1–11

www.neuropsychopharmacology.org

Open

Overexpression of Reelin Prevents the Manifestation of Behavioral Phenotypes Related to Schizophrenia and Bipolar Disorder

Cátia M Teixeira*[,1], Eduardo D Martín[2], Ignasi Sahún[3], Nuria Masachs[1], Lluís Pujadas[1], André Corvelo[4], Carles Bosch[1], Daniela Rossi[1], Albert Martinez[1], Rafael Maldonado[5], Mara Dierssen[3] and Eduardo Soriano*[,1]

[1]Developmental Neurobiology and Regeneration Unit, Institute for Research in Biomedicine, Parc Cientific de Barcelona; Centro de Investigación Biomédica en Red sobre Enfermedades Neurodegenerativas (CIBERNED), and Department of Cell Biology, University of Barcelona, Barcelona, Spain; [2]Laboratory of Neurophysiology and Synaptic Plasticity. Albacete Science and Technology Park (PCyTA). Institute for Research in Neurological Disabilities (IDINE), University of Castilla-La Mancha, Albacete, Spain; [3]Genes and Disease Program, Center for Genomic Regulation (CRG), Barcelona Biomedical Research Park (PRBB) and CIBER de Enfermedades Raras (CIBERER), Barcelona, Spain; [4]Centro Nacional de Análisis Genómico, Barcelona, Spain; [5]Departament de Ciències Experimentals i de la Salut, Laboratory of Neuropharmacology, Universitat Pompeu Fabra, Barcelona, Spain

Despite the impact of schizophrenia and mood disorders, which in extreme cases can lead to death, recent decades have brought little progress in the development of new treatments. Recent studies have shown that Reelin, an extracellular protein that is critical for neuronal development, is reduced in schizophrenia and bipolar disorder patients. However, data on a causal or protective role of Reelin in psychiatric diseases is scarce. In order to study the direct influence of Reelin's levels on behavior, we subjected two mouse lines, in which Reelin levels are either reduced (Reelin heterozygous mice) or increased (Reelin overexpressing mice), to a battery of behavioral tests: open-field, black–white box, novelty-suppressed-feeding, forced-swim-test, chronic corticosterone treatment followed by forced-swim-test, cocaine sensitization and pre-pulse inhibition (PPI) deficits induced by *N*-methyl-D-aspartate (NMDA) antagonists. These tests were designed to model some aspects of psychiatric disorders such as schizophrenia, mood, and anxiety disorders. We found no differences between Reeler heterozygous mice and their wild-type littermates. However, Reelin overexpression in the mouse forebrain reduced the time spent floating in the forced-swim-test in mice subjected to chronic corticosterone treatment, reduced behavioral sensitization to cocaine, and reduced PPI deficits induced by a NMDA antagonist. In addition, we demonstrate that while stress increased NMDA NR2B-mediated synaptic transmission, known to be implicated in depression, Reelin overexpression significantly reduced it. Together, these results point to the Reelin signaling pathway as a relevant drug target for the treatment of a range of psychiatric disorders.

Neuropsychopharmacology advance online publication, 3 August 2011; doi:10.1038/npp.2011.153

Keywords: depression; behavior; cocaine sensitization; pre-pulse inhibition; corticosterone; NR2B

INTRODUCTION

Schizophrenia, mood, and anxiety disorders are devastating diseases with high prevalence and comorbidity rates (Altamura *et al*, 2011; Kessler *et al*, 2005). Despite the immense impact of these diseases, knowledge about their pathophysiology is limited. According to the stress–diathesis model, these diseases result from interaction between genetic predisposition and environmental risk factors. Research into how genetic makeup interacts with the environmental factors implicated in the triggering of these diseases is crucial. This implies not only understanding the genetic risk factors but also identifying genetic variations that confer resilience to disease, which may lead to the development of new treatments.

Reelin, an extracellular protein essential for neuronal migration and positioning during development (D'Arcangelo *et al*, 1995; Tissir and Goffinet, 2003), has received recent attention because of its connection to bipolar disorder and schizophrenia. In fact, comprehensive databases of

*Correspondence: Drs E Soriano or CM Teixeira, Cell and Developmental Biology Programme, Developmental Neurobiology and Regeneration Unit, Institute for Research in Biomedicine (IRB) Barcelona, Parc Científic de Barcelona, Centro de Investigación Biomédica en Red sobre Enfermedades Neurodegenerativas (CIBERNED), and Department of Cell Biology, University of Barcelona, Baldiri Reixac 10, Barcelona E-08028, Spain, Tel: +34 93 4037117, Fax: +34 93 4037116, E-mail: eduardo.soriano@irbbarcelona.org or catia.teixeira@irbbarcelona.org
Received 25 March 2011; revised 28 June 2011; accepted 28 June 2011

3. Neurodegeneration and functional impairments associated with glycogen synthase accumulation in a mouse model of Lafora disease. EMBO Mol Med. 2011 Nov;3(11):667-81

Valles-Ortega J, Duran J, Garcia-Rocha M, BOSCH C, Saez I, Pujadas L, Serafin A, Cañas X, Soriano E, Delgado-García JM, Gruart A, Guinovart JJ.

EMBO Molecular Medicine

Neurodegeneration and functional impairments associated with glycogen synthase accumulation in a mouse model of Lafora disease

Jordi Valles-Ortega[1,2†], Jordi Duran[1,3†], Mar Garcia-Rocha[1], Carles Bosch[1,4,5], Isabel Saez[1,2], Lluís Pujadas[1,4,5], Anna Serafin[6], Xavier Cañas[6], Eduardo Soriano[1,4,5], José M. Delgado-García[7], Agnès Gruart[7], Joan J. Guinovart[1,2,3]*

Keywords: glycogen synthase; glycogen; Lafora; malin; neurodegeneration

DOI 10.1002/emmm.201100174

Received June 20, 2011
Revised July 22, 2011
Accepted July 29, 2011

Lafora disease (LD) is caused by mutations in either the laforin or malin gene. The hallmark of the disease is the accumulation of polyglucosan inclusions called Lafora Bodies (LBs). Malin knockout (KO) mice present polyglucosan accumulations in several brain areas, as do patients of LD. These structures are abundant in the cerebellum and hippocampus. Here, we report a large increase in glycogen synthase (GS) in these mice, in which the enzyme accumulates in LBs. Our study focused on the hippocampus where, under physiological conditions, astrocytes and parvalbumin-positive (PV^+) interneurons expressed GS and malin. Although LBs have been described only in neurons, we found this polyglucosan accumulation in the astrocytes of the KO mice. They also had LBs in the soma and some processes of PV^+ interneurons. This phenomenon was accompanied by the progressive loss of these neuronal cells and, importantly, neurophysiological alterations potentially related to impairment of hippocampal function. Our results emphasize the relevance of the laforin–malin complex in the control of glycogen metabolism and highlight altered glycogen accumulation as a key contributor to neurodegeneration in LD.

INTRODUCTION

Glycogen is the principal storage form of glucose in animal and human cells. It is mainly produced in the liver and muscles, and glycogen levels in the brain are low compared to these two tissues. In the brain, this polysaccharide is stored in astrocytes, while most neurons do not accumulate it under normal conditions (Cataldo & Broadwell, 1986; Wender et al, 2000).

Glycogen is produced by glycogen synthase (GS), the only enzyme able to synthesize glucose polymers in mammals, and degraded by glycogen phosphorylase (GP). Mammals express two isoforms of GS encoded by *GYS1* and *GYS2*. The latter encodes the liver isoform (LGS) and its expression is restricted to the liver, while the former encodes the muscle isoform (MGS) and is widely expressed excluding the liver. MGS is regulated by phoshorylation at nine serine residues located in the amino- and carboxy-terminal domains of the enzyme. Phoshorylation by

(1) Institute for Research in Biomedicine (IRB Barcelona) Barcelona, Spain
(2) Department of Biochemistry and Molecular Biology, University of Barcelona, Barcelona, Spain
(3) Centro de Investigación Biomédica en Red de Diabetes y Enfermedades Metabólicas Asociadas (CIBERDEM), Madrid, Spain
(4) Department of Cell Biology, University of Barcelona, Barcelona, Spain
(5) Centro de Investigación Biomédica en Red para Enfermedades Neurodegenerativas (CIBERNED), Madrid, Spain
(6) Laboratory Animal Applied Research Platform, Barcelona Science Park, Barcelona, Spain
(7) Division of Neurosciences, Pablo de Olavide University, Seville, Spain
***Corresponding author:** Tel: +34 93 403 71 11; Fax: +34 93 403 71 14; E-mail: guinovart@irbbarcelona.org

†These authors contributed equally to this work.

4. Accelerated aging of the GABAergic septohippocampal pathway and decreased hippocampal rhythms in a mouse model of Alzheimer's disease. FASEB J. 2012 Nov;26(11):4458-67

Rubio SE, Vega-Flores G, Martínez A, BOSCH C, Pérez-Mediavilla A, del Río J, Gruart A, Delgado-García JM, Soriano E, Pascual M.

The FASEB Journal • Research Communication

Accelerated aging of the GABAergic septohippocampal pathway and decreased hippocampal rhythms in a mouse model of Alzheimer's disease

Sara E. Rubio,[*,†,‡] Germán Vega-Flores,[§] Albert Martínez,[*,†,‡] Carles Bosch,[*,†,‡] Alberto Pérez-Mediavilla,[‡,‖] Joaquín del Río,[‡,‖] Agnès Gruart,[§] José María Delgado-García,[§] Eduardo Soriano,[*,†,‡] and Marta Pascual[*,†,‡,1]

*Developmental Neurobiology and Regeneration Laboratory, Institute for Research in Biomedicine, Barcelona, Spain; [†]Department of Cell Biology, University of Barcelona, Barcelona, Spain; [‡]Centro de Investigación Biomédica en Red para Enfermedades Neurodegenerativas, Madrid, Spain; [§]Division of Neurosciences, Pablo de Olavide University, Seville, Spain; and [‖]Division of Neurosciences, Centro de Investigación Médica Aplicada, Universidad de Navarra, Pamplona, Spain

ABSTRACT **Patients with Alzheimer's disease (AD) display altered functioning of cortical networks, including altered patterns of synchronous activity and a serious deficit in cholinergic septohippocampal (SH) innervation. However, the mechanisms underlying these alterations and the implication of the GABAergic SH component in AD are largely unknown. In addition, the GABAergic septohippocampal pathway (SHP) is believed to regulate synchronous hippocampal activity by controlling the activity of interneurons. Here we show, using well-characterized pathway tracing experiments, that innervation of the GABAergic SHP decreases during normal aging. Furthermore, in an AD mouse model ($hAPP_{Sw,Ind}$; J20 mice), the GABAergic SHP shows a dramatic and early onset of this decrease in 8-mo-old mice. This decline is not caused by neuronal loss, but by the reduced number and complexity of GABAergic SH axon terminals. Finally, we demonstrate that hippocampal θ and γ rhythm power spectra are markedly diminished in 8-mo-old behaving mice expressing mutated hAPP. In addition to the well-known loss of cholinergic input to the hippocampus in AD, these data suggest that the altered patterns of synchronous activity seen in patients with AD could be caused by the loss of GABAergic SH axons, which modulate hippocampal network activities.—Rubio, S. E., Vega-Flores, G., Martínez, A., Bosch, C., Pérez-Mediavilla, A., del Río, J., Gruart, A., Delgado-García, J. M., Soriano, E., Pascual, M. Accelerated aging of the GABAergic septohippocampal pathway and decreased hippocampal rhythms in a mouse model of Alzheimer's disease. *FASEB J.* 26, 4458–4467 (2012). www.fasebj.org**

Key Words: θ *rhythm* · *J20 mice* · *medial septum*

The most typical neuropathological hallmarks of Alzheimer's disease (AD) are amyloid-β (Aβ) deposits and Tau tangles. However, one of the earliest manifestations of this disease is the progressive deterioration of the cholinergic component of the basal forebrain system, including the medial septum/diagonal band of Broca (MS/DB) and the nucleus basalis magnocellularis (NBM), and thus of the cholinergic input to the cerebral cortex, including the hippocampal complex (1–3). This phenomenon has been described during normal aging in experimental animals, and several abnormalities in the cholinergic system have also been reported in aged human brains (4–6). Moreover, it is believed that reduced function of the cholinergic septohippocampal pathway (SHP) may underlie early impairment of hippocampus-based episodic memory. Indeed, pharmacological intervention of the cholinergic neurotransmitter system (*e.g.*, cholinesterase inhibitors) is used to treat early AD symptoms (7).

In addition to the cholinergic pathway, the SHP has a second important component, the GABAergic SHP. This inhibitory pathway terminates specifically on GABAergic hippocampal interneurons (8, 9), which, in turn, control the activity of pyramidal neurons. It has been proposed that activation of GABAergic SHP neurons leads to the selective inhibition of inhibitory interneurons, thereby allowing the synchronous activa-

Abbreviations: Aβ, amyloid-β; AD, Alzheimer's disease; BDA, biotinylated dextran amine; CALR, calretinin; DB, diagonal band of Broca; FAD, familial Alzheimer's disease; GAD65/67, glutamic acid decarboxylase isoforms 65 and 67; hAPP, human amyloid precursor protein; MS, medial septum; NBM, nucleus basalis magnocellularis; PARV, parvalbumin; SH, septohippocampal; SHP, septohippocampal pathway; WT, wild type

[1] Correspondence: Developmental Neurobiology and Regeneration Laboratory, Institute for Research in Biomedicine, Baldiri i Reixac, 10, E-08028 Barcelona, Spain. E-mail: marta.pascual@irbbarcelona.org

doi: 10.1096/fj.12-208413

This article includes supplemental data. Please visit *http://www.fasebj.org* to obtain this information.

5. Cell-autonomous inactivation of the reelin pathway impairs adult neurogenesis in the hippocampus. J Neurosci. 2012 Aug 29;32(35):12051-65.

Teixeira CM, Kron MM, Masachs N, Zhang H, Lagace DC, Martinez A, Reillo I, Duan X, BOSCH C, Pujadas L, Brunso L, Song H, Eisch AJ, Borrell V, Howell BW, Parent JM, Soriano E.

The Journal of Neuroscience, August 29, 2012 • 32(35):12051–12065 • **12051**

Development/Plasticity/Repair

Cell-Autonomous Inactivation of the Reelin Pathway Impairs Adult Neurogenesis in the Hippocampus

Catia M. Teixeira,[1]* Michelle M. Kron,[2]* Nuria Masachs,[1]* Helen Zhang,[2] Diane C. Lagace,[4] Albert Martinez,[1] Isabel Reillo,[8] Xin Duan,[5] Carles Bosch,[1] Lluis Pujadas,[1] Lucas Brunso,[1] Hongjun Song,[5] Amelia J. Eisch,[6] Victor Borrell,[8] Brian W. Howell,[7] Jack M. Parent,[2,3] and Eduardo Soriano[1]****

[1]Developmental Neurobiology and Regeneration Laboratory, IRB Barcelona, Parc Cientific de Barcelona, Centro de Investigación Biomédica en Red sobre Enfermedades Neurodegenerativas (CIBERNED, ISCIII), Department of Cell Biology, University of Barcelona, Barcelona E-08028, Spain, [2]Department of Neurology and Neuroscience Graduate Program, University of Michigan Medical School, Ann Arbor, Michigan 48109, [3]Ann Arbor Veterans Administration Healthcare System, Ann Arbor, Michigan 48105, [4]Department of Cellular and Molecular Medicine, University of Ottawa, Ottawa, Ontario K1H 8M5, Canada, [5]Institute for Cell Engineering, Departments of Neurology and Neuroscience, Johns Hopkins University School of Medicine, Baltimore, Maryland 21205, [6]Department of Psychiatry, University of Texas Southwestern Medical Center, Dallas, Texas 75390-9070, [7]Department of Neuroscience and Physiology, State University of New York, Syracuse, New York 13210, and [8]Instituto de Neurociencias, Consejo Superior de Investigaciones Científicas-Universidad Miguel Hernández, Sant Joan d'Alacant E-03550, Spain

Adult hippocampal neurogenesis is thought to be essential for learning and memory, and has been implicated in the pathogenesis of several disorders. Although recent studies have identified key factors regulating neuroprogenitor proliferation in the adult hippocampus, the mechanisms that control the migration and integration of adult-born neurons into circuits are largely unknown. Reelin is an extracellular matrix protein that is vital for neuronal development. Activation of the Reelin cascade leads to phosphorylation of Disabled-1, an adaptor protein required for Reelin signaling. Here we used transgenic mouse and retroviral reporters along with Reelin signaling gain-of-function and loss-of-function studies to show that the Reelin pathway regulates migration and dendritic development of adult-generated hippocampal neurons. Whereas overexpression of Reelin accelerated dendritic maturation, inactivation of the Reelin signaling pathway specifically in adult neuroprogenitor cells resulted in aberrant migration, decreased dendrite development, formation of ectopic dendrites in the hilus, and the establishment of aberrant circuits. Our findings support a cell-autonomous and critical role for the Reelin pathway in regulating dendritic development and the integration of adult-generated granule cells and point to this pathway as a key regulator of adult neurogenesis. Moreover, our data reveal a novel role of the Reelin cascade in adult brain function with potential implications for the pathogenesis of several neurological and psychiatric disorders.

Introduction

Neurogenesis persists throughout adulthood in the hippocampal dentate gyrus (DG) (Altman and Das, 1965; Cameron et al., 1993; Kuhn et al., 1996). Continuous generation of neurons in the adult hippocampus is essential for learning and has been proposed recently to contribute to the development of psychiatric disorders (Eisch et al., 2008). DG neuroblasts arise in the subgranular zone, migrate a short distance into the granule cell layer (GCL), and differentiate into dentate granule cells (DGCs) (van Praag et al., 2002; Ge et al., 2008; Toni et al., 2008). Thus, adult neurogenesis is a multistep process comprising the regulation of stem cell niches, cell proliferation, differentiation and *de novo* formation of dendrites and axons, and the integration of adult-generated neurons into functional circuits. While recent studies have identified key factors for the regulation and proliferation rates of neuroprogenitor cells, much less is known about the mechanisms that control the migration and functional recruitment of adult-generated neurons. *Disrupted in Schizophrenia-1* (*DISC1*), a schizophrenia susceptibility gene, was recently found to regulate process development and migration of adult-generated DGCs (Duan et al., 2007; Faulkner et al., 2008; Kim et al., 2009). Other molecules, including cyclin-dependent kinase 5 (cdk5), NeuroD, Sonic hedgehog, Prox1 and Wnts, are also implicated in controlling several steps of adult DGC neurogenesis (Lie et al., 2005; Jessberger et al., 2008; Lagace et al., 2008; Gao et al., 2009; Karalay

Received April 17, 2012; revised July 1, 2012; accepted July 9, 2012.

Author contributions: C.M.T., M.M.K., D.C.L., X.D., H.S., A.J.E., V.B., B.W.H., J.M.P., and E.S. designed research; C.M.T., M.M.K., N.M., D.C.L., H.Z., A.M., I.R., X.D., C.B., L.P., and L.B. performed research; D.C.L., X.D., H.S., A.J.E., V.B., and B.W.H. contributed unpublished reagents/analytic tools; C.M.T., M.M.K., N.M., H.Z., D.C.L., A.M., H.S., A.J.E., J.M.P., and E.S. analyzed data; C.M.T., M.M.K., D.C.L., H.S., A.J.E., B.W.H., J.M.P., and E.S. wrote the paper.

This project was supported by Grant BFU2008-3980 from the Ministerio de Ciencia e Innovacion (MICINN), Spain; by grants from the Centro de Investigación Biomédica en Red sobre Enfermedades Neurodegenerativas (CIBERNED) and Caixa Catalunya-Obra Social Foundations to E.S.; by grants from the Spanish Ministry of Science and Innovation (SAF2009-07367 and CONSOLIDER CSD2007-00023) to V.B.; by the Fred Annegers Fellowship from the Epilepsy Foundation (M.M.K.); and by NIH Grant NS058585 to J.M.P. I.R. was recipient of a Formación de Personal Universitario predoctoral fellowship from MINECO (Spain). We also thank Ashraf Muhaisen for technical help; Tanya Yates for editorial assistance; and F. Gage and S. Jessberger for reagents.

*C.M.T., M.M.K., and N.M. contributed equally to this study.

**J.M.P. and E.S. are co-senior authors.

Correspondence should be addressed to either of the following: Dr. Eduardo Soriano, IRB Barcelona, Baldiri Reixac 10, Barcelona E-08028, Spain, E-mail: eduardo.soriano@irbbarcelona.org; or Dr. Jack M. Parent, 5021 Biomedical Sciences Research Building, 09 Zina Pitcher Place, Ann Arbor, MI 48109. E-mail: parent@umich.edu.

DOI:10.1523/JNEUROSCI.1857-12.2012

 0270-6474/12/3212051-15$15.00/0

6. Transient downregulation of Dab1 protein levels during development leads to behavioral and structural deficits: relevance for psychiatric disorders. Neuropsychopharmacology. 2014 Feb; 39(3):556-68

Teixeira CM, Masachs N, Muhaisen A, BOSCH C, Pérez-Martínez J, Howell B, Soriano E.

Neuropsychopharmacology (2014) 39, 556–568

www.neuropsychopharmacology.org

Transient Downregulation of Dab1 Protein Levels during Development Leads to Behavioral and Structural Deficits: Relevance for Psychiatric Disorders

Catia M Teixeira*[,1,2,6], Nuria Masachs[1,2,6], Ashraf Muhaisen[1,2], Carles Bosch[1,2], Javier Pérez-Martínez[3], Brian Howell[4] and Eduardo Soriano*[,1,2,5]

[1]Department of Cell Biology, University of Barcelona, Barcelona, Spain; [2]Centro de Investigación Biomédica en Red sobre Enfermedades Neurodegenerativas (CIBERNED), Barcelona, Spain; [3]Institute of Neurosciences, CSIC and Miguel Hernández University, Alicante, Spain; [4]Department of Neuroscience and Physiology, SUNY Upstate Medical University, Syracuse, NY, USA; [5]Fundación CIEN, Vallecas, Spain

Psychiatric disorders have been hypothesized to originate during development, with genetic and environmental factors interacting in the etiology of disease. Therefore, developmentally regulated genes have received attention as risk modulators in psychiatric diseases. Reelin is an extracellular protein essential for neuronal migration and maturation during development, and its expression levels are reduced in psychiatric disorders. Interestingly, several perinatal insults that increase the risk of behavioral deficits alter Reelin signaling. However, it is not known whether a dysfunction in Reelin signaling during perinatal stages increases the risk of psychiatric disorders. Here we used a floxed *dab1* allele to study whether a transient decrease in Dab1, a key component of the Reelin pathway, is sufficient to induce behavioral deficits related to psychiatric disorders. We found that transient Dab1 downregulation during perinatal stages leads to permanent abnormalities of structural layering in the neocortex and hippocampus. In contrast, conditional inactivation of the *dab1* gene in the adult brain does not result in additional layering abnormalities. Furthermore, perinatal Dab1 downregulation causes behavior impairments in adult mice, such as deficits in memory, maternal care, pre-pulse inhibition, and response to cocaine. Some of these deficits were also found to be present in adolescence. We also show that D-cycloserine rescues the cognitive deficits observed in floxed *dab1* mice with layering alterations in the hippocampus and neocortex. Our results indicate a causal relation between the downregulation of Dab1 protein levels during development and the structural and behavioral deficits associated with psychiatric diseases in the adult.
Neuropsychopharmacology (2014) **39,** 556–568; doi:10.1038/npp.2013.226; published online 16 October 2013

Keywords: Reelin; Dab1; schizophrenia; mouse model; behavior; D-cycloserine

INTRODUCTION

Dysregulation of key developmental processes, caused by environmental and/or genetic risk factors, is associated with the pathogenesis of neuropsychiatric diseases (Ansorge *et al*, 2007; Brown and Patterson, 2011; Krishnan and Nestler, 2008; Nestler and Hyman, 2010). For example, maternal infection and early-life stress have been proposed as environmental risk factors for psychiatric disorders, although little is known about the mechanisms involved (Ansorge *et al*, 2007; Brown and Patterson, 2011; Krishnan and Nestler, 2008; Nestler and Hyman, 2010). Nevertheless, developmental dysregulation of a few factors, such as Disc1 (Li *et al*, 2007), NR1 in cortical interneurons (Belforte *et al*, 2009), serotonin (Ansorge *et al*, 2008; Ansorge *et al*, 2004), and dopamine (Kellendonk *et al*, 2006), have been shown to cause dysfunctions related to these diseases.

Reelin, an extracellular protein essential for neuronal migration, has been shown to regulate glutamatergic neurotransmission in both developing and adult neurons (Pujadas *et al*, 2010; Tissir and Goffinet, 2003). Reelin signals through ApoER2 and VLDLR receptors and leads to the phosphorylation of the adapter Dab1, which subsequently activates several pathways. The phenotypes of Dab1- and ApoER2/VLDLR-knockout mice are indistinguishable from Reelin-deficient mice, thereby indicating that these signaling components are essential for the Reelin pathway (Hiesberger *et al*, 1999; Howell *et al*, 1997b; Tissir and Goffinet, 2003). Reelin expression is decreased in psychiatric disorders. In addition, *reelin* genetic variants are associated with these diseases, and Reelin overexpression protects against psychiatric disease-related phenotypes (Fatemi *et al*, 2000; Jia *et al*, 2010; Kim and Webster, 2009; Teixeira *et al*, 2011; Torrey *et al*, 2005). Interestingly, perinatal insults that cause behavioral deficits in the adult, such as alcohol exposure during pregnancy, maternal viral infection or exposure to Poly I:C, and serotonin

*Correspondence: Dr E Soriano or Dr CM Teixeira, Department of Cell Biology, University of Barcelona, Baldiri Reixac 10, Barcelona E-08028, Spain, Tel: +34 93 4037117, Fax: +34 93 4037116, E-mail: esoriano@ub.edu or teixeira.catia@gmail.com
[6]These authors contributed equally to this work.
Received 8 April 2013; revised 9 August 2013; accepted 11 August 2013; accepted article preview online 13 September 2013